TEAD1 is regulator of cardiomyocyte proliferation and differentiation

Inaugural-Dissertation

zur Erlangung des akademischen Grades

doctor rerum naturalium

(Dr. rer. nat.)

Vorgelegt beim Fachbereich für Biologie (FB 17)

der Philipps-Universität Marburg

von

Polina Zarjitskaya-Thierling

(M. Sc.)

aus

Taschkent (Usbekistan)

Marburg, Mai 2019

Die Untersuchungen zur vorliegenden Arbeit wurden am Max-Planck-Institut für Herz- und Lungenforschung (W. G. Kerckhoff-Institut) in Bad Nauheim unter Leitung von Prof. Dr. Dr. Thomas Braun durchgeführt.

Vom Fachbereich Biologie
der Philipps-Universität Marburg als Dissertation am 08.07.2019 angenommen

Erstgutachter (*intern*): Prof. Dr. Renate Renkawitz-Pohl
Fachbereich für Biologie (FB 17)
Abteilung Entwicklungsbiologie
Philipps-Universität Marburg
Karl-von-Frisch-Straße 8
D-35043 Marburg

Zweitgutachter (*extern*): Prof. Dr. Dr. Thomas Braun
Abteilung für Entwicklung und Umbau des Herzens
Max-Planck-Institut für Herz- und Lungenforschung
Ludwigstraße 43
D-61231 Bad Nauheim

Tag der mündlichen Prüfung am: 31.07.2019

Ehrenwörtliche Erklärung:

Ich versichere, dass ich meine Dissertation

TEAD1 is regulator of cardiomyocyte proliferation and differentiation

unter der Leitung von Prof. Dr. Dr. Thomas Braun (Max-Planck-Institut für Herz- und Lungenforschung, Bad Nauheim) selbstständig und ohne unerlaubte Hilfe angefertigt und mich dabei keiner anderen als der von mir ausdrücklich angegebener Quellen und Hilfen bedient habe.
Die Dissertation wurde in der jetzigen oder einer ähnlichen Form noch bei keiner anderen Hochschule eingereicht und hat noch keinen sonstigen Prüfungszwecken gedient.

Marburg, den 24.05.2019

_____

Polina Zarjitskaya-Thierling

I. ZUSAMMENFASSUNG

Die embryonale Herzentwicklung ist ein sehr präzise regulierter Vorgang, der hauptsächlich mittels Zellproliferation und Differenzierung der Herzmuskelzellen (Kardiomyozyten) stattfindet. Nach der Geburt verlieren Kardiomyozyten sukzessive ihre Proliferationsfähigkeit, so dass das Herzwachstum überwiegend durch die physiologische Größenzunahme sowie eine Reifung der Kardiomyozyten erfolgt. Diese Prozesse werden durch eine große Zahl an Transkriptionsfaktoren gesteuert, deren Störung zu Defekten und einem Versagen des Herzens führen kann. TEAD1 ist ein Transkriptionsfaktor, der die Expression von vielen muskelspezifischen Genen reguliert und dennoch bleibt vieles über seine Rolle in Kardiomyozyten unbekannt. Um die biologische Funktion von TEAD1 im Herzen zu untersuchen, wurde die vorliegende Studie an die Analyse unterschiedlicher Kardiomyozyten-spezifischer konditioneller *Tead1* Knockout- und Überexpression-Mauslinien sowie an die Identifizierung von Kardiomyozyten-spezifischen TEAD1-regulierten Genen gerichtet. Die Ergebnisse der Studie zeigen, dass TEAD1 für die Proliferation, Differenzierung und Reifung der embryonalen sowie postnatalen Kardiomyozyten erforderlich ist. Der spezifische Verlust von *Tead1* in embryonalen Kardiomyozyten führt zu einer frühen embryonalen Sterblichkeit, die durch eine erniedrigte Kardiomyozyten-Proliferation sowie eine erhöhte Apoptose gekennzeichnet ist. Außerdem weisen Kardiomyozyten eine Verzögerung in der Entwicklung von Myofibrillen- sowie Glanzstreifen auf. Die spezifische Inaktivierung von *Tead1* in postnatalen Stadien führt zu einer frühen Sterblichkeit, die durch die Entwicklung einer Herzinsuffizienz sowie darauffolgendem Herzversagen gekennzeichnet ist und bis spätestens 30 Tage nach der Geburt eintritt. Darüber hinaus geht der Verlust von *Tead1* in postnatalen Kardiomyozyten mit einer verminderten Kardiomyozyten-Plastizität einher, die zu einer frühzeitigen Reifung führt. Die Untersuchung des Transkriptions-Profils von isolierten *Tead1* Knockout-Kardiomyozyten kombiniert mit einem genomweiten TEAD1-Bindungsmuster in isolierten Wildtyp-Kardiomyozyten zeigt, dass TEAD1 für die Regulation der Gene verantwortlich ist, die in Wachstum, Differenzierung, Reifung, Kontraktion, Organisation des Zytoskellets, Umbau von Sarkomeren, sowie Energiehomöostase der Kardiomyozyten involviert sind. Alle diese Untersuchungsergebnisse deuten auf eine wichtige biologische Funktion von TEAD1 in Entwicklung und Reifung, sogenannte Plastizität, von embryonalen sowie postnatalen Kardiomyozyten hin, die einen regelrechten, physiologischen Herzumbau erlauben.

II. ABSTRACT

Heart development is a tightly regulated process directed to control cardiomyocyte proliferation and differentiation. After birth, cardiomyocytes steadily lose the ability to proliferate and the heart growth is maintained by physiological hypertrophy and differentiation of the cardiomyocytes. Numerous transcription factors are involved in these processes and deregulation of them can lead to heart defects, heart failure and death. TEAD1 is a transcription factor that governs the expression of numerous muscle specific genes, however, little is known about the role of TEAD1 in cardiomyocytes. In order to study the role of TEAD1 in the heart, the present study aimed at analyzing TEAD1 function in cardiomyocytes based on loss- and gain-of-function studies to decipher postnatal TEAD1 regulated transcriptional networks. Our data indicate an essential role of TEAD1 for the cardiomyocyte differentiation and maturation in both, embryonic and postnatal hearts. Specifically, early deletion of *Tead1* in cardiomyocytes is embryonically lethal and characterized by decreased cardiomyocyte proliferation and increased apoptosis. In addition, cardiomyocytes displayed delay in the development of myofibrils and intercalated discs. In contrast, mice harboring cardiomyocyte-specific *Tead1* inactivation in postnatal stage die within 4 weeks after birth due to impaired cardiac function and heart dilatation. Moreover, postnatal *Tead1*-deficient cardiomyocytes showed decreased proliferation and increased apoptosis rate. In addition, in postnatal cardiomyocytes, *Tead1* inactivation leads to diminished cardiomyocyte plasticity characterized by premature differentiation of cardiomyocytes. Importantly, the lethal heart phenotype of our conditional *Tead1*-deficient mice was rescued by cardiomyocyte-specific *Tead1* overexpression. Transcriptome profiling of *Tead1*-deficient cardiomyocytes combined with genome-wide TEAD1 binding studies in wild-type cardiomyocytes revealed that TEAD1 regulates genes responsible for cardiomyocyte growth, differentiation, maturation, contraction, energy homeostasis, sarcomere and cytoskeleton organization. Taken together, these data indicate an important role of TEAD1 in embryonic and postnatal cardiomyocyte plasticity thus enabling proper physiological heart remodeling.

III. ACKNOWLEDGEMENTS

I would like to express my very great gratitude to a large number of people that supported me during these years working at Max Planck Institute for Heart and Lung Research in Bad Nauheim, where I was supported by International Max Planck Research School for Heart and Lung Research fellowship.

First, I would like to express my deep appreciation to Prof. Dr. Dr. Thomas Braun, my research supervisor, for his valuable and constructive suggestions during the planning and development of this research work. I am particularly grateful for advice given by Dr. André Schneider and his extraordinary support in keeping my progress.

My grateful thanks are also addressed to PD Dr. Thomas Böttger for his cooperation in processing and analysis of microarray data, to Dr. Stefan Günther for his help in analyzing the ChIP-Seq, to Dr. Astrid Wietelmann, who helped me with MRI measurements, to PD. Dr. Sava Costin for his help in processing TEM analysis and to Marion Wiesnet for her support in isolation of adult mouse cardiomyocytes. I would like also to thank Dr. Thomas Kubin for helping in isolating of adult rat cardiomyocytes and performing siRNA knockdown experiments.

My special thanks are extended to the members of AG Schneider group, who supported me greatly and always willing to help.

I would also like to extend my thanks to all Lab members, PhD students, technicians, bioinformatics group and animal caretakers, especially from Room 2, for their help in offering me recourses in running my PhD program.

Moreover, I gratefully acknowledge Prof. Dr. Renate Renkawitz-Pohl from Philipps-University Marburg for supporting me during my doctoral graduation.

Finally, I wish to thank my family and friends for their contribution to my emotional well-being and encouragement throughout my PhD time.

IV. TABLE OF CONTENTS

1 INTRODUCTION

The cellular and molecular processes of myocardial remodeling leading to heart diseases have been studied intensively both, *in vivo* and *in vitro*. However, the underlying mechanisms are largely unknown and more studies are certainly needed to understand whether the regulation of cardiomyocyte-specific gene expression in the pathological heart differs from that in normal, physiological hearts. Therefore, identification of signaling pathways and transcription factors regulating the expression of these genes in normal and pathological hearts may give important mechanistical insights into the pathogenesis of cardiac diseases and new therapeutic strategies.

Cardiomyocytes are the major cell type in the heart and any changes of their structural and functional characteristics can potentially lead to heart dysfunction [1-4]. It has been shown that activation of cardiomyocyte-specific genes is regulated by multiple transcription factors (TFs), including GATA4, MEF2, NKX2-5 and HAND [5-9]. Recently, transcription enhancer factor 1 (TEAD1) has been identified as an important regulator of muscle specific genes. In cardiomyocytes, however, only a few genes, which are directly regulated by TEAD1 have been documented so far [10-19].

1.1 Heart development and myocardial remodeling

During mammalian embryogenesis, the heart grows primarily *via* cardiomyocyte proliferation referred to as hyperplasia [20-23]. After birth, cardiomyocytes undergo a switch from cell division to incomplete cell cycle, resulting in approximately 80–90% binucleated cardiomyocytes in adult mice and rats (Figure 1) [24-27]. In contrast, the non-cardiomyocyte cell fraction of the heart (*e.g.* fibroblasts, smooth muscle cells, endothelial cells, *etc.*) retain their proliferation capacity.

The adult mammalian heart is able to functionally and structurally adapt to alternations of the workload settings [28] *via* cardiomyocyte cell enlargement referred to as hypertrophy [29, 30]. The major features of physiological and pathological hypertrophy are schematically presented in Figure 2.

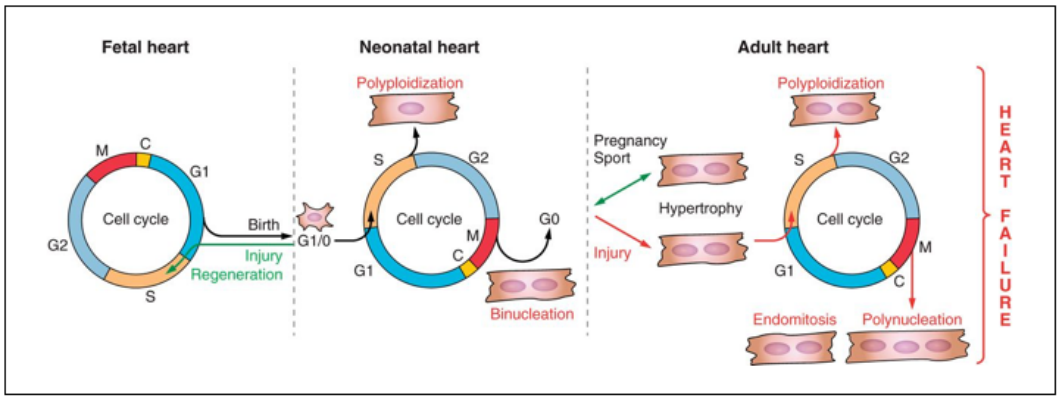

Figure 1. ***Cell cycle activities in fetal, postnatal and adult mammalian cardiomyocytes.*** *During embryogenesis, the ballooning of the chamber and further growth of the heart are sustained by cardiomyocyte proliferation. After birth, cardiomyocytes gradually stop proliferation and exit the cell cycle (G0/G1 phase). Initially this arrest is reversible so that newborn cardiomyocytes can re-enter the cell cycle and proliferate upon injury. During postnatal development, cardiomyocytes undergo additional incomplete cycles lacking cytokinesis, which finally results in binucleated or polyploid postnatal cardiomyocytes. In pathological hypertrophy, adult cardiomyocyte re-enter cell cycle and undergo polyploidization, endomitosis and polynucleation. This is a common feature of heart failure (adapted from [31]).*

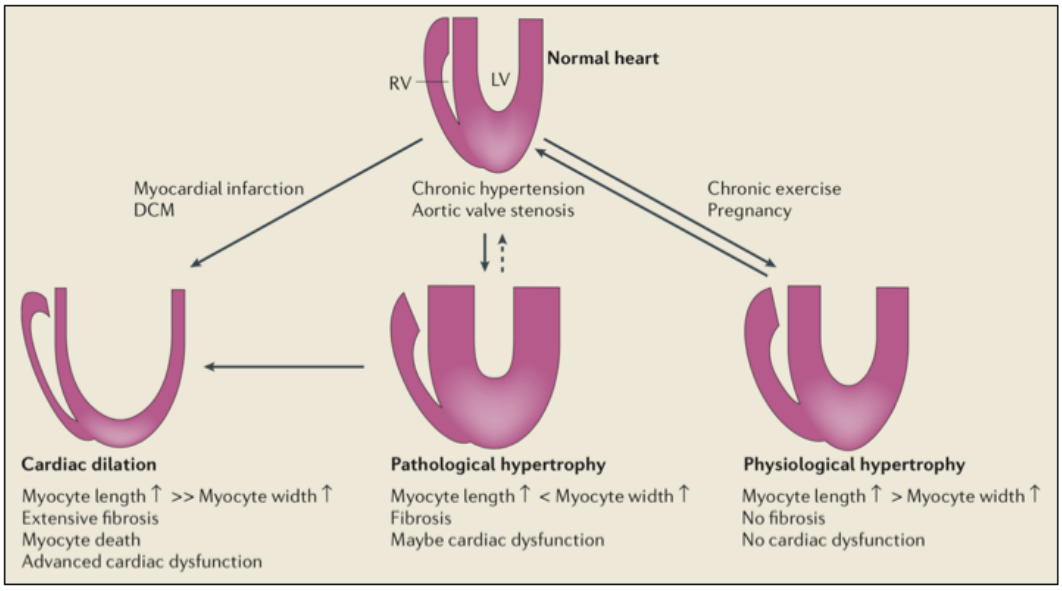

Figure 2. ***Types of cardiac hypertrophy. Physiological hypertrophy*** *is characterized by a uniform ventricular wall and septum growth leading to proportional increase in chamber dimension. This phenotype is associated with cardiomyocyte hypertrophy in which sarcomeres are added both, in series to lengthen the cell (longitudinal area) or at the periphery to increase the cell width (cross-sectional area).* ***Pathological cardiac hypertrophy*** *can produce concentric hypertrophy in which the ventricular wall and septum thicken with a net decrease in ventricular chamber dimensions. This remodeling is associated with a greater and disproportional increase in cardiac myocyte width than length.* ***Cardiac dilation*** *can result from a growth response in which sarcomeres are predominantly added in series to individual myocytes. DCM - dilated cardiomyopathy; LV - left ventricle; RV - right ventricle (adapted from [30]).*

During acute myocardial infarction (MI), cardiomyocytes die due to necrosis, apoptosis and autophagy. Cardiomyocyte loss in the infarct area is partially compensated by proliferating fibroblasts and extracellular matrix deposition [32-34]. This process, which is also referred to as replacement fibrosis, finally results in loss of contractility and in increased heart stiffness, whereby the remaining cardiomyocytes compensate the increased workload *via* hypertrophic growth referred to as hypertrophic remodeling processes (Figure 3). During this process cardiomyocytes undergo an extensive remodeling, which includes re-expression of fetal genes, like *Myh7 (*Myosin Heavy Chain 7, cardiac muscle β Isoform) and *Acta2* (Smooth Muscle α-Actin 2), as well as reorganization of the cytoskeletal and contractile apparatus (Figure 4) [35-37]. However, under certain conditions cardiomyocyte remodeling can also lead to heart failure, which is defined as inability of the heart to adequately pump blood in response to systemic demands [38].

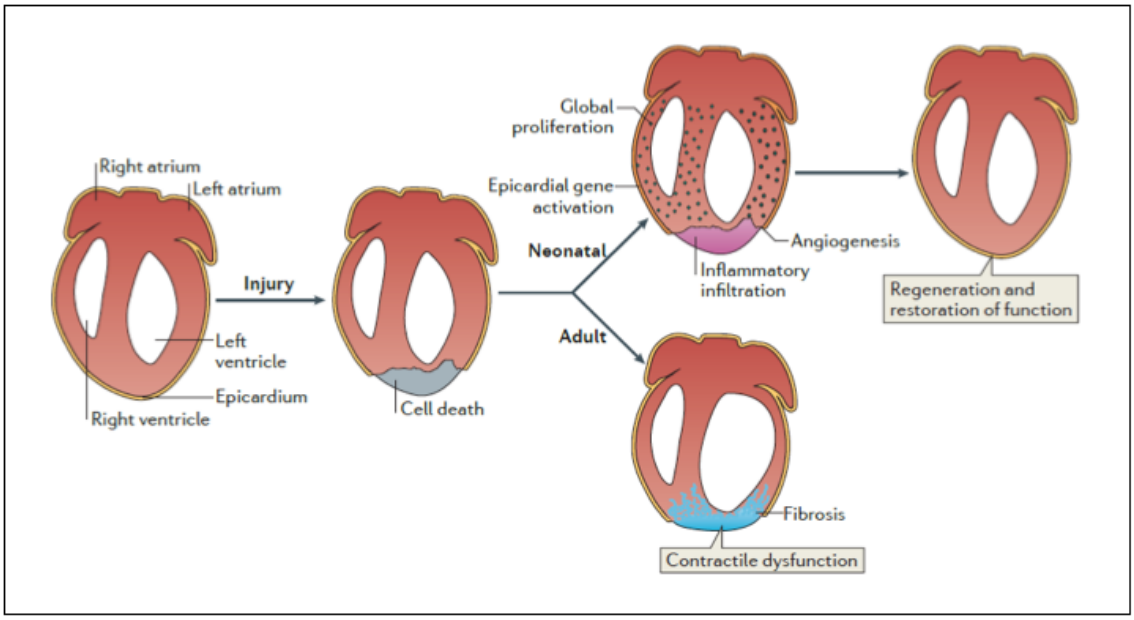

Figure 3. ***Regeneration of mammalian postnatal and adult hearts after myocardial infarction.*** *The postnatal mouse heart possesses regenerative capacity, which is characterized by an early response to cardiac injury-induced cardiomyocyte loss, accompanied by an inflammatory infiltration, activation of epicardial-specific genes and angiogenesis. Global proliferation of cardiomyocytes in the injured heart replaces the scar tissue with cardiomyocytes and restores cardiac function within 3 weeks after injury. The regenerative capacity of the mammalian postnatal heart declines with age, whereas cardiac fibrosis increases with age in response to injury. The regenerative potential of the murine heart upon injury is lost from the postnatal day 7, when fibrotic scar tissue replaces dead cardiomyocytes culminating in reduced cardiac function and heart failure (adapted from [39]).*

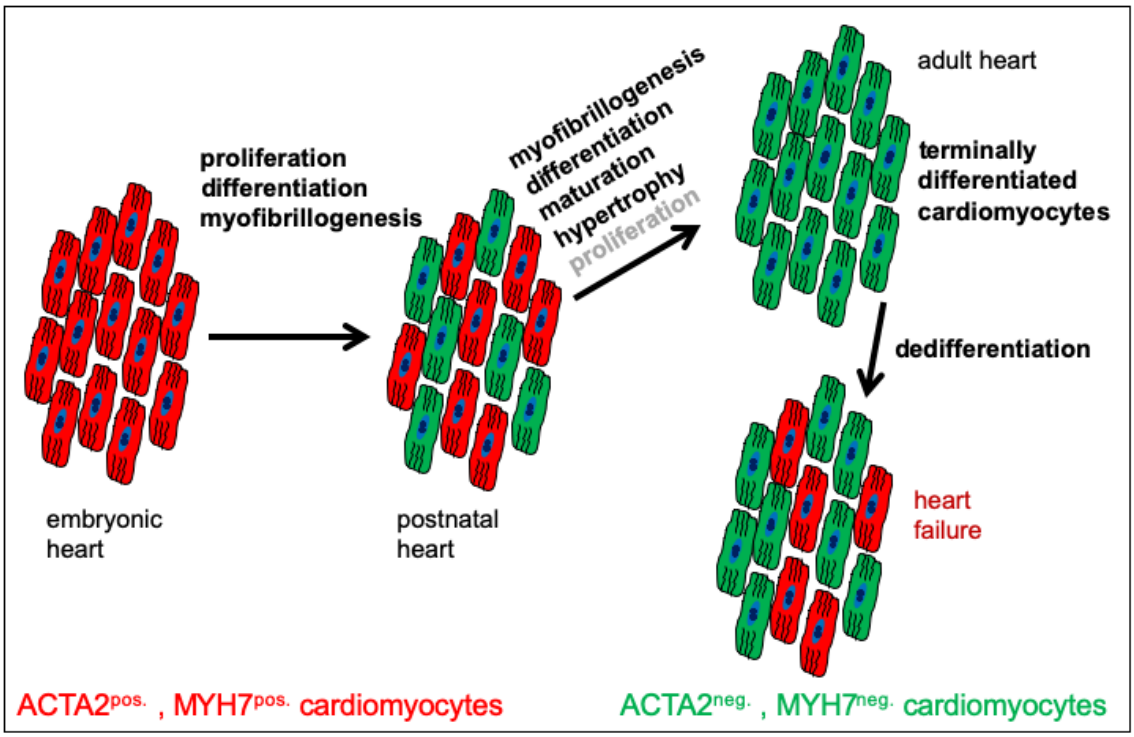

Figure 4. ***Acta2 and Myh7 expression in embryonic and adult cardiomyocytes under physiological and pathological conditions.*** *Embryonic cardiomyocytes express Acta2 and Myh7. During differentiation and maturation processes, postnatal cardiomyocytes successively loose Acta2 and Myh7 expression. Under pathological conditions adult cardiomyocytes dedifferentiate and re-express Acta2 and Myh7.*

1.2 TEAD transcription factors

The TEAD transcription factor family comprises four members, TEAD1 (TEF1, NTEF-1), TEAD2 (TEF4, ETEF), TEAD3 (TEF5, DTEF-1, ETFR-1) and TEAD4 (TEF3, RTEF-1, ETFR-2, FR-19). All four family members share a highly conserved N-terminal 68 amino acid TEA/ATTS DNA binding motif, which binds to muscle specific MCAT (5´- CATTCCT-3´) as well as to SV40 GT-IIC, SphI and SphII enhancer-motives [10, 40]. The TEA/ATTS DNA binding motif is evolutionary conserved from fungi (AbaA), yeast (Tec1), fly (Scalloped) to vertebrates. In *Aspergillus nidulans* AbaA regulates terminal development of specialized hyphal brunches, which produce spore in asexual way [41]. The yeast orthologue Tec1 (Transposon Enhancement Control 1) has been identified to control Ty1-mediated gene activation, regulating independently transcription or acting in combination with additional transcription factors, like Ste12, which enables promoter-specific transcriptional activation and controls development, cell adhesion and filament formation [42, 43]. The *Drosophila melanogaster* TEAD ortholog Scalloped forms with the cofactor Vestigial a protein complex and

regulates wing morphogenesis *via* binding to essential sites in wing-specific enhancers [44]. Transcriptional activation of target genes can also be controlled under certain physiological conditions by interaction with additional transcription factors as well as cofactors to provide tissue-specific control of gene expression during cell fate decisions and organogenesis [45].

Several studies have shown that *Tead1*, *Tead3* and *Tead4* are widely expressed in the mammalian organism including heart, skeletal muscles, vessels, lung, pancreas, placenta and digestive system from early embryonic to adult stages. On the contrary, *Tead2* expression is restricted to a subset of embryonic tissue including fore- and hindlimb, tail bud, testis and cerebellum during murine embryonic development [46].

TEAD1 was initially identified in HeLa cells as a 53 kDa protein, which binds to a specific sequence of the SV40 enhancer motif [40]. In 1994 Chen *et al.* showed that gene-trap based constitutive *Tead1* inactivation resulted in early embryonic lethality at embryonic day (E)11.5 [12]. Mutant embryonic hearts displayed an enlarged pericardial cavity with abnormal thin and hypotrabeculated ventricular walls (Table 1). It is worth noting that transmission electron microscopy analysis of homozygous mutant hearts showed no obvious alterations in mitochondria, fascia adherens and sarcomeric structures of the cardiomyocytes. Interestingly, expression levels of potential TEAD1 downstream target genes including *Tnnt2* (Troponin T2, cardiac type), *Tnni3* (Troponin I3, cardiac type) and *Myosins* were not altered.

Striated muscle specific overexpression of *Tead1* under control of the muscle creatine kinase (MCK) promoter displayed age-dependent heart dysfunction characterized by decreased cardiac output, stroke volume, ejection fraction and fractional shortening as well as an increased MYH7 protein level [17]. At the transcriptional level, TEAD1 gain-of-function (GOF) mutants displayed an elevated expression of fetal genes including *Nppa* (Natriuretic Peptide A), *Nppb* (Natriuretic Peptide B), *Myh7* and *Acta1* (Skeletal Muscle α-Actin), which remained constantly high from fetal stages until adulthood. Moreover, histological analysis revealed altered alignment of cardiomyocytes, septal wall thickening and myocardial fibrosis. Importantly, these mice were unable to tolerate pressure-induced overload leading to heart failure and death (Table 1).

In skeletal muscle *Tead1* overexpression shifted the expression of contractile proteins towards slow muscle phenotype resulting in reduction of shortening velocity as well as longer contraction and relaxation times [47].

Table 1. ***Overview of relevant mouse models for TEAD TFs gain- and loss of function mutants.*** *DCM – dilated cardiomyopathy, E – embryonic day*

Genetic modification	**Method**	**Effects**	**Ref.**
Tead1 knockout	constitutive, retroviral gene trap in embryonic stem cells	• Embryonic lethal at E11.5 Heart: • Enlarged pericardial cavity and thin hypotrabeculated ventricular walls	[48]
Tead1 overexpression	conditional, under control of striated muscle-specific *MCK*-Cre	Heart: • Decreased cardiac output, stroke volume, ejection fraction and fractional shortening • Altered alignment of cardiomyocytes, septal wall thickening and fibrosis, no cardiac hypertrophy. Skeletal muscle: • Transition toward a slow muscle contractile protein phenotype	[17, 47]
Tead1 knockout	conditional, inducible deletion under control of cardiomyocyte- specific *Myh6*-Cre	Deletion in adult cardiomyocytes: • Severe, lethal DCM • Impaired excitation-contraction coupling • Decreased SERCA2a activity	[18]
Tead2 knockout	Conditional, under control of the ubiquitous *Ella*-Cre	• Elevated risk for neural tube closer defects during embryonic development.	[49]
Tead1/Tead2 double knockout	constitutive	• Growth retardation and severe morphological abnormalities at E8.5, • Defects in mesoderm development, especially in the notochord.	[50]
Tead4 knockout	conditional, under control of the ubiquitous *EIIa*-Cre	• Defects in preimplantation stages of specification and development of the trophectoderm lineage	[51, 52]
Tead4 overexpression	conditional, under control of cardiomyocyte-specific *Myh6*-Cre	• Impaired cardiac conduction and arrhythmias. • Increased dephosphorylation of cardiac connexin40 and 43. Impaired gap-junctional conductance.	[53]

TEAD2 is exclusively expressed in embryonic tissues and constitutive *Tead2* knockout mutants displayed an incomplete penetrance of neural tube closure defects [49, 54]. Moreover, *Tead1* and *Tead2* double-knockout (dKO) led to embryonic lethality at embryonic stage E9.5 accompanied by severe growth defects, morphological abnormalities, reduced proliferation and increased

apoptosis rate [50]. This aggravated phenotype of *Tead1/Tead2* dKOs is indicative for redundant function of both genes.

TEAD3 is highly expressed in cardiac muscle and to a lesser degree in skeletal muscle [55]. Adrenergic stimulation of postnatal rat cardiomyocytes enhances TEAD3 binding to MCAT-elements and activation of corresponding target genes including *Acta1*. This finding indicates that in addition to TEAD1, also TEAD3 is able to regulate expression of *Acta1* in response to the α_1-adrenergic signaling pathway in postnatal rat cardiomyocytes, although, a *Tead3* KO mutant has not been described so far [56].

TEAD4 was initially described in 1996 by Hsu *et al*. as a TEF-1- (TEAD1)-related gene, which is activated by FGF-1 (Fibroblast Growth Factor 1) mediated mitogenic stimulation of quiescent fibroblasts as well as during differentiation of C2C12 myoblasts [57]. *Tead4* is highly expressed in skeletal muscles and lung, whereas the heart and placenta display lower expression levels [58]. TEAD4 as well as TEAD1 can activate *Myh7* and *Acta1* promoters in response to α-adrenergic signal indicating that TEAD4 can mediate α_1-adrenergic response in hypertrophic myocytes [59]. Cardiac specific *Tead4* GOF mice displayed chronic elevation of protein phosphatase 1β, which resulted in an enhanced dephosphorylation of the gap junctional connexin-40 and -43, decreased impulse velocity and thus cardiac conduction defects [53].

Notably, TEAD4 in myofibroblasts regulates *Acta2* transcription, whereas, TEAD1 in differentiated smooth muscle cells (SMCs) controls *Acta2* expression [60]. *Tead4* overexpression in endothelial cells upregulates vascular endothelial growth factor B, which in turn is able to stimulate hypertrophic gene expression in cardiomyocytes [61]. Constitutive inactivation of *Tead4* in mouse resulted in a lethal preimplantation phenotype, caused by absence of trophoblast stem cells due to failed expression of the trophectoderm-specific genes, such as *Cdx2*, whereas deletion of *Tead4* after implantation state did not influence embryonic development [51].

Chromatin immunoprecipitation sequencing (ChIP-seq) of mature mouse muscle fibers identified a number of TEAD4-occupied sites, which are highly enriched for promoters of muscle-specific actins and cytoskeletal binding proteins. Inactivation of *Tead4* in mature muscle fibers caused no obvious phenotype

under physiological conditions, however, under pathological condition in the settings of myotoxic injury, *Tead4* inactivation delayed muscle regeneration indicating an important role of TEAD4 during myogenic differentiation. It is worth to note that the concomitant inactivation of *Tead4* and *Tead1* in differentiating C2C12 cells resulted in impaired differentiation, whereas the inactivation in primary myoblasts revealed a relatively mild phenotype [48].

Taken together, it is becoming increasingly evident that each member of the TEAD TF family regulates specific and unique downstream-target genes. On the other hand, several TEAD TFs can regulate expression of a single gene by providing a back-up network.

1.3 Regulation of TEAD TFs target genes *via* MCAT-elements

TEAD TFs bind predominantly to conserved DNA sequences, so called MCAT elements (Muscle Specific Cytidine-Adenosine-Thymidine-Sequence (5´-CATTCCT-3`). Initially MCAT elements have been discovered in promoter regions of numerous skeletal-, heart- and smooth muscle gene promoters *e.g*. cardiac *Tnnt2*, *Myh7*, *Acta2* as well as *Acta1* (Table 2), where they play a crucial role in transcriptional regulation of these genes [10, 62-64]. However, MCAT-elements are not restricted exclusively to the muscle-specific genes but are also located in promoter regions of non-muscle genes, like simian virus 40 enhancer, human papilloma virus type 16, *E6* and *E7* oncogenes, chorionic somatomammotropin as well as *Foxo2* (Forkhead Box A2) genes [40, 65-67]. MCAT-elements can occur as a single regulatory element (*Acta1* promoter), as well as in clusters (*Tnnt2* or *Myh7* promoters) [10, 62, 64].

Tnnt2 promoter studies have shown that the maximal transcriptional activation requires activation of both MCAT-elements [10]. In addition, it has been shown that the distance between two MCAT-elements play an important role in the transcription activation efficiency [68]. These findings indicate that not only one MCAT-element, but also combinations of several MCAT-elements as well as their interplay with additional regulatory elements are important for a specific transcriptional activation of target genes.

Myh7 promoter studies revealed, that two MCAT-elements regulate transcriptional activation in cardiomyocytes under normal as well as under

hypertrophic conditions and mutations within these MCAT-elements diminish the basal promotor activity. In addition, the binding rate of MCAT-elements in cardiomyocytes were increased upon stimulation with α_1-adrenergic agonists, *e.g.* phenylephrine, and during chronic pressure overload of the heart [69].

Table 2. ***MCAT-elements in muscle-specific genes.*** *Myh6 - Myosin Heavy Chain 6, cardiac muscle α Isoform; Chrnb1- β-Acetylcholine Receptor; Myocd -Myocardin; Adra1c - α_{1c}-Adrenergic Receptor; Tpm1 - α-Tropomyosin (adapted and modified from [70]).*

Genes	Species	Sequence and Position	References
Tnnt2	chicken	MCAT1: CATTCCT (−95/−89 bp) MCAT2: CATTCCT (−72/−66 bp)	[10]
Myh7	mouse	distal: CATTCCA (−275/−281 bp) proximal: CATGCCA (−205/−211 bp)	[62]
Acta2	Rat	MCAT1: CATTCCT (−178/−184 bp) MCAT2: CATTCCT (−314/−320 bp)	[63]
Acta1	mouse	CATTCCT (−69/−63 bp)	[64]
Myh6	Rat	CATTCCA (−42/−48 bp)	[13]
Chrnb1	Rat	CATTCCT (−49/−43 bp)	[71]
Myocd	mouse	CATTCCA (~−30 kb)	[16]
Adra1c	mouse	CATGCCA (−916/−910 bp)	[72]
Tpm1	frog	CATTCCT (−59/−65 bp)	[73]

1.4 TEAD TFs are involved in Hippo-pathway mediated cellular processes

The Hippo-pathway is a crucial signal transduction pathway, which partially signals *via* TEAD TFs to activate the expression of downstream target genes. This pathway is involved in multiple processes including regeneration, proliferation, stem cell function as well as controlling organ size and development (reviewed in [74]).

Initially, the Hippo-pathway was discovered in a tumor suppressor screen in *Drosophila melanogaster* and comprises the kinases Hippo and Warts as well as the kinase-binding proteins Salvador and Mats1. Loss-of-function (LOF) mutations of these proteins led to increased cell proliferation and decreased cell apoptosis [75, 76].

In recent years, a number of Hippo-pathway components have been identified and characterized in mammals. The key components of the mammalian Hippo-pathway are the protein kinases MST1 and MST2 (STE20-like Protein Kinase 1 and 2) as well as LATS1 and LATS2 (Large Tumor Suppressor Kinases 1 and 2), which phosphorylate and thereby trap transcriptional coactivators YAP1 (Yes-Associated Protein 1) and WWTR1 (WW Domain Containing Transcription Regulator 1, TAZ) in cytoplasm (Figure 5). However, in the case of inactive Hippo-pathway, unphosphorylated YAP1 and WWTR1, enter the nucleus, where they interact with transcription factors, *e.g.* TEAD TFs, to drive the expression of target genes. In addition, there is increasing evidence suggesting that additional signaling cascades, such as WNT or GPCR, can also interfere with the Hippo-pathway [77].

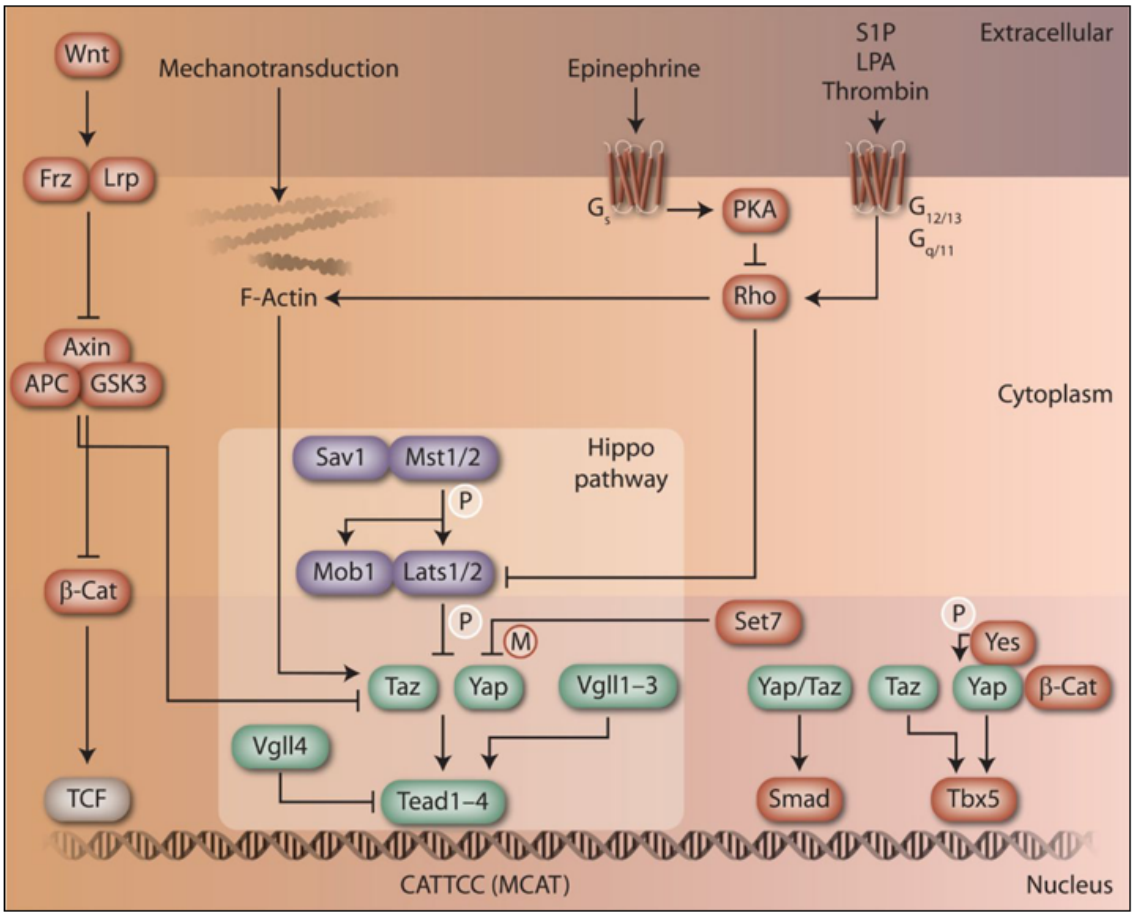

Figure 5. ***Schematic view of key players of the Hippo signal transduction network and its interaction with other signaling pathways.*** *P - phosphorylation; M - methylation; LPA - lysophosphatidic acid; S1P - sphingosine 1-phosphate (adapted from [78]).*

Cardiac-specific *Mst1* overexpression in mice activates caspases resulting in increased apoptosis and dilated cardiomyopathy (DCM). In contrast, suppression of *Mst1* by a dominant-negative approach in mice prevents cardiomyocyte apoptosis as well as myocardial fibrosis and hence abolishes cardiac dysfunctions [79, 80]. MST1 in turn activates LATS 1 or 2 *via* phosphorylation. Moreover, it has been shown that LATS2 limits cardiomyocyte hypertrophy without affecting cardiomyocyte apoptosis in the heart. Inactivation of Hippo-pathway by a dominant negative *Lats2* approach resulted in hypertrophied cardiomyocytes accompanied by inhibited apoptosis, whereas activation of *Lats2* caused heart atrophy with unchanged cardiomyocyte apoptosis rate [81]. These results underline a role of LATS2 in cardiomyocyte hypertrophy, which are supported by the observation of increased endogenous *Lats2* expression in chronic pressure overloaded hearts [81].

1.5 Crosstalk between TEAD TFs and Hippo-pathway *via* cofactors

A typical feature of TEAD TFs is the lack of a transactivation domain, which implicates TEAD interaction with specific cofactors to activate transcription of target genes. So far, several TEAD TFs cofactors have been reported including paralogs YAP1 and WWTR1, VGLL-1 (Vestigial Like Family Member 1), VGLL-2 (Vestigial Like Family Member 2, VITO-1) as well as VGLL-4 (Vestigial Like Family Member 4) (Figure 6) [82-86]. A characteristic feature of these cofactors is the lack of a DNA binding domain and therefore the transactivation of downstream transcriptional networks relies on a physical interaction of TEAD TFs and cofactors. This in turn implicate a tightly regulated activation, based on differential TEAD-cofactor interaction. In particular YAP1 and WWTR1 are broadly expressed and play an important role in Hippo-pathway mediated control of organ size *via* cell proliferation, cell differentiation as well as stemness. During Hippo-pathway activation, both cofactors, YAP1 and WWTR1 are phosphorylated and excluded from the nucleus, whereas Hippo-pathway inactivation results in nuclear translocation of YAP1 and WWTR1 and subsequent transcriptional activation of target genes *via* complex formation with transcription factors, *e.g.* TEAD TFs [87].

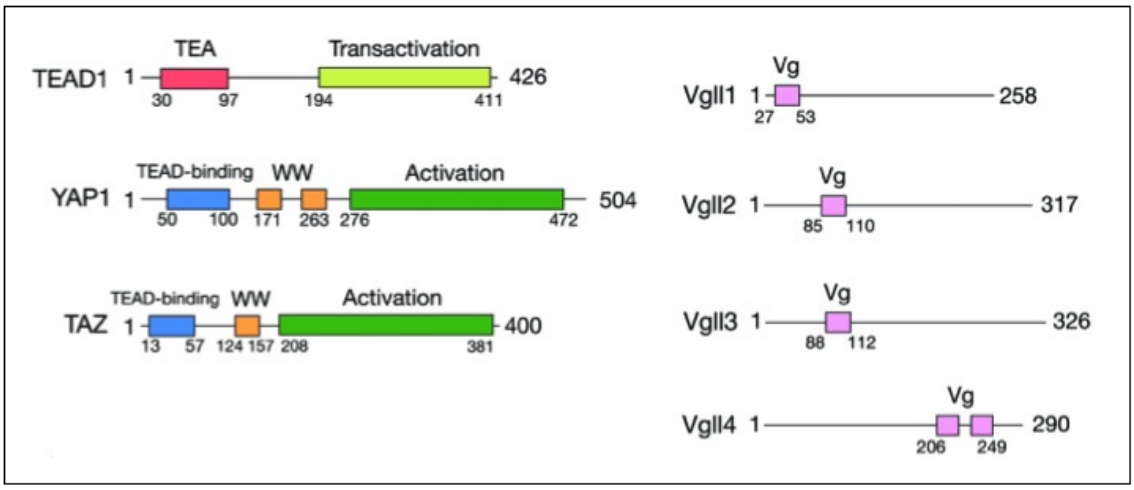

Figure 6. ***Domain architecture of TEAD1 and corresponding coactivators.*** *TEADs contain a N-terminal TEA domain that binds DNA and a C-terminal transactivation domain, which interacts with corresponding coactivators. YAP1 and TAZ (WWTR1) encode a N-terminal TEAD-binding motif, one or two WW domains and an activation domain. VGLL-1,-2,-3 cofactors contain one conserved Vg-motif (*TDU-domain*), which facilitates interaction with TEAD TFs, whereas VGLL-4 encodes two Vg motifs (adapted from [88]).*

In the myocardium, TEAD TFs and YAP1 regulate cardiomyocyte proliferation, cardiac morphogenesis and myocardial trabeculation [89-91]. Lin *at al.* showed that α-catenin modulates subcellular localization as well as transcriptional activity of YAP1, triggered by extracellular signals, which facilitated the release of YAP1 from the α-, β- and γ-catenin complex located in intercalated disks of cardiomyocytes, which in turn caused YAP1 translocation to the nucleus and subsequent activation of mitogenic gene expression [91]. Early cardiac specific inactivation of *Yap1* resulted in hypoplasia of the myocardium as well as in reduction of proliferative cardiomyocytes during embryonic development, leading to late gestational lethality around E16.5. Specific overexpression of *Yap1* in the embryonic heart led to hypertrabeculation and increased cardiomyocyte proliferation, however, cardiac-specific overexpression of *Yap1* in adult mouse hearts promoted cardiomyocyte proliferation without affecting heart function. Moreover, *Yap1* overexpression after myocardial infarction led to improved cardiac function indicating positive impact of *Yap1* overexpression in terms of improving heart regeneration [89, 90].

WWTR1 is 45% identical to YAP1 and contains 3 conserved domains: WW-domain, a 14-3-3-binding site and a C-terminal PDZ-binding motif [92, 93]. WWTR1 and YAP1 co-regulate distinct cellular processes such as myoblast

proliferation, whereas myogenic differentiation is exclusively regulated by WWTR1 [94].

The Vestigial-like family, deduced from the *Drosophila* Vestigial gene, represent an additional TEAD TFs cofactors and consists of 4 members: VGLL-1, VGLL-2, VGLL-3 and VGLL-4. A key motif of the Vestigial family is the tondu (TDU)-domain which mediates physically and functionally interaction with TEAD TFs [85]. VGLL-1 and VGLL-3 expression is mainly restricted to placenta and therefore might function in combination with TEAD TFs in proliferative processes of placenta cells. VGLL-2, also referred to as VITO-1, is exclusively expressed in skeletal muscle tissue starting from E8.5 in somatic myotome of the mouse embryo and contributes to a myogenic program [95, 96]. Moreover, Günther *et al.* showed that VGLL-2 interacts with TEAD1 and enhances MYOD-mediated myogenic program [84]. In contrast to VGLL-2, VGLL-4 is highly expressed in the heart. Cardiac specific VGLL-4 overexpression enhances the TEAD1 mediated activation of Acta1 promoter [97]. On the contrary, Lin *et al.* reported that VGLL-4 negatively regulates TEAD TFs stability as well as TEAD-YAP1 interaction and serves thereby as a repressor of the TEAD1-YAP1 driven cardiac growth [86].

1.6 Orchestrated TEAD TFs mediated gene activation in transcriptional networks

Multiple lines of evidence indicate that a regulatory network of TFs is involved in muscle-specific gene activation. Among them, muscle restricted as well as broadly expressed TFs regulate cell type specific transcriptional networks. It has been previously demonstrated that TEAD TFs have the potential to interact with numerous transcription factors including MAX (MYC Associated Factor X), SRF (Serum Response Factor), MEF2 (Myocyte Enhancer Factor 2), IRF2BP2 (Interferon Regulatory Factor 2 Binding Protein 2) and FOXO to specifically activate transcription of target genes [14, 16, 98-101]. Gupta *et al.* showed that the basic Helix-Loop-Helix-Leucine zipper protein, MAX, binds in a complex with TEAD1 to E-box-M-CAT-hybrid motif, which in turn regulates basal transcription of the cardiac *Myh6* gene in rat cardiomyocytes, indicating a concomitant activation of gene expression [14]. In this study the authors also reported a physical interaction of TEAD1 and SRF *in vitro* as well as *in vivo*, which in turn

synergistically induces the promoter activity of the *Acta1* gene in cardiomyocytes [98]. In contrast, Liu *et al*. showed that TEAD1 suppresses expression of smooth muscle-specific genes including *Acta2* in SMCs *via* competition with Myocardin (MYOCD) for SRF binding. This subsequently results in the disruption of MYOCD-SRF interaction, which finally lead to a decreased expression of smooth muscle-specific genes [102]. Furthermore, two additional studies suggest TEAD TFs interactions with MEF2 and FOXO to control muscle specific gene expression [16, 99]. In addition, TEAD TFs have been reported to form a complex with several transcription factors simultaneously, *e.g.* downstream of TGFβ (Transforming Growth Factor β) pathway. In malignant mesothelioma cells, TEAD4 forms a complex with YAP1-SMAD2/3-P300 on a specific site of the *Ctgf* (Connective Tissue Growth Factor) promoter indicating a synergistic action of TEAD4 and SMAD3 [101].

1.7 Muscle related genes regulated by TEAD TFs

In recent years, several studies have attempted to identify direct TEAD TFs target genes. One of the best characterized TEAD1 target gene in striated muscle cells is *Myh7*, which encodes β heavy chain subunit of cardiac myosin. MYH7 is a crucial member of the cardiomyocyte contractile apparatus, which exerts an important role in heart maturation as well as in myocardial remodeling. *Myh7* is predominantly expressed during fetal heart development and replaced after birth by *Myh6*, an additional member of myosin proteins family. In the adult heart, *Myh7* is re-expressed under pathophysiological conditions such as chronic pressure overload or DCM [103, 104]. In cultured hypertrophied postnatal cardiomyocytes, *Myh7* expression is mediated by α_1-adrenergic stimulation and β protein kinase C, which in turn facilitates binding of TEAD1 to the MCAT-sequence of the *Myh7* promoter, resulting in transcriptional activation [105]. Moreover, the mammalian *Myh7* promoter contains four MCAT-elements, which are involved in the maximal promoter activity. Under basal conditions TEAD1 binding is restricted to one MCAT-element, whereas under hypertrophic conditions TEAD1 binds to all 4 MCAT-sequences to enhance *Myh7* expression [15]. In addition, it has been shown that TEAD1 is recruited to the promoter region of *Acta1*, a key component of the cardiac muscle cell contractile apparatus [106]. In contrast to the *Myh7*

expression, which is activated by TEAD1 *via* MCAT-elements, the activation of *Acta1* is orchestrated by a combinatorial recruitment of several regulatory elements including MCAT, CArG as well as Sp1 and therefore simultaneous binding of multiple transcription factors including TEAD1 and SRF is required [64]. These findings demonstrate the divergence in TEAD1 transcriptional regulation of target genes within one cell type.

Apart from facilitating gene activation, TEAD TFs can function as transcriptional repressors under certain conditions, *e.g.* target genes or cell types. In cultured SMCs, binding of TEAD TFs to MCAT-elements repress transcription of *Acta2*, whereas in cultured myoblasts, fibroblasts and endothelial cells TEAD binding activates transcription [63]. TEAD4 knockdown experiments showed that TEAD4 regulates *Acta2* expression in cultured myofibroblasts, but not in differentiated SMCs. Furthermore, quantitative ChIP assays in myofibroblasts revealed that TEAD4 binds preferentially to the MCAT-containing regions within the *Acta2* promoter, whereas in undifferentiated SMCs TEAD1 binds to the same region of *Acta2* promoter [60]. In addition, analyses of transgenic mice harboring mutations within MCAT-elements of *Acta2* promoter showed delayed as well as reduced *Acta2* activation in SMCs, cardiac and skeletal muscle cells during early embryogenesis, whereas expression in adult SMCs remained unaltered [60]. A possible explanation for delayed *Acta2* expression in MCAT mutants might be compensatory effects of Myocardin (MYOCD), which is one of the key regulators of smooth as well as cardiac muscle gene expression [107]. In this regard, it has been shown that TEAD TFs act also upstream of MYOCD, thereby regulating smooth muscle development during embryogenesis [16]. Strikingly, in proliferating SMCs TEAD1 represses the expression of the smooth muscle-specific genes including *Acta2* by abolishing the MYOCD function *via* competition with MYOCD for the direct binding to SRF, indicating opposing transcriptional mechanisms mediated by TEAD TFs [102]. This competitive binding is of biological importance in healing processes after arteria injury, where TEAD1 induction and binding to SRF enables SMCs to proliferate. These findings suggest multiple functions of TEAD TFs in cell-type specific regulation of *Acta2* gene.

In summary, the published data suggest that TEAD TFs are involved in transcriptional regulation of muscle specific gene program. In cardiomyocytes,

however, only a few direct TEAD1 cardiomyocyte-specific target genes have been investigated so far [10, 14-18, 64, 73, 108]. Importantly, genome-wide TEAD1 binding studies, especially in cardiomyocytes, are still pending.

1.8 Aim of the present study

The present study aimed at investigating the biological function of TEAD1 transcription factor in murine embryonic and postnatal cardiomyocytes by analyzing cardiomyocyte-specific conditional *Tead1* knockout and *Tead1*-overexpressing mice. In addition, this study set out to identify target genes that are regulated by TEAD1 in cardiomyocytes by using global transcriptome analysis combined with genome-wide TEAD1 binding studies. Finally, it was intended to investigate the effects of the FGF2-FGFR1 pathway on TEAD1 in cardiomyocytes.

2 MATERIAL AND METHODS

2.1 Transgenic mice

The animal experiments in this study were performed in full agreement with institutional guidelines and with approval of the Committee for Animal Rights Protection of the State of Hessen (Regierungspräsidium Darmstadt; B2/1125, B2/K5312). The animals were kept in individual ventilated cages accompanied with environmental enrichment under sterile approved conditions with an appropriate day and night cycle in the Animal House Facility of Max Planck Institute for Heart and Lung Research, Bad Nauheim, Germany. For separate experiments were used age-matched littermates. The number of animals used in each experiment is listed in the figure legends.

2.1.1 Generation of mice with cardiomyocyte-specific Tead1 deletion

Conditional *Tead1* mutant mice (*Tead1*$^{fl/fl}$) carrying exon 3 to 5 flanked by *loxP* sites, encoding for DNA-binding TEA-domain of TEAD1 were generated by Nadine Kirchner *in domo*. The crossing of conditional *Tead1* mutant mice with deleter mouse strain carrying cell-type specific Cre-recombinase resulted in non-functional TEAD1 protein in a cell-type specific manner.

Conditional, Cre-recombinase mediated *Tead1* deletion in cardiomyocytes was achieved by crossbreeding of *Tead1*$^{fl/fl}$ *with* either XMLC2-Cre [109] or MCK-Cre [110] deleter mouse strains to facilitate deletion in embryonic (genotype: *XMLC2::Tead1*$^{fl/fl}$) or postnatal (genotype: *MCK-Cre::Tead1*$^{fl/fl}$) mice, accordingly. Inducible Cre-mediated deletion of *Tead1* in isolated P3 cardiomyocytes was performed by crossbreeding of *Tead1*$^{fl/fl}$ mice with tamoxifen-inducible *Rosa26-CreER*^{T2} transgenic mice [111] and subsequent administration of 2 µmol/L 4-Hydroxytamoxifen (4-HT) (Sigma, H7904-5MG) for 8 days in culture.

2.1.2 Conditional overexpression of Tead1 tagged by Flag-HA

Conditional transgenic overexpressing *Tead1-Flag-HA* mice were generated *in domo* utilizing a modified *ROSA26* targeting locus carrying a synthetic *CAG* promoter [112]. The Flag-HA tagged plasmid of mouse *Tead1* was PCR-amplified

(primers used: *FlagHA-BigT-forward* and *FlagHA-BigT-revers*) to introduce NheI and NotI sites, and cloned into the *pBigT-CAG* vector. The generated *pBigT-CAG-Tead1-Flag-HA* cassette was subcloned in PacI and AscI site of the *pRosa26-PA* construct. The final construct was electroporated into V6.5 F1 hybrid embryonic stem cells and targeted stem cell clones were selected by G418 treatment and screened by Southern blotting with 5' genotyping by EcoRV. Positive embryonic stem cell clones were injected into C57BL/6 (B6) blastocysts. The resulted chimeric mice were backcrossed to C57BL/6 mice to generate transgenic mice harboring a single mutant allel (genotype: *Tead1-Flag-HA*$^{Tg/+}$). Conditional Cre-mediated overexpression of *Tead1-Flag-HA* in embryonic cardiomyocytes was achieved by crossbreeding of *Tead1-Flag-HA*$^{Tg/+}$ transgenic mice with *XMLC2-Cre* mice (genotype: *XMLC2-Cre::Tead1-Flag-HA*$^{Tg/+}$). The *XMLC2-Cre::Tead1-Flag-HA*$^{Tg/+}$ allele were used as heterozygous in all experimental studies.

Table 3. ***List of primers used for mouse cloning experiments***

Name	Sequence
pBigT-rev1	5'-AGTTTGTCCTCAACCGCGAG-3'
pBigT-for1	5'-TGGGAAGACAATAGCAGGCA-3'
Flag-HA-for	5'-CTCTTAATTAAGGATCCAATATACTCGAGGACTACAAGGACGACGATGA-3'
Flag-HA-rev	5'-GAGGGCGCGCCCTAGGCGTAGTCGGGCACGT-3'

2.2 Genotyping of mice

2.2.1 Extraction of genomic DNA from mouse tail biopsies

The mouse-tail biopsies were digested in 500 µL TENS-buffer (Table 17) with 5 µL Proteinase K (10 mg/mL Proteinase K; Roth) overnight at 56°C. After complete digestion, the samples were centrifuged (Centrifuge 5417R, Centrifuge 5430 - Eppendorf) at 14000 rpm for 5 minutes. Thereafter, each supernatant was transferred to a new 1.5 mL tube containing 500 µL 100 % Isopropanol and vortexed. After another 10 minutes centrifugation step (14000 rpm), the pellets containing genomic DNA were washed with 70 % Ethanol (EtOH) for 5 minutes at 14000 rpm. Finally, the dried DNA pellets were dissolved in 300 µL sterile TE-

Buffer (Table 17) for 3h at 56 °C. The tail DNA was then ready to use for genotyping PCRs with self-designed primers (listed in Table 4) using appropriate cycling conditions (2.2.2).

2.2.2 Genotyping Polymerase Chain Reaction (PCR)

The genotyping of distinct mouse strains was performed on extracted genomic tail DNA (2.2.1) using corresponding primer combinations (Table 4) either with a homemade Taq-mix or with the REDTaq® ReadyMix™ PCR Reaction Mix (Sigma-Aldrich, R2523).

The master mix using a homemade Taq-Polymerase for one PCR reaction was prepared as followed:

Components	Concentration
10 x PCR buffer	1 x
$MgCl_2$	1.5 mmol/L
Primer-for	0.2 µmol/L
Primer-rev	0.2 µmol/L
dNTP	0.2 mmol/L
Taq-Polymerase	1.25 U
dd. H_2O	up to 25 µL

Table 4. ***List of primers used for genotyping-PCR and corresponding PCR-product sizes.*** *WT -wild-type allel, TG – transgenic allel, bp – base pair*

Gene name	**Name**	**Sequence**	**Product size (bp)**
Tead1	*Tead1-LoxP-for* *Tead1-LoxP-rev*	5'-GCAGTGGTCACTGGCTCACT-3' 5'-GCTCTTATGTCTGAACACAGGT-3'	WT - 340 TG – 370
Cre	*Cre61-for* *Cre63-rev*	5'-GACCAGGTTCGTTCACTCATGG-3' 5'-AGGCTAAGTGCCTTCTCTACAC-3'	TG – 250
SRY	*SRY-for* *SR Y-rev*	5'-TTGTCTAGAGAGCATGGAGGGCCATGTCAA-3' 5'-CCACTCCTCTGTGACACTTTAGCCCTCCGA-3'	273
RosaCAGG	*AS2645-for* *AS2648-rev1* *AS2427-rev2*	5'-CTTGCTCTCCCAAAGTCGCTCTGAG-3' 5'-CTTTAAGCCTGCCCAGAAGACTCCC-3' 5'-ACCGTAAGTTATGTAACGCGGAACTCC-3'	WT - 249 TG – 325
MCM-Cre	*MCM-for* *MCM-rev*	5'-CAA CAT GAA ATG CAA GAA CG-3' 5'-GGA AAC CAT TTC CGG TTA TTC-3'	TG - 400

PCRs were performed in a Thermocycler (Mastercycler Nexus – Eppendorf, Labcycler – Sensoquest) at a cycle program corresponding to the PCR conditions. The PCR products were loaded on a 1 – 2% agarose gel (LE Agarose, Biozym, 840004) and separated in TAE (Tris-acetate- EDTA) buffer (Table 17) at 100 – 180 mV (Power Supply: E455 – Consort, Power Pack P25 T – Biometra, T100 Thermal Cycler – Biorad). Gel documentation was performed with a UV light and gel documentation device (BioDocAnalyze - Biometra).

The following Thermocycler conditions were used for the genotyping of:

***Tead1*:**

Steps	Temperature (°C)	time	Repeat
1. Initialization	94	3 min	
2. Denaturation	94	30 sec	Step 2 to 4
3. Annealing	60	30 sec	35 times
4. Elongation	72	30 sec	
5. Final elongation	72	5 min	
6. Final hold	12	∞	

***MCK-Cre, XMLC2-Cre, MCM-Cre*:**

Steps	Temperature (°C)	time	repeat
1. Initialization	94	3 min	
2. Denaturation	94	30 sec	Step 2 to 4
3. Annealing	55	30 sec	36 times
4. Elongation	72	30 sec	
5. Final elongation	72	5 min	
6. Final hold	12	∞	

***RosaCAGG*:**

Steps	Temperature (°C)	time	repeat
1. Initialization	94	3 min	
2. Denaturation	94	30 sec	Step 2 to 4
3. Annealing	57	30 sec	36 times
4. Elongation	72	30 sec	
5. Final elongation	72	5 min	
6. Final hold	12	∞	

***SRY*:**

Steps	Temperature (°C)	time	repeat
1. Initialization	94	3 min	
2. Denaturation	94	30 sec	Step 2 to 4
3. Annealing	58	30 sec	34 times
4. Elongation	72	40 sec	
5. Final elongation	72	5 min	
6. Final hold	12	∞	

2.3 Cloning and preparation of plasmid DNA

2.3.1 Generation of Tead1-GFP and Tead1-Flag-HA expression constructs

Expression constructs containing TEAD1 tagged either by GFP or Flag-HA were obtained by using a *pCAGIPuroxPA*-vector containing ampicillin and puromycin resistance cassettes (Figure 7).

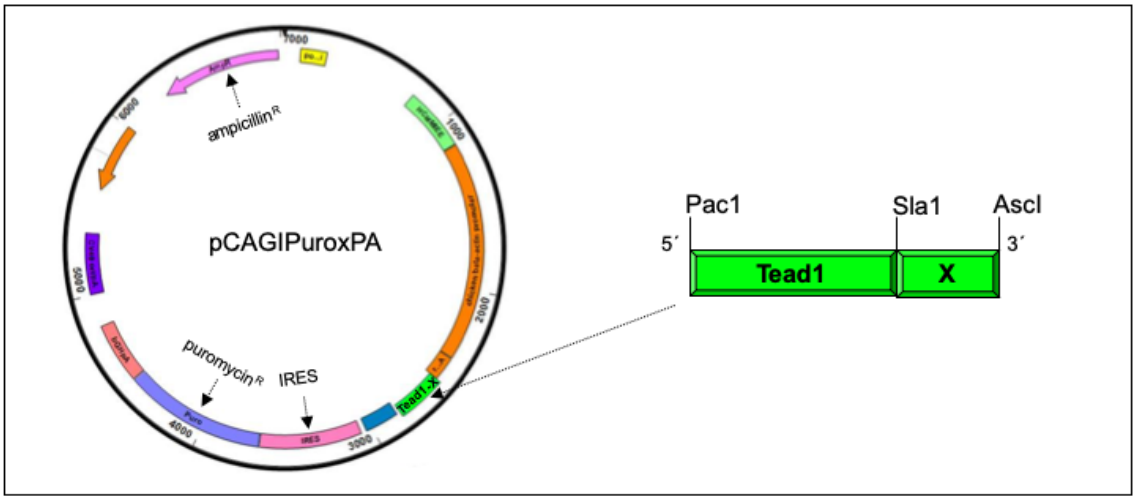

Figure 7. ***Scheme of the pCAGIPuroxPA-vector containing ampicillin and puromycin resistance cassettes. Left panel:*** *Puromycin resistance cassette is located on 3´-end of IRES element (pink). Gene of interest (Tead1-X in green) is subcloned into pCAGIPuroxPA-vector via AscI and Pac1 restriction sites.* ***Right panel:*** *Schematic drawing of the insert encoding Tead1 tagged either with GFP (X) or Flag-HA (X) containing Pac1, Sla1 and AscI restriction sites. X = GFP or Flag-HA*

The sequence of murine *Tead1* was amplified using specific primers containing on the 5'-end the Pac1 and on the 3'-end the Sla1 restrictions sides. The *Tead1* amplicon was than ligated by using T4-DNA-Ligase (Promega, M1801) with amplified either FGP- or Flag-HA-tag containing on the 5'-end the Sla1 and on the 3'-end the AscI restrictions sides at 16°C overnight. Thereafter, the inserts containing *Tead1* tagged either by *GFP* or *Flag-HA* were subcloned in PacI and

AscI sites of the *pCAGIPuroxPA* vector by using T4-DNA-Ligase (Promega, M1801) overnight by 16 °C in molar ration vector-to-insert as followed:

$$\frac{Vector\ (ng) \cdot Insert\ size(kb)}{Vectorsize\ (kb)} \cdot Molar\ ratio \frac{Insert\ (3)}{Vector\ (1)} = ng\ Insert$$

The ligation reaction was prepared as followed:

Components	Volume
DNA (Insert)	x µL
2 x Ligation-Puffer	5 µL
pCAGIPuroxPA (Vector)	1 µL
T4 DNA-Ligase	1 µL
Total	10 µL

Table 5. ***List of primers used for cloning***

Name	Sequence
TEAD1-GFP-for	5'-CTCTTAATTAACGTCCACCATGGAAAGGATGAGCGACTC-3'
TEAD1-GFP-rev	5'-GAGGGCGCGCCTTACTTGTACAGCTCGTCCATG-3'
Flag-HA-for	5'-CTCTTAATTAAGGATCCAATATACTCGAGGACTACAAGGACGACGATGA-3'
Flag-HA-rev	5'-GAGGGCGCGCCCTAGGCGTAGTCGGGCACGT-3'

2.3.2 Preparation of electrocompetent bacteria

One XL1 blue *E. coli* colony was placed in Erlenmeyer flask containing 50 mL lysogeny broth medium (LB-Medium (Lennox) - Roth, X964.2) without antibiotics and incubated for 16-18 hours (h) at 37°C and 220 rpm, overnight. Next, 3-4 mL of this culture were transferred to 200 mL LB-medium in a new Erlenmeyer flask and incubated by 37°C at 220 rpm. During incubation the optical density (OD) of culture was constantly measured in order to reach the value of 0.5 - 0.6 indicating the exponential growth phase of bacteria. Bacterial cultures with optimal OD were transferred to 200 mL centrifuge tubes and cooled down on ice for 30 min. Thereafter, the precooled cultures were centrifuged (Sorvall Evolution RC) for 15 min, at 0°C and 3500 rpm. After centrifugation the supernatants were discarded, pellets were gently resuspended in 200 mL of ice-cold sterile water each on ice and centrifuged again. The wash step in 200 mL of ice-cold sterile water was

repeated two times more. After the third wash step, pellets were gently resuspended in 40 mL of ice-cold sterile 10 % glycerol (10 % glycerol / 90 % sterile water), transferred in a precooled 50 mL centrifuge tube and centrifuged at 0°C, 6000 rpm for 20 min. After centrifugation the supernatant was discarded, pellets were gently resuspended in 2 mL ice-cold 10 % glycerol and aliquoted *á* 50 µL in precooled 1.5 mL centrifuge tubes. The aliquots were snap frozen in liquid nitrogen and stored at -80°C.

2.3.3 Transformation of electrocompetent bacteria with plasmid DNA

The amplification of plasmids was performed by means of bringing a foreign DNA into bacterial microorganisms. For this purpose, electrocompetent XL1 blue *E. coli* bacteria (see: 2.3.2), were transformed by electroporation with an electroporator (Gene Pulser^{TM}– Bio-Rad). At first, a 50 µL of XL1blue bacteria stock was diluted with an appropriate amount of pre-cooled sterile H_2O (maximum 500 µL) and 100 µL of this bacterial dilution was transferred into a pre-cooled electroporation cuvette (Electroporation Cuvettes, blue cap – Peqlab, 71-2020). Thereafter, 250 ng – 1 µg of plasmid DNA was added and the cuvettes were subjected to electroporation. Sterile H_2O instead of plasmid DNA served as the transformation control. The electroporation was performed at 2.5 kV for 4.6 to 4.7 ms. The electroporated bacteria were resuspended in 400 µL cold LB-medium (LB-Medium (Lennox) - Roth, X964.2) without antibiotics and incubated at 37°C on a heating block (Thermo Mixer F 1.5 - Eppendorf) for 30 min. Thereafter the bacteria suspension was transferred and uniformly distributed to antibiotic containing (50-100 µg e.g. Ampicillin, Amp) agar dishes (LB-Agar (Lennox) – Roth, X965.2). Finally, the agar dishes were dried and placed in a bacteria incubator (Heraeus, 26126010) at 37°C overnight.

2.3.4 Preparation of plasmid DNA

Successfully transformed bacteria with the plasmid DNA of interest (see: 2.3.3), formed colonies on the Amp-agar dish. Thereafter, the colonies were picked with a sterile pipet tip, placed in a glass tube containing 2 mL LB-Amp and then incubated at 37°C in a bacteria shaker (Innova® 44 Incubator Shaker Series – New Brunswick Scientific) overnight. For mini-DNA preparation, the bacteria

suspension was transferred in a 1.5 mL tube and centrifuged at 14000 rpm for 3 minutes. After removing the supernatant, the pelleted bacteria were resuspended in 150 µL ice-cold Buffer I. Then, 200 µL Buffer II was added and the samples were inverted several times to mix both buffers and incubated at room temperature (RT) for 5 minutes. After incubation, 200 µL Buffer III was added and samples were centrifuged for 20 minutes at 14000 rpm. Following centrifugation, for DNA precipitation the supernatant was transferred to a new 1.5 mL tube containing 400 µL Isopropanol (Roth; 6752.4) and well shacked. The mixed samples were centrifuged for 10 minutes at 14000 rpm. Following supernatant removal, the pellets were washed with 500 µL 70 % EtOH (Roth; 9065.4) at 14000 rpm for 5 minutes. Afterwards the DNA-palettes were air-dried and resuspended in 100 µL TE-buffer (Table 17) supplemented with 10 µg RNaseA. Finally, the isolated DNA was validated by restriction enzyme digest, which was controlled on a 1% agarose gel and sequenced with corresponding primers.

High amounts of Plasmid-DNA were obtained using a commercially obtained NucleoBond® Xtra Maxi-kit (Macherey-Nagel; 740414) in accordance to the manufacturer's instructions. The DNA purity and concentration were measured in a spectrophotometer (NanoDrop® ND-2000c - Peqlab)

2.4 Cell culture

2.4.1 Human Embryonic Kidney Cells (HEK 293T)

Human Embryonic Kidney Cells (HEK 293T) were cultured in medium (Table 8) containing DMEM/10%FCS/1% PSG (1 x Dulbecco's Modified Eagle Medium (DMEM 4.5 g/L D-Glucose – Gibco, 42430-025). The cells were passaged every 2nd day, followed by washing the cells and incubating them for 2 min with 1 x Trypsin-EDTA (Sigma; T4174) in PBS. After complete cell detachment, trypsin activity was stopped with a cell medium containing FCS. Cell suspension was transferred into a 15 mL centrifugation tube and pelleted at 1000 rpm, RT in the centrifuge (Universal 320R; Hettich Zentrifugen). After centrifugation, the supernatant was discarded and the pellet was resuspended in an appropriate amount of medium and seeded to a culture dish at a density of 2 x 10^5 cells/100 mm.

2.4.2 Transfection of HEK 293T

For the transfection of HEK293T cells with expression constructs, a TurboFect™ Transfection Reagent (ThermoFisher Scientific, R053) was used according to the supplier's protocol.

2.4.3 Luciferase Reporter Assay

HEK 293T cells were plated on a 48 well plate and next day were transfected with *4 x MCAT-Luc*, *VGLL-2* (kindly provided by Dr. Stefan Günther [84]) and *TEAD1*, *TEAD1-GFP*, *TEAD1-Flag-HA* constructs (Table 6) using TurboFect (ThermoFisher scientific; R0531) according to the manufacturer's protocol. Two days after transfection, HEK 293T cells were prepared for Luciferase Reporter Assay processed with Dual-Luciferase® Reporter 1000 Assay Systems (Promega; E1980) according to the supplier's protocol. The bioluminescence was measured in Multimode Microplate Reader (Mithras LB 940 - Berthold Technologies). Untransfected HEK 293T cells were used as a control.

Table 6. ***List of*** **constructs used in Luciferase Reporter Assay**

Plasmid name	Insert	Cloning vector
4 x MCAT-Luc [84]	4 *MCAT* repeats (CATTCCA)	*pTa-Luc*
VGLL-2 (VITO1) [84]	Complete *Vito-1* orf	*pCS2 MT*
TEAD1	Complete *Tead1* orf	*pCAGIPuroxPA*
TEAD1-GFP	Complete *Tead1* with N-terminal GFP tag	*pCAGIPuroxPA*
TEAD1-Flag-HA	Complete *Tead1* with N-terminal Flag-HA tag	*pCAGIPuroxPA*

2.4.4 Isolation of early postnatal mouse cardiomyocytes

In order to isolate early postnatal mouse cardiomyocytes (PCMs), 2-3 days old postnatal mice (P2-P3) were rinsed quickly with 70% EtOH to sterilize the skin. Pups were quickly sacrificed using sterile scissors and the chest was opened along the sternum to allow the access to the heart. The hearts were prepared with Dumont forceps (#7 curved tip, F.S.T., 11272-30) and directly transferred to a new bacterial dish containing PBS on ice. The surrounded heart tissues (lung, big vessels) were removed with Vannas Spring Scissors (straight, sharp tip, F.S.T., 15018-10) and transferred to a 2 mL tube containing ice-cold PBS.

Cardiac cell dissociation was performed using the Neonatal Heart Dissociations Kit (Miltenyi Biotec; 130-098-373) and gentleMACS Octo Dissociator with Heaters (Miltenyi Biotec; 130-096-427) according to the manufacture's protocol. After dissociation, the cardiomyocyte cell fraction was isolated using a mouse Neonatal Cardiomyocyte Isolation Kit (Miltenyi Biotec; 130-100-825) according to the manufacture's protocol. Both protocols are available at www.miltenyibiotec.com.

Freshly isolated cardiomyocytes were used either directly for RNA and protein extraction or cultured for further experiments. Another set of freshly isolated cardiomyocytes was gently resuspended in DMEM, supplemented with 5 % FCS and 1 % L-glutamine-penicillin-streptomycin (P/S/G) (Table 8), and seeded on a precoated with 10 % fibronectin (PromoCell; C-43050) cell culture dish at the density of 1.5 x 10^5 cells per cm^2. Cardiomyocytes were maintained at 37°C and 5 % CO_2.

2.4.5 Adenoviral transduction of cultured early postnatal mouse cardiomyocytes (P2-P3)

The required multiplicity of infection (MOI) was calculated using the titer of adenoviral solution (Cre Recombinase Adenovirus (Ad-CMV-iCre), titer 1x10^10 PFU/mL - VECTOR BIOLABS, 1045N) and formula:

$$\frac{Plaque\ forming\ units\ (PFU)}{number\ of\ cells} = MOI$$

The calculated amount of virus solution was added to culture dishes with cardiomyocytes and kept for 6 h in a 5 % CO_2 incubator at 37 °C. After incubation, the medium containing virus was removed, cardiomyocytes were washed with PBS to completely remove virus particles and further maintained in culture in fresh medium (Table 8). Cultured cells were monitored with Live-Cell Analysis System (IncuCyte®, Essenbioscience). Extraction of RNA and proteins was performed 4 days after viral transduction.

2.4.6 Isolation of adult mouse cardiomyocytes

Adult cardiomyocytes were isolated from 8 weeks old male mice. The animals were anesthetized by *intraperitoneal* (*i.p.*) injection of Buprenorphine/Ketamine in 0.9 % NaCl with 0.2 mL heparin (Braun, 1708.00.00) to prevent blood clotting. The chest was rinsed with 70 % EtOH and opened along the sternum to allow access to the heart. The heart with parts of the lungs was prepared and transferred into Petri dish filled with PBS. The lung tissue was removed and the aorta was cut below the aortic arch. Thereafter, the heart was connected to a Langendorff perfusion system and perfused with 15 mL of Ca^{2+}-free buffer (Table 17) as previously described [113, 114]. Then the heart was perfused with an Enzyme-Buffer containing Liberase und Trypsin (Table 17) for 30 min. After perfusion the heart was removed from the cannula, the ventricles were dissected from the atria and transferred to a new Petri dish containing 5 mL Stop-Buffer 1 (Table 17). The ventricles were carefully cut into small pieces using forceps and transferred to a 50 mL tube for centrifugation at 300 rpm for 3 minutes. The supernatant was transferred to a 15 mL tube and centrifuged at 300 rpm for 1 minute. The pellets from both, 50 mL and 15 mL centrifugation tubes were combined and resuspended in 10 mL Stop-Buffer 2 (Table 17). Cell suspensions were passed through a 100 µm cell strainer to a new 50 mL centrifugation tube. Thereafter Ca^{2+} concentration was adjusted up to 1 mmol/L in 5 steps every 4 min. After adjustment of Ca^{2+} concentration, the cell suspension was centrifuged at 300 rpm for 1 min and the supernatant was discarded. Freshly isolated cardiomyocytes were used either directly for RNA and protein extraction or for cell culture. For the latter experiments, freshly isolated cardiomyocytes were seeded on pre-coated with laminin (10 µg/µL laminin in MEM media) cell culture dishes and cultured in 5 % CO_2 in incubator at 37°C. After firm cardiomyocyte attachment to the culture substrate (2-3 h), the medium was replaced by freshly prepared medium (Table 8) to remove cell debris and non-cardiomyocytes.

2.4.7 Isolation of adult rat cardiomyocytes

The chest of anesthetized (Buprenorphine/Ketamine in 0.9 % NaCl, *i.p.*) 10 weeks old adult male rat (Sprague–Dawley rat) was rinsed with 70 % EtOH and opened along the sternum to allow the access to the heart. The heart with parts of lung tissue was prepared and transferred into a Petri dish filled with PBS (Table

17). The lung tissue was removed and the aorta was resected below the aortic arch. Adult rat cardiomyocytes were isolated as described by Lorchner *et al.* [115]. Briefly, the aorta was connected to a Langendorff perfusion system and the heart was perfused with Krebs-Henseleit bicarbonate buffer (Table 17) constantly mixed with 95 % O_2 and 5 % CO_2 at 37°C for 8 min. Thereafter, 0.04 % collagenase II (Worthington; LS004176) and 40 µmol/L Ca^{2+} (Roth; 5239.2) were added to the Perfusion Buffer and further perfused of 30 min. After perfusion the ventricles were carefully cut into small pieces using forceps in the same collagenase solution containing 1.25 % fatty acid-free albumin (BSA - Sigma; A8806). Dissociated heart cells were washed with increasing calcium concentration of 0.2 and 0.5 mmol/L at 200 rpm for 3 min. Next, cardiomyocytes were sedimented using MEM media with 4 % BSA and 1 mmol/L Ca^{2+} followed by centrifugation at 200 rpm for 1 min. The cell pellet consisting mostly of cardiomyocytes was resuspended in the Cell Medium (Table 8). The cardiomyocytes were seeded on precoated with laminin (10 µg/mL, Sigma; # L2020) 24 well cell culture plates at the density of 1.5 x 10^4 cells/cm^2. Two hours later, the medium was replaced by 2 % fetal bovine serum (FBS - Sigma, F6178) containing medium and cultured for two days. The medium was changed every second day.

2.4.8 FGF2 stimulation of cultured adult rat cardiomyocytes

To study the effects of FGF2 stimulation on TEAD1 in cultured adult rat cardiomyocytes, freshly isolated adult rat cardiomyocytes were cultured for two days in medium (Table 8) containing 2 % FBS (Sigma; F6178). On the 3rd day, either FGF2 (Recombinant Human FGF-basic - ReproTech; 100-1813) at concentration of 50 ng/mL for stimulation, or BSA (Sigma, A8806), as a control, were added to the culture medium and were replaced every second day.

2.4.9 SiRNA knockdown in cultured adult rat cardiomyocytes

To study the effects of the impairment in FGF2-FGFR1 pathway and of TEAD TFs deficiency in cultured adult rat cardiomyocytes, siRNA mediated knockdown (KD) experiments were performed. For this purpose, cultured adult rat cardiomyocytes were transfected with 0.5 µmol/L of appropriate siRNA (Table 7)

per well using DharmaFECT 2 transfection reagent (Dharmacon; T-2002-01) according to the manufacturer's instruction. FGF2-stimulation (2.4.8) was started 2 days after siRNA-mediated KD.

Table 7. ***List of siRNAs used in this study***

siRNA	Company	Catalog No.
ON-TARGETplus Rat Tead1 siRNA- SMARTpool	Dharmacon (GE Healthcare)	L-083793-00-0005
ON-TARGETplus Rat Tead2 siRNA-SMARTpool	Dharmacon (GE Healthcare)	L-082568-02-0005
ON-TARGETplus Rat Tead3 siRNA-SMARTpool	Dharmacon (GE Healthcare)	L-094426-02-0005
ON-TARGETplus Rat Tead4 siRNA-SMARTpool	Dharmacon (GE Healthcare)	L-107973-01-0005
ON-TARGETplus Rat Fgfr1 siRNA- SMARTpool	Dharmacon (GE Healthcare)	L-095313-02-0005
ON-TARGETplus Non-targeting Control Pool	Dharmacon (GE Healthcare)	D-001810-10-20

Table 8. ***Components of cell culture media***

Medium	Composition
HEK 293T cell culture medium	DMEM with 4.5 g glucose supplemented with 10 % FBS; 100 u/mL Penicillin; 0.1 mg/mL Streptomycin; 2 mmol/L Glutamine
Early postnatal cardiomyocyte culture medium (P2-P3)	DMEM with 4.5 g glucose supplemented with 5 % FBS; 100 u/mL Penicillin; 0.1 mg/mL Streptomycin; 2 mmol/L Glutamine
Adult mouse cardiomyocyte culture medium (pH 7.4)	M 199 (Earle's salt) supplemented with 5 mmol/L creatinine x H_2O; 2 mmol/L L-carnitine x HCl; 5 mmol/L taurine; 25 mmol/L HEPES; 100 U/mL penicillin; 100 µg streptomycin; 10 % FCS (Insulin, Transferrin, Selenium supplements)
Adult rat cardiomyocyte culture medium	M 199 medium supplemented with 25 mmol/L HEPES; 25 mmol/L $NaHCO_3$; 100 U/mL penicillin; 100 µg streptomycin; 2 mmol/L L-carnitine; 5 mmol/L creatine; 5 mmol/L taurine

2.5 RNA preparation and cDNA synthesis

2.5.1 RNA preparation with peqGold® TriFast™ reagent

In order to isolate RNA of mouse heart tissue, the isolated hearts were perfused with PBS and then snap frozen in liquid nitrogen. The frozen hearts were either stored at -80°C until use or directly placed in 2 mL tubes, resuspended in 1 mL of peqGold® TriFast™ reagent (VWR Peqlab; 30-2010) with a help of 1 sterile grinding ball (grinding balls ss 5 mm – Retsch, 22.455.0003) in a tissue homogenizer (Retsch, MM301) for 5 min with frequency of 30/s. After homogenization, cell debris were removed *via* centrifugation at 14 000 rpm for 5 min and the supernatant was transferred to a new 1.5 mL tube. Further RNA isolation was proceeded following the manufacturer's instruction. The final RNA pellets were fully dissolved in in 20-40 µL of RNase free water or TE Buffer (TE buffer pH 7.0 - Ambion; AM9860) and stored at –80°C until further use. The RNA concentration of the purified RNA samples was measured with a spectrophotometer (NanoDrop ND-2000c Spectrophotometer - Peqlab). and 0.5 – 2 µg of RNA were used for the synthesis (2.5.2).

To isolate RNA from cells, the cultures were first washed with PBS (Table 17) and then 1mL peqGold® TriFast™ reagent per 5-10 x 10^6 cells was directly added to the dish and incubated for 1 min at RT. Thereafter cells were harvested using cell scraper (Sarstedt, 83.1830), transferred to a fresh 1.5 mL tube and resuspended by gentle pipetting. Samples obtained from cultured cells were further processed for RNA isolation using a protocol identical to that of heart tissue.

2.5.2 Complimentary DNA (cDNA) synthesis

In order to perform relative quantitation of RNA expression levels (qRT-PCR, 2.6), cDNA was synthesized. Therefore, 1 µg RNA was reverse transcribed to cDNA using the SuperScriptTM II Reverse Transcriptase (Table 19) according to the manufacture protocol as followed:

Volume	Components
X µL (1 µg)	RNA
1 µL	Oligo$(dT)_{15}$ Primer (Promega; C110A)
1 µL	dNTP (Fermentas; R0186)
10 – x µL	MilliQ H_2O

Reactions were adjusted to 65°C for 5 min and after cooling down, 8 µL of synthesis mixture were added.

Synthesis mixture setup:

Volume	Components
4 µL	5 X first strand buffer (Invitrogen; P/N y02321)
2 µL	0,1 M DTT (Invitrogen; P/N y00147)
1 µL	RNasin RNase Inhibitor (Promega; N261B)
1 µL	SuperScript®II reverse transcriptase (Invitrogen; P/N 100004925)

Reactions were adjusted to 42°C for 50 min and further to 70°C for 15 min. After cooling down, 1 µL of RNaseH (Promega; M428C) per reaction was added and kept at 37°C for 20 min. After synthesis, cDNA was stored at -80°C until further use.

2.6 Quantitative real-time polymerase chain reaction using TaqMan® Gene Expression Assays

In order to perform quantitative real-time polymerase chain reaction (qRT-PCR), the synthesized cDNA (2.5.2) was diluted 1:100 with MilliQ H_2O for use in TaqMan® Gene Expression Assays (Applied Biosystems) using specific TaqMan probes (Table 9) on a StepOnePlus Real-Time PCR System.

The master mix for one qRT-PCR reaction was prepared as followed:

Volume	Components
0.5 µL	Specific TaqMan Gene Expression Assay (20x)
0.5 µL	GAPDH TaqMan Gene Expression Assay (20x)
5 µL	TaqMan Gene Expression Master Mix (2x)
4 µL	cDNA Template (1-100 ng)

Thermocycler condition were used as followed:

Steps	Temperature (°C)	Time	Number of cycles
1	50	2 min	
2	95	10 min	
1	95	15 sec	40x
2	60	1 min	

Each sample was examined in triplicates. The quantitation was performed using a qPCR thermocycler (Step OnePlus Real-Time PCR Cycler – Applied Biosystems). The calculated fold changes (RQ-values) of the examined samples were based on their ΔΔCt values normalized to *Gapdh*, as an internal housekeeping control, using a Step One Software (StepOneTM Software v2.3).

Table 9. ***List of specific TaqMan Gene Expression Assay (20x)***

Gene	Assay	Dye	Species
Tead1	Mm01271498_m1	FAM	mouse
Crhr2	Mm00438303_m1	FAM	mouse
Acta2	Mm00725412_s1	FAM	mouse
Myocd	Mm01325105_m1	FAM	mouse
Myh7	Mm00600555_m1	FAM	mouse
Mylk4	Mm01161239_m1	FAM	mouse
Coro6	Mm01241331_m1	FAM	mouse
GAPDH	mm999999915_g1	VIC	mouse

2.7 Microarray analysis and Gene Set Enrichment Analysis (GSEA)

For microarray analysis, the total RNA was extracted from isolated cardiomyocytes using RNA isolation kit (Direct-zol™ RNA MiniPrep - Zumo research, R2050). For this purpose, the cardiomyocytes were lysed in 600 µL (for up to 5 x 10^6 cells) TRI Reagent (Zumo research, R2050-1-50) and the extraction was processed following the manufacturer's instructions. The quality of extracted RNA was verified with RNA 6000 Nano Kit on an Agilent 2100 Bioanalyzer. RNA was labeled accordingly to the Affymetrix Whole Transcript Sense Target Labeling protocol and hybridized to Affymetrix ClariomTM D assays. The data were processed and analyzed by RMA algorithm using the Affymetrix Expression Console. The statistical analysis was performed using DNAStar Arraystar 11 to calculate FC values in combination with students t- test of log2-transformed data to identify significantly differentially expressed transcripts [116].

The functional gene set enrichment analysis of microarray data in this study was performed and visualized using GSEA software (available on http://software.broadinstitute.org/gsea/index.jsp [117]). GraphPad Prism 6 was used to generate the heat maps and graph bars.

2.8 Protein extraction and immunoblot analysis

2.8.1 Protein extraction from cultured cells and tissue samples

Protein extraction from cultured cells was performed using EB/LB-Buffer (Table 17) supplemented with protease inhibitors (Table 21) to homogenize the samples. For this purpose, the cultured cells were washed with PBS (Table 17) and harvested with a cell scraper (Sarstedt, 83.1830) after adding EB/LB-Buffer (1 mL per one confluent 10 cm dish) directly to the dish. After transfer to a fresh 1.5 mL tube, the samples were resuspended by gentle pipetting and homogenized with a sonicator (Sonicator - Bandelin Sonopuls, HD2070). After sonication, the protein homogenates were centrifuged at 14000 rpm for 5 min at RT to remove debris. The supernatant containing pure protein lysate was then transferred to a fresh 1.5 mL tube and the protein concentration was measured using Bradford Method (2.8.2). Protein lysates were diluted to a concentration of 1-2 µg/µL with a corresponding lysis buffer, denatured by supplementation of 1 mol/L DTT (4 µL per 100 µL sample) and subsequent heating up to 99°C for 2 min and stored at –20°C until further use.

Protein extraction from isolated mouse hearts was performed using Extraction Buffer (EB Buffer; Table 17) supplemented with protease inhibitors (Table 21) to homogenize the samples. For this purpose, the frozen mouse heart tissues were sonified and centrifuged at 14000 rpm for 5 min to remove debris. The supernatant containing pure protein lysate was then transferred to a fresh 1.5 mL tube and protein concentration was measured using Bradford Method (2.8.2). Samples obtained from heart tissue were further processed identical to those of cells.

2.8.2 Determination of protein concentration with Bradford Method

The determination of protein concentration was performed using DC™ ProteinAssay (BioRad; Reagent A - 500-0113; Reagent B - 500-0114) in 96 well

plate (Microplate - Greiner-Bio-One, 655101) according to the manufacturer's instruction and measured on Microplate reader (FLUOstar Galaxy - BMG). A blank (only lysis buffer) and a BSA protein standard row (BSA dilution series: 1, 5, 10, 20, 30 µg; 100x BSA – NEB, B9001S) was used for calibration. All samples were prepared in duplicates. The protein concentrations were calculated based on the standard regression curve in an Excel sheet.

2.8.3 Polyacrylamide gel electrophoresis (PAGE)

Western Blot technique was employed to analyze proteins, which were loaded in equal amounts (10 – 15 µg per well) on a self-made polyacrylamide gel (Table 10). The gels were filled in a purchased NOVEX® Cassettes (1 mm – Invitrogen, NC2010) to perform a separation of the proteins by their mass *via* electrophoresis. The electrophoresis was performed in a gel running chamber (NOVEX® Electrophoresis Mini-Cell - Invitrogen, EI001) at separation time of 1.5 – 2 h using MES running buffer (Table 17). For a better separation, the running buffer was supplemented with 5 mmol/L sodium bisulfite (1 mol/L sodium bisulfite). The protein mass was detected by using the Protein-Marker VI (Peqlab, 27-2311). After electrophoresis, the immunoblotting was processed (2.8.4).

Table 10. ***Composition of gel electrophoresis 9 % Bis-Tris Polyacrylamid gel (PAA)***

Separation gel:	**9%**
Rotiphorese® Gel 30 (37.5:1) (Roth, 3029.1)	2.1 mL
3.5 x bis-Tris pH 6.5 – 6.8	2 mL
Milli-Q H_2O	2.9 mL
10 % Ammoniumperoxodisulfat (APS – Merck, 1.01201)	25 µL
TEMED (Roth, 2367.1)	7 µL
Stacking gel:	**5%**
Rotiphorese® Gel 30 (37.5:1) (Roth, 3029.1)	0.29 mL
3.5 x bis-Tris pH 6.5 – 6.8	0.5 mL
Milli-Q H_2O	0.96 mL
10 % Ammoniumperoxodisulfat (APS – Merck, 1.01201)	8 µL
TEMED	3 µL

2.8.4 Western Blot Analysis (protein immunoblotting)

For Western Blot analysis, the proteins were transferred from a polyacrylamide gel to a nitrocellulose membrane (Amersham™ Protran™ 0.45 µm NC - GE Healthcare, 10600002). The protein transfer was performed using Transfer Buffer (Table 17) and blotting time of 2 h at 30 mV (Power Pac 200 – Bio-Rad) in a blotting chamber (NOVEX® X Cell II™ Blot Module - Invitrogen; EI9051). To visualize transferred proteins, the membrane was stained with 1x Red Alert (dilution of 10 x RedAlert™ Western Blot Stain – Millipore, 71078-50ML) for 10 min on a shaker (Rotamax120 – Heidolph). After documentation, the staining was removed by washing with TBST (Table 17) and the unstained membrane was blocked in 5 % skimmed milk powder solution (Fluka®, 70166-500G) in TBST (Table 17) for 1h at RT. After blocking, the membrane was incubated with primary antibodies (Table 11) diluted in 3 % skimmed milk (Table 21) in TBST overnight at 4°C. After incubation with a primary antibody, the membrane was washed with TBST for 5 min and then incubated with a corresponding secondary antibody (Table 12) diluted in 3 % skimmed milk in TBST for 1h at RT. After this step, the membrane was washed again with TBST and then treated with Super Signal® West Femto Maximum Sensitivity Substrate (Thermo Scientific; 34096), according to the manufacturer's instructions. Then, the membrane was exposed to the Chemiluminescence Analyzer (ChemiDoc™ MP Imaging System – BioRad, 731BR01764) to detect the protein bands. Densitometry and data analysis were performed using Image Lab 5.1 software (Bio-Rad).

Table 11. ***List of primary antibodies for immunoblotting***

Antibody	**Source**	**Company**	**Catalog No.**	**Dilution**
Tead1 (D9X2L)	rabbit	Cell Signaling	12292	1:1000
antiTEF-1	mouse	BD Biosciences	610923	1:1000
anti HA	rat	Roche	11867423001	1:1000
GFP	rabbit	Abcam	ab6556	1:1000
GAPDH	rabbit	Cell Signaling	2118	1:1000

Table 12. ***List of secondary antibodies for immunoblotting***

Antibody	Source	Company	Catalog No.	Dilution
anti-Rabbit IgG HRP-conjugated	goat	ThermoFisher SCIENTIFIC	31460	1:1000
anti-Rat IgG HRP-conjugated	goat	R&D Systems	HAF005	1:1000
anti-Mouse IgG HRP-conjugated	goat	ThermoFisher SCIENTIFIC	G-21040	1:1000

2.9 Chromatin immunoprecipitation (ChIP)

In order to analyze the direct binding of TEAD1 in promoter regions of protentional target genes, TEAD1 Chromatin Immunoprecipitation (ChIP) experiments were performed in early postnatal cardiomyocytes isolated (P2-P3) from wild-type mice.

2.9.1 Chromatin shearing using Covaris Focused-Ultrasonicator

Freshly isolated early postnatal mouse cardiomyocytes (P2-P3) were prepared for ChIP using truChIP™ Chromatin Shearing Reagent Kit (Covaris, 520154) according to the manufacturer's instructions. In brief, approximately 2 x 10^7 of freshly isolated cardiomyocytes (2.4.4) were washed with PBS, transferred to 1.5 mL Protein LoBind tubes (Eppendorf, 0030108.116) and fixed in 1 mL Fixing Buffer containing 11.1 % formaldehyde (16% Formaldehyde Solution, Methanol free - Thermo scientific, 28906) for 5 minutes. The fixation was stopped with 48 µL Quenching Buffer and washed twice with 1 mL ice-cold DPBS (Gibco, 14190144). To shear chromatin, the DNA pellets were lysed with 1 mL Lysis Buffer for 10 min on a rocker at 4°C. The lysed samples were centrifuged at 1700 rpm for 5 min and pellets containing nuclei were washed with 1 mL Washing Buffer. Thereafter, the samples were shortly centrifuged and equilibrated with Shearing Buffer. After equilibration, pellets containing nuclei were resuspended in 130 µl Shearing Buffer per 3 x 10^6 cells and suspensions were transferred to microTUBEs (microTUBE AFA Fiber Pre-Slit Snap, Cap 6x16mm (25) – Covaris, 520045) for shearing by Adaptive Focused Acoustics™ (AFA) in Covaris Focused-Ultrasonicator (S220, Covaris) for 10 min using conditions described in Covaris protocol. Sheared samples were transferred to 0.5 mL DNA LoBind tubes (Eppendorf, 0030108.035) and centrifuged at 4500 rpm for 5 min. Afterwards,

supernatants were transferred to new 0.5 mL DNA LoBind tubes and stored at -80°C for further immunoprecipitation experiments (2.9.3).

2.9.2 Analysis of chromatin shearing efficiency

For analysis of chromatin shearing efficiency, 25 µL of sheared chromatin was treated with 1 µL RNase A (10 mg/mL) at 37°C for 30 min to remove RNA. For reverse cross-linking, 1 µL Proteinase K (10 mg/mL) was added and samples were incubated overnight at 65°C. After incubation, the probes were purified with NucleoSpin Gel and PCR Clean-up kit for SDS containing samples (Macherey-Nagel, 740609.250) according to the manufacturer's instructions. The concentration of purified DNA was measured with spectrophotometer (NanoDrop 2000c) and the quality of shearing was analyzed on 2 % agarose gel.

2.9.3 Chromatin Immunoprecipitation (ChIP)

For ChIP experiments, 20 µL protein A/G magnetic beads (Magna ChIP™ Protein A+G Magnetic Beads – Millipore, 16-663) per each immunoprecipitation (IP) reaction were used. For this purpose, protein A/G magnetic beads were transferred to 0.5 mL DNA LoBind tubes and placed on a magnetic separator (MagneSphere® Technology Magnetic Separation Stand (twelve-position) – Promega, Z5341) for 30 sec. After separation, the supernatant was discarded and the beads were washed with 300 µL Binding/Blocking Buffer (Table 17) and placed on magnetic separator again. For coupling magnetic beads to antibodies, a solution containing magnetic beads and desired antibodies (Table 13) in appropriate amounts in 300 µL Binding/Blocking Buffer (Table 17) was mixed for 1 h on a rotating wheal at RT. Afterwards, antibody-coupled beads were washed in 300 µL Binding/Blocking Buffer (Table 17) and added to 200 µL of sheared chromatin (concentration: 50 ng/µL) and incubated at 4°C on a rotating wheal overnight. After incubation, IP reactions were placed on a magnetic separator for 30 sec and supernatant was discarded. The probes were then washed with 400 µL Low Salt Buffer, 400 µL High Salt Buffer, 400 µL LiCl-Buffer and 400 µL TE (Table 17) for 10 min at 4°C each. After the washing steps, beads were dried at RT. Then to dried beads was added 50 µL Direct Elution Buffer (Table 17) supplemented with 5 µL mixture containing 3 µL Direct Elution Buffer and 2 µL

RNase (RNase, DNase free – Roche, 11119915001) per reaction and incubated at 37°C for 30 min. In parallel, 20 µL of input sample was adjusted to a total volume of 50 µL with Direct Elution Buffer (Table 17) supplemented with 5 µL mixture containing 3 µL Direct Elution Buffer and 2 µL RNase and incubated with all samples at 37°C for 30 min. For reverse cross-linking, each sample was supplemented with 5 µL mixture containing 2.5 µL Proteinase K (Proteinase K Solution, RNA Grade – Invitrogen, 25530-049), 1 µL Glycogen (Glycogen for mol. biol. – Roche, 10901393001) and 1,5 µL Direct Elution Buffer (Table 17) and incubated at 65°C overnight. After incubation, the probes were purified with NucleoSpin Gel and PCR Clean-up kit (Macherey-Nagel, 740609.250) using NTB buffer (Macherey-Nagel, 740595.150) for SDS containing samples according to the manufacturer's instruction. The concentration of purified DNA samples was measured on Fluorometer (Qubit® 2.0, Q32866) using a Qubit dsDNA HS Assay Kit (ThermoFisher scientific, Q32854) in 0.5 mL Qubit® Assay tubes (Invitrogen, Q32856) according to the manufacturer's instructions.

Table 13. ***List of antibodies used for chromatin immunoprecipitation***

Antibody	Source	Company	Catalog No.	Amount
Tead1 (D9X2L)	rabbit	Cell Signaling	12292	5 µg
H3K9Ac	rabbit	Abcam	Ab10812	5 µg
ChIPAb+ RNA Pol II - ChIP	mouse	MILLIPORE	17-620	5 µg
Rabbit IgG Isotype control	rabbit	Cell Signaling	2729S	5 µg
Mouse (G3A1) mAb IgG1 Isotype control	mouse	Cell Signaling	5415S	5 µg

2.9.4 ChIP sequencing and analysis

For ChIP sequencing (seq), 0.5-10ng of DNA was used as input for TruSeq ChIP Library Preparation Kit (Illumina) with following modifications. Instead of gel-based size selection before final PCR step, libraries were size selected by SPRI-bead based approach after 18 cycles of PCR. For this purpose, the samples were purified using 1x bead/1xDNA ratio to eliminate residuals from the PCR reaction, followed by 2-sided-bead cleanup step with a 0.6x bead/1xDNA solution to exclude larger fragments. The supernatant was transferred to a new tube and

incubated with additional beads in a 0.2x bead/1xDNA solution for eliminating smaller fragments, such as adapter and primer dimers. Bound DNA samples were washed with 80% EtOH, dried and resuspended in TE buffer. Library integrity was verified with a BioAnalyzer 2100 (Agilent) or LabChip Gx Touch 24 (Perkin Elmer). Sequencing was performed on the NextSeq500 instrument (Illumina) using v2 chemistry with 1x75bp single end setup.

The resulting raw reads were assessed for quality, adapter content and duplication rates with FastQC (Andrews S. 2010, FastQC: a quality control tool for high throughput sequence data. Available online at: http://www.bioinformatics.babraham.ac.uk/projects/fastqc). Reaper version 13-100 was employed to trim reads after a quality drop below a mean of Q20 in a window of 10 nucleotides [118]. Only reads between 30 and 150 nucleotides were cleared for further analyses.

Trimmed and filtered reads were aligned versus the mm10 (GRCm38) version of the mouse genome using STAR 2.5.2b with the parameter "--outFilterMismatchNoverLmax 0.1" to increase the maximum ratio of mismatches to mapped length to 10% [119] and retaining only unique alignments to exclude reads with uncertain arrangement. Reads were further deduplicated using Picard 2.9.0 (Picard: A set of tools (in Java) for working with next generation sequencing data in the BAM format) to mitigate PCR artefacts leading to multiple copies of the same original fragment.

The MUSIC peakcaller (version from Dec. 2015) [120] was employed to detect enriched regions. In order to determine thresholds for significant peaks per IP, the data were manually inspected in Integrative Genomics Viewer (IGV 2.3.52) [121]. Thresholds ranged from 1000-5000 for the p-value normalization window length (l_p), with a minimum enrichment of treatment versus input reads of 2 – 4-fold, and a maximum FDR of 0.05 to 1. Peaks overlapping ENCODE blacklisted regions (known misassemblies, satellite repeats) were excluded.

For assessment of the peak's reproducibility, the resulting lists of significant peaks were overlapped and unified to represent identical regions. A background-correction was performed to correct read counts on various regions (unified peaks, promoters, genes). Treatment and Input samples were normalized for sequencing depth, before subtracting reads of the Input sample from reads of the respective Treatment sample in windows of 50nt length [122]. All windows with

negative values (Input > Treatment) were set to zero [123]. Background-corrected counts for regions were calculated using bigWigAverageOverBed (UCSC Tools) and normalized with DESeq2 [124]. For Peaks were annotated with the promoter (TSS ± 5000 nt) of the gene most closely located to the center of the peak based on reference data from GENCODE v25. Spearman correlations were produced to assess the degree of reproducibility between samples. To permit comparative display of samples in Integrative Genomics Viewer (IGV), raw BAM files were scaled with DESeq2 size factors based on all unified peaks using bedtools genomecov resulting in normalized BigWig files [125].

For analysis of MCAT motifs in TEAD1-occupied sites, Tead1 ChIP seq data were screened for the enrichment of the following nucleotide sequences: CATTC, CATTCC(TA) and their combination. In brief, a region of 100 nucleotides was centered on summit of identified in ChIP seq peaks, background regions of promoters were set to 100 < TSS > 0 and background repetitions number to 100. Summit of peaks was found and extracted ± 50 bp using Fuzznuc (http://www.bioinformatics.nl/cgi-bin/emboss/fuzznuc). Background distribution was calculated by random promoter sequence of same number (same as input peaks) and size (100 < TSS > 0) and repeated 100-times. List of hits was ranked and, for significant enrichment, *P*-values were calculated.

2.9.5 Verification of TEAD1 ChIP by qRT-PCR using SYBR® Green

In order to verify selected binding peaks identified in ChIP-seq (2.9.3), the qRT-PCR method was performed using specific self-designed primers showed in Table 14. The purified DNA was diluted 1:100 with MilliQ H_2O for use in KAPA SYBR® FAST qPCR Master Mix (Kapa Biosystems, KM4104) on a StepOnePlus Real-Time PCR System.

The master mix for one qRT-PCR reaction was prepared as followed:

Volume	Components
7.5 µL	KAPA SYBR® FAST qPCR Master Mix (2x) (Kapa Biosystems)
4 µL	Purified DNA (1-100 ng)
2.7 µL	MilliQ H_2O
0.4 µL	Primer forward
0.4 µL	Primer reverse

Each sample was performed in triplicates. The quantitation was performed by a qPCR thermocycler (Step OnePlus Real-Time PCR Cycler – Applied Biosystems) that identified *Ct* values, which were further log2-transformed and normalized to 10% Input using Microsoft Excel. GraphPad Prism 6 was used to generate graph bars.

Table 14. ***List of primers used for verification of ChIP-seq results***

Name	Sequence
PZ84-Myh7-ChIP-for *PZ85-Myh7-ChIP-rev*	5'-TGGTCGTGGTCAGCTTACTCT-3' 5'-CCTTCCCTTGTCCAAACAGT-3'
PZ96-Acta2-ChIP-for *PZ97-Acta2-ChIP-rev*	5'-CCTTCCTTATCCAAGTCCTCAGCT-3' 5'-GCTCAGCTGCTTATGGGGATAAAC-3'

2.10 Histology

2.10.1 Preparation of paraffin embedded hearts

The mice were narcotized (Buprenorphine/Ketamine in 0.9 % NaCl, *i.p.*) and perfused first with PBS (Table 17) and then with freshly prepared 4% paraformaldehyde (PFA - Roth, 0335.4) (Table 17) *via* the left heart ventricle. Hearts were then isolated and fixed with 4 % PFA overnight at 4°C. After fixation the hearts were rinsed with PBS for 10 min at RT and further processed in a dehydration series of 70 %-, 80 %-, 90 %- and 100 %- EtOH (Rothipuran® Ethanol > 99.8 % (EtOH) – Roth, 9065.4) for 2 h on a shaker at RT each step. Heart samples were than incubated with 100 % isopropanol for maximum 2h at RT on a shaker and then transferred to 50 % isopropanol/ 50 % paraffin mixture at 56°C overnight. For a better paraffin penetration, the samples were transferred to 100 % liquid paraffin and immersed for 3 h in a vacuum chamber at -3 bar and 56°C. Finally, the hearts were embedded in paraffin using a tissue embedding center (Leica EG1150C). Thick sections (10 µm) were obtained using a microtome (Leica RM2125RT) and collected on a glass slide (Superfrost Ultra Plus® - Thermo Scientific, J3800AMNZ). Sections were dried on a heating plate (42°C; HI1220 – Leica) and stored in a box at RT.

2.10.2 Hematoxylin and eosin staining

Paraffin sections (2.10.1) were first deparaffinized by dipping two times in 100 % xylene (Roth, 9713.3) for 2 min and rehydrated in decreasing EtOH concentration series (100 %-, 90 %-, 80 %- and 70 %- EtOH) (Table 17) and thoroughly rinsed with dd.H_2O. Afterwards, sections were exposed to Mayer's Hematoxylin (Haemalaum, acidic Mayer – WALDECK, 2E-038) (Table 17) for 10 minutes at RT and then dipped 2-times in dd.H_2O. Thereafter, the sections were dipped 10 times in 70% RtOH/ 1% hydrochloric acid solution (Table 17) and then 5-times in tap water followed by a 5 min staining with eosin (Eosine Solution – WALDECK, 2C-140) (Table 17) at RT. Afterwards, the tissue slides were dehydrated again in increasing EtOH concentration series (70 %-, 80 %-, 90 %-EtOH – 2 dips each and 100 % EtOH 10 min) and 100 % xylene (Roth, 9713.3) for 5 min. Finally, the sections were mounted in Entellan (Merck-Millipore, 1.07961.0100) and photographed with a Keyence (Keyence BZ-9000) or Zeiss Axioplan 2 microscopes.

2.10.3 Preparation of mouse hearts or mouse embryos for cryosections

The mice were narcotized (Buprenorphine/Ketamine in 0.9 % NaCl, *i.p.*) and perfused with PBS (Table 17) *via* the left heart ventricle. For this purpose, the chest was opened and the perfusion system was connected to the left heart ventricle. After perfusion with PBS, the hearts were dissected and directly frozen in liquid nitrogen and stored at –80 °C until further use. The embryos were isolated from pregnant mice and immersed in FSC 22® clear (Leica, 3801480) for 12 h at 4°C followed by embedding in FSC 22® clear at 20°C and stored at –80 °C until further use.

The embedded hearts and embryonic tissue were fixed on a special metal holder followed by cryosectioning using a Leica cryotome (Leica CM1950). Cryosections (6 µm thick) were mounted on a glass slide (Superfrost ultra plus - Thermo scientific, J3800AMNZ), shortly dried at RT and fixed in fresh 4% PFA (Table 17) for 2 min at RT, washed with PBS (Table 17) and either directly proceeded with staining or stored at 4°C.

2.10.4 Beta galactosidase (LacZ) staining

Cryosections were fixed in Fixing Solution (Table 17) for 5 min at RT and rinsed with Wash Solution (Table 17) for 10 min at RT. Thereafter, the slides were incubated in Staining Solution (Table 17) at 37°C overnight, in the dark. Afterwards, the sections were rinsed with Wash Solution (Table 17) for 10 min at RT and stained with eosin (2.10.2). After eosin staining, the sections were dehydrated in 70 %-, 80 %-, 90 %- and 100 %- EtOH series followed by 10 min 100% xylene (Roth, 9713.3). Finally, the sections were mounted in Entellan (Merck-Millipore, 1.07961.0100). Images were acquired with Keyence microscope (Keyence BZ-9000) or Zeiss Axioplan 2 microscope.

2.10.5 Immunofluorescence analysis

Immunofluorescence labeling of fixed cultured cells and tissue sections was performed using standard antibody staining protocols in accordance to the data sheet of antibodies (Tables 15 and 16) and adjusted depending on the examined cells or tissues. For immunofluorescence analysis, cells were either cultured on cover slips (cover slips 13 mm - Hecht-Assistant, 41001113) or chamber slides (Lab Tek® Chamber Slide™ system, 4-well Permanox® Slide - Nunc/Sigma-Aldrich, 177437). Cultured cells were fixed with freshy prepared 4 % PFA (Table 17) for 2 min at RT, washed 3-times with PBS (Table 17) for 5 min to remove fixative solution.

Prior to immunolabeling, tissue sections (2.10.3) and cultured cells were permeabilized with 0.5 % Triton-X1 (Roth, 6683.1) in PBS for 2 min. Permeabilized cells and cryosections were incubated with the primary antibodies (Table 15) in a humidified chamber over night at 4°C or for 2h at RT. After incubation, tissue sections or cells were washed 3-times with PBS for 5 min at RT and incubated with the corresponding secondary antibodies (Table 16) for 1h at RT in a humidified chamber. Cell nuclei were stained with DAPI (Molecular Probes™, Thermo Fisher, D1306) for 5 min at RT in a humidified chamber (dark), washed 3-times with PBS for 5 min at RT and mounted with Mowiol (Millipore, 475904-100GM).

Table 15. ***List of primary antibodies for immunofluorescence analysis***

Antibody	Source	Company	Catalog No.	Dilution
ACTN2	Mouse	Sigma	A 7811	1:200
Dystrophin	Mouse	Sigma	D 8168	1:200
Dystrophin (H-300)	Rabbit	SantaCruz	sc-15376	1:200
Tead1 (D9X2L)	Rabbit	Cell Signaling	12292	1:200
antiTEF-1	Mouse	BD Biosciences	610923	1:200
Smooth muscle Actin –Cy3	Mouse	Sigma	C6198	1:200
Mylk4 Antibody	Rabbit	Abcam	ab107994	1:200
Collagen1	Rabbit	Rockland	600-401-103-0.5	1:200
anti HA high affinity	Rat	Roche	11867423001	1:200
GFP	Rabbit	Abcam	ab6556	1:500
anti-FLAG	Mouse	Sigma	F1804	1:200

Table 16. ***List of secondary antibodies and detection systems for immunofluorescence analysis***

Antibody	Source	Company	Catalog No.	Dilution
Phalloidin-FITC (F-Actin)	Amanita phalloides	Sigma	P5282	1:200
Phalloidin-TRITC (F-Actin)	Amanita phalloides	Sigma	P1951	1:200
Phalloidin-633 (F-Actin)	Amanita phalloides	Invitrogen	A22284	1:200
DAPI		Roche	10236276001	1:1000
anti-Mouse Alexa 594	Goat	Invitrogen	A11005	1:200
anti-Rabbit Alexa 594	Goat	Invitrogen	A11012	1:200
anti-Mouse Alexa 488	Goat	Invitrogen	A11001	1:200
anti-Rabbit Alexa 488	Goat	Invitrogen	A11070	1:200
anti-Rat Alexa Fluor 488	Goat	Invitrogen	A-11006	1:200

2.10.6 EdU-based assay for DNA synthesis and cell cycle analysis

EdU assay is based on incorporation of alkyne-containing thymidine analog EdU (5-ethynyl-2´-deoxyuridine) into DNA during active synthesis, which then can be detected by a click reaction [126]. For EdU incorporation analysis of the embryonic hearts (E12.5), pregnant mice were injected *i.p*. with 1 mg EdU diluted in 0.9 % NaCl. The embryos were isolated 24 h after EdU administration and immersed in PBS with 30 % sucrose at 4°C overnight. Next day, the embryos were transferred into 1:1 of FSC 22® clear:30% sucrose in PBS solution for 2 h at RT, embedded in FSC 22® clear on dry-ice and stored at -80°C for further use or directly proceeded for cryosectioning (2.10.3). 6 µm tick cryosections were fixed with 4 % PFA for 2 min at RT, permeabilized with 0.5 % Triton X-100 in PBS (Table 17) for 2 min at RT and further processed for EdU detection.

For the assessment of cardiomyocyte proliferation in early postnatal hearts (P3), the P2 mice were *i.p.* injected with EdU diluted in 0.9 % NaCl, (50 µg per 1 g of body weight). After 24 h, the mice were sacrificed, the hearts were isolated and snap-frozen in liquid nitrogen. 6 µm thick cryosections were fixed with 4 % PFA, permeabilized with 0.5 % Triton X-100 in PBS (Table 17) and further processed for EdU detection.

EdU detection was performed using EdU Click-iT Plus Alexa Fluor® 594 Imaging Kit (Invitrogen, C10639) according to the manufacture's protocol. For quantification of EdU^{pos} cardiomyocytes in embryonic and postnatal hearts, tissue sections were immunolabeled with antibodies against dystrophin (DMD) and counterstained with phalloidin-Alexa633 for F-Actin and DAPI for nuclei. This technique allows a clear delineation of the cardiomyocyte cell borders owing to the fact that DMD is present only at the lateral sarcolemma. Quantification of EdU^{pos} cardiomyocytes was performed per high-power field (hpf) using a 63-objective lens (x600, image size 250x250 µm). Five (embryonic hearts) to ten hpf (postnatal hearts) were investigated per each mouse. Quantification of EdU was performed blindly by counting the total number of cardiomyocytes containing nuclei followed by the determination of EdU^{pos} cardiomyocytes. The results are presented as percent of EdU^{pos} cardiomyocytes from the total cardiomyocyte number.

For quantification of EdU^{pos} cardiomyocytes in cell cultures, the slides were stained with either phalloidin-Alexa633 or with antibodies against sarcomeric

alpha-actinin (ACTN2) that permits an unequivocal cardiomyocyte detection. Ten hpf were investigated per each culture.

2.10.7 In situ Cell Death Detection

TUNEL labeling of DNA strand breaks using fluorescein-dUTP method enables detection and quantification of apoptosis at single-cell level [127]. For detection of cell death (apoptosis), 6 µm thick cryosections (2.10.3) were fixed with 4 % PFA (Table 17) for 5 min at RT and processed to TUNEL detection using *In Situ* Cell Death Detection Kit, TMR red (Roche, 2156792910) according to the manufacture's protocol.

Quantification of $TUNEL^{pos}$ cardiomyocytes in embryonic and postnatal hearts was similar to that of EdU^{pos} cardiomyocytes (2.10.6). The results are presented as percent of $TUNEL^{pos}$ cardiomyocytes from the total number of cardiomyocytes.

2.10.8 Isolation of late postnatal cardiomyocytes from PFA fixed hearts

In order to analyze the morphology of late postnatal cardiomyocytes (P16), cardiomyocytes were isolated from PFA-fixed hearts as described by Mollova *et al.* [128]. Briefly, mice were sacrificed, perfused with PBS *via* the left heart ventricle. Perfused hearts were cut in small pieces about 1-2 mm^2 of size and fixed with 4% PFA at 4°C. For cardiomyocyte isolation, small PFA-fixed heart pieces were transferred into a 37°C warm collagenase mixture consisting of 1.8 mg/mL collagenase B (Roche, 11088807001) and 2.4 mg/mL collagenase D (Roche, 11088858001) in $CaCl_2$ (20 µL of 10 mmol/L $CaCl_2$ pro 1 mL DPBS) in DPBS (Gibco™, 14190144) and incubated at 37°C overnight shaking at 220 rpm. After incubation the supernatant containing separated cardiomyocytes was transferred to a 0.5 mL tube, centrifuged at 300 rpm for 5 min, resuspended in PBS and stored at 4°C until further use. For immunofluorescence labeling, isolated cardiomyocytes were washed with PBS containing 1 % BSA for 5 min at RT and shortly centrifuged. The pelleted cardiomyocytes were incubated with an appropriate primary antibody (Table 15) diluted in PBS supplemented with 0.1 % triton-X 100 in PBS for 2h at 30°C, shaking at 160 rpm. After incubation, the cardiomyocytes were shortly centrifugated and the pellet was incubated with appropriate secondary antibodies (Table 16) in PBS with 0.1 % triton-X 100 for 1

h at 30 °C. Cell nuclei were stained with DAPI (Molecular Probes™, Thermo Fisher, D1306) for 5 min at 30 °C. For cardiomyocyte transfer to glass slides, the suspensions were centrifuged in Cytospin™ (ThermoFisher scientific) at 500 rpm for 5 min. Glass slides with cardiomyocytes were mounted in Mowiol (Millipore, 475904-100GM).

2.10.9 Transmission electron microscopy

For transmission electron microscopy (TEM) the animals were anesthetized (Buprenorphine/Ketamine in 0.9 % NaCl, *i.p.*) and the hearts were perfused with PBS and fixed with 4 % PFA. To isolate embryonic hearts, the pregnant mice were sacrificed and the embryos were isolated and placed separately into a fresh petri dish containing 4 % PFA to carefully isolate the hearts. Both, isolated embryonic or 2 mm thick sections of postnatal hearts were immersion fixed in 2.5 % glutaraldehyde and 2 % PFA in 0.1 M cacodylate buffer (pH 7.2) for 48 h followed by en-bloc staining in cold 0.5 % osmium tetroxide for 60 min and 2 % uranyl acetate in the dark for 30 min. The tissue samples were then dehydrated through a graded ethanol series, embedded in epoxy resin (Epon 812) from which 70 nm thin sections were cut with a diamond knife. Ultrathin (70 nm) sections were mounted on 300 mesh hexagonal grids and stained with 2 % uranyl acetate and lead citrate. Images were obtained using a FEI CM10 and a JEOL 1400 electron microscopes equipped with 2K and 4K digital cameras. Both TEM microscopes were operated at 80 kV.

2.11 Magnetic resonance imaging of the mouse hearts

Magnetic resonance imaging (MRI) was used to analyze the mouse heart function *in vivo*. The MRI was performed on a 7.0 Bruker PharmaScan, equipped with a 300 mT m^{-1} gradient system, using a custom-built circularly polarized birdcage resonator and Early Access Package for self-gated cardiac imaging (Intragate, Bruker). First, mice were anesthetized with 1.5 % - 2.0 % Isoflurane (CP-Pharma, 1214) and then measured. The measurement was based on the gradient echo method (repetition time, 6.3 ms; echo time, 1.6 ms; field of view, 2.20 × 2.20 cm; slice thickness, 1.0 mm; matrix, 128 × 128; repetitions, 100). The imaging plane was placed using scout images showing transverse- and four-

chamber views of the heart and images were then acquired in short-axis view, orthogonal to the septum in both scout images. Multiple contiguous short-axis slices consisting of six to seven slices were acquired for complete coverage of the left ventricle. MRI images were analyzed with MASS 4Mice 7.1 program. Only left ventricular data sets in transversal plane were used for data analysis. Therefore, the area of heart in end-diastole (the maximum of ventricular volume) and end-systole (the minimum of ventricular volume) by highlighting of endo- and epicardial borders in all transversal imaged of the heart were defined and calculated in the program (MASS 4Mice 7.1).

2.12 Statistical Analysis

The data reported in this study were analyzed with Microsoft Excel 2016 (Microsoft) and Prism Software Version 6 (GraphPad Software, San Diego, CA). The results are presented as means ±SD. *P*-values were determined by two-tail Student's *t*-test (unpaired) for two groups. One-way ANOVA followed by Benferroni's multiple comparison test was used for three or more groups. Survival curve analysis was performed using Kaplan-Meier log-rank (Mantel-Cox) test. Values of $P < 0.05$ were considered as statistically significant and *n* represents the number of separate experiments performed.

2.13 Materials

Table 17. ***Buffers and solutions***

Buffer	**Composition**
Common buffers	
TE buffer	10 mmol/Lol/L Tris-HCl (pH 8.0); 1 mmol/L EDTA (pH 8.0)
PBS (pH 7.4)	137 mmol/L NaCl; 2.7 mmol/L KCl; 10 mmol/L Na_2HPO_4; 1.8 mmol/L KH_2PO_4; in MilliQ H_2O
Genomic DNA extraction	
TENS buffer (pH 7.4)	50 mmol/L Tris/HCl (pH 8.0); 40 mmol/L EDTA (pH 8.0); 100 mmol/L NaCl; 1% SDS; in milliQ H_2O

Plasmid DNA Preparation	
Buffer I	10 mmol/L EDTA; 50 mmol/L Tris/HCl, pH 8,0; 100 µg/mL RNase A
Buffer II	0,2 M NaOH; 1% (w/v) SDS
Buffer III (pH 5.5)	3 M Potassium acetate
50 x TAE	Dilute 242 g Tris Base; 57.1 mL acetic acid; 100 mL 0.5 mol L^{-1} EDTA, pH 8.0 in 1000 mL Aqua dest.
Adult mouse cardiomyocytes isolation	
Calcium-free buffer	113 mmol/L NaCl; 4.7 mmol/L KCl; 0.6 mmol/L KH_2PO_4; 0.6 mmol/L Na_2HPO_4; 1.2 mmol/L $MgSO_4$; 12 mmol/L $NaHCO_3$; 10 mmol/L $KHCO_3$; 10 mmol/L Hepes; 30 mmol/L Taurine; 10 mmol/L 2,3-Butanedionemonoxime; 5.5 mmol/L Glucose
Enzyme-buffer	0.25 mg/mL Liberase DH; 0.14 mg/mL Trypsin; 12.5 µmol/L $CaCl_2$
Stop buffer 1	90% Enzyme-buffer; 10% FCS; 12.5 µmol/L $CaCl_2$
Stop buffer 2	95% Enzyme-buffer; 5% FCS; 12.5 µmol/L $CaCl_2$
Adult rat cardiomyocytes isolation	
Perfusion solution (Ca^{2+}-free Krebs-Henseleit bicarbonate buffer (KHB, pH 7.4)	110 mmol/L NaCl; 2.6 mmol/L KCl; 1.2 mmol/L KH_2PO_4; 1.2 mmol/L $MgSO_4$; 11 mmol/L glucose; 10 mmol/L HEPES
Western Blot	
LB buffer	67 mmol/L Tris-HCl; 2% SDS;27% Glycerol; in milliQ H_2O
EB buffer	100 mmol/L Tris-HCl; 10 mmol/L EDTA; 10% SDS; in milliQ H_2O
EB/LB buffer	60% EB buffer; 40% LB buffer
MES buffer	20 x MES buffer 1:20 dilution in milliQ H_2O
Transfer buffer	190 mmol/L Bicine; 25 mmol/L BisTris; EDTA; 20% Methanol; in milliQ H_2O
TBST buffer	150 mmol/L NaCl; 20 mmol/L Tris, pH 7.5; 0,1 Tween 20
5 % Immunoblot blocking solution	Dilute 5 g skim milk in 100 mL 1 x TBS-T
Chromatin Immunoprecipitation	
Binding/blocking buffer	0,5 % BSA; 0,5 %Tween in PBS (without Ca^{+2},Mg^{+2})
Dilutions buffer	16.7 mmol/Lol/L Tris-HCl (pH 8.0); 1.2 mmol/L EDTA (pH 8.0); 167 mmol/L NaCl; 1.1 % Triton X-100; 0.01 % SDS; in molecular biology-grade water supplemented with protease inhibitors (cOmplete ULTRA Tablets)

Low salt buffer	10 mmol/L Tris-HCl (pH 8.0); 1 mmol/L EDTA (pH 8.0); 140 mmol/L NaCl; 1 % Triton X-100; 0.1 % SDS; 0.1 % Na-DOC; in molecular biology-grade water supplemented with protease inhibitors (cOmplete ULTRA Tablets)
High salt buffer	10 mmol/L Tris-HCl (pH 8.0); 1 mmol/L EDTA (pH 8.0); 500 mmol/L NaCl; 1 % Triton X-100; 0.1 % SDS; 0.1 % Na-DOC; in molecular biology-grade water supplemented with protease inhibitors (cOmplete ULTRA Tablets)
LiCl wash buffer	10 mmol/L Tris-HCl (pH 8.0); 1 mmol/L EDTA (pH 8.0); 250 mmol/L LiCl; 0.5 % NP-40; 0.5 % Na-DOC; in molecular biology-grade water supplemented with protease inhibitors (cOmplete ULTRA Tablets)
Direct elution buffer	10 mmol/Lol/L Tris-HCl (pH 8.0); 5 mmol/Lol/L EDTA (pH 8.0); 300 mmol/L NaCl; 0.5 % SDS; in molecular biology-grade water
Common Histology	
4 % PFA (pH 7.4)	4 % PFA in 1 x PBS
0.5 % Triton-X100	0.5 % Triton-X100; in 1 x PBS
0.1 % Triton-X100	0.1 % Triton-X100; in 1 x PBS
Beta galactosidase (LacZ) staining	
SPP buffer	77.4 mmol/L Na_2HPO_4; 22.6 mmol/L NaH_2PO_4
Fixing solution	0.4 % glutaraldehyde, 2 mmol/L $MgCl_2$; 5 mmol/L EGTA (pH 7.5); in SPP buffer
Wash solution	2 mmol/L $MgCl_2$; 0.01 % Na-desoxycholate; 0.02% NP-40; in SPP buffer
Stain solution	5 mmol/L K_3FeCN_6; 5 mmol/L K_4FeCN_6; 0.1 % X-Gal
X-β-Gal stock solution	50 mg X-β-Gal in 1 mL dimethylformamide
HE staining	
90% ethanol	90% ethanol; in dd. H_2O
80% ethanol	80% ethanol; in dd. H_2O
70% ethanol	70% ethanol; in dd. H_2O
Ethanol/HCl	1% HCl (37%); in 70% ethanol
Eosin stock solution	2% eosin G; in dd. H_2O
Eosin working solution	0.1% eosin G; 0.0005% acetic acid; in dd. H_2O

Table 18. ***Agents and Viruses***

Agents / Viruses	Company	Catalog No.
4-Hydroxytamoxifen	SIGMA-ALDRICH	H7904-5MG
EdU (5-ethyl-2´-deoxyuridine)	Invitrogen	A10044
FGF2 (Recombinant Human FGF-basic)	ReproTech	100-1813
Ad-CMV-iCre	VECTOR BIOLABS	1045N

Table 19. ***Transfection reagents***

Reagents	Company	Catalog No.
TurboFect™ Transfection Reagent	ThermoFisher Scientific	R0531
DharmaFECT 2 transfection reagent	Dharmacon	T-2002-01

Table 20. ***List of enzymes and their appropriate reagents****

Enzyme	Company	Catalog No.
Proteinase K	Carl Roth	7528.2
SuperScript® II Reverse transcriptase	Invitrogen	P/N 100004925
Oligo(dT)$_{15}$ Primer *	Promega	C110A
dNTP *	Fermentas	R0186
5 x First strand buffer *	Invitrogen	P/N y02321
0.1 M DTT *	Invitrogen	P/N y00147
RNasin RNase Inhibitor *	Promega	N261B
RNaseH	Promega	M428C
T4-DNA-Ligase	Promega	M1801
2 xRapid Ligation-Buffer *	Promega	C6711
Taq Polymerase	Homemade	
REDTaq® ReadyMix™ PCR Reaction Mix	Sigma-Aldrich	R2523
collagenase II	Worthington	LS004176
PureLink™ RNase A* (20 mg/mL)	Invitrogen	12091021
RNase, DNase free	Roche	11119915001
Proteinase K Solution, RNA Grade	Invitrogen	25530-049
KAPA SYBR® FAST qPCR Master Mix	Kapa Biosystems	KM4104

collagenase B	Roche	11088807001
collagenase D	Roche	11088858001
Trypsin-EDTA	Sigma	T4174
Trypsin	Sigma	T0303
EcoR I	Jena Bioscience	EN-113S
Sla I	Jena Bioscience	EN-134S
Bgl II	Jena Bioscience	EN-106S
Sfi I	Jena Bioscience	EN-132S
AscI	NEB	R0558S
10x universal Buffer *	Jena Bioscience	EN-300
10x restriction Buffer 2 *	Jena Bioscience	EN-302
10x restriction Buffer 3 *	Jena Bioscience	EN-303
10x restriction Buffer 4 *	Jena Bioscience	EN-304
NEBuffer 4 *	NEB	B7204

Table 21. ***List of protease inhibitors***

Inhibitor	**Company**	**Catalog No.**
Aprotinin	Sigma	10820
Leupeptin	Sigma	L8511-5MG
Sodium fluoride (NaF)	Sigma	S7920-100G
Sodium orthovanadate (Na_3Vo_4)	Sigma	450243
Phenylmethylsulfonyl fluoride (PMSF)	Sigma	P7626
protease inhibitors (cOmplete ULTRA Tablets, Mini, EASYpack)	Roche	05892970001

Table 22. ***Kits and Assays***

Kits	**Company**	**Catalog No.**
NucleoBond® Xtra Maxi-kit	Macherey-Nagel	740414
Dual-Luciferase® Reporter 1000 Assay Systems	Promega	E1980
Neonatal Heart Dissociations Kit	Miltenyi Biotec	130-098-373
Mouse Neonatal Cardiomyocyte Isolation Kit	Miltenyi Biotec	130-100-825
Direct-zol™ RNA MiniPrep	Zumo research	R2050
DC™ ProteinAssay Reagent A	BioRad;	500-0113

Reagent B		500-0114
truChIP™ Chromatin Shearing Reagent Kit	Covaris	520154
NucleoSpin Gel and PCR Clean-up kit for SDS containing samples	Macherey-Nagel	740609.250
NTB buffer	Macherey-Nagel	740595.150
Magna ChIP™ Protein A+G Magnetic Beads	Millipore	16-663
Qubit dsDNA HS Assay Kit	ThermoFisher	Q32854
EdU Click-iT Plus Alexa Fluor® 594 Imaging Kit	Invitrogen	C10639
In Situ Cell Death Detection Kit, TMR red	Roche	2156792910

Table 23. ***List of chemicals***

Chemicals	**Company**	**Catalog No.**
0.9 % NaCl	B. Braun	9511040
1 x DPBS	Gibco	14190144
1,4-Dithiothreit (DTT)	Carl Roth	6908.2
10 x RedAlert™ Western Blot Stain	Millipore	71078-50ML
100x BSA	NEB	B9001S
16 % Formaldyhyde Solution, Methanol free	ThermoScientific	28906
2,3-Butanedionemonoxime	Sigma	B0753
20 x MES buffer	Invitrogen	NP000202
Acetic acid	Roth	3738.5
Ammoniumperoxodisulfat (APS)	Merck	101.201
Bicine	Sigma	B3876-1KG
BisTris	AppliChem	A1025,0500
Bovine Serum Albumin (BSA) solution	Sigma	A9576
Calcium (Ca^{2+})	Roth	5239.2
Creatinine x H_2O	Sigma	C3630
Dimethyl sulfoxide (DMSO)	Sigma	D-4540
Dimethylformamide	Sigma	319937-500ml
Disodium hydrogen phosphate (Na_2HPO_4)	Sigma	P030.2
DPBS, no calcium, no magnesium	Gibco™	14190144
Dulbecco's Modified Eagle Medium (DMEM) 4.5 g/L D-Glucose,	Sigma	D5796
EDTA	Roth	8040.3
EGTA	Roth	3054.3

Entellan	Merck-Millipore	1.07961.0100
Eosine Solution	WALDECK	2C-140
Ethanol	Roth	9065.4
Ethidium bromide solution (1 %)	AppliChem	A1152,0100
Fatty acid-free BSA	Sigma	A8806
Fetal bovine serum (FBS)	Sigma	F7524
Fetal calf serum (FCS)	Sigma	F7524
Fibronectin	PromoCell	C-43050
FSC 22® clear Frozen Section Compound	Leica	3801480
Glucose	Roth	X997.2
Glutaraldehyde	Sigma	G5882
Glycerol	Roth	7533.1
Glycogen for mol. biol.	Roche	10901393001
Haemalaum, acidic Mayer	WALDECK	2E-038
Heparin	Braun	1708.00.00
HEPES	Gibco	15630-056
Hydrochloric acid (HCl (37%))	Roth	4625.1
Insulin-Transferrin-Sodium-Selenite	Sigma	11074547001
Isoflurane	CP-Pharma	1214
Isopropanol	Roth	6752.4
K_3FeCN_6	Merck	1.04973.0250
K_4FeCN_6	Merck	1.04984.0500
L-carnitine x HCl	Sigma	A6706
Laminin	Sigma	L2020
LB-Agar (Lennox)	Roth	X965.2
LB-Medium (Lennox)	Roth	X964.2
LE Agarose	Biozym	840004
Lithium chloride (LiCl)	Roth	P007.1
M 199	Sigma	M4530-500ML
M 199 (Earle's salt)	Gibco	31153
Magnesium chloride x $6H_2O$ ($MgCl_2$)	Roth	2189.1
Magnesium sulfate ($MgSO_4$)	Merck	1.05886.1000
Methanol	Roth	4627.5
Molecular biology-grade water	Sigma	W4502

Mowiol	Millipore	475904100GM
Na-desoxycholate (Na-DOC)	Sigma	30970-100G
Nonidet P-40 (NP-40)	Fluka	74385
NuPAGETM MES SDS Running Buffer	ThermoFisher	NP000202
Paraformaldehyde (PFA)	Roth	0335.4
Penicillin	Roth	K029.2
Penicillin/Streptomycin/Glutamine	Sigma	G6784
peqGold® TriFast™ reagent	VWR Peqlab	30-2010
Potassium acetate	Roth	T874.1
Potassium bicarbonate ($KHCO_3$)	Merck	1.04854.0500
Potassium chloride (KCl)	Roth	6781.3
Potassium dihydrogen phosphate (KH_2PO_4)	Roth	P018.1
Rotiphorese® Gel 30 (37.5:1)	Roth	3029.1
SDS	Roth	2326.3
Skimmed milk powder	Fluka®	70166-500G
Sodium bicarbonate ($NaHCO_3$)	Merck	1.06329.1000
Sodium bisulfite	Sigma	243973
Sodium chloride (NaCl)	Roth	3957.2
Sodium dihydrogen phosphate (NaH_2PO_4)	Roth	2370.3
Sodium hydroxide (NaOH)	Roth	6771.2
Streptomycin	Roth	HP66.1
Sucrose	Carl Roth	9097.1
Super Signal® West Femto Maximum Sensitivity Substrate	ThermoScientific	34096
TaqMan Gene Expression Master Mix (2x)	Applied Biosystems	10525395
Taurine	Sigma	T8691
TE buffer pH 7.0	Ambion	AM9860
TEMED	Roth	2367.1
TRI Reagent	Zumo research	R2050-1-50
Tris-HCl	Roth	5429.2
Triton X-100	Roth	6683.1
Tween 20	Roth	9127.2
X-β-Gal	Roth	2315.4
Xylene	Roth	9713.3

Table 24. ***Protein and DNA-markers***

Marker	Company	Catalog No.
Protein-Marker VI	Peqlab	27-2311
PUC Marker (DNA)	Homemade	

Table 25. ***List of equipment***

Equipment	Company
0.5 mL DNA LoBind tubes	Eppendorf (0030108.035)
0.5 mL Qubit® Assay tubes	Invitrogen (Q32856)
1.5 mL Protein LoBind tubes	Eppendorf (0030108.116)
10 cm cell culture dishes	Greiner
7.0 Bruker PharmaScan	Bruker
96 well plate	Greiner- Bio-One (655101)
Amersham™ Protran™ 0.45 µm NC	GE Healthcare (10600002)
Bacteria incubator	Heraeus
BioDocAnalyze	Biometra
cell culture plate (6-, 12-, 24- and 48 well)	Greiner
Cell scraper	Sarstedt (83.1830)
Centrifuge 5417R	Eppendorf
Centrifuge 5430	Eppendorf
Centrifuge Universal 320R	Hettich Zentrifugen
ChemiDoc™ MP Imaging System	BioRad (731BR01764)
Covaris Focused-Ultrasonicator S220	Covaris
Cover slips 13 mm	Hecht-Assistant (41001113)
Cryotome Leica CM1950	Leica
Dumont forceps - #7 curved tip	F.S.T.
E455 – Consort, Power Pack P25 T	Biometra
EG1150C Tissue Embedding Center	Leica
Electron microscope CM10	FEI
Electron microscope1400	JEOL
Electroporation Cuvettes (blue cap)	Peqlab
Eppendorftubes, (0.5 mL, 1.0 mL, 2.0 mL)	Eppendorf
Filter tips (10 µl, 20 µl, 100 µl, 1000 µl)	Fisher Scientific
Fluorometer Qubit® 2.0	Q32866

Gene Pulser™	Bio-Rad
gentleMACS Octo Dissociator with Heaters	Miltenyi Biotec (130-096-427)
Glass slides Superfrost Ultra Plus®	Thermo Scientific (J3800AMNZ)
Greiner centrifuge tubes (15 mL, 50 mL)	Sigma-Aldrich
Grinding balls ss 5 mm	Retsch (22.455.0003)
Heating block	IKA Labortechnik
HERA Cells150i, CO_2 cell culture incubator	Thermo Scientific
HERAsafe KS laminar flow hood	Thermo Scientific
Incucyte Zoom life cell imager	Essen BioScience
Innova® 44 Incubator Shaker Series	New Brunswick Scientific
Lab Tek® Chamber Slide™ system, 4-well Permanox® Slide	Nunc/Sigma-Aldrich (177437)
Labcycler	Sensoquest
MagneSphere® Technology Magnetic Separation Stand (twelve-position)	Promega (Z5341)
Mastercycler Nexus	Eppendorf
Microplate reader FLUOstar Galaxy	BMG
Microscope Biorevo BZ-9000	Keyence
Microscope Imager Z1 Axio	Zeiss
Microscope M205 FA	Leica
Microscope Zeiss Axioplan 2	Zeiss
Microtome Leica RM2125RT	Leica
microTUBE AFA Fiber Pre-Slit Snap – Cap 6x16mm (25)	Covaris (520045)
Multimode Microplate Reader - Mithras LB 940	Berthold Technologies
NanoDrop ND-2000c Spectralphotometer	Peqlab
Neubauer improved cell counting chamber	Marienfeld
NOVEX® Cassettes 1 mm	Invitrogen (NC2010)
NOVEX® Electrophoresis Mini-Cell	Invitrogen (EI001)
NOVEX® X Cell II™ Blot Module	Invitrogen (EI9051)
pH meter	HANNA instruments
Pipettes	Rainin
Power Pac 200	Bio-Rad
Shaker Rotamax120	Heidolph
Sonicator Bandelin Sonopuls	Bandelin Sonopuls (HD2070)
Sorvall Evolution RC	Sorvall

Step OnePlus Real-Time PCR Cycler	Applied Biosystems
T100 Thermal Cycler	Biorad
Thermo Mixer F 1.5	Eppendorf
Tissue homogenizer	Retsch (MM301)
UV Transilluminator	INTAS
Vannas Spring Scissors straight, sharp tip,	F.S.T.
Vortex mixer	Scientific Industries, Inc.
Waterbath	Leica

Table 26. ***Analysis software***

Software	**Company**
MASS 4Mice 7.1	Medis medical imaging systems
StepOne™ Software v2.3	Applied Biosystems™
GSEA	GSEA/MSigDB
GraphPad Prism 6	GraphPad Software
Image Lab 5.1 software	Bio-Rad
Excel 2016	Microsoft
Image J / Fiji	NIH
SeqBuilder Pro	DNAStar, Inc.
Integrative Genomic Viewer (IGV)	Broad Institute and the Regents of the University of California
IncuCyte S3 Software	Essen BioScience

3 RESULTS

3.1 TEAD1 expression and protein abundance in embryonic end postnatal mouse hearts

In order to analyze TEAD1 mRNA and protein levels during embryogenesis as well as postnatal heart growth, qRT-PCR (Quantitative Real-Time Polymerase Chain Reaction) and western blot analysis of the wild-type (WT) mouse hearts were performed.

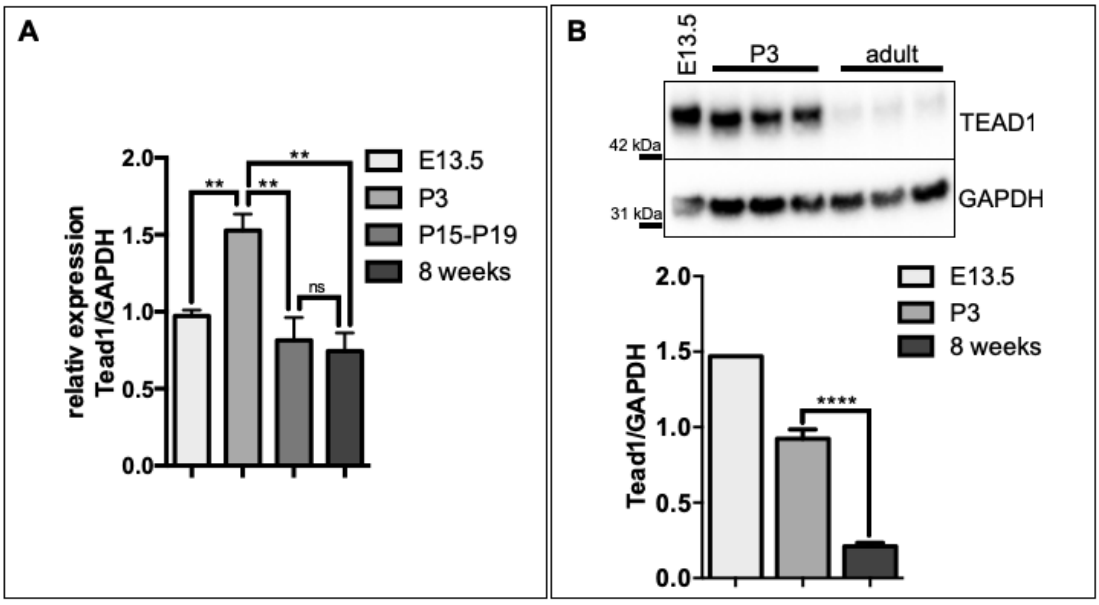

Figure 8. ***TEAD1 mRNA expression and protein levels in embryonic and postnatal hearts. (A)*** *Tead1 mRNA expression levels in embryonic (E13.5, n=2), postnatal (P3, n=3 and P15-P19, n=3) and adult (8 weeks, n=3) WT mouse hearts. Tead1 expression level initially increases about 1.5-times from embryonic to early postnatal (P3) stage and afterwards gradually decreases in late postnatal (P15-P19) and adult (8 weeks) stages. Tead1 expression levels were normalized to Gapdh expression.* ***(B)*** *Representative western blots of embryonic (E13.5, n=1), postnatal (P3, n=3) and adult (8 weeks, n=3) WT mice hearts show that the protein levels of TEAD1 constantly decrease from embryonic to adult stages. Protein levels of TEAD1 were normalized to GAPDH protein levels. Data are means ± SD; ns = not significant (P ≧ 0.05); ** = P < 0.005; **** = P < 0.001.*

As shown in figure 8A, *Tead1* mRNA expression initially increased form embryonic (embryonic day (E)13.5) to early postnatal stage (postnatal day (P)3) and afterwards began gradually to decrease until adult stage (8 weeks). At both,

late postnatal stage (P15-P19) and 8 weeks adult hearts, *Tead1* mRNA levels were approximately 2-times lower compared to P3 hearts. There were no significant differences between P15-P19 and 8 weeks hearts in the *Tead1* mRNA expression levels. Concomitant western blot analysis indicated that TEAD1 protein levels gradually decreased from embryonic (E13.5) to adult (8 weeks) stages (Figure 8B). In adult hearts, the TEAD1 protein abundance was 4.5-fold lower in comparison to P3 hearts.

3.2 Loss of *Tead1* in embryonic mouse cardiomyocytes results in embryonic lethality

In order to investigate the role of TEAD1 in cardiomyocytes *in vivo*, a conditional *Tead1* knockout mouse approach (*Tead1*$^{fl/fl}$) was used by insertion of *loxP* sites in introns 2 and 5 of *Tead1* gene (Figure 9). This conditional inactivation resulted in deletion of exon 3 to 5 accompanied by a frameshift and premature translational stop. In order to analyze TEAD1 function during early embryonic heart development, a *XMLC2-Cre::Tead1*$^{fl/fl}$ mouse line, which were later referred to as e(embryonic)Tead1-cKO, was generated. Cardiomyocyte-specific *Tead1*-deletion in this mice is achieved in the early myocardium starting at E7.5 [109].

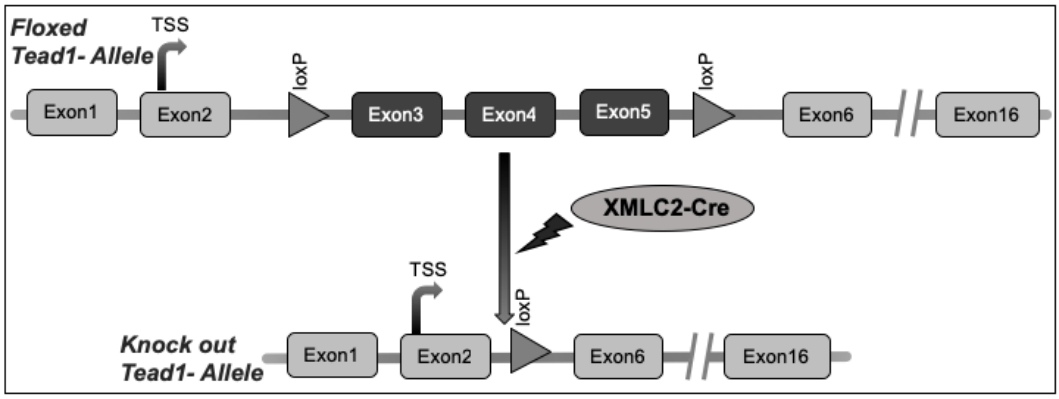

*Figure 9**. Schematic view of XMLC2-Cre driven recombination in the eTead1-cKO mouse line results in a conditional deletion of Tead1 Exon3 to Exon5.***

Homozygous eTead1-cKO mice were embryonic lethal at E13.5 and were characterized by a smaller body size compared to control littermates. Morphological analysis revealed that mutant embryos displayed dilated heart ventricles and pericardial cavity, enlarged fourth brain ventricle and cranial hemorrhages (Figure 10A). The heart ventricular walls in eTead1-cKO mice were

approximately 2-fold thinner compared to control embryos, although no difference between *Tead1* mutants and controls in the atrial wall thickness was observed (Figure 10B). In addition, the heart ventricles of eTead1-cKO embryos consistently exhibited thinner trabecular layer (hypotrabeculation) as compared to controls (Figure 10C).

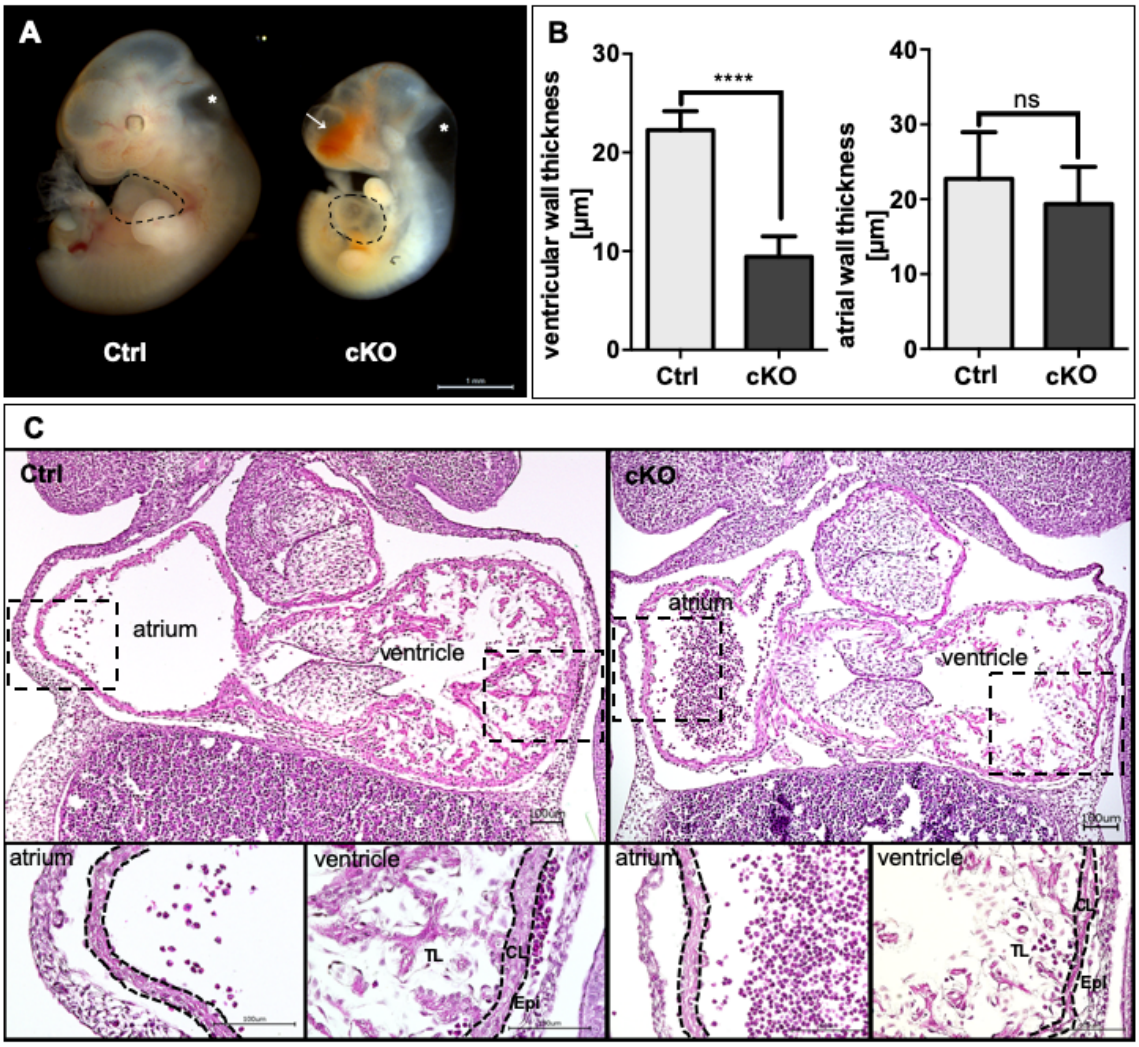

Figure 10. ***Embryonic retardation, enlarged cardiac cavity, thin ventricular wall and hypotrabeculation in eTead1-cKO (E11.5).*** *(**A**) Representative example of eTead1-cKO (right panel, cKO) and control (left panel, Ctrl) embryos. Note that eTead1-cKO embryo exhibits enlarged fourth brain ventricles (asterisk), cranial hemorrhages (arrow), developmental retardations and dilated heart cavities (outlined with dashed line) in comparison to control. (**B**) Reduced ventricular wall thickness in eTead1-cKOs (mean 9.4 µm, n=3) compared to controls (mean 22 µm, n=3), however there is no significant difference in atrial wall thickness. Data are means ± SD; ns = not significant (P ≧ 0.05); **** = P < 0.001. (**C**) HE-stained paraffin sections of a representative eTead1-cKO (right panel) embryo in comparison to control (left panel). eTead1-cKO embryo displays a thinner ventricular wall (outlined with dashed black line) and reduced trabeculation (TL) in comparison to control. Notice that the atrial wall thickness is not altered. TL – trabecular layer, CL – compact layer (outlined with dashed black line), Epi – epicardium.*

Immunohistochemical analysis of control embryos (E12.5) showed that TEAD1 localizes in nuclei of the vast majority of cardiac cells, including cardiomyocytes as well as non-cardiomyocytes (Figure 11). In contrast, in eTead1-cKO hearts (E12.5) residual TEAD1 protein was restricted to non-cardiomyocytes, demonstrating cardiomyocyte-specific deletion of TEAD1 (Figure 11).

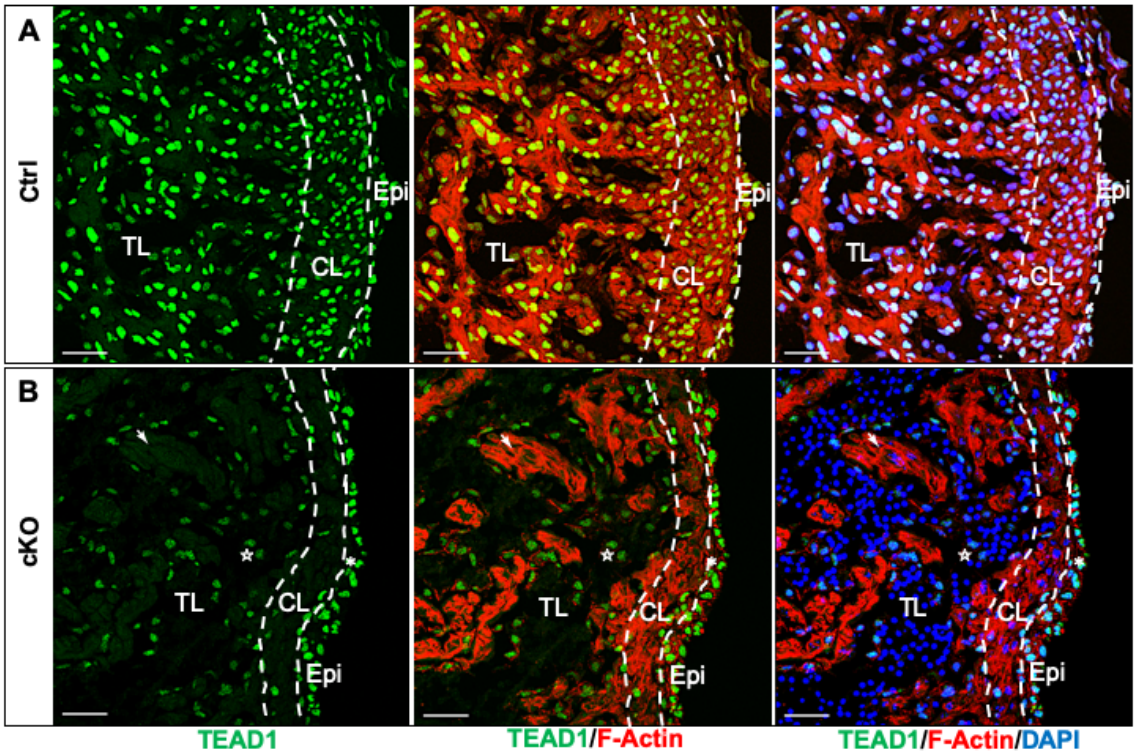

Figure 11. ***Absence of TEAD1-positive cardiomyocytes in eTead1-cKO embryonic hearts (E12.5).*** *Fluorescent images of control (**A**) and eTead1-cKO (**B**) embryonic hearts. Note that in mutant hearts (B), TEAD1 is present in non-cardiomyocytes (asterisk) of the trabecular layer (TL) and in epicardial cells while almost all cardiomyocytes of the trabecular layer are TEAD1^{neg} (arrow). In contrast, all cardiomyocytes and non-cardiomyocytes of compact and trabecular layer as well as epicardial cells in control embryonic heart are TEAD1^{pos}. CL – compact layer (outlined with dashed white line); Epi – epicardium; green – TEAD1, red – F-Actin, blue – DAPI. Scale bar: 30 µm.*

Next, it was reasoned that deficient cardiomyocyte proliferation might be a cause for severe heart phenotype in eTead1-cKO mutants. The proliferation assay at E12.5 showed that eTead1-cKO hearts exhibited 3.4-times less EdU^{pos} cardiomyocytes compared to control heterozygous littermates (Figure 12).

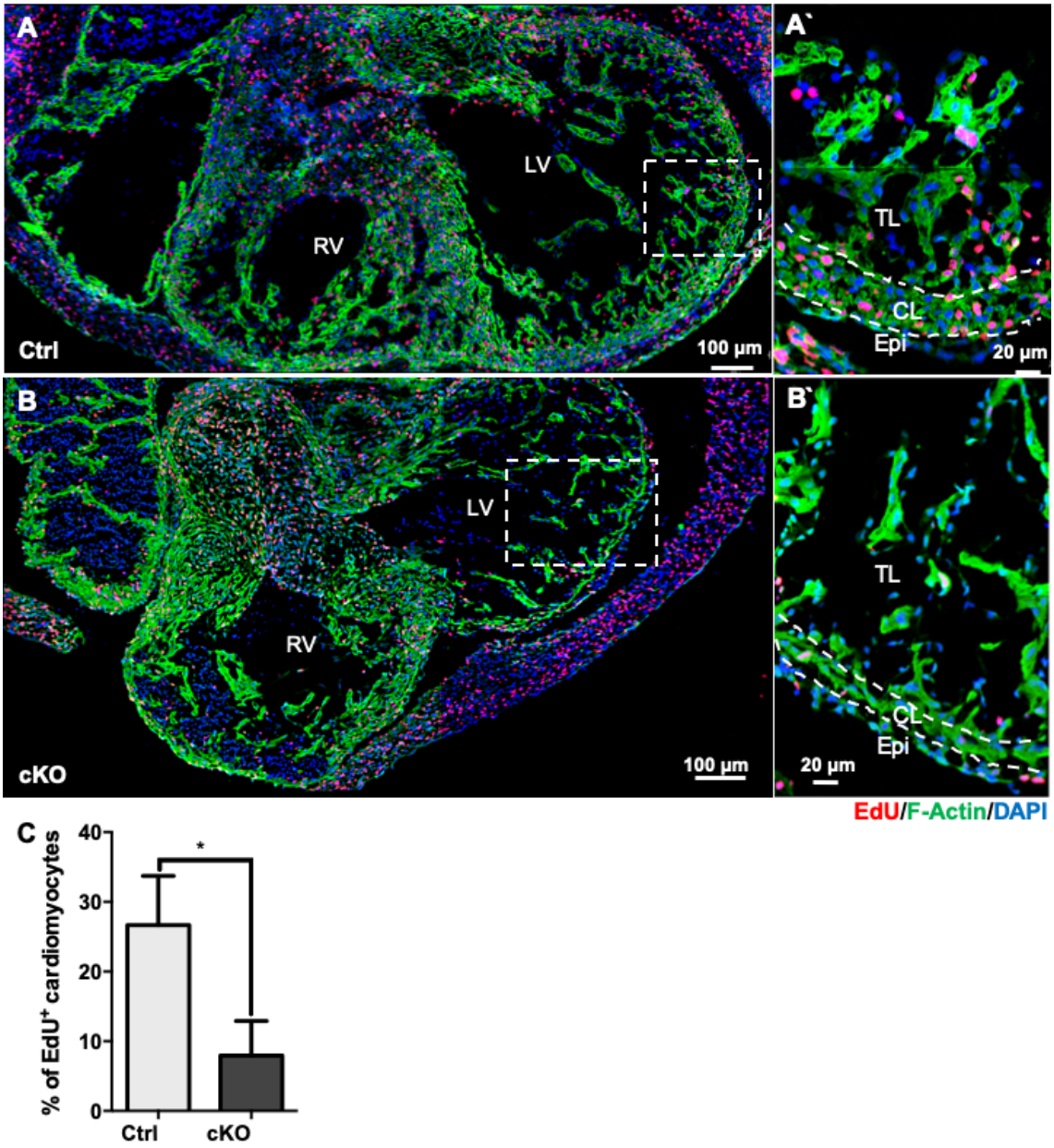

Figure 12. ***Reduced cardiomyocyte proliferation in eTead1-cKO embryonic hearts (E12.5).*** *Fluorescent images of EdU labeling in control (**A**) and eTead1-cKO (**B**) embryonic hearts showing reduced number of EdU^{pos} (red) cardiomyocytes (F-Actin, green) in eTead1-cKO hearts (B). Red – EdU, green - F-Actin, blue - DAPI; RV – right ventricle, LV – left ventricle, TL – trabecular layer, CL – compact layer (outlined with dashed white line), Epi – epicardium. (**C**) The number of EdU^{pos} cardiomyocytes in eTead1-cKO (mean 8%, n=3) is approximately 3-times lower than in control hearts (mean 27%, n=3). Data are means ± SD; ∗ = P < 0.05.*

Further it was also reasoned that cell death might be involved in the manifestation of the severe heart phenotype in eTead1-cKO embryos. The number of TUNEL^{pos} apoptotic cells in eTead1-cKO embryonic hearts was 5-fold increased compared to control hearts (Figure 13).

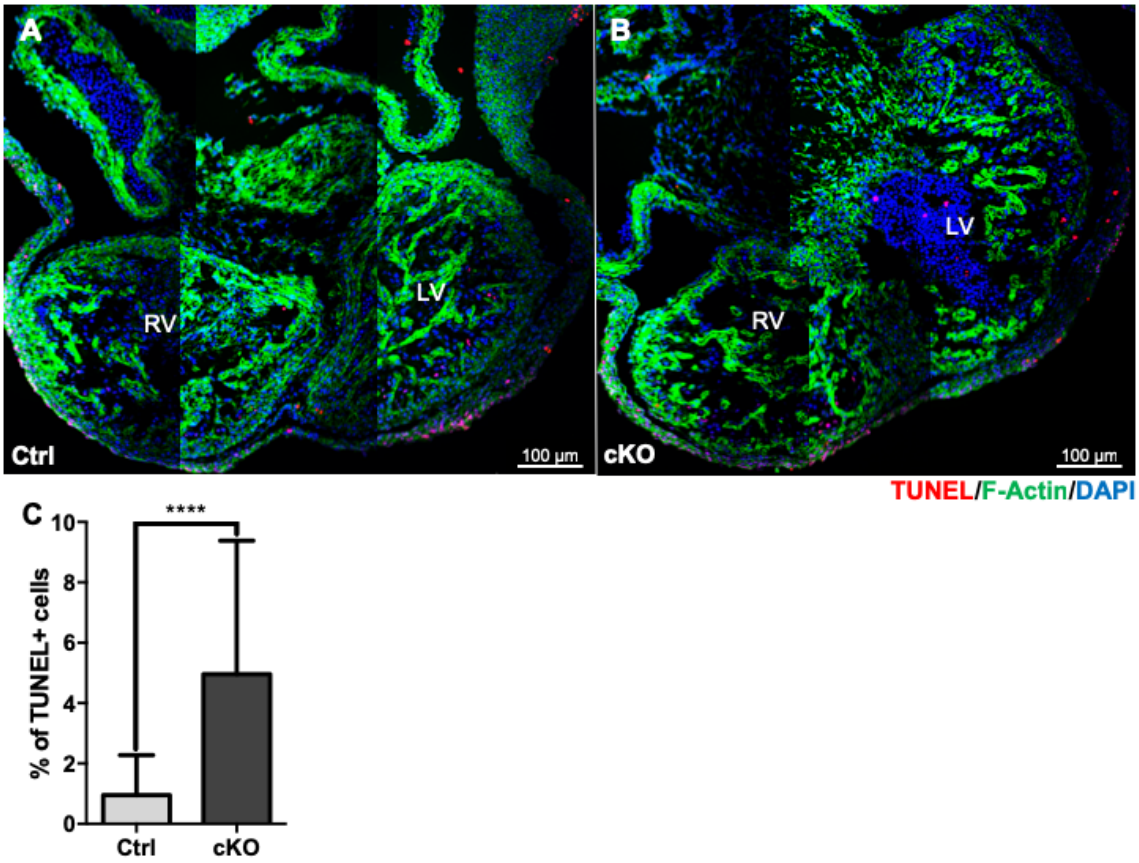

Figure 13. ***Increased number of apoptotic cells in eTead1-cKO embryonic hearts (E12.5)****. TUNEL staining of control (**A**) and corresponding eTead1-cKO (**B**) embryonic hearts shows increased number of TUNEL^{pos} cells in eTead1-cKO embryonic hearts compared to control. RV – right ventricle, LV – left ventricle; red -TUNEL, green - F-Actin, blue - DAPI. (**C**) The percent of TUNEL^{pos} cells in eTead1-cKO (n=3) hearts is approximately 5% compared to 1% in controls (n=3). Data are means ± SD, **** = P < 0.001. Scale bar: 100 µm.*

Next, transmission electron microscopy (TEM) was performed to analyze the ultrastructure of eTead1-cKO and control E12.5 embryonic hearts revealing a reduced ventricular wall thickness and a reduced trabeculation in eTead1-cKO hearts. The size of individual cardiomyocytes in eTead1-cKO hearts was smaller than that in controls. Moreover, the packing density of cardiomyocytes within the ventricular wall appeared more dispersed in eTead1-cKO hearts than in control hearts. (Figure 14). Despite the more condensed myofibrillar pattern in control hearts, there were no differences between control and eTead1-cKO hearts in the ultrastructural organization of individual sarcomeres (Figure 15). In both groups, sarcomeres had a similar length and exhibited discernible Z-discs in the absence of M-bands.

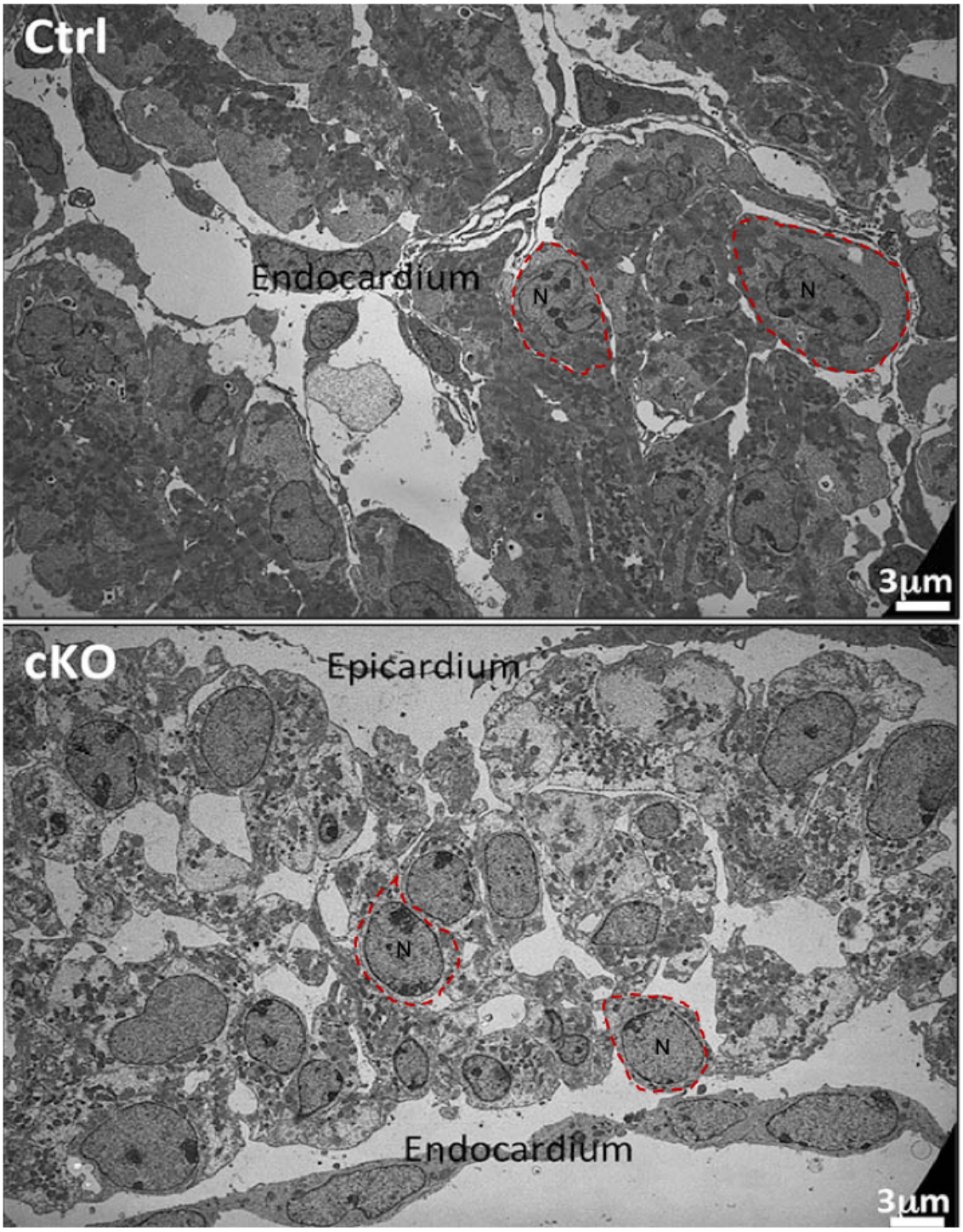

Figure 14. ***Representative TEM images comparing the left ventricular wall in control and eTead1-cKO embryonic hearts (E12.5).*** *eTead1-cKO (**low panel**) heart displays a more disperse packing pattern of cardiomyocytes and thinner ventricular wall compared to control (**upper panel**). Note the difference between groups by comparing the outlined cardiomyocytes. N - nuclei*

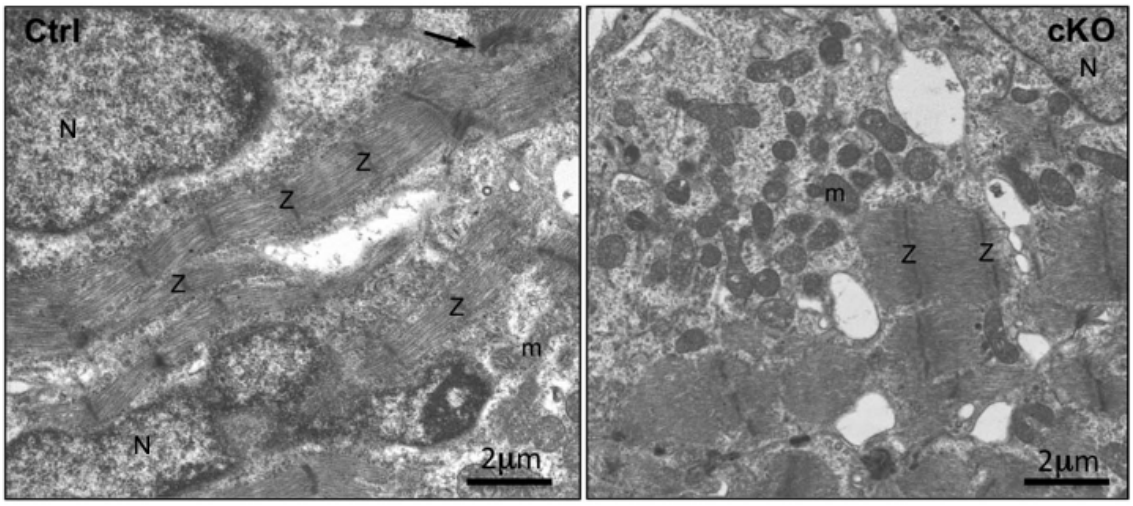

Figure 15. ***The ultrastructure of sarcomeres in control and eTead1-cKO cardiomyocytes (E12.5).*** *Note that the sarcomeres in both, control (**left panel**) and eTead1-cKO (**right panel**) display discernible Z-disks (Z). There are no apparent differences in the sarcomere length of both groups. Arrows denote fascia adherents, m – mitochondria, N – nuclei, Z – Z-disks.*

Taken together, cardiomyocyte-specific deletion of *Tead1* during embryogenesis led to severe defects in heart development and embryonic lethality. The most obvious feature of eTead1-cKO hearts was a decrease of cell proliferation and an increase of apoptotic cardiomyocytes. These latter findings were also documented by TEM analysis (Figure 16).

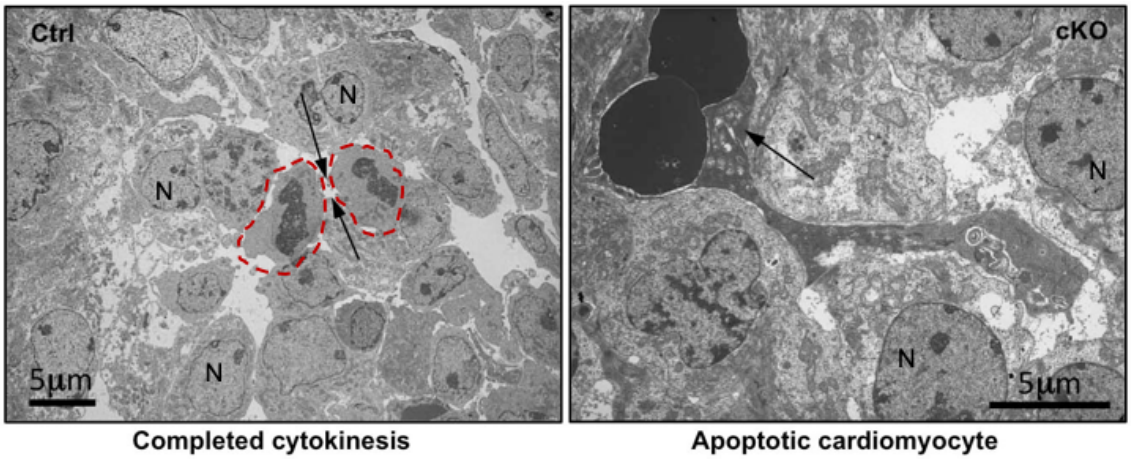

Figure 16. ***TEM images show completed cytokinesis*** *(arrows, cardiomyocytes are outlined with dashed line)* ***in control hearts*** *(left panel)* ***and apoptotic cells*** *(arrow)* ***in eTead1-cKO embryonic hearts*** *(right panel)* ***(E12.5).*** *N – nuclei.*

3.3 Loss of TEAD1 in postnatal mouse cardiomyocytes leads to dilated cardiomyopathy, heart failure and premature death

In order to analyze TEAD1 function in postnatal cardiomyocytes, a *MCK-Cre::Tead1*$^{fl/fl}$ mouse line, which were later referred to as p(postnatal)Tead1-cKO was generated. Myocardial specific recombination in these mice starts at late fetal stages and reaches its maximum around postnatal day 10 (P10) [110, 129].

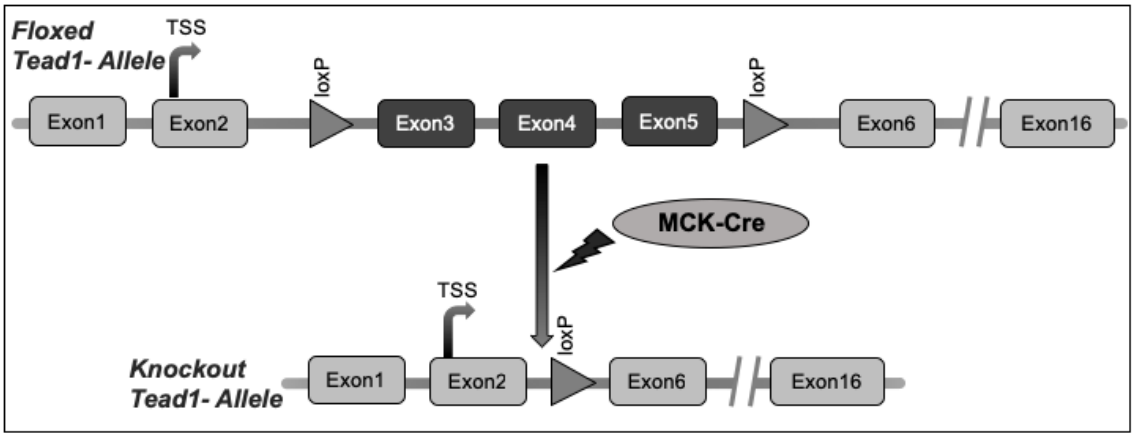

Figure 17. ***Recombination in pTead1-cKO mouse line after crossing to MCK-Cre-deleter mouse leads to the deletion of Tead1 Exon3 to Exon5.***

As shown in Figure 17, deletion of *Tead1* exons 3 to 5 results in a frame shift of subsequent codons and premature stop. In order to determine the time-point of highest MCK-Cre (Muscle Creatine Kinase) recombinase activity in the heart, the *MCK-Cre* mouse line was crossed with *ROSA26-LacZ* (Reverse Oriented Splice Acceptor, Clone 26) Cre-reporter line to monitor Cre-recombinase activity [130]. To achieve this aim hearts of P0 to P15 knock-in (*MCK-Cre::Rosa26*$^{fl/+}$) and control (*MCK-Cre::Rosa26*$^{+/+}$) mice were isolated and stained for LacZ. Figure 18 shows that LacZ^{pos} cardiomyocytes were present in knock-in hearts at all stages, which are gradually increase from P0 to P15. In contrast, control hearts were LacZ^{neg} at all stages. It is worth to note that not all cardiomyocytes of knock-in mice were LacZ^{pos} as indicated by some islands of LacZ^{neg} cells.

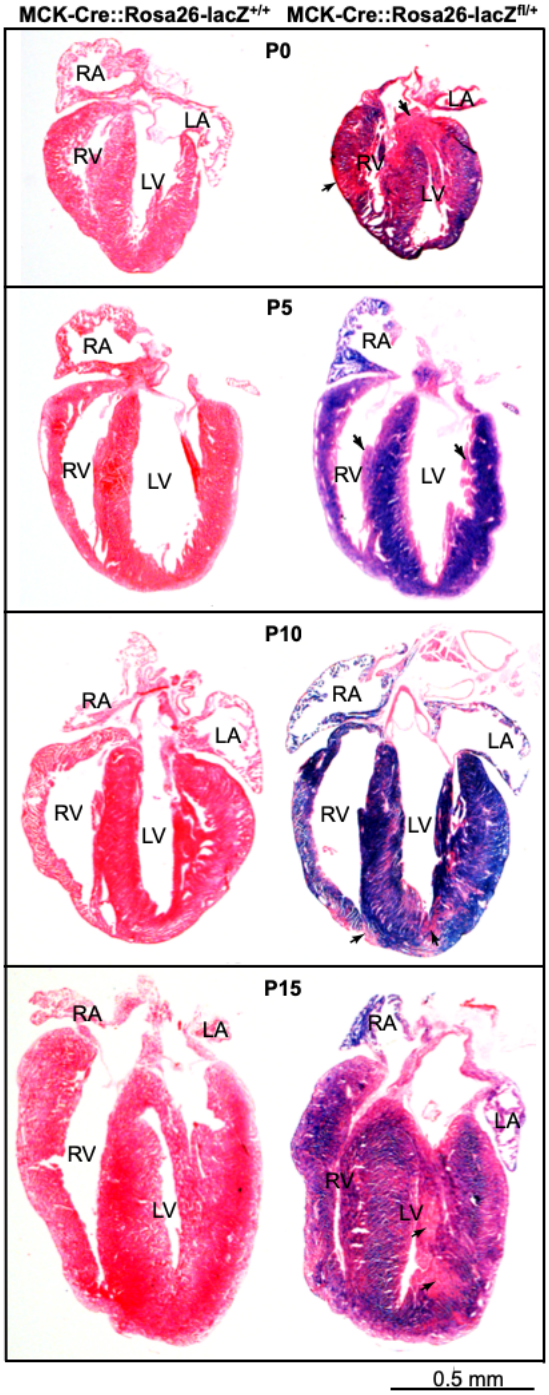

Figure 18. ***Stepwise increase in Rosa26-LacZ^{pos} cardiomyocytes during postnatal heart maturation (P0 to P15) representing activation of CRE recombinase driven by the MCK promoter.*** *Representative images of heart coronal sections at different stages (P1, P5, P10 and P15) stained for LacZ. Sections on the left side depict control (MCK-Cre::Rosa26-lacZ$^{+/+}$) littermate hearts which show no Rosa26-lacZ-reporter activation (red). Sections on the right side depict knock-in (Cre::Rosa26-lacZ$^{+/-}$) hearts with an active Rosa26-lacZ-reporter, which is represented by LacZ-staining (blue). The number of Lac-Z^{pos} cardiomyocytes is gradually increasing during the observation period. RA – right atrium, LA – left atrium, RV – right ventricle, LV – left ventricle.*

The efficiency of cardiomyocyte-specific inactivation of *Tead1* in pTead1-cKO mice (*MCK-Cre::Tead1$^{fl/fl}$*) was determined by immunohistochemistry, qRT-PCR and western blot. Immunohistochemical analysis of P10 and P24 heterozygous control animals showed that almost all cardiomyocytes displayed strong TEAD1 signal confined to nuclei (Figures 19A - 19D). In contrast, pTead1-cKO hearts steadily decreased the population of TEAD1^{pos} cardiomyocytes from P10 toward P24 (Figures 19E - 19H). Immunohistochemical analysis also revealed that in

both, pTead1-cKO and control hearts, the non-cardiomyocyte cell population was positive for nuclear TEAD1 signal irrespective of the postnatal stage, implying that TEAD1 was specifically deleted in pTead1-cKO cardiomyocytes.

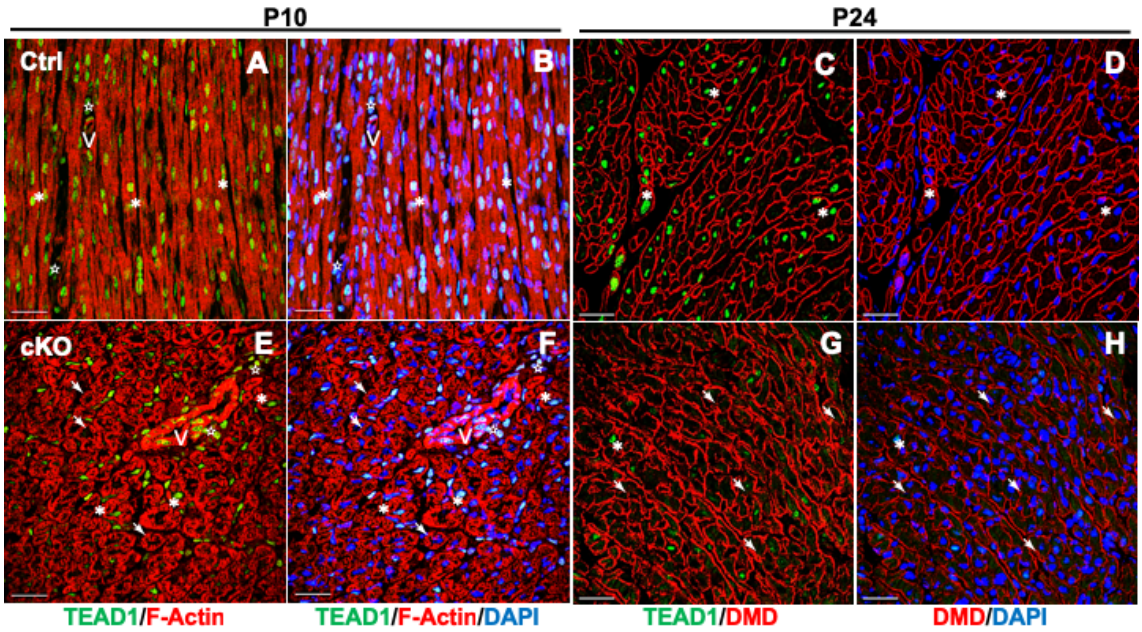

Figure 19. ***Gradual cardiomyocyte-specific inactivation of Tead1 in pTead1-cKO mutants during postnatal period.*** *(**A** and **B**) panels show fluorescent images of P10 control heart sections in which the vast majority of cardiomyocytes is TEAD1^{pos} (asterisk), whereas almost all cardiomyocytes in pTead1-cKO mutant hearts are TEAD1^{neg} (panels **E**, **F**, arrows). Stars denote non-cardiomyocyte population cell. (**G** and **H**) show that almost all cardiomyocytes are surrounded by Dystrophin (DMD) in P24 pTead1-cKO mutants and are TEAD1^{neg} (arrows). Cardiomyocytes in control hearts (panels **C**, **D**) are TEAD1^{pos} (asterisk). V – vessels; green – TEAD1, red –DMD, blue – DAPI. Scale bar: 30 µm.*

As a next step, isolated cardiomyocytes from different postnatal stages were used to determine *Tead1* mRNA levels in control and mutant animals. *Tead1* mRNA expression levels in isolated early postnatal (P3) pTead1-cKO cardiomyocytes were reduced by approximately 3-times compared to controls (Figure 20A) whereas in late postnatal cardiomyocytes (P15-P18), *Tead1* mRNA transcript levels in pTead1-cKO decreased 12-times in comparison to controls (Figure 20A). Western blot analysis of P17 pTead1-cKO mutant hearts revealed approximately a 4-fold decrease of TEAD1 protein in comparison to control hearts (Figure 20B). Taken together, these data indicate an effective age-dependent inactivation of TEAD1 in postnatal cardiomyocytes of pTead1-cKO mutants.

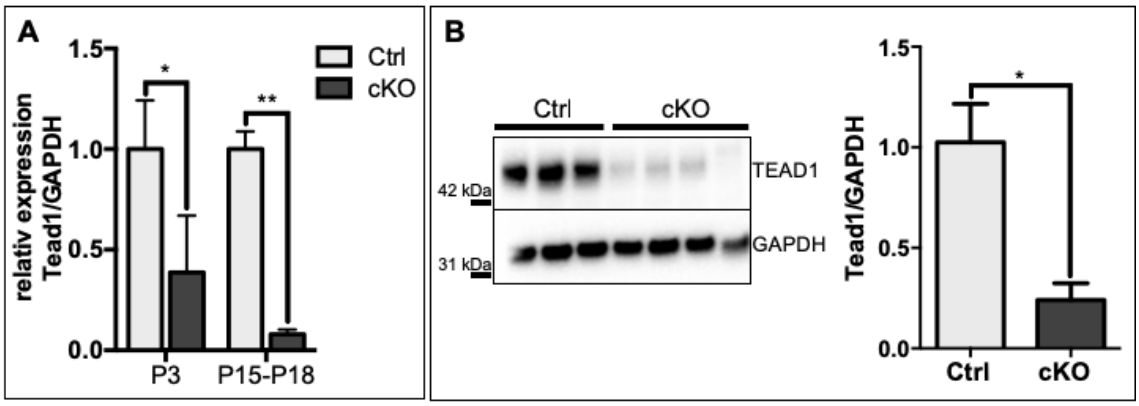

Figure 20. ***Reduced TEAD1 mRNA and protein levels in pTead1-cKO mice.*** *(**A**) The mean Tead1 expression in isolated pTead1-cKO cardiomyocytes) is 2.5-fold reduced in P3 mice (n=3) and 12.5-fold reduced in P15-P18 mice (n=3) in comparison to their age-matched controls (n=3). Tead1 expression levels are normalized to Gapdh expression. (**B**) Western blot and corresponding densitometry measurements of heart protein lysates at P17 show reduced TEAD1 levels of approximately 25% in pTead1-cKO hearts (n = 4) in comparison to TEAD1 protein content in control hearts (n = 3). Protein levels of TEAD1 are normalized to GAPDH protein levels. Data are means ± SD, ns = not significant (P ≧ 0.05), ∗ = P < 0.05, ∗∗ = P < 0.005.*

The present study documented that effective deletion of *Tead1* in postnatal cardiomyocytes culminated in the lethality of pTead1-cKO mice between P11 – P30, while the heterozygous littermates (*MCK-Cre::Tead1$^{fl/+}$*, referred to as control) had a normal life span (Figure 21A). There were no significant differences in body weight and heart weight to tibia length ratio between pTead1-cKO and control animals at P12 (Figures 21B and 21C).

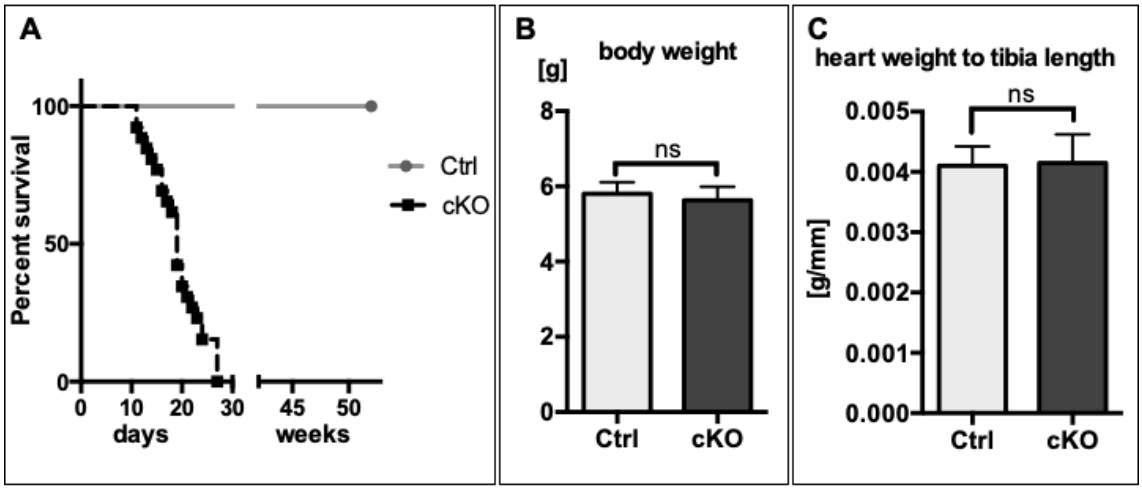

Figure 21. ***pTead1-cKO mice die postnatally between P11 and P28.*** *(**A**) Kaplan-Meier curve shows the survival of pTead1-cKO mice (n = 24) in comparison to control littermates (n = 9). Note that pTead1-cKO mice die between P11 and P28. (**B** and **C**) are quantifications of the body weight and heart weight to tibia length demonstrating no significant changes in these parameters between pTead1-cKO (n = 3) and control (n = 6) mice at P12. Data are means ± SD, ns = not significant (P ≧ 0.05).*

Next, pTead1-cKO hearts were examined macroscopically and microscopically at different time points. All pTead1-cKO mice conspicuously displayed dilated hearts accompanied by thinner left and right ventricular walls in comparison to control littermates (Figures 22A, 22B, 22D and 22E). Morphometric analysis showed that the left and right ventricular wall thickness of P16 pTead1-cKO animal hearts were 2-fold and 1.5-fold, respectively, decreased compared to control hearts (Figures 22G and 22H).

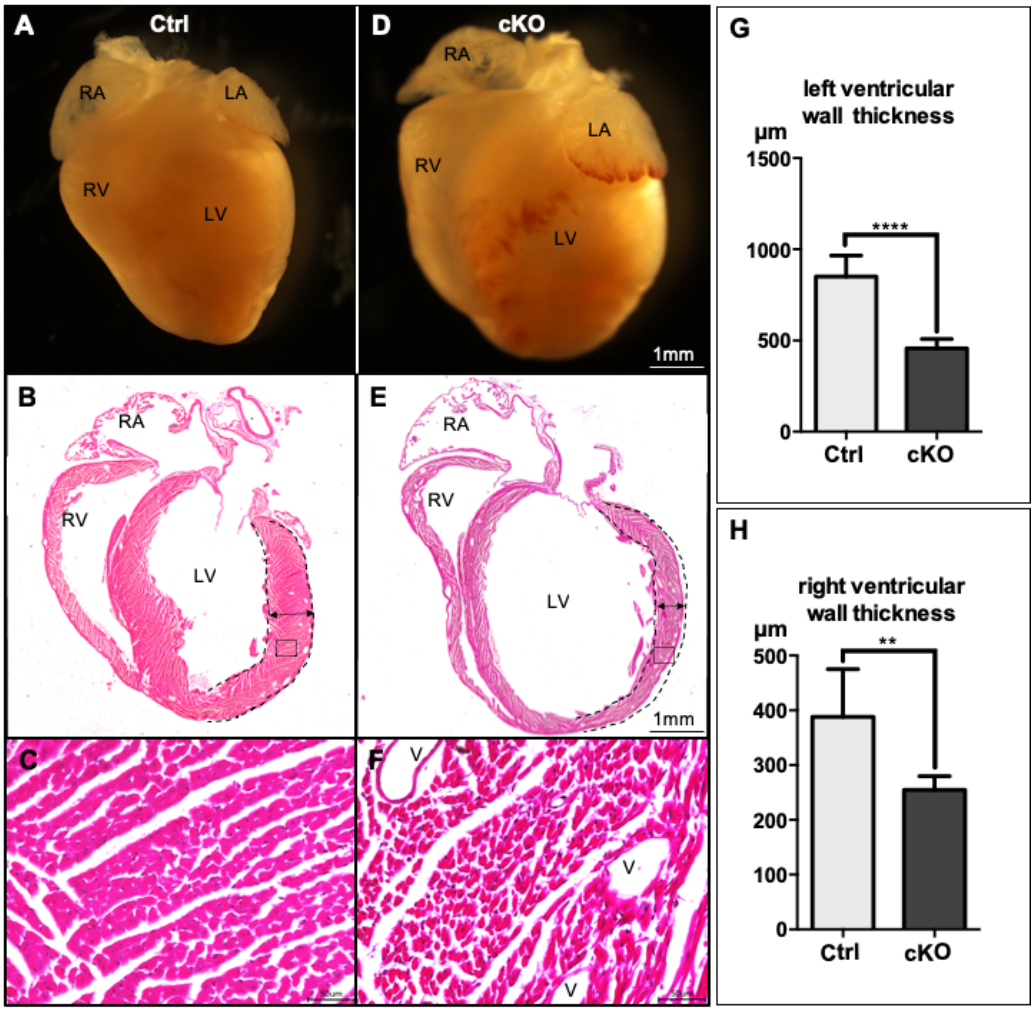

Figure 22. ***Dilated ventricles and thin myocardial walls in P16 pTead1-cKO hearts.*** *(**A** and **D**) macroscopic views comparing hearts from P16 pTead1-cKO and control littermates. pTead1-cKO hearts (D) display dilated left and right ventricles. (**B** and **E**) Microscopic view of paraffin sections of corresponding hearts. The left-ventricular wall and interventricular septum of pTead1-cKO (E) are thinner in comparison to control (B). (**C** and **F**) are detailed views of the corresponding left ventricular walls. Notice that the intercellular space in left ventricular wall of pTead1-cKO (F) is augmented in comparison to control (C). RA – right atrium, LA – left atrium, RV – right ventricle, LV – left ventricle, V – vessel. (**G**) The mean value of left ventricular wall thickness in control hearts is 851 µm (n = 3) and in pTead1-cKO hearts is 456 µm (n = 3). (**H**) The mean value of right ventricular wall thickness of control hearts is 388 µm (n = 3) and of pTead1-cKO hearts is 255 µm (n = 3). Data are means ± SD, **** = P < 0.001, ** = P < 0.005. Scale bar in C and F: 50 µm.*

Moreover, morphometric analysis revealed that pTead1-cKO cardiomyocytes of P16 animals were 1.2-times longer and 1.2-times thinner than control cardiomyocytes. (Figure 23A). Histogram distribution of the measured cardiomyocyte length and width showed that pTead1-cKO cardiomyocytes are shifted towards longer and thinner morphology compared to controls (Figure 23B), which was further confirmed by electron microscopy (Figure 24).

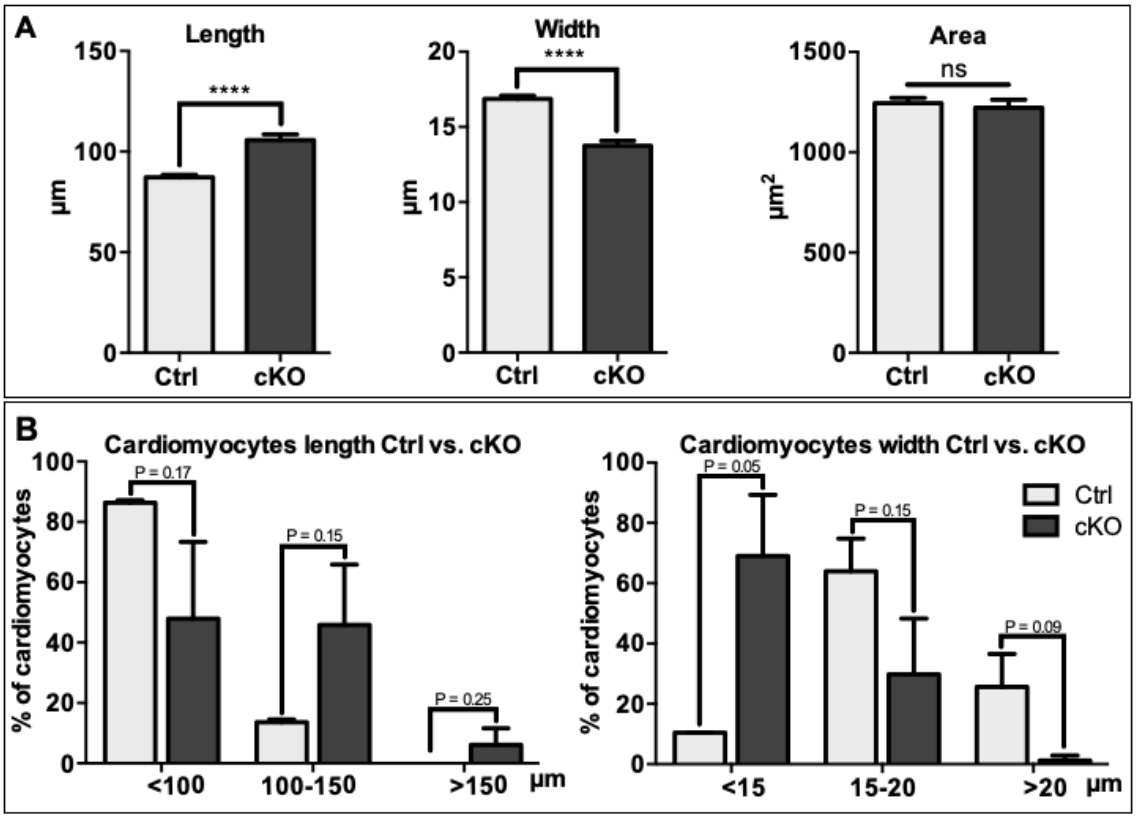

Figure 23. ***Shift of pTead1-cKO cardiomyocytes towards longer and thinner morphology (P16).*** *(**A**) Cardiomyocytes show significant length differences between control (mean length 87 µm, n=3) and pTead1-cKO mice (mean length 106 µm, n=3). Conversely, the cardiomyocytes width of pTead1-cKO mutant is reduced (mean width 14 µm, n=3) in comparison to controls (mean width 17 µm, n=3). There is no significant difference in cardiomyocyte area between control (mean area 1244 µm², n=3) and pTead1-cKO (mean area 1223 µm², n=3). (**B**) Length and width distribution of pTead1-cKO cardiomyocytes is shifted towards longer and thinner cardiomyocyte morphology compared to controls. Data are means ± SD, ns = not significant (P ≧ 0.05), **** = P < 0.001.*

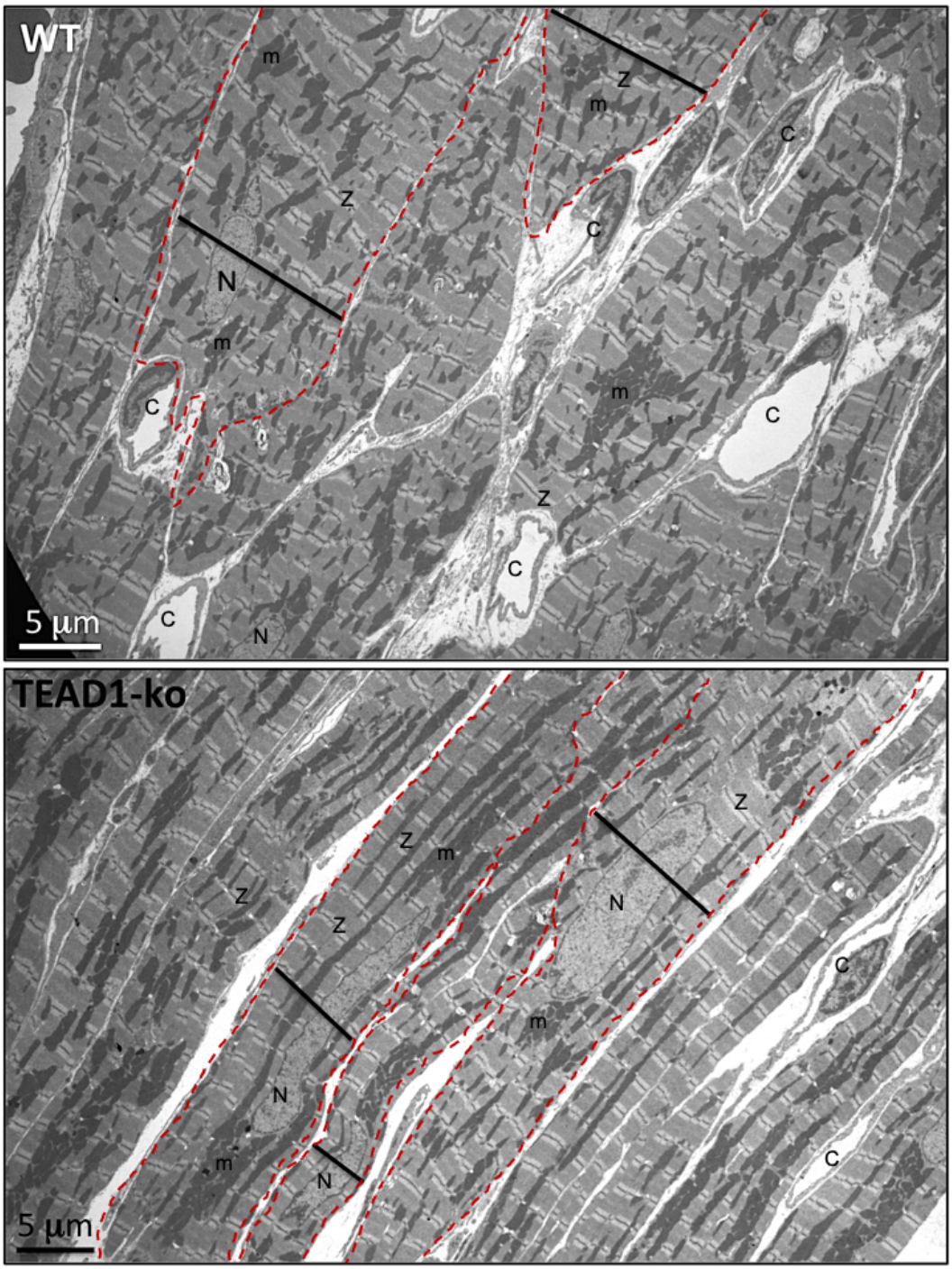

Figure 24. ***Representative TEM images of the left ventricle comparing the width*** *(black lines)* ***of individual cardiomyocytes at the nuclear level in control and pTead1-cKO mice (P16).*** *Note that cardiomyocytes (outlined in red) in pTead1-cKO hearts (**lower panel**) are thinner in comparison to control hearts (**upper panel**). N – nuclei, C – capillary, Z – Z-disks, m – mitochondria.*

Magnetic Resonance Imaging (MRI) analysis of left ventricular parameters of 12 controls and 12 age-matched pTead1-cKO hearts (between P10 and P18) revealed contractile dysfunction in pTead1-cKO mice (Figures 25A and 25B). In particular, left ventricular ejection fraction (LVEF), which is an important

parameter for proper heart function, decreased below 40 % in pTead1-cKO mutant and averaged 27 %, in comparison to approximately 60 % in control mice (Figure 25C). The severe reduction of LVEF provides a strong evidence for contractile heart insufficiency in pTead1-cKO mice.

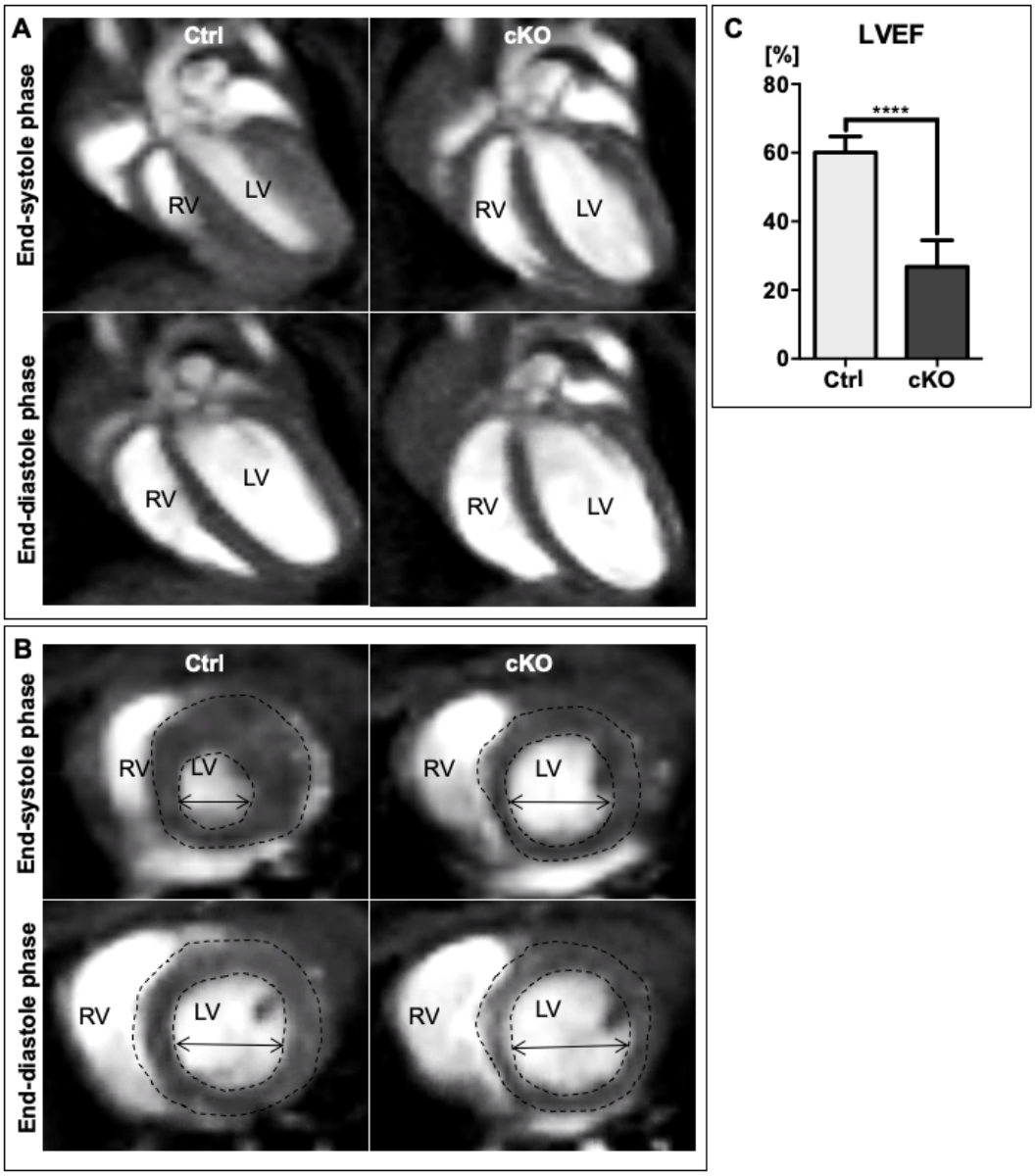

Figure 25. ***Contractile heart dysfunction in pTead1-cKO animals.*** *(**A**) MRI images show representative four chamber views of control and pTead1-cKO mutant hearts in end-systole and end-diastole phases. pTead1-cKO hearts display contractile dysfunction in systole phase and are massively dilated in diastole phase compared to control hearts (P16). (**B**) Short axis view visualizes the dilatation of the pTead1-cKO heart in systole and diastole compared to control heart (P16). RV – right ventricle, LV – left ventricle. (**C**) Quantitative reduction of LVEF in pTead1-cKO mice (n = 12) with the mean value of 27% in comparison to controls (n = 12) with the mean value of 60% (P10-P18). Data are means ± SD; **** = P < 0.001.*

TEM and immunofluorescent techniques were employed to study ultrastructural alterations of the myocardium in pTead1-cKO mutants. TEM analysis revealed that cardiomyocytes from pTead1-cKO mutant hearts are smaller in size and surrounded by numerous fibroblasts accompanied by massive depositions of thick collagen fibers (Figure 26). These findings were confirmed by immunolabeling for the major fibrillar collagen type I in combination with laser confocal microscopy. The images presented in Figure 27 show that collagen fibers are more abundant in pTead1-cKO in comparison to controls. Taken together, accumulation of fibroblasts and deposition of collagen fibers might contribute to contractile heart-dysfunction in pTead1-cKO mutants.

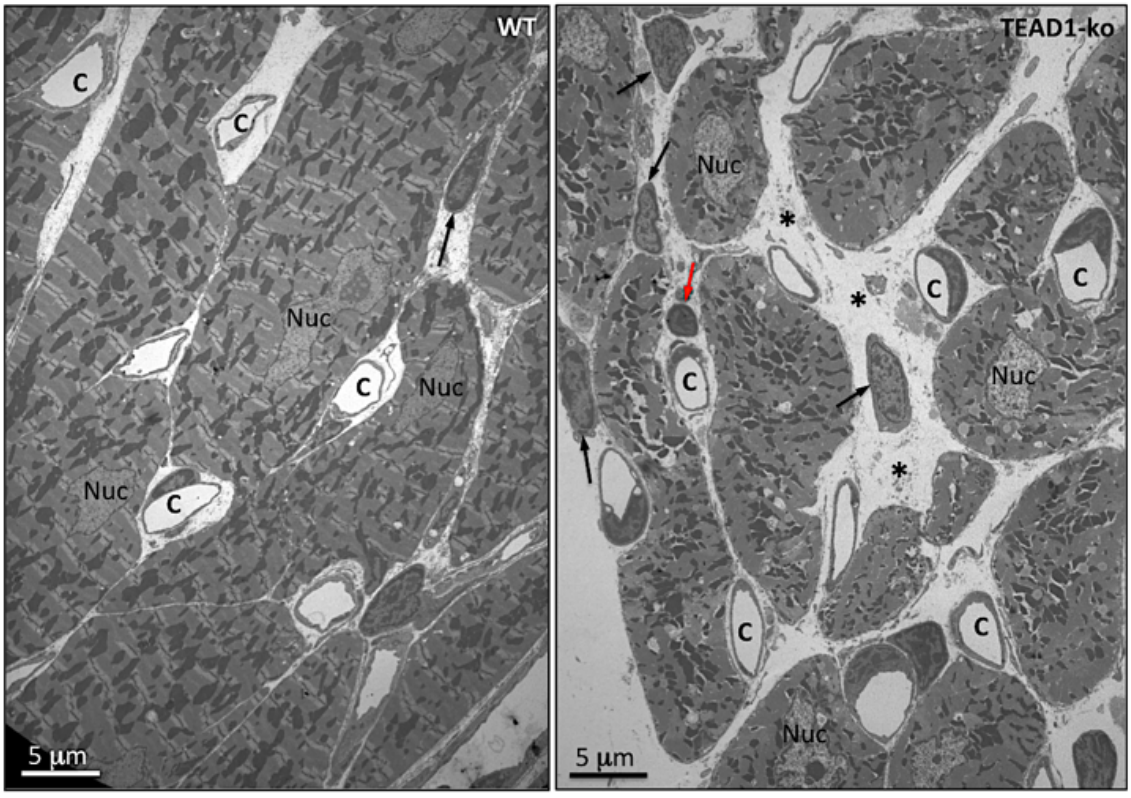

Figure 26. ***Representative TEM images comparing the left heart ventricle in control and pTead1-cKO mice (P16).*** *Note numerous fibroblasts (arrows) and severe deposition of collagen fibers (asterisk) in pTead1-cKO (**right panel**) hearts compared to control counterparts (**left panel**). Nuc – nuclei, C – capillary, red arrow – lymphocyte.*

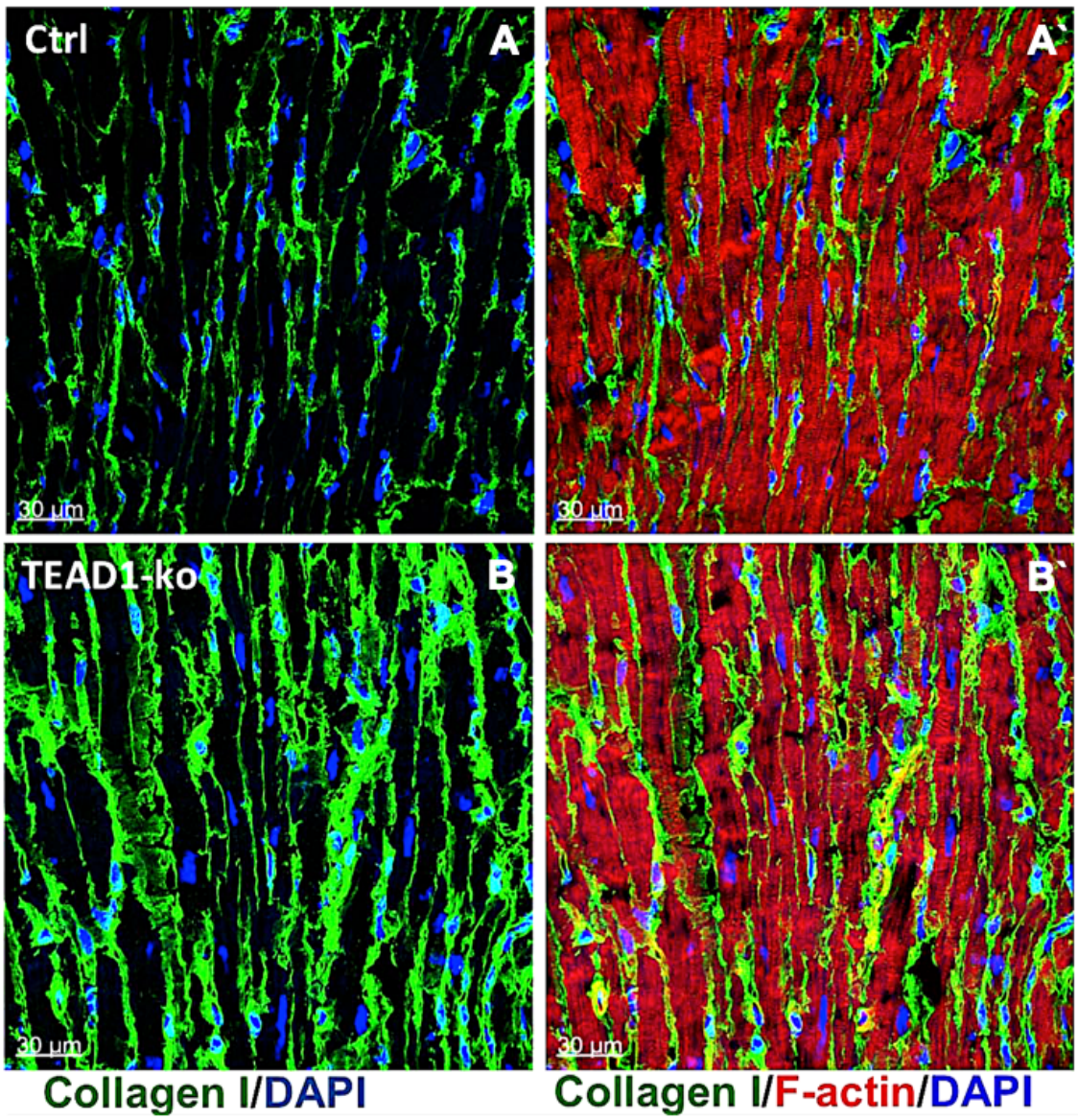

Figure 27. ***Increased fibrosis in pTead1-cKO mutants (P16).*** *Confocal micrographs displaying an increased abundance of collagen I fibers (green) in pTead1-cKO (**B**) compared to control (**A**) hearts. Nuclei are labeled in blue, F-actin in red. Scale bar: 30 µm.*

Multiple studies have shown that tightly controlled processes of postnatal cardiomyocyte proliferation and apoptosis have a fundamental impact on the onset of a cardiomyopathic phenotype (reviewed in [131, 132]). In order to investigate the proliferation capacity of postnatal control and pTead1-cKO mutant cardiomyocytes, 24 hours (h) EdU incorporation in P3 littermates was analyzed. The number of EdU^{pos} cardiomyocytes comprised 9 % of the total cardiomyocyte number in control hearts, whereas in pTead1-cKO hearts the number of EdU^{pos} cardiomyocytes was significantly lower (approximately 3 %). Representative

fluorescent images of EdU stained heart sections and quantifications of EdU^{pos} cardiomyocytes are depicted in the Figure 28.

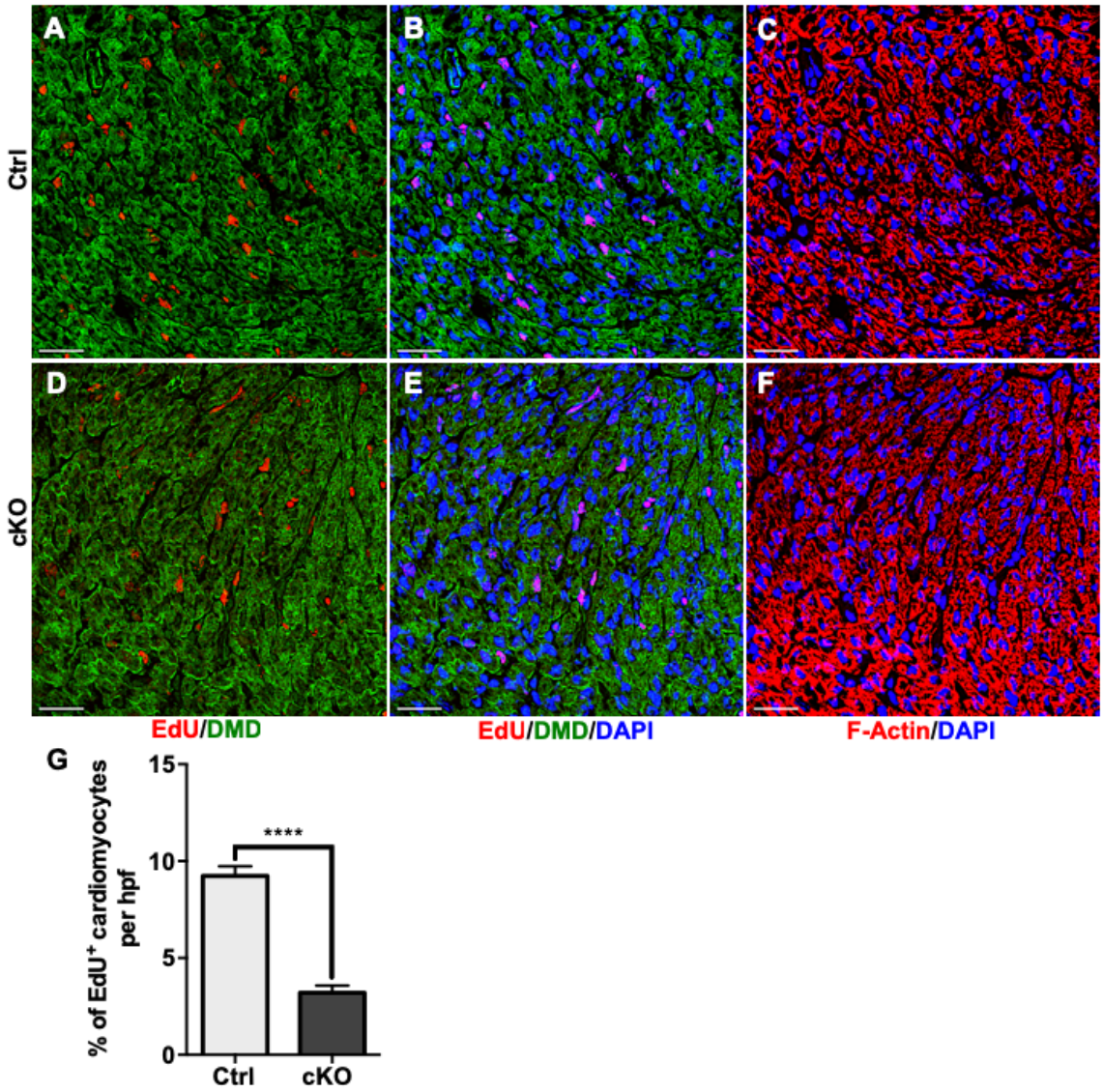

Figure 28. ***Reduced cardiomyocyte proliferation in pTead1-cKO (P3).*** *(**A** - **F**) Representative fluorescent images from sections of EdU-labelled hearts of P3 animals. The number of EdU^{pos} cardiomyocytes in pTead1-cKO hearts (D, E) is reduced in comparison to controls (A, B). Red – EdU, green – DMD, blue – DAPI. (**G**) Hearts of pTead1-cKO mutants (n = 3) manifest approximately 3-fold reduction of EdU^{pos} cardiomyocytes compared to control (n = 3). Data are means ± SD, ** = P < 0.005; hpf – high-power field. Scale bar: 30 µm.*

The number of apoptotic cardiomyocytes, defined here as TUNEL^{pos} cardiomyocytes, was increased by 3-fold in pTead1-cKO P12 hearts compared to control hearts (Figure 29). An increased apoptosis rate was even more pronounced at later time points (P24) (Figure 30).

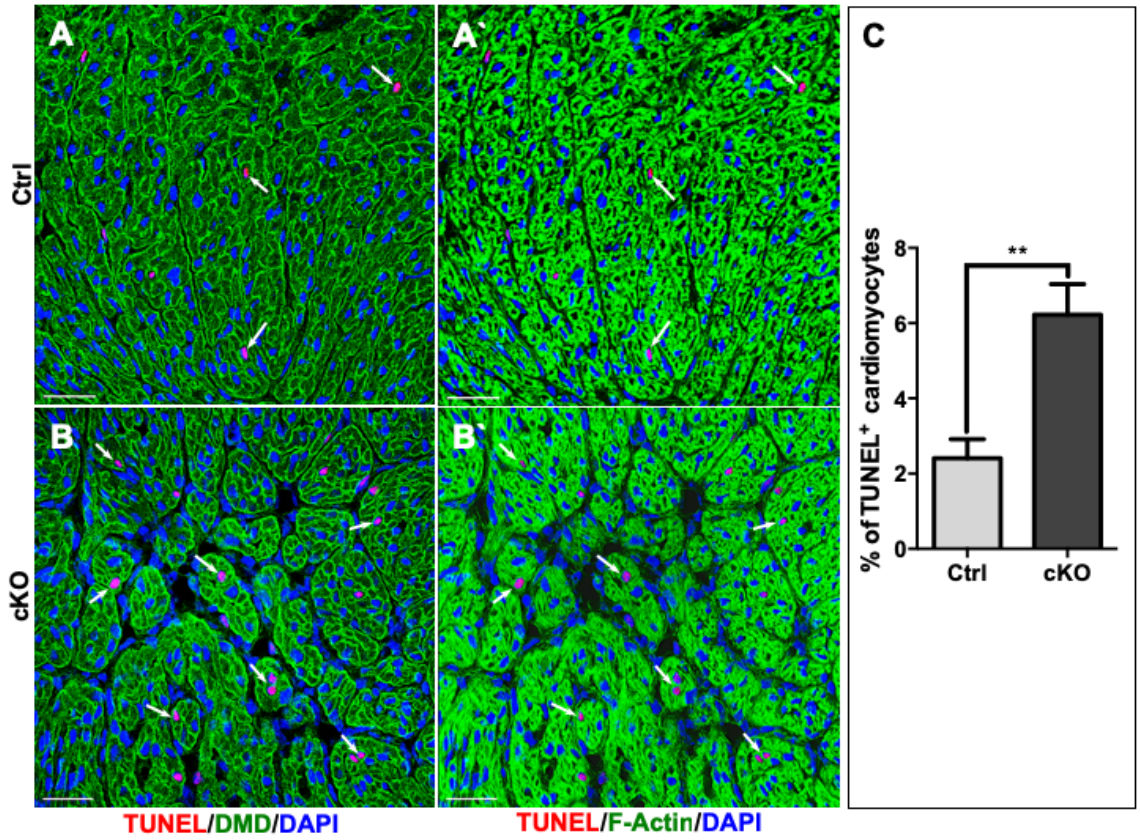

Figure 29. ***Increased cardiomyocyte apoptosis in P12 pTead1-cKO hearts.*** *Representative fluorescent images of heart sections of control (**A**) and pTead1-cKO (**B**) stained using TUNEL assay representing apoptotic cardiomyocytes (arrows, TUNEL^{pos}/DMD^{pos}/F-Actin^{pos}). Red – TUNEL, green – DMD / F-Actin, blue – DAPI. (**C**) pTead1-cKO hearts exhibit approximately 3-times more TUNEL^{pos} cardiomyocytes than control hearts. Data are means ± SD, ** = P < 0.005. Scale bar: 30 µm.*

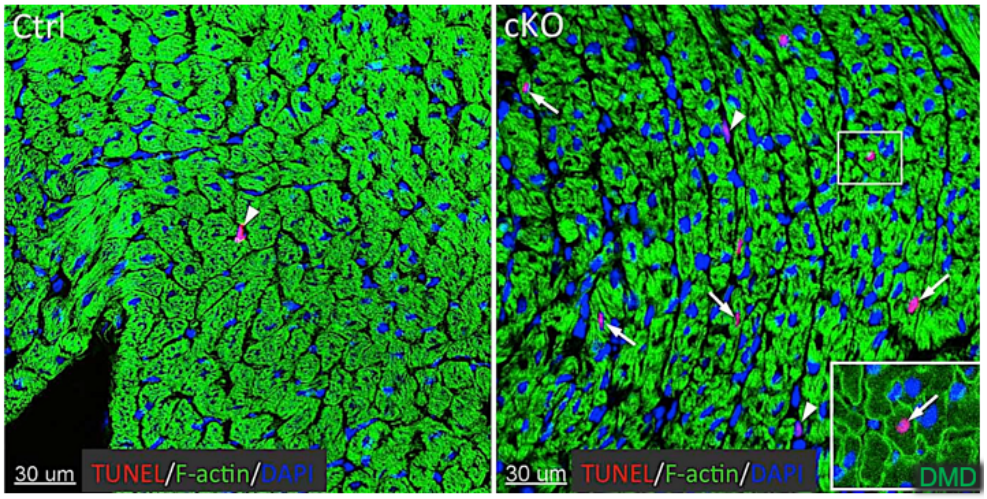

Figure 30. ***Increased number of apoptotic cardiomyocytes in pTead1-cKO mice compared to controls (P24).*** *Representative fluorescent images of heart sections stained using TUNEL assay. pTead1-cKO hearts (**right panel**) show more TUNEL^{pos} cardiomyocytes (arrows) than control hearts (**left panel**). Arrowheads denote apoptotic interstitial cells. Red – TUNEL, green – F-actin / DMD (boxed region), blue – DAPI.*

Taken together, these findings indicate that pTead1-cKO hearts are characterized by an imbalance between cardiomyocyte proliferation and cardiomyocyte cell death. The latter may predispose the pTead1-cKO hearts to develop severe myocardial fibrosis and contractile dysfunction.

3.4 Epitope tagged TEAD1 binds to MCAT-elements *in vitro*

In order to further study the function of TEAD1 in cardiomyocyte, we generated two expression constructs in which TEAD1 was tagged with either Flag-HA or GFP and expressed under control of *CAGG*-promotor. Generation of stable *Tead1*-overexpressing cell lines by random integration of transgenes was achieved by an IRES-puromycin-cassette and concomitant puromycin selection. For this purpose, HEK 293T cells were transfected with *Tead1*, *Tead1-GFP*, *Tead1-Flag-HA* and *GFP* alone as control vector. Figure 31 shows that immunolabeling signal of TEAD1-Flag-HA is confined to nuclei of transfected cells. As expected, the GFP signal in *GFP* control vector transfected cells was localized in both, the cytoplasm as well as in the nucleus in contrast to *Tead1-GFP* transfected cells where the signal was restricted to nuclei.

To analyze the abundance of fusion proteins, the lysates of transfected cells were validated by western blot with specific antibodies against GFP (GFP and TEAD1-GFP fusion protein) and HA (TEAD1-Flag-HA fusion protein). According to calculation, a 27 kDa band was detected in lysates of transfected cells with *GFP* control, an 80 kDa band in lysates of *Tead1-GFP* transfected cells and a 60 kDa band in lysates of *Tead1-Flag-HA* transfected cells (Figure 32A).

In order to test the functionality of the *Tead1*-overexpression constructs, dual-luciferase reporter assays (Figure 32B) with a TEAD1-Reporter construct containing four copies of TEAD1 consensus binding sites (CATTCCA) combined with a minimal promoter were performed as previously described in Günter *et al.* [84]. To monitor the transfection efficiency, *Renilla* Luciferase containing expression vector was co-transfected. Due to the fact that TEAD1 lacks a transactivation domain and is not able to activate transcription by itself, VGLL-2 (VITO-1) [84], a well-known TEAD1-cofactor, was co-transfected. Cells co-transfected with TEAD1 and VGLL-2 constructs displayed a 4.5-times higher reporter activity in comparison to transfection with TEAD1 in the absence of

VGLL-2. Co-transfection of TEAD1-GFP and VGLL-2 activated the luciferase reporter construct 4-times higher than single TEAD1-GFP transfection. Similarly, the luciferase activity in TEAD1-Flag-HA and VGLL-2 co-transfection was roughly 7-times higher compared to single transfection.

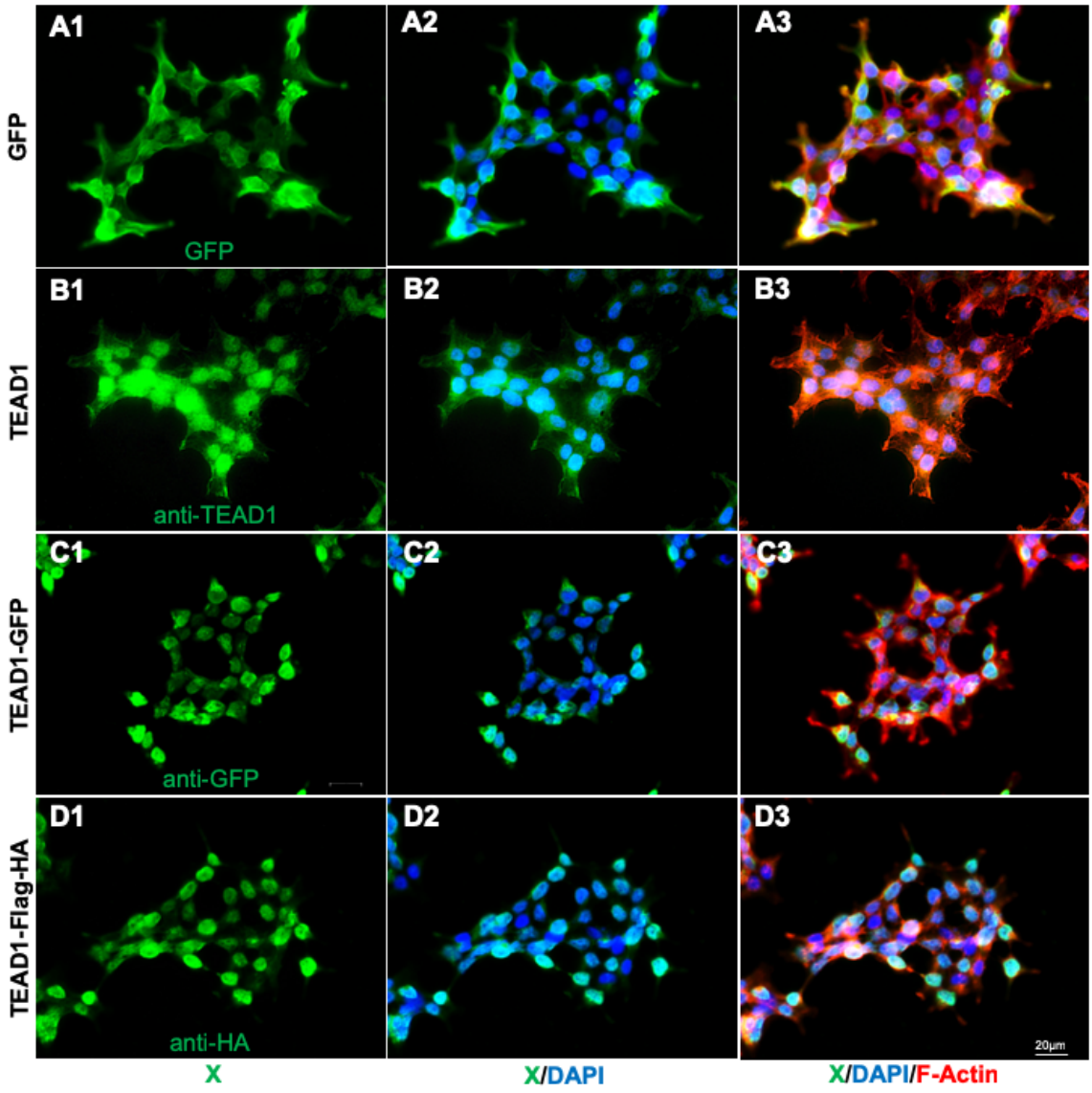

Figure 31. ***Nucleus-restricted localization of TEAD1-Flag-HA and TEAD1-GFP in transfected HEK 293T cells.*** *(**A**) In cells transfected with GFP control vector, GFP signal (green) localizes to cytoplasm and nuclei. (**B**) In cells transfected with Tead1, TEAD1 signal is detected in cell nuclei. (**C**) In Tead1-GFP transfected cells the GFP signal is restricted to nuclei. (**D**) In Tead1-Flag-HA transfected cells the HA signal (green) is restricted to nuclei. In all images - DAPI signal in blue marks nuclei and F-Actin in red marks the cytoplasm. Green – X = GFP / TEAD1 / HA. Scale bar: 20 µm.*

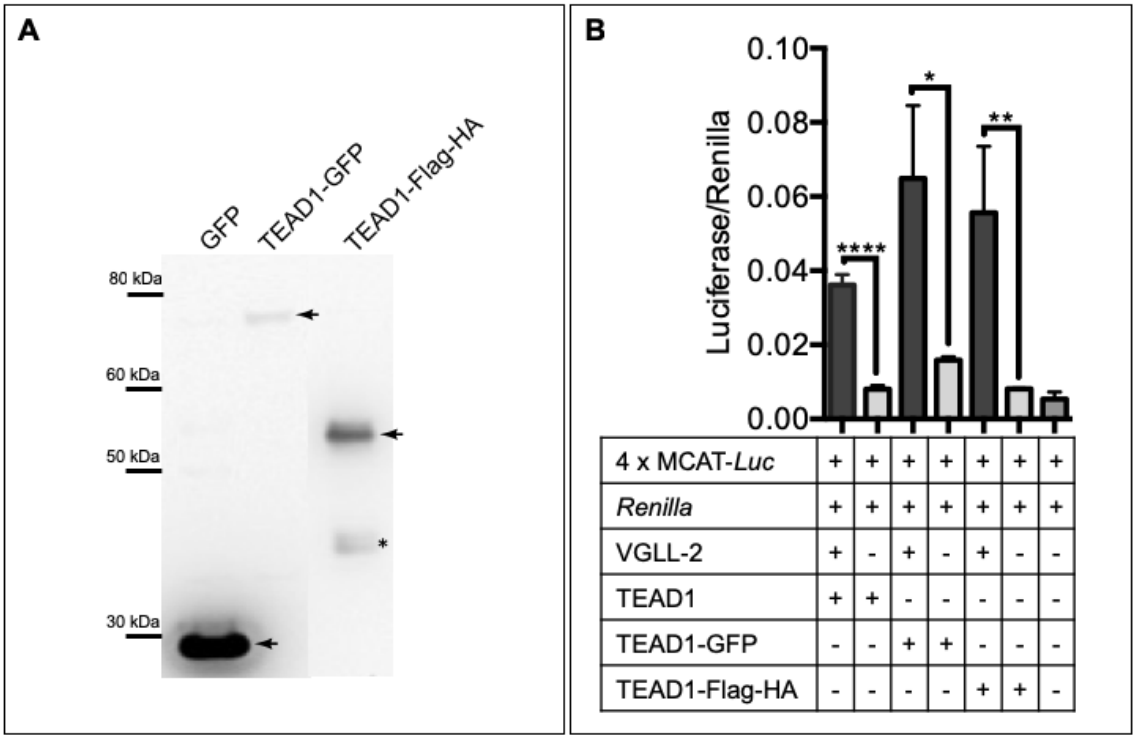

Figure 32. ***TEAD1-Flag-HA and TEAD1-GFP fusion proteins activate MCAT-elements in vitro.*** *(**A**) Western blot of lysates from HEK 293T cells transfected with vectors containing GFP; TEAD1-GFP and TEAD1-Flag-HA. Control GFP protein is represented by a 27 kDa band (arrow). TEAD1-GFP fusion protein is represented by a calculated 80 kDa band (53 kDa (TEAD1) + 27 kDa (GFP), arrow). TEAD1-Flag-HA fusion protein is represented by a calculated 60 kDa band (53 kDa (TEAD1) + 7 kDa (Flag-HA, arrow)). The asterisk indicates an unspecific band. (**B**) Dual-Luciferase reporter assay of transfected HEK 293T cells. Transfected cells with TEAD1 and VGLL-2, as a cofactor, activate the luciferase reporter 4.5-fold higher compared to TEAD1 single transfection. In cells transfected with TEAD1-GFP and VGLL-2, activation of luciferase is 4-fold higher than in cells transfected with TEAD1-GFP alone. TEAD1-Flag-HA transfected with VGLL-2 activate luciferase-reporter about 7-fold higher compared to TEAD1 single transfection. There is almost no activation of luciferase-reporter in untransfected control and single transfected cells. Data are means ± SD, ∗ = P < 0.05, ∗∗ = P < 0.005, ∗∗∗∗ = P < 0.001, n = 3.*

3.5 Cardiomyocyte-specific overexpression of *Tead1-Flag-HA* rescues the loss of endogenous *Tead1* and results in increased cardiomyocyte proliferation

In order to analyze the impact of an elevated *Tead1* expression in cardiomyocytes a *Rosa26*-based CRE-inducible *Tead1-Flag-HA* overexpression mouse line (*Tead1-Flag-HA*$^{Tg/Tg}$) was generated. Figure 33 depicts a scheme of the overexpression constructs design encoding a *Tead1* cDNA tagged with *Flag-HA* and *PolyA*-tail under the transcriptional control of a *CAGG* promoter, which is inserted between 1st and 2nd exons of *Rosa26* locus [133]. The conditional

activation of *Tead1-Flag-HA* is achieved by a Cre-mediated removal of floxed *PGK-neo* cassette in the early myocardium E7.5 mediated by the *XMLC2-Cre* deleter allele [109].

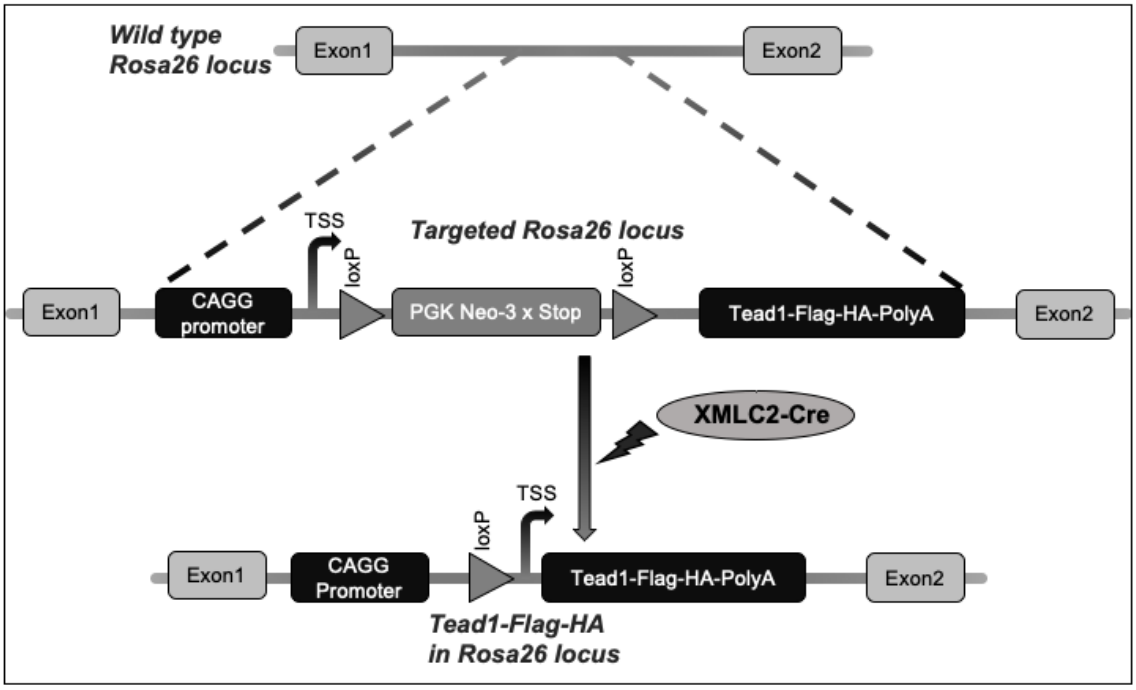

Figure 33. ***Schematic view of Tead1-Flag-HA recombination in Rosa26 locus.*** *The upper part resembles the WT Rosa26 locus. The middle part displays the modified Rosa26 locus containing a CAGG promoter followed by a transcriptional stop cassette (PGK Neo), which is flanked by two loxP sites and a Tead1 cDNA fused to a Flag-HA double-tag. The lower part resembles the mutant allel after Cre-mediated deletion of transcriptional stop cassette.*

Heterozygous (*XMLC2-Cre::Tead1-Flag-HA*$^{Tg/+}$) as well as homozygous (*XMLC2-Cre::Tead1-Flag-HA*$^{Tg/Tg}$) gain-of-function (GOF) mice (later referred to as e(embryonic)Tead1-cOE) have a normal life span similar to control (Cre^{neg}) mice (data not shown). Macroscopic examination of homozygous overexpression hearts revealed no obvious alterations in comparison to hearts from control littermates (Cre^{neg} *Tead1*$^{Tg/Tg}$ littermates) (Figure 34A). At P16, eTead1-cOE mice displayed a slightly increased weight in comparison to their control littermates, however, there were no significant differences in the heart weight to tibia length ratio in control and eTead1-cOE mice (Figures 34B and 34C). Isolated cardiomyocytes of P16 eTead1-cOE hearts were 6 % increased in length by an unaltered width, which resulted in an 8.5% increased cross-sectional area

compared to controls (Figure 34D). TEM analysis revealed no ultrastructural alterations of eTead1-cOE cardiomyocytes (Figure 35).

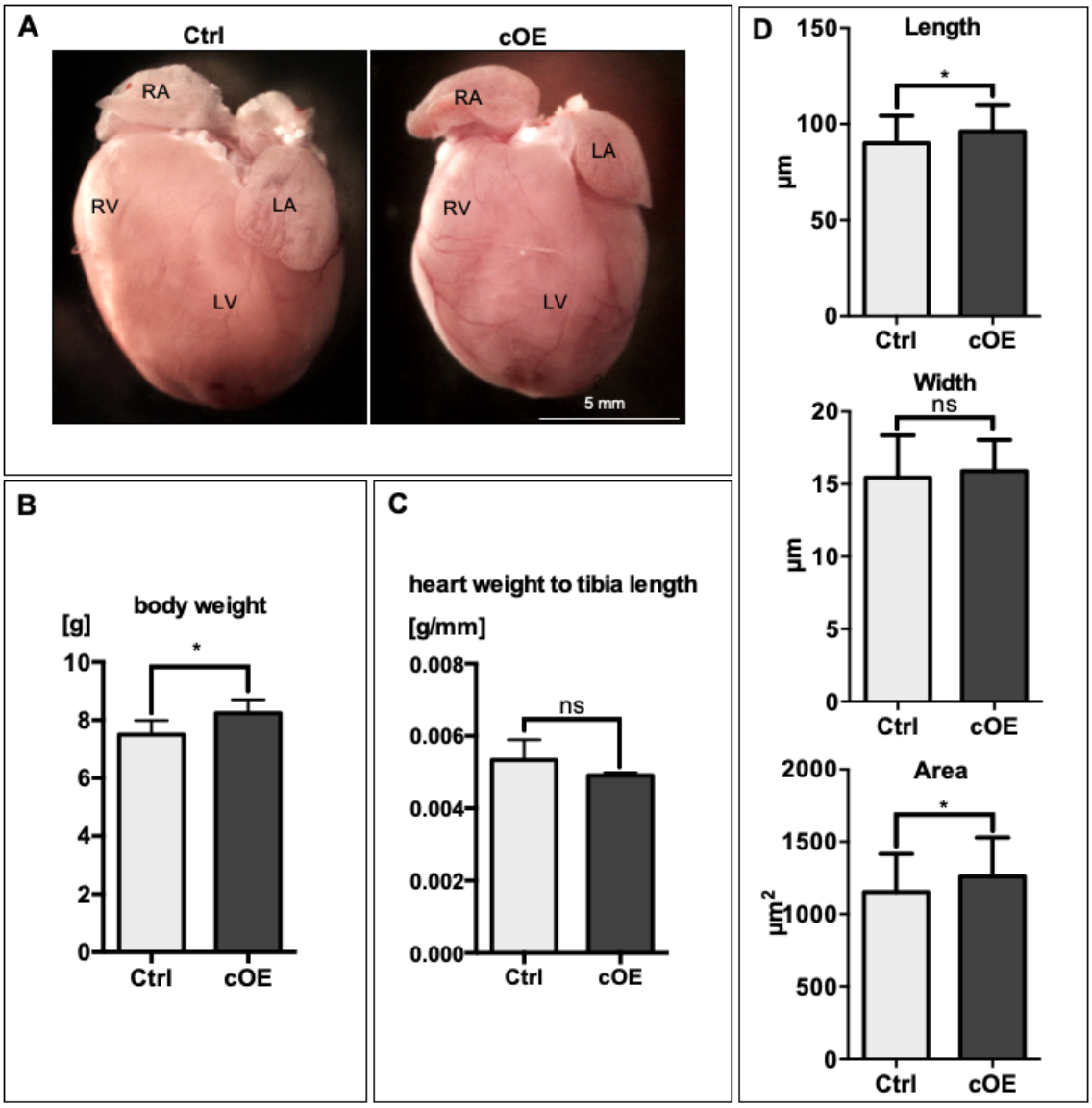

Figure 34. ***No major macroscopic differences between eTead1-cOE and control hearts (P16).*** *(**A**) Macroscopic view of P16 hearts shows no obvious morphological differences between eTead1-cOE and controls. RA – right atrium, LA – left atrium, RV – right ventricle, LV – left ventricle. (**B**) Slight increase in the body weight of eTead1-cOE mice (mean 8.2 g, n=5) compared to controls (mean 7.5 g, n=6) at P16. (**C**) eTead1-cOE mice display no significant differences in the heart weight to tibia length ratio compared to controls at P16. (**D**) Isolated cardiomyocytes from P16 eTead1-cOE hearts (n=3) show a slight increase in cell length (mean 96 µm) compared to control (mean 90 µm, n=3). The width of cardiomyocytes in eTead1-cOE mice (mean 15.9 µm, n = 3) is not significantly different from controls (mean 15.4 µm, n = 3). The cardiomyocyte area in eTead1-cOE (mean area 1261 µm^2, n = 3) is slightly bigger compared to controls (mean area 1153 µm^2, n = 3). Data are means ± SD, ns = not significant (P ≧ 0.05), ∗ = P < 0.05, ∗∗ = P < 0.005, ∗∗∗∗ = P < 0.001.*

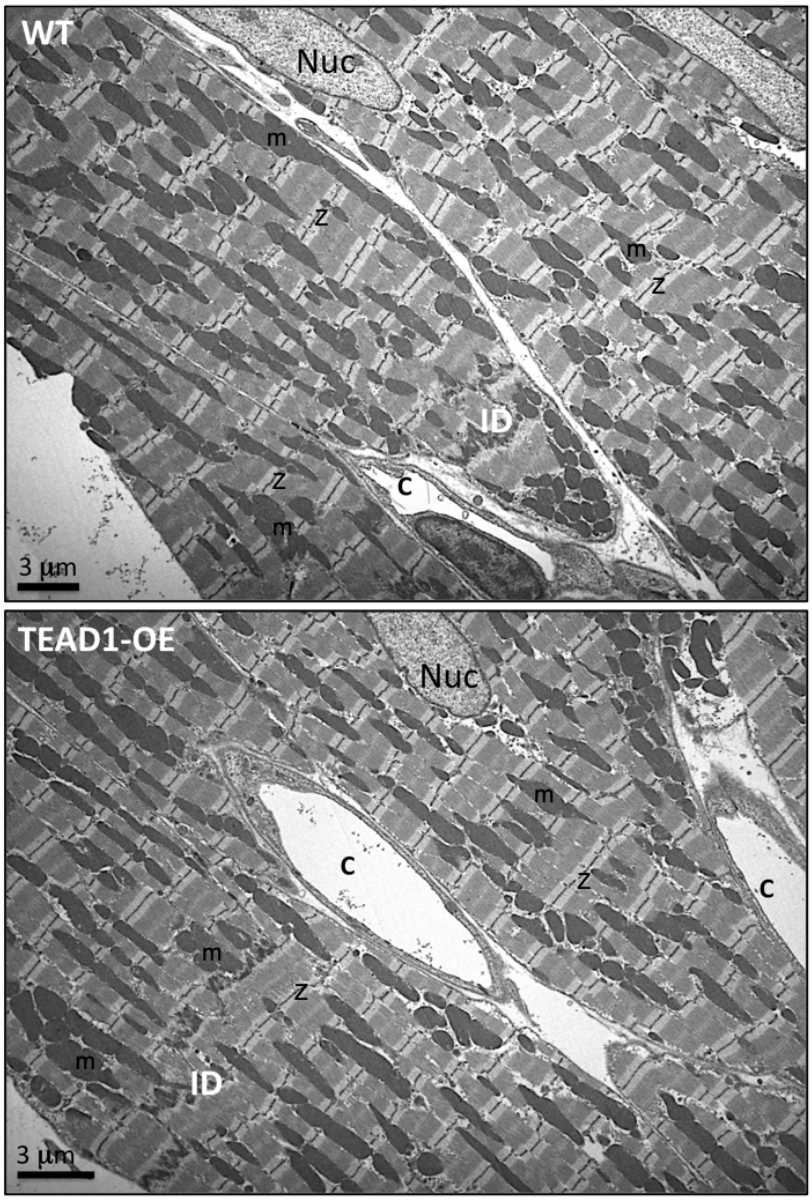

Figure 35. ***TEM images of control*** *(upper panel)* ***and eTead1-cOE*** *(lower panel)* ***cardiomyocytes demonstrate no ultrastructural differences between groups (P16)****. NUC – nucleus, ID – intercalated disk, C – capillary, Z – Z-disks, m – mitochondria.*

Immunohistochemical analysis of P16 eTead1-cOE mice hearts showed enhanced TEAD1 signal in cardiomyocytes compared to control hearts. As expected, HA as well as FLAG epitope tagged TEAD1 localized exclusively to cardiomyocyte nuclei detected in eTead1-cOE cardiomyocytes as shown in Figures 36A - 36F. These observations were in line with qRT-PCR results, which displayed a 2.5-fold (P2-P3) or a 13-fold (P16-17) increased *Tead1* level in isolated cardiomyocytes from *Tead1* GOF mice (Figure 36G).

Western blot analysis (anti-HA antibody) of heart protein lysates detected TEAD1-Flag-HA fusion protein exclusively in eTead1-cOE hearts (Figure 36H).

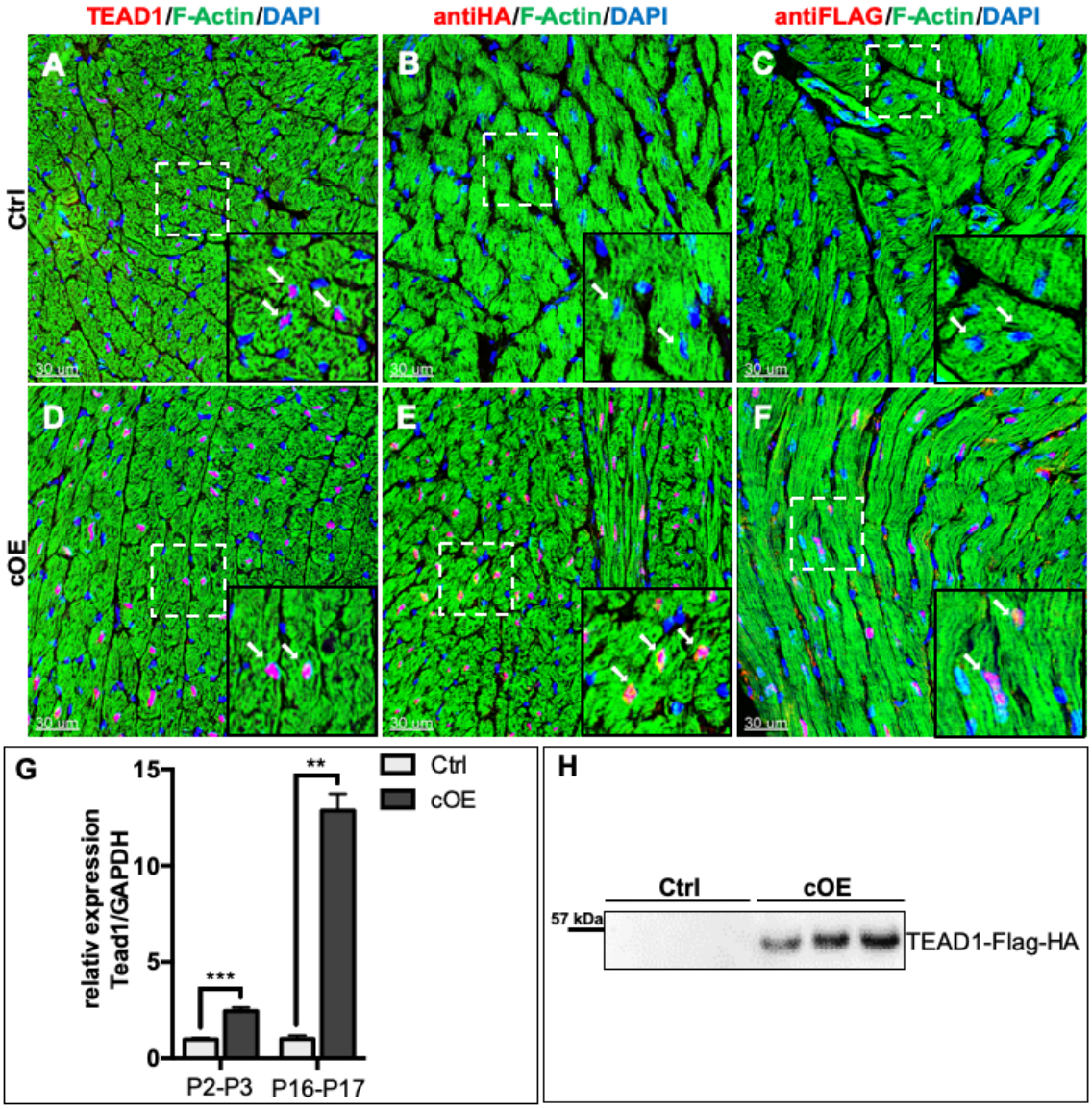

Figure 36. ***Cardiomyocyte restricted Tead1-Flag-HA overexpression in eTead1-cOE mice (P16).*** *(**A** – **F**) Representative fluorescent images of P16 eTead1-cOE and P16 control heart sections. HA and FLAG signals are absent in controls (panels B, C) and detectable in cardiomyocyte nuclei of eTead1-cOE hearts (panels E, F; labeled with arrows in boxed regions at higher magnification). Note that endogenous TEAD1 protein is detected in eTead1-cOE as well as in control (panels A, D; labeled with arrows in boxed regions at higher magnification). Red – TEAD1 / FLAG / HA; green – F-actin; blue – DAPI. (**G**) The mean expression of Tead1 in isolated P2-P3 cardiomyocytes is 2.5-times increased in eTead1-cOE mice (n=3) compared to control (n=3). Isolated cardiomyocytes from P16-P17 eTead1-cOE mice (n=3) express 13-times more Tead1 than their control counterparts (n=3). Tead1 expression levels were normalized to Gapdh expression. Data are means ± SD, ns = not significant (P ≧ 0.05), ∗ = P < 0.05, ∗∗ = P < 0.005, ∗∗∗ = P < 0.002, n = 3. (**H**) Western bolt analysis shows detection of the TEAD1-Flag-HA fusion protein at the calculated size of 55 kDa by the use of a HA antibody exclusively in heart lysates of P16 eTead1-FlagHA overexpressing mice (n=3). Scale bar: 30 µm.*

The functionality of the *Tead1* GOF allele was validated on conditional *Tead1*-deficient genetic background. For this purpose, conditional *MCK-Cre::Tead1*$^{fl/fl}$ mice were crossed to *Tead1-Flag-HA*$^{Tg/Tg}$ mice to create *MCK-Cre::Tead1*$^{fl/fl}$ *Tead1-Flag-HA*$^{Tg/Tg}$ mice, referred to as p(postnatal)Tead1-Rescue mice (Figure 37A). These mice have a normal life span comparable to controls, whereas pTead-cKO mice died within 4 weeks after birth (Figure 37B) demonstrating the functionality of the exogenous *Tead1-Flag-HA* construct. Importantly, these data demonstrate that overexpression of *Tead1-Flag-HA* rescues the lethal heart phenotype of pTead1-cKO mice.

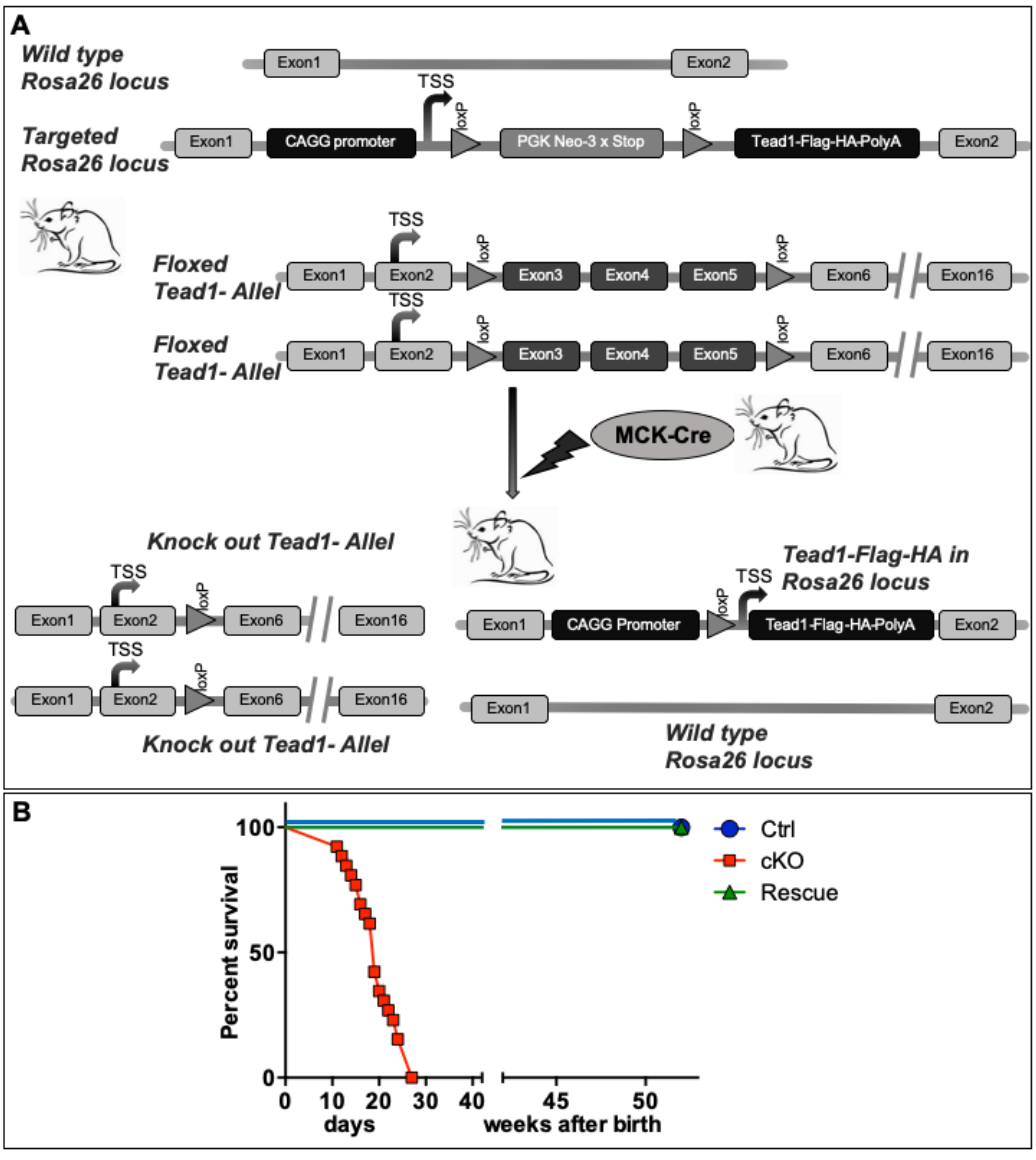

Figure 37. ***Survival of mice with cardiomyocytes specific Tead1 deletion is rescued by cardiomyocytes specific overexpression of Tead1-Flag-HA (pTead1-Rescue mice).*** *(**A**) Schematic illustration of MCK-Cre driven recombination in pTead1-Rescue mice. (**B**) Kaplan-Meier curve of the survival rate shows no differences in the life span of control (n = 5) and rescued mice (n = 5). All pTead1-cKO mutants (n = 24) died within first 4 weeks after birth. Blue – control; green – pTead1-Rescue; red – pTead1-cKO.*

As a next step, the proliferation capacity of embryonic and postnatal *Tead1-Flag-HA* overexpressing cardiomyocytes was analyzed based on EdU incorporation. The results presented in Figure 38 and 39 show that the number of proliferative (EdU^{pos}) cardiomyocytes was increased by approximately 1.5-fold in both, E12.5 and P3 Tead1-Flag-HA overexpressing mice in comparison to control littermates. Interestingly, Tead1 GOF hearts displayed a higher number of EdU^{pos} proliferating cardiomyocytes in the trabecular layer in comparison to the compact layer (Figures 38H and 38I).

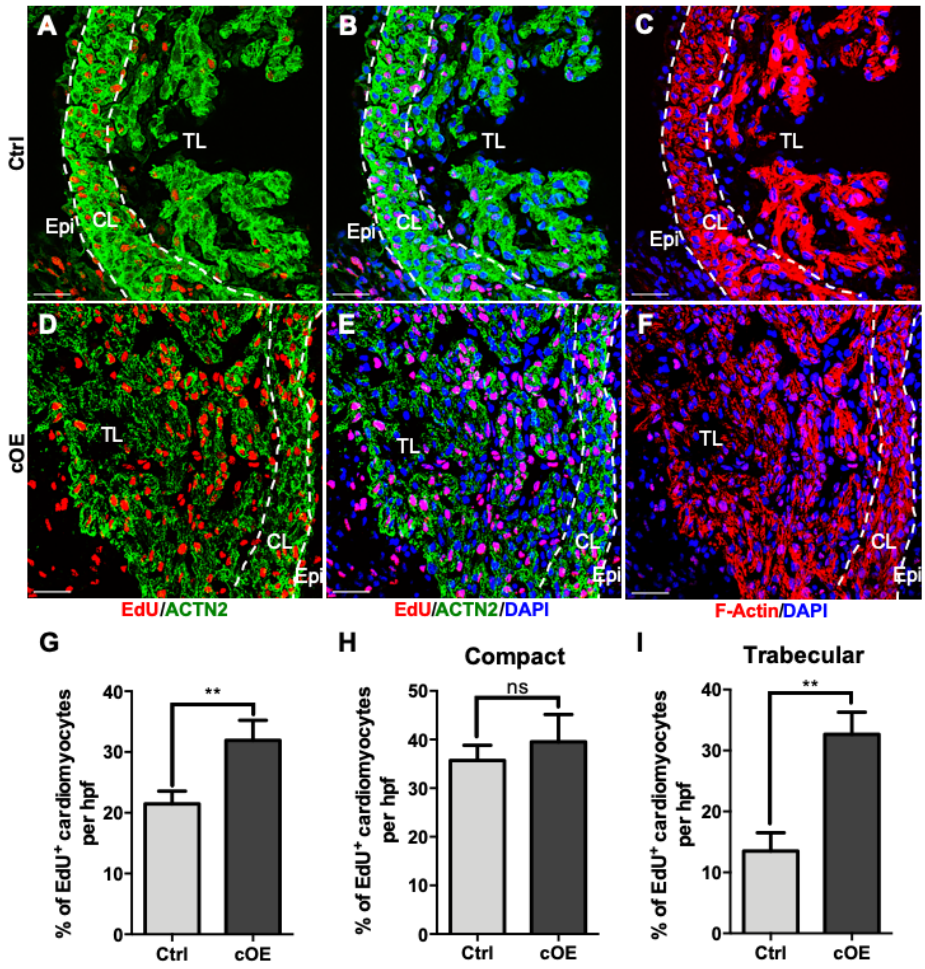

Figure 38. ***Increased proliferation of embryonic eTead1-cOE cardiomyocytes (E12.5).*** *(**A** - **C**) Representative fluorescent images of EdU-labelled E12.5 control hearts. (**D** - **F**) EdU-labeling in E12.5 eTead1-cOE heart sections displays increased number of EdU^{pos} (red) cardiomyocytes, especially in the trabecular layer of eTead1-cOE hearts. Of note, eTead1-cOE hearts are hypertrabeculated in comparison to control hearts. Red – EdU, green – ACTN2, blue – DAPI; TL – trabecular layer, CL – compact layer (outlined with dashed white line), Epi – epicardium. (**G**) eTead1-cOE hearts (n=3) comprise 32% and control hearts (n=3) approximately 21.5% of EdU^{pos} cardiomyocytes. (**H**) No difference in the number of EdU^{pos} cardiomyocytes are detected between compact layers of control (n=3) and eTead1-cOE hearts (n=3). (**I**) The number of EdU^{pos} cardiomyocytes in the trabecular layer of eTead1-cOE hearts (n=3) is 2.5-fold increased in comparison to control (n=3). Data are means ± SD, ns = not significant ($P \geqq 0.05$), ** = $P < 0.005$; hpf – high-power field. Scale bar: 30 µm.*

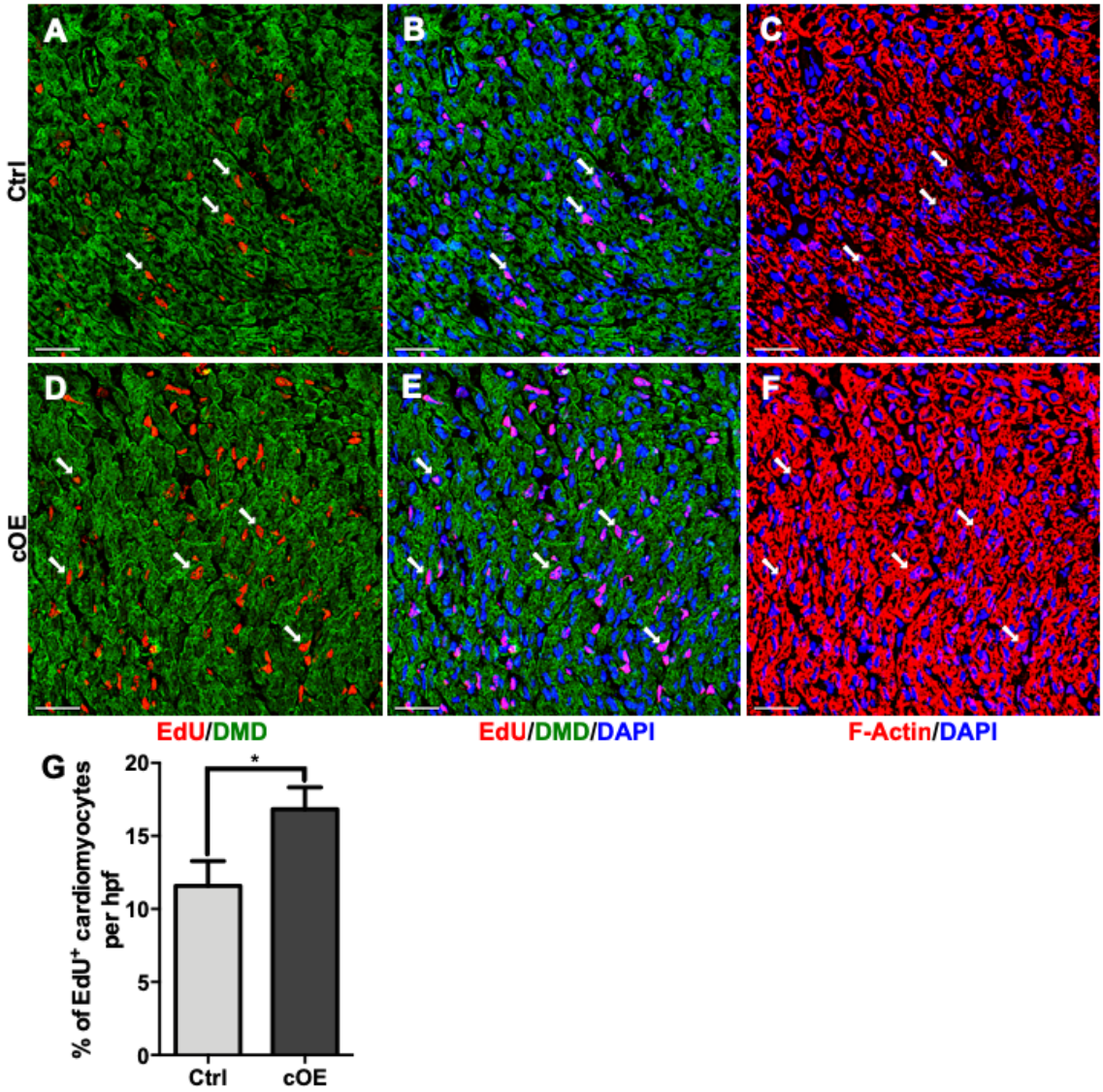

Figure 39. ***Increased cardiomyocyte proliferation in eTead1-cOE mutants at P3.*** *(**A** - **F**) Representative fluorescent images show increase in number of EdU^{pos} cardiomyocytes in eTead1-cOE hearts (D-F) compared to control (A-C). Red – EdU, green – DMD (dystrophin), blue – DAPI. (**G**) eTead1-cOE hearts (n=3) display about 17% and control hearts (n=3) approximately 11.5% of EdU^{pos} cardiomyocytes. Data are means ± SD, ∗ = P < 0.05; hpf – high-power field. Scale bar: 30 µm.*

In contrast, apoptosis rates at P12 displayed no significant differences in the number of TUNEL^{pos} cardiomyocytes in eTead1-cOE and control mice. Figure 40 depicts representative images resulting from TUNEL staining reactions and corresponding quantifications, which indicate comparable rates of TUNEL^{pos} cardiomyocytes (around 2%) in both groups.

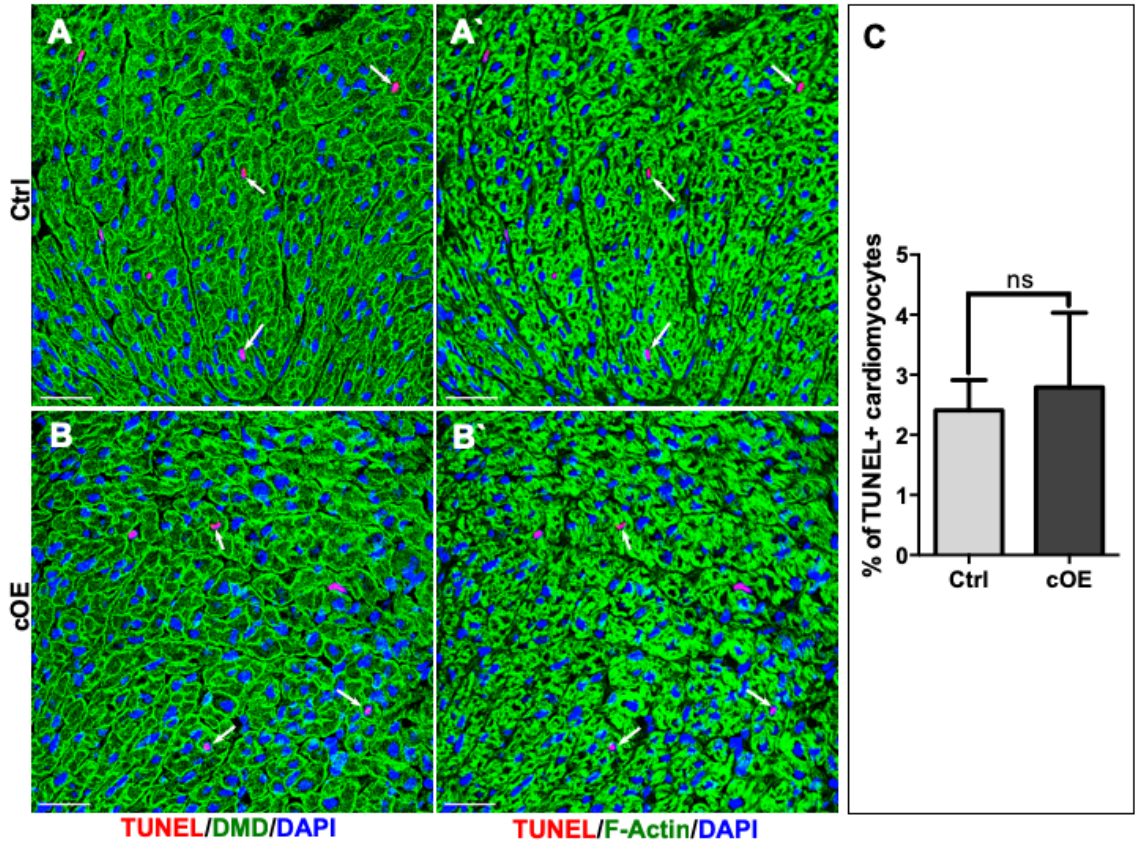

Figure 40. ***Confocal micrographs showing no differences in the number of TUNEL^{pos} cardiomyocytes in P12 control and eTead1-cOE hearts.*** *(**A** and **B**) TUNEL^{pos} cardiomyocytes (red) are indicated with arrows. Dystrophin (DMD) is immunolabeled in green (left panels), F-Actin is labeled with phalloidin633 in green (right panels) and nuclei are blue labeled in all panels. (**C**) eTead1-cOE (n=3) and control (n=3) hearts display comparable number of TUNEL^{pos} cardiomyocytes (around 2%). Data are means ± SD, ns = not significant (P ≧ 0.05). Scale bar: 30 µm.*

Taken together, increased cardiomyocyte proliferation in *Tead1* GOF mutants indicates a phenotypic shift of the heart towards a transient hyperplasia without morphological and functional alterations.

3.6 Altered TEAD1 expression influences proliferation and growth of isolated postnatal cardiomyocytes

For a more comprehensive analysis of postnatal *Tead1* knockout as well as *Tead1-Flag-HA* overexpressing cardiomyocytes, P3 cardiomyocytes from pTead1-cKO and eTead1-cOE mice were isolated and cultured for 2 days. Figure 41 compares the overall appearance of cultured control, pTead1-cKO and eTead1-cOE cardiomyocytes. By immunofluorescence, cardiomyocytes of pTead1-cKO mice were loosely distributed in culture dish and displayed a

heterogeneous population of TEAD1^{pos} and TEAD1^{neg} cardiomyocytes due to incomplete recombination mediated by MCK-Cre at early postnatal stages as previously observed in heart tissue sections of pTead1-cKO hearts (see Figure 56B). Noticeably, TEAD1^{neg} cardiomyocytes were smaller in size compared to TEAD1^{pos} cardiomyocytes (Figure 41B). In marked contrast, *Tead1-Flag-HA* overexpressing cardiomyocytes were apparently larger in size and formed a uniform confluent cell layer (Figure 41C).

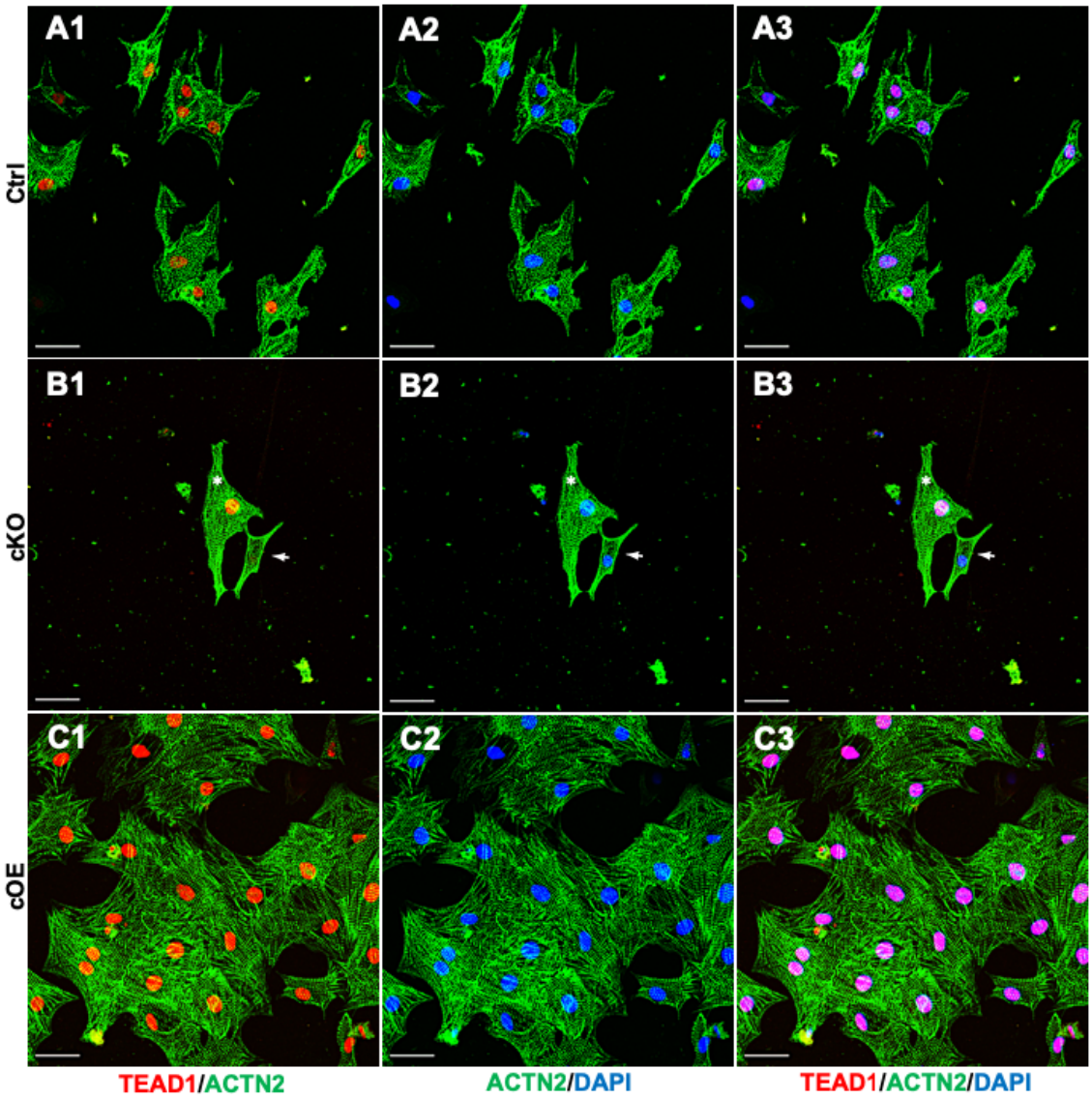

Figure 41. ***Effects of Tead1 deletion and Tead1 overexpression on isolated P3 cardiomyocytes.*** *(**A**) Postnatal cardiomyocytes from control hearts show nuclear TEAD1 signal. (**B**) Cardiomyocyte cultures from pTead1-cKO hearts display heterogeneous TEAD1^{pos} and TEAD1^{neg} cardiomyocyte populations. Note that TEAD1^{neg} cardiomyocyte (arrow) is much smaller than TEAD1^{pos} cardiomyocyte (asterisk). (**C**) Tead1-Flag-HA overexpressing cardiomyocytes from eTead1-cOE hearts display more intense TEAD1 signal and are enlarged in size compared to control cardiomyocytes. Red – TEAD1, green – ACTN2, blue – DAPI. Scale bar: 30 µm.*

In order to validate our *in vivo* observations of *Tead1* loss- and gain-of-function hearts we cultured in the next step cardiomyocytes from pTead1-cKO and eTead1-cOE P3 hearts and scored for proliferation based on 24 h of EdU incorporation. The data presented in Figure 42 show that cultured *Tead1-Flag-HA* overexpressing cardiomyocytes display a 4-fold increase of EdU^{pos} cells compared to control. In marked contrast, isolated cardiomyocytes from pTead-cKO mutants showed almost no EdU^{pos} cardiomyocytes (less than 0.5% of cells) compared to control (about 9%), which is in line with our *in vivo* data shown in Figures 28 and 39.

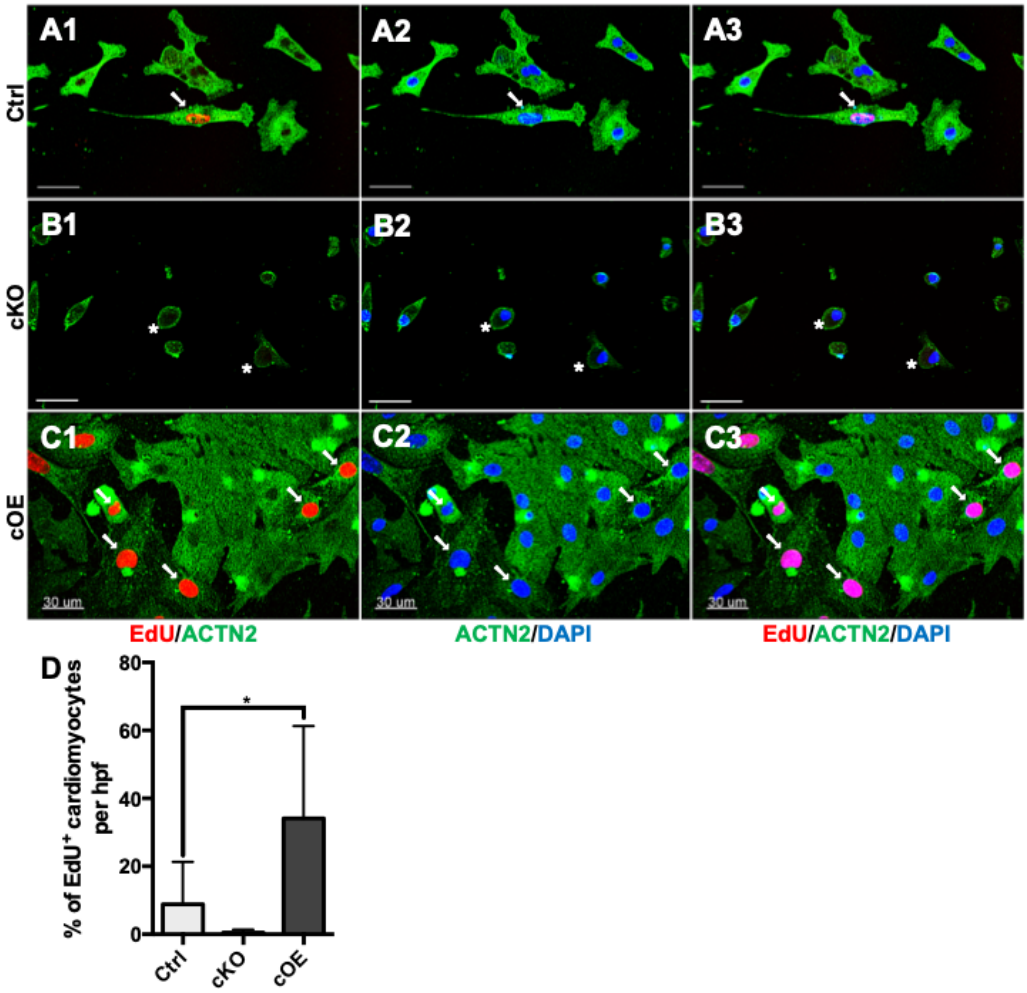

Figure 42. ***Tead1 overexpression stimulates proliferation of cultured P3 cardiomyocytes, whereas Tead1 deficiency reduces proliferation.*** *(**A** - **C**) Representative fluorescent images of EdU labelled isolated cardiomyocytes show almost no EdU^{pos} cardiomyocytes in pTead1-cKO (B, arrow) compared to control (A). Isolated and cultured Tead1-Flag-HA overexpressing cardiomyocytes (C) show an increased number of EdU^{pos} cardiomyocytes (arrows) as compared to controls (A). (B) Note that pTead1-cKO cardiomyocytes are small in size and display only a peripheral rim of $ACTN2^{pos}$ contractile filaments (asterisk). Red – EdU, green – ACTN2, blue – DAPI. (**D**) Cultures of eTead1-cOE cardiomyocytes comprise approximately 34%, control about 9% and pTead1-cKO less than 0.5% of EdU^{pos} cardiomyocytes. Data are means ± SD, ∗ = $P < 0.05$, n=3; hpf – high-power field. Scale bar: 30 µm.*

3.7 TEAD1 regulates genes involved in cardiomyocyte differentiation, maturation, contraction and energy homeostasis in postnatal mouse cardiomyocytes

An important objective of this study was the identification of TEAD1 target genes in the context of myocardial development and maturation. For this purpose, microarray-based transcriptome analysis of isolated P2-P3 (later referred to as "early") postnatal cardiomyocytes (PCMs) from conditional loss-of-function (pTead1-cKO) as well as gain-of-function (eTead1-cOE) mutants were performed. The rationale for using early PCMs resided in the fact that TEAD1 is highly abundant on mRNA as well as on protein levels at this stage (Figure 8). Expression changes in both, *Tead1* loss- and gain-of-function mutants, were compared to control (Cre^{neg}) littermates and quantified as downregulated by fold changes (FC) ≤ 0.75 or as upregulated by FCs ≥ 1.5 with adjusted *P*-value < 0.05. Since multiple studies have shown that TEAD TFs enhance the transcription of target genes [67, 134-137], we focused on genes downregulated upon Tead1 deletion and upregulated upon Tead1 overexpression in PCMs. In total, expression of 462 genes was downregulated in *Tead1* loss-of-function mutants whereas only 12 genes displayed an enhanced expression. In contrast, the analysis of *Tead1* gain-of-function early PCMs revealed 364 upregulated and 245 downregulated genes. In total, only 3 genes were identified, which were downregulated in Tead1 loss-of-function and upregulated in gain-of-function mutants including *Olfr1382*, *Vmn2r86* and *Gm15698*.

Due to incomplete MCK-Cre mediated deletion of *Tead1* during early postnatal stages (Figures 20A, 41B and 56B), a microarray-based transcriptome analysis of isolated PCMs at a more advanced stage, P15-P19 (later referred to as "late") was performed. This analysis revealed 742 downregulated and 312 upregulated genes upon *Tead1* deletion. In contrast, cardiomyocyte-specific *Tead1* overexpression enhanced the expression of 70 genes and repressed the expression 725 genes, respectively.

Gene set enrichment analysis (GSEA) of late PCMs isolated from pTead1-cKO mutants showed a negative enrichment score representing downregulation of genes involved in cardiac muscle contraction (ES = -0.61), which was inversely correlated with upregulation (positive enrichment score, ES = 0.39) in *Tead1*-

overexpressing cardiomyocytes (Figure 43A). Similar transcriptional changes were detected for genes involved in oxidative phosphorylation, which were downregulated (ES = -0.70) upon *Tead1* deletion and upregulated (ES = 0.47) upon *Tead1* overexpression (Figure 43B).

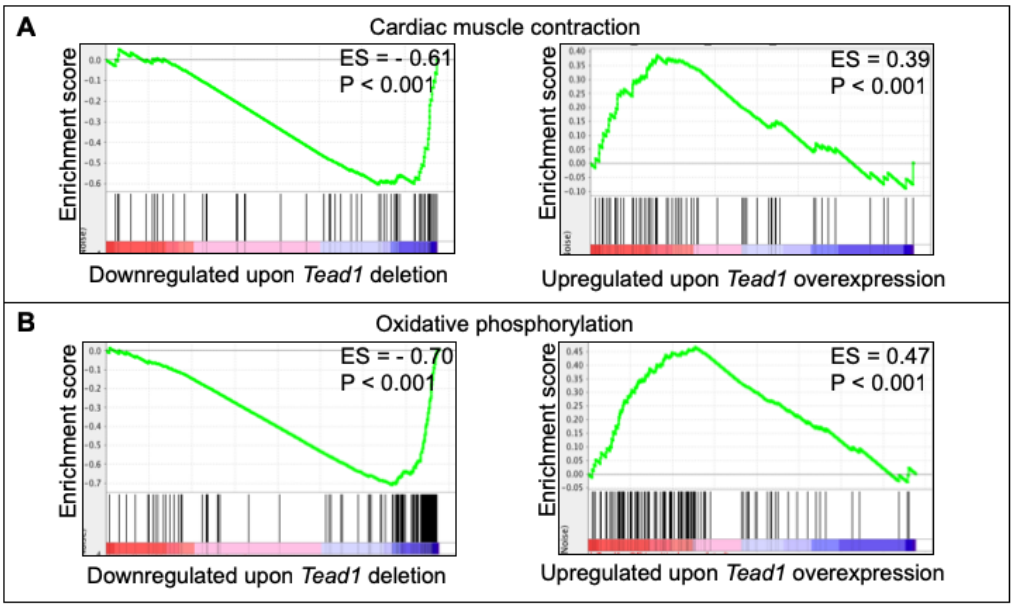

Figure 43. ***GSEA of TEAD1 regulated genes.*** *(**A**) Genes involved in cardiac muscle contraction were downregulated (ES = -0.61, P < 0.001) upon Tead1 deletion and upregulated (ES = 0.39, P < 0.001) upon Tead1 overexpression. (**B**) Expression of genes involved in oxidative phosphorylation was decreased (ES = -0.70, P < 0.001) upon Tead1 deletion and enhanced (ES = 0.47, P < 0.001) upon Tead1 overexpression. ES - enrichment score. (pTead1-cKO: n = 3; eTead1-cOE: n = 2; control: n = 4).*

In contrast, gene clusters for extracellular matrix (ECM) receptor interaction, focal adhesion, cell adhesion molecules (CAMS) as well as gap junction were enhanced in Tead1-cKO mutants and *vice-versa* silenced upon *Tead1* overexpression in late PMCs indicating indirect effects of TEAD1 on these gene clusters (Figure 44).

In addition, GSEA revealed upregulation of the gene clusters encoding the TGF-β signaling pathway (ES = 0.71) in pTead1-cKO cardiomyocytes (Figure 45A). Moreover, gene clusters of adherens junction (ES = 0.64) and VEGF (Vascular Endothelial Growth Factor) signaling pathway (ES = 0.56) were also enriched. On the contrary, the genes involved in fatty acid metabolism (ES = -0.72), which is a common observed phenomenon during heart failure (reviewed in [138]), were downregulated (Figure 45A). In *Tead1* gain-of-function PCMs genes involved in cell proliferation processes including Insulin- (ES = 0.46), mTOR- (ES = 0.45),

ERBB- (ES = 0.37) and WNT-signaling pathways (ES = 0.37) were upregulated (Figure 45B).

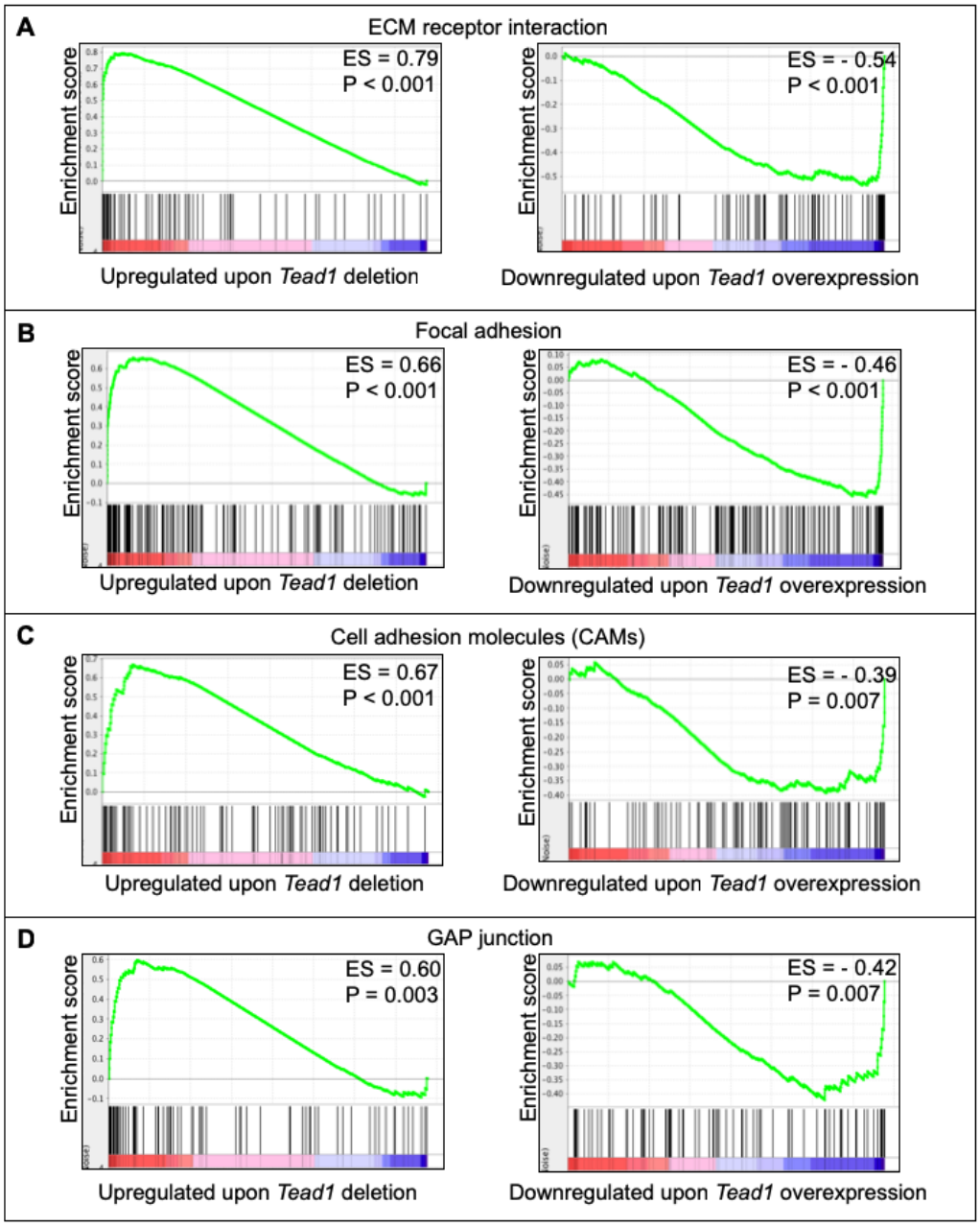

Figure 44. ***GSEA of TEAD1 regulated genes.*** *(**A**) Upregulation (ES = 0.79, P < 0.001) of genes involved in ECM receptor interaction in pTead1-cKO cardiomyocytes and downregulation (ES = -0.54, P < 0.001) upon Tead1 overexpression. (**B**) Upregulation (ES = 0.66, P < 0.001) of genes involved in focal adhesion upon Tead1 deletion and downregulation (ES = -0.46, P < 0.001) upon Tead1 overexpression. (**C**) Upregulation (ES = 0.67, P < 0.001) of genes involved in cell adhesion molecules in pTead1-cKO cardiomyocytes and downregulation (ES = -0.39, P = 0.007) in eTead1-cOE cardiomyocytes. (**D**) Upregulation (ES = 0.60, P = 0.003) of genes involved in GAP junctions upon Tead1 deletion and downregulation (ES = -0.42, P < 0.007) upon Tead1 overexpression. ES - enrichment score. (pTead1-cKO: n = 3; eTead1-cOE: n = 4; control: n = 2).*

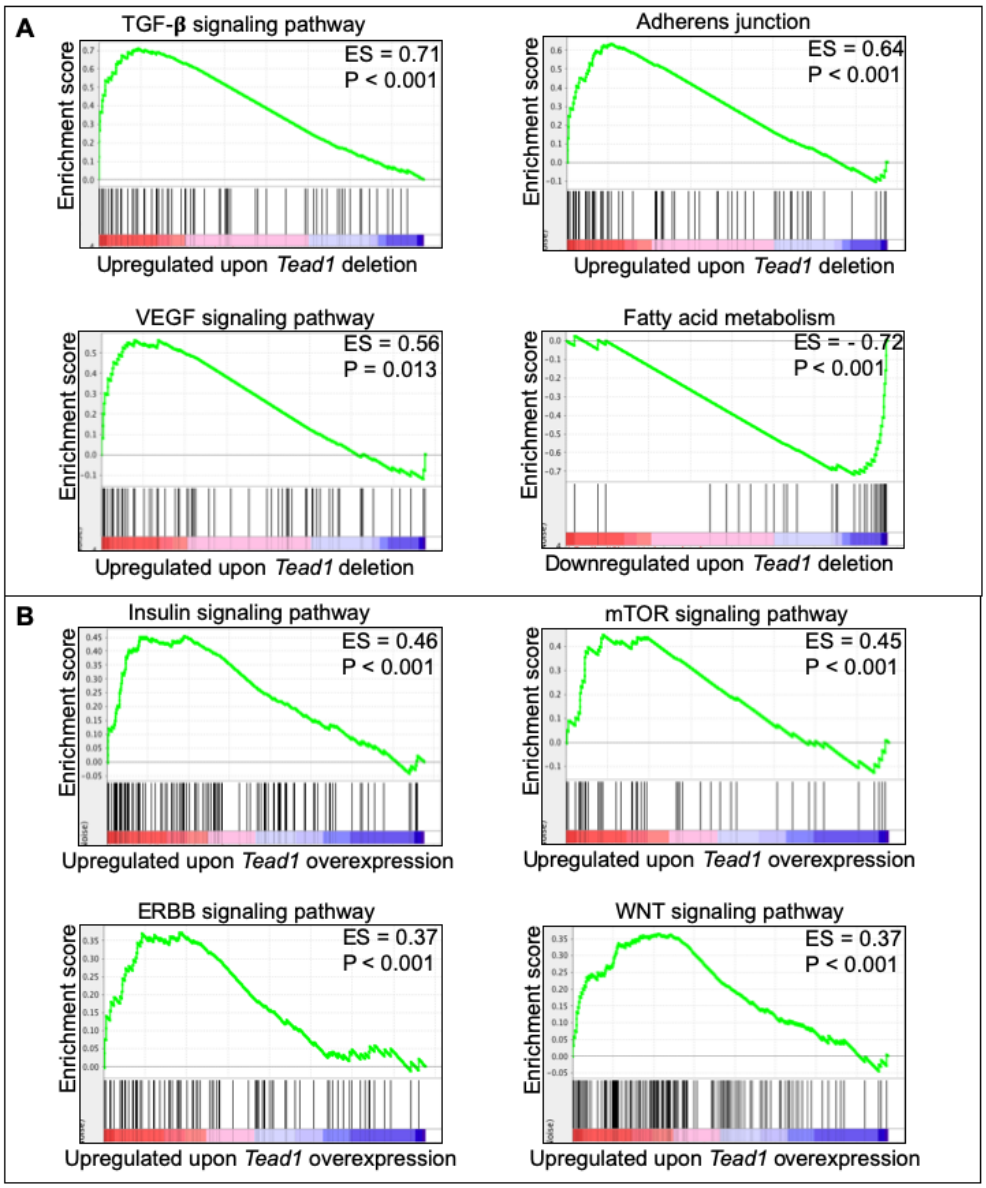

Figure 45. ***GSEA of TEAD1 regulated genes.*** *(**A**) Enrichment plots show enhancement of TGF-beta signaling pathway (ES = 0.71, P < 0.001), adherens junction (ES = 0.64, P < 0.001) and VEGF signaling pathway (ES = 0.56, P = 0.013) as well as downregulation of genes involved in fatty acid metabolism (ES = -0.72, P < 0.001) upon Tead1 deletion in late PCMs. (**B**) Enrichment plots show enhancement of Insulin- (ES = 0.46, P < 0.001), mTOR- (ES = 0.45, P < 0.001), ERBB- (ES = 0.37, P < 0.001) and WNT-signaling pathways (ES = 0.37, P < 0.001) upon Tead1 overexpression in late PCMs. ES - enrichment score. (pTead1-cKO: n = 3; eTead1-cOE: n = 2; control: n = 4)*

Merging datasets of downregulated genes in early and late pTead1-cKO PCMs resulted in total of 8 genes: *Mylk4*, *Lrtm1*, *Scd4*, *Abcc8*, *Crhr2*, *Emp2*, *Tns1* and *nR5s25* (Figure 46A).

In order to analyze the direct binding of TEAD1 in promoter region of potential target genes, TEAD1 chromatin immunoprecipitation combined with sequencing analysis (ChIP-seq) in early PCMs isolated from WT mice was performed. This analysis revealed that TEAD1-occupied 1675 binding sites in total, 606 of them

were located in promoter regions, which were defined as transcription start site (TSS) plus 5000 nucleotides up- and down-stream, respectively. In order to identify MCAT consensus sequences in TEAD1-occupied sites, the data were analyzed for two common consensus MCAT-motives (CATTC and CATTCC[TA]). Both consensus sequences were strongly enriched in TEAD1-occupied sites (CATTC 4-fold and CATTCC[TA] 2-fold).

In order to identify direct TEAD1 target genes, downregulated genes of pTead1-cKO late PCMs were merged with TEAD1 promoter occupied sites obtained from ChIP-seq analysis, which finally resulted in 63 matched genes, out of them 36 contained MCAT-elements in the corresponding promoter regions (Figure 46B). The histone 3 acetylation on lysine 9 (H3K9Ac) is highly corelated with active promoters [139], therefore the ChIP-seq analysis using antibody directed against H3K9Ac was performed in murine WT early PCMs and revealed in total 8361 peaks, among them 7257 were located in promoter regions. In order to identify active TEAD1-occupied promoters, the 63 downregulated genes upon *Tead1* deletion were merged with H3K9Ac peaks from our ChIP-seq analysis and identified 26 candidates, which displayed TEAD1-occupied sites with active H3K9Ac-marked regulatory elements (Figure 46B).

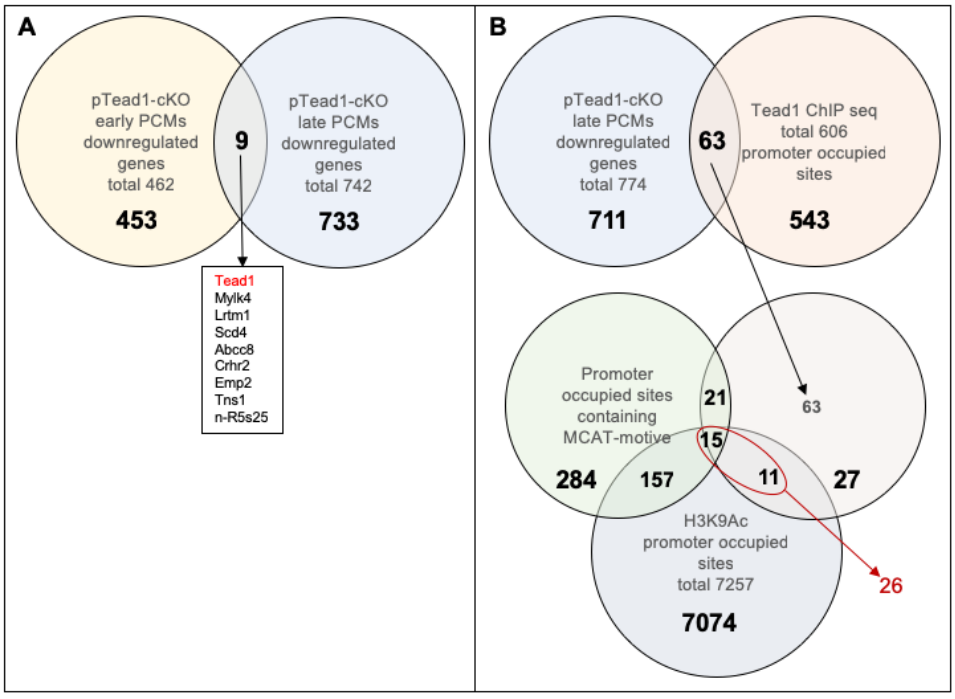

Figure 46. ***Combined transcriptome profiling and genome-wide binding analysis identified multiple cardiomyocyte-specific TEAD1 regulated genes.*** *(**A**) Comparison of downregulated genes (FC ≤ 0.75) during early and late stages of pTead1-cKO PCMs resulted in 8 genes plus Tead1. (**B**) Merging of downregulated genes in late Tead1-cKO PCMs (FC ≤ 0.75) with TEAD1-occupied promoter sites in WT early PCMs revealed 63 candidates, 36 of them contained conserved MCAT-motives and 26 contained H3K9Ac peaks.*

In our analysis, we defined direct TEAD1 targets if they fulfill the following 3 criteria: 1) reduced expression upon *Tead1* deletion; 2) direct TEAD1 binding in promoter region, and 3) transcriptionally active region. These stringent criteria resulted in totally 26 targets, out of them 6 have been previously associated with striated muscle dysfunctions including *Crhr2*, *Adprhl1*, *Nnt*, *Foxo3*, *Coro6* and *Irf2bp2* (Figures 47 and 48). Furthermore, reduced expression of *Crhr2* (by 87 %) and *Coro6* (by 40 %) could be validated by qRT-PCR in late *Tead1*-deficient PCMs (Figure 50A).

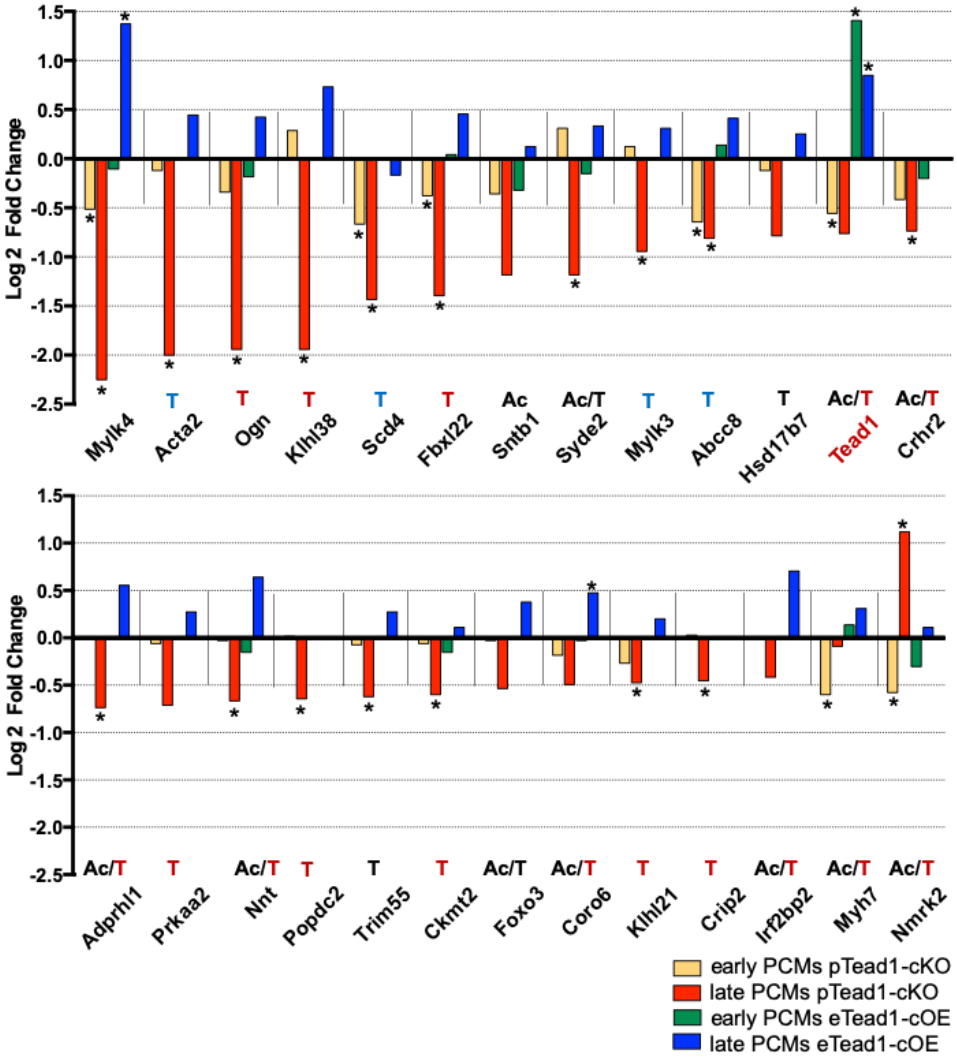

Figure 47. ***Examples of candidate genes regulated by TEAD1 in murine cardiomyocytes and their Log2 fold changes upon Tead1 deletion*** *(bars: yellow – early PCMs and red – late PCMs)* ***and overexpression*** *(bars: green - early PCMs and blue - late PCMs)* ***in PCMs.*** *Black* ***T*** *below gene aliases represents TEAD1 peaks, red* ***T*** *represents a presence of MCAT sequences as well as TEAD1 peaks,* ***Ac*** *represents H3K9Ac peaks, which were detected by our in-house bioinformatics analysis, blue* ***T*** *represents peaks identified manually using IGV.* ***Asterisk*** *above the corresponding bars resembles transcriptional fold changes with a P-value < 0.05. Early PCMs were isolated from control (n = 4), pTead1-cKO (n = 2) and eTead1-cOE (n = 2) hearts. Late PCMs were isolated from control (n = 4), pTead1-cKO (n = 3) and eTead1-cOE (n = 2) hearts.*

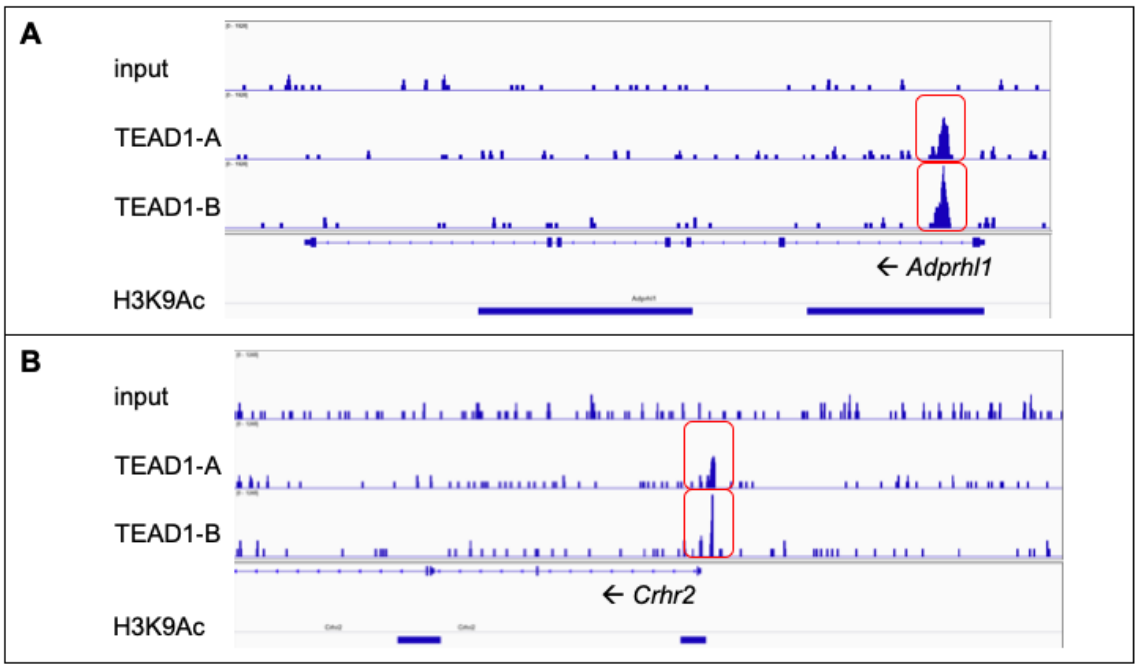

Figure 48. ***TEAD1 binds to the promoter region of transcriptional active Adprhl1 (A), and Crhr2 (B) in early WT PCMs.*** *Promoter regions of Adprhl1 (A), and Crhr2 (B) revealed an intense TEAD1 binding (TEAD1-A and TEAD1-B) visualized by a strong peak highlighted by red boxes without comparable peaks in the input (n = 2). H3K9Ac is visualized by horizontal blue bars at the bottom, n = 1 (visualized in IGV).*

Given that some of strongly dysregulated genes identified in *Tead1* loss- or gain-of-function cardiomyocytes using transcriptome analyses (Figure 47) were not detected by our in-house bioinformatics settings for ChIP-seq analysis, the TEAD1 ChIP-seq data were manually analyzed with Integrative Genomic Viewer (IGV) software (available at: https://software.broadinstitute.org/software/igv/). Using this approach, TEAD1 binding sites were identified in promoter regions of *Acta2*, *Scd4*, *Mylk3* and *Abcc8* (Figure 47). Although *Mylk4* was found to be one of the most downregulated genes in *Tead1* loss-of-function cardiomyocytes (Figure 47), no TEAD1 occupancy of *Mylk4* promoter was detected using IGV. qRT-PCR validation of *Acta2* and *Mylk4* expression in *Tead1*-deficient late PCMs confirmed our transcriptome profiling and revealed strongly reduced mRNA levels of *Mylk4* (by 94%) as well as *Acta2* (by 93%) (Figure 50A). Surprisingly, *Myocd* expression was unaltered in *Tead1*-deficient cardiomyocytes (Figures 50A).

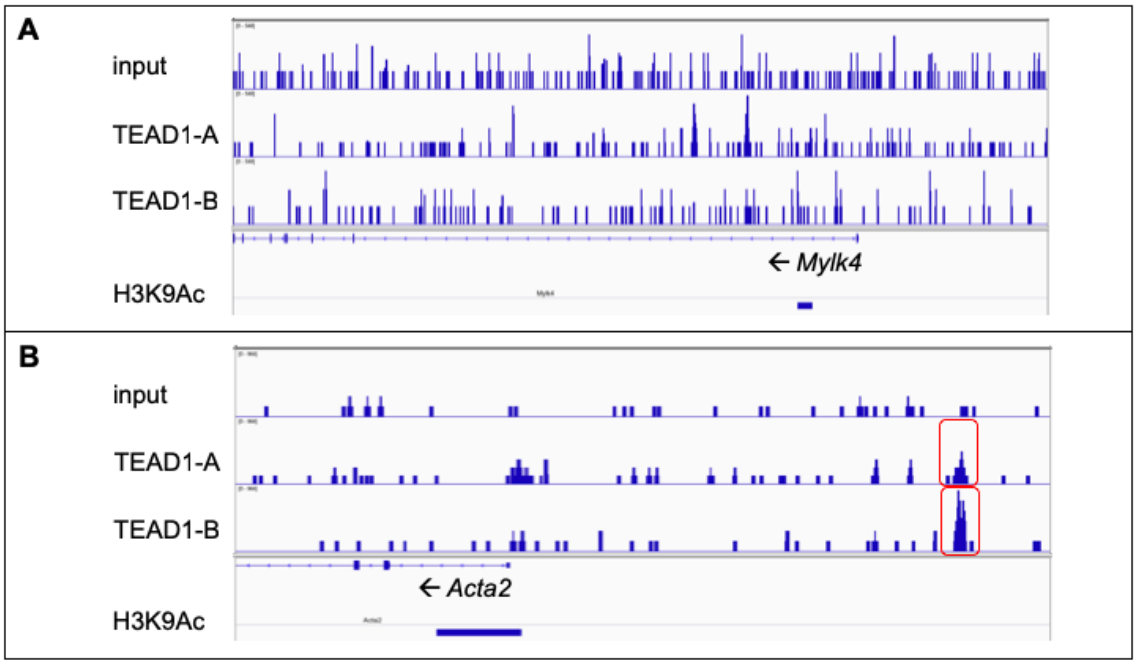

Figure 49. ***Acta2 promoter displays TEAD1 binding, whereas Mylk4 promoter shows no TEAD1 binding.*** *(**A**) In Mylk4 promoter region as well as gene body no TEAD1-occupied sites are present. (**B**) Acta2 display TEAD1 peaks (red boxes) without comparable peaks in the input. H3K9Ac is visualized by horizontal blue bars at the bottom (visualized in IGV).*

Myh7 has been previously reported as a direct TEAD1 target gene in rat and mouse cardiomyocytes and is a typical marker for the fetal myocardial gene program ([15, 105] and reviewed in [104]). According to our ChIP-Seq analysis results, *Myh7* showed a strong promoter occupancy by TEAD1 and H3K9Ac, respectively, in early PCMs indicating a direct regulation of *Myh7* expression by TEAD1 (Figures 47 and 51A). Although *Myh7* expression was unaltered in *Tead1*-deficient late PCMs (Figures 47 and 50A), elevated *Myh7* mRNA levels were detected in *Tead1*-overexpressing cardiomyocytes (Figures 47 and 50B), which might be explained by the physiological *Myh7* downregulation during cardiomyocyte differentiation and maturation shown in Figure 50C.

Another gene, which partially fulfilled our criteria was *Nmrk2,* indicated by a strong TEAD1 and H3K9Ac promoter occupancy. Early *Tead1*-deficient PCMs displayed a strong downregulation of *Nmrk2*, whereas in late PCMs *Nmrk2* expression was 2-fold increased (Figure 47).

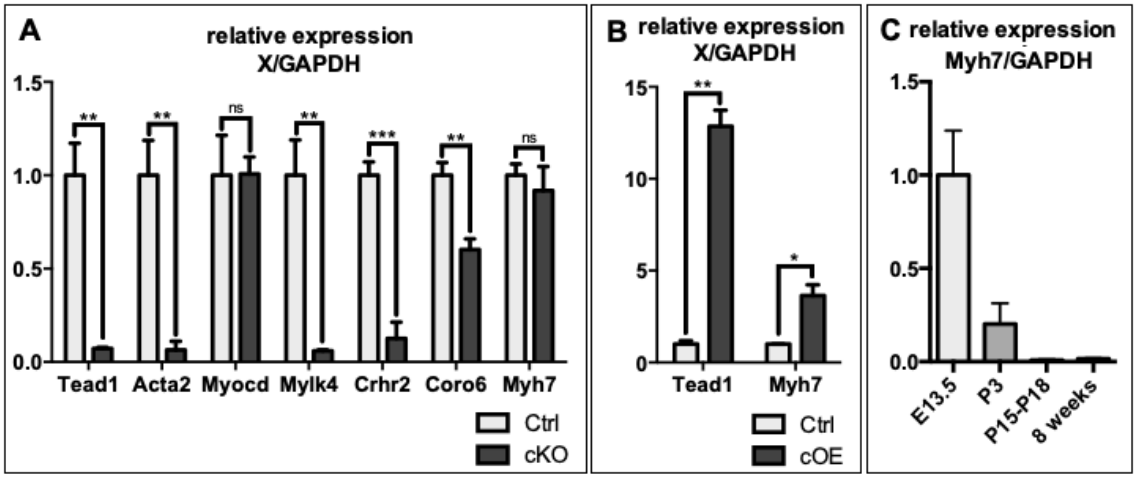

Figure 50. ***Tead1-deficient late PCMs display reduced Acta2, Mylk4, Crhr2, Coro6 mRNA levels, whereas Myh7 and Myocd remains unaltered.*** *(**A**) Tead1 deletion results in downregulation of Acta2, Mylk4, Crhr2 and Coro6 mRNAs, whereas, Myh7 and Myocd expression levels are unaltered. (**B**) Tead1 overexpression results in an enhanced Myh7 expression. (**C**) Continuous downregulation of Myh7 expression (by 98%) during cardiomyocyte differentiation and maturation in WT mice (from E13.5 to 8 weeks)**. Values were normalized to Gapdh mRNA levels. X – gene. Data are means ± SD, ns = not significant (P ≧ 0.05), ∗ = P < 0.05, ∗∗ = P < 0.005, ∗∗∗ = P < 0.002, n = 3.*

TEAD1 binding to *Myh7* and *Acta2* loci was validated by qChIP-PCR using specific primers located in the corresponding promoter regions. Our analysis revealed an enrichment for TEAD1 as well as RNA-Pol2 and H3K9Ac binding, indicating a transcriptionally active promoter for *Myh7* and *Acta2*. No enrichment was observed for IgG binding, which served as a background control (Figure 51).

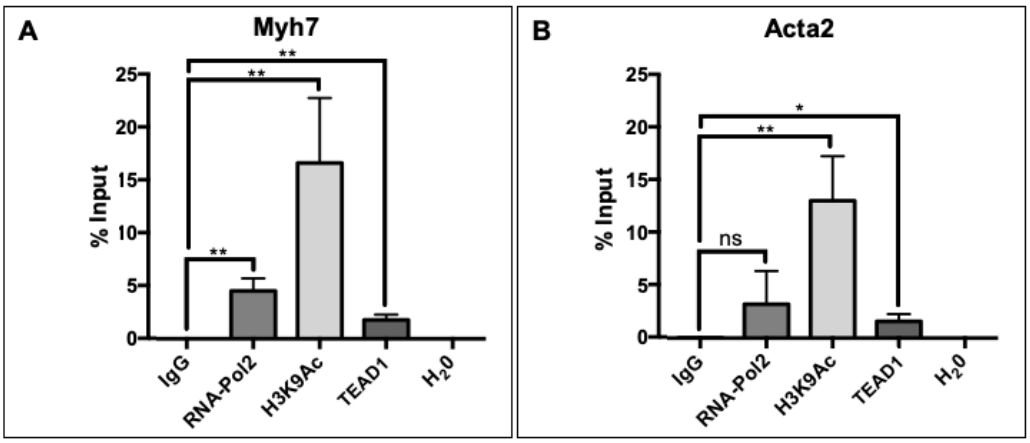

Figure 51. ***qChIP-PCR validation of TEAD1-occupied Myh7 and Acta2 promoters.*** *(**A**) PCR results display an enrichment of RNA-Pol2 (4.5%), H3K9Ac (16.5%) and TEAD1 (1.8%) binding in comparison to control IgG (0.02%) in Myh7 promoter, relative to 10 % input. (**B**) PCR results revealed an enrichment of H3K9Ac (13%) and TEAD1(1.6%) binding in comparison to control IgG (0.3%) in Acta2 promoter, relative to 10 % input. Data are means ± SD, ns = not significant (P ≧ 0.05), ∗ = P < 0.05, ∗∗ = P < 0.005, n = 3.*

Another group of genes comprising *Amotl2* and *Ctgf*, which have been previously reported as TEAD1 target genes [48, 140], displayed strong occupancy by TEAD1 and H3K9Ac (Figure 52), however expression levels were nearly unaltered in *Tead1* loss- and gain-of-function cardiomyocytes (data not shown).

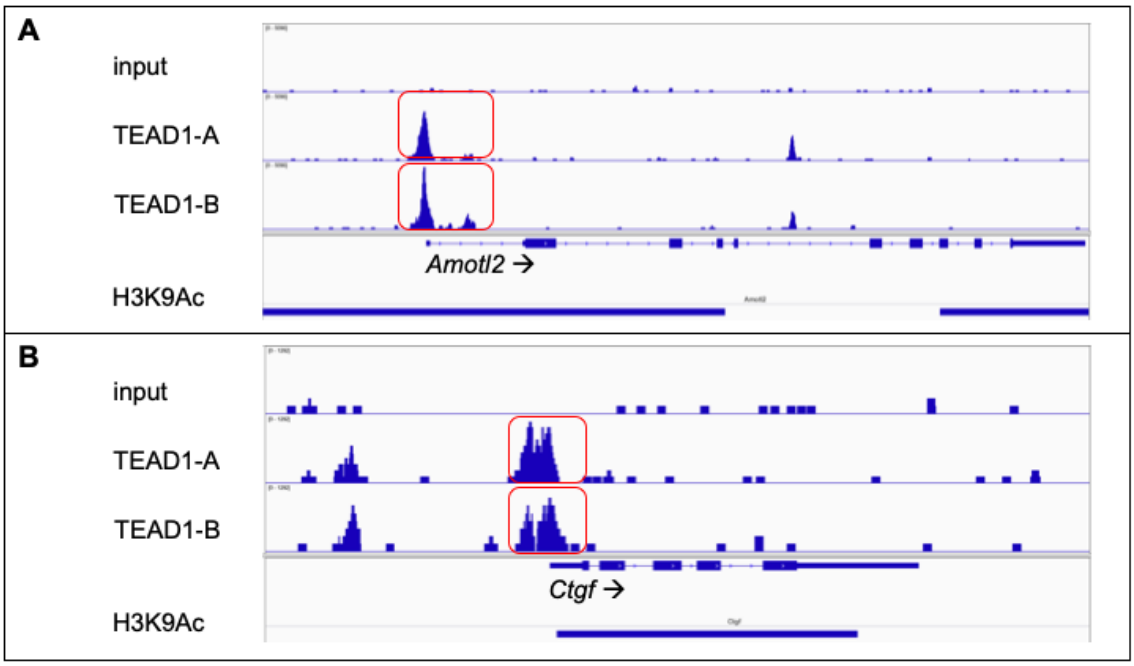

Figure 52. ***TEAD1 occupies promoter regions of transcriptional active Amotl2 and Ctgf genes in early PCMs.*** *(**A**) Amotl2 and (**B**) Ctgf peaks are highlighted by red boxes. H3K9Ac is visualized by horizontal blue bars at the bottom representing transcriptional activity of this gene (visualized in IGV).*

Expression of several known players of the Hippo-pathway downstream targets was nearly unaltered in *Tead1* loss- and gain-of-function cardiomyocytes with the exception of *Vgll-2* and *Ajuba* (Figure 53). *Vgll-2* showed a 4-fold enhanced expression in pTead1-cKO late PCMs. In contrast, *Ajuba* revealed a 1.65-fold upregulation upon *Tead1* deletion and a slight downregulation while *Tead1* overexpression in early PCMs. In addition, TEAD1-occupied also promoter regions of *Tead4*, *Vgll-4*, *Yap1* and *Wwtr1*, however the expression of the corresponding transcripts was unaltered in *Tead1* loss- and gain-of-function cardiomyocytes (Figure 53).

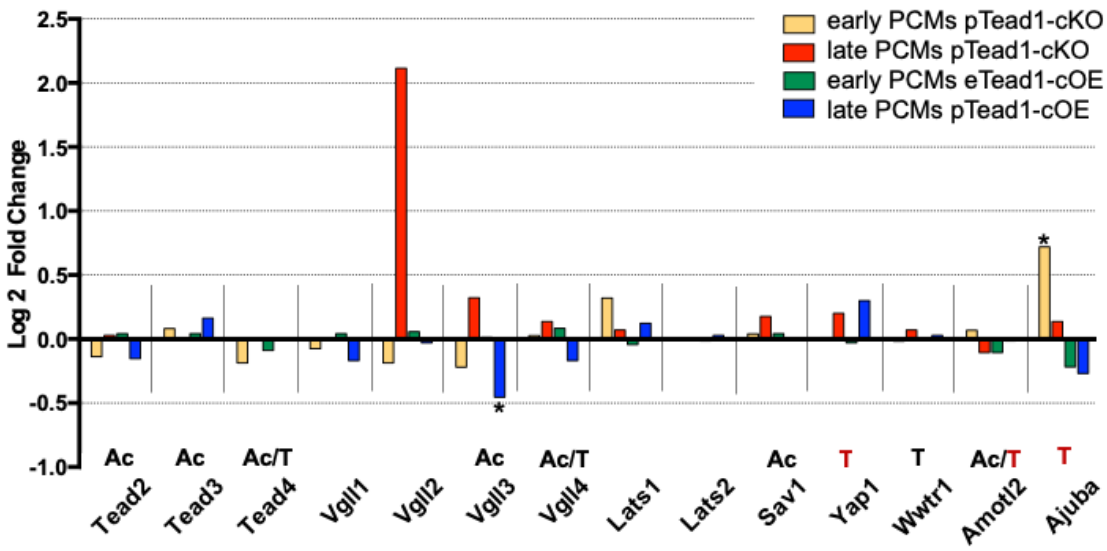

Figure 53. ***Examples of expressional changes of characterized Hippo-pathway players upon Tead1 deletion*** *(yellow and red bars)* ***and overexpression*** *(green and blue bars)* ***in early versus late PCMs.*** *Black* ***T*** *above gene aliases represents TEAD1 peaks, red* ***T*** *represents a presence of MCAT sequences as well as TEAD1 peaks,* ***Ac*** *represents an H3K9Ac peaks, which were detected by our in-house bioinformatics analysis.* ***Asterisk*** *above the corresponding bars resembles transcriptional fold changes with a P-value < 0.05. Early PCMs were isolated from control (n = 4), pTead1-cKO (n = 2) and eTead1-cOE (n = 2) hearts. Late PCMs were isolated from control (n = 4), pTead1-cKO (n = 3) and eTead1-cOE (n = 2) hearts.*

Interestingly, TEAD1 binds to its own promoter in H3K9Ac-marked region suggesting that TEAD1 positively regulates its own expression (Figure 54).

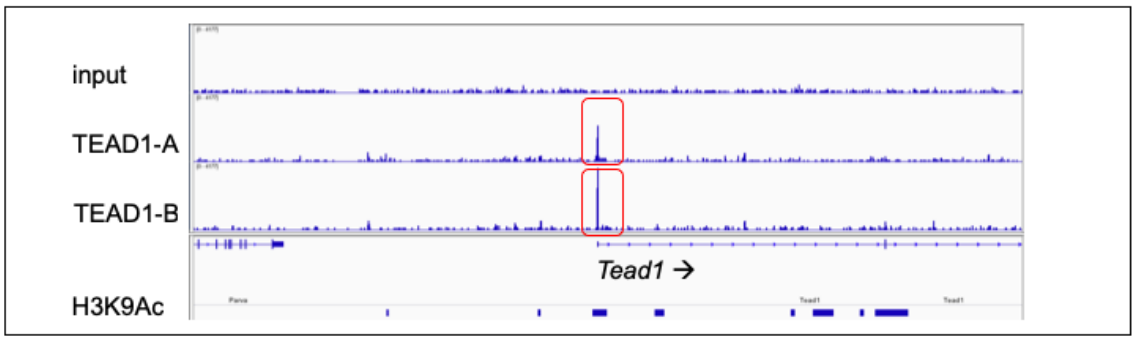

Figure 54. ***Binding of TEAD1 to its own transcriptional active promoter.*** *TEAD1 bindings peaks are highlighted by red boxes. H3K9Ac peaks are visualized by horizontal blue bars at the bottom representing transcriptional activity of Tead1 gene (visualized in IGV).*

3.8 TEAD1 activates *Acta2* expression in cardiomyocytes

Smooth muscle actin (ACTA2) has been previously identified as a direct TEAD1 target in mouse SMCs and myofibroblasts [60, 63]. In the present study, ChIP-seq analysis of early PCMs showed TEAD1 occupancy in *Acta2* promoter region

and microarray analysis of pTead1-cKO cardiomyocytes revealed a significant *Acta2* downregulation indicating a direct transcriptional regulation of *Acta2* by TEAD1 (Figures 47, 49B, 50A and 51B). To elucidate whether *Acta2* expression is impaired in embryonic cardiomyocytes of eTead1-cKO mutants, E12.5 embryonic hearts were co-stained for ACTA2, TEAD1 and F-Actin. Figure 55 shows that cardiomyocytes in control embryonic hearts were positive for both, ACTA2 and TEAD1. In contrast, cardiomyocytes in eTead1-cKO hearts displayed reduced ACTA2 signal in TEAD1^{neg} cardiomyocytes.

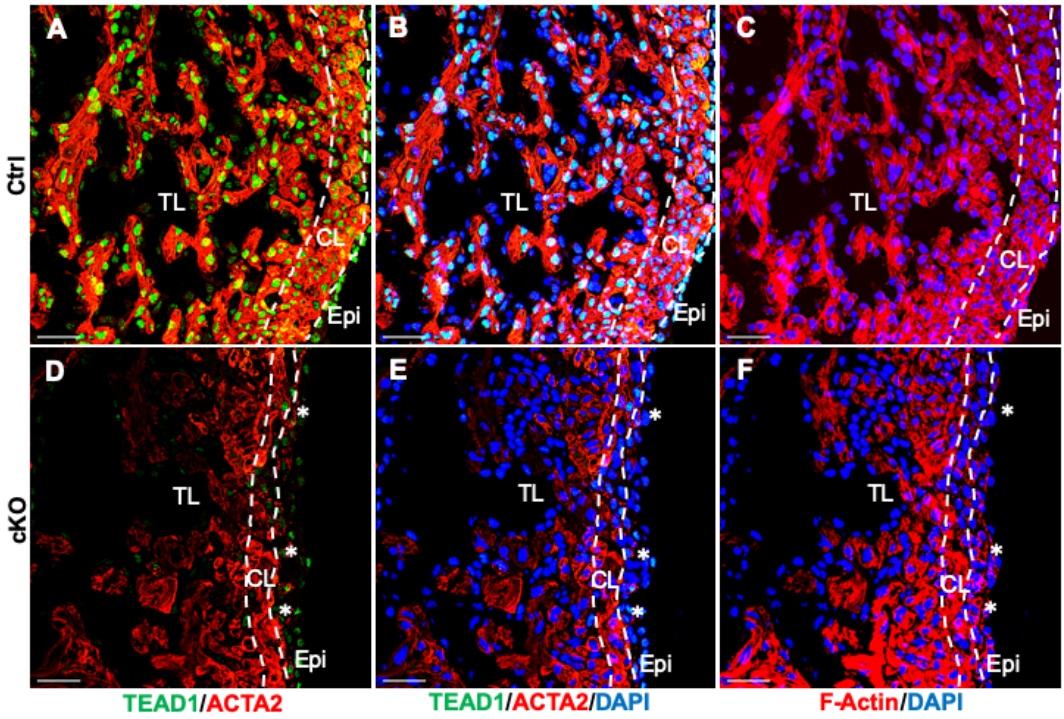

Figure 55. ***Embryonic cardiomyocytes display decreased ACTA2 in E12.5 eTead1-cKO hearts.*** *Representative images of E12.5 heart sections co-stained for ACTA2, TEAD1, F-Actin and DAPI. (**A** – **C**) Embryonic TEAD1^{pos} cardiomyocytes in control hearts are ACTA2^{pos}. (**D** - **F**) Cardiomyocytes in eTead1-cKO hearts exhibit decreased abundance of ACTA2. F-Actin signal intensity is almost unaltered in both, control and eTead1-cKO hearts. Note that in eTead1-cKO hearts only epicardial cells are TEAD1^{pos} (asterisk in panels D, E, F). Of note, cardiomyocytes in both, control and eTead1-cKO hearts display comparable F-Actin staining intensities. Green – TEAD1, red – ACTA2 / F-Actin, blue – DAPI, TL – trabecular layer, CL – compact layer (outlined with dashed white line), Epi – epicardium. Scale bar: 30 µm.*

Numerous studies demonstrated a step-wise decline of *Acta2* expression in postnatal cardiomyocytes [35, 141, 142]. Therefore, analysis of ACTA2 abundance was examined by immunofluorescence upon *Tead1* deletion and overexpression at postnatal stages P3, P12 and P24. Analysis revealed that cardiomyocytes of Tead1-cKO mutants at P3 displayed reduced ACTA2 signal compared to control hearts (Figure 56). In contrast to Tead1-cKO mutants,

Tead1-overexpressing hearts at P3 showed increased ACTA2 intensity in cardiomyocytes.

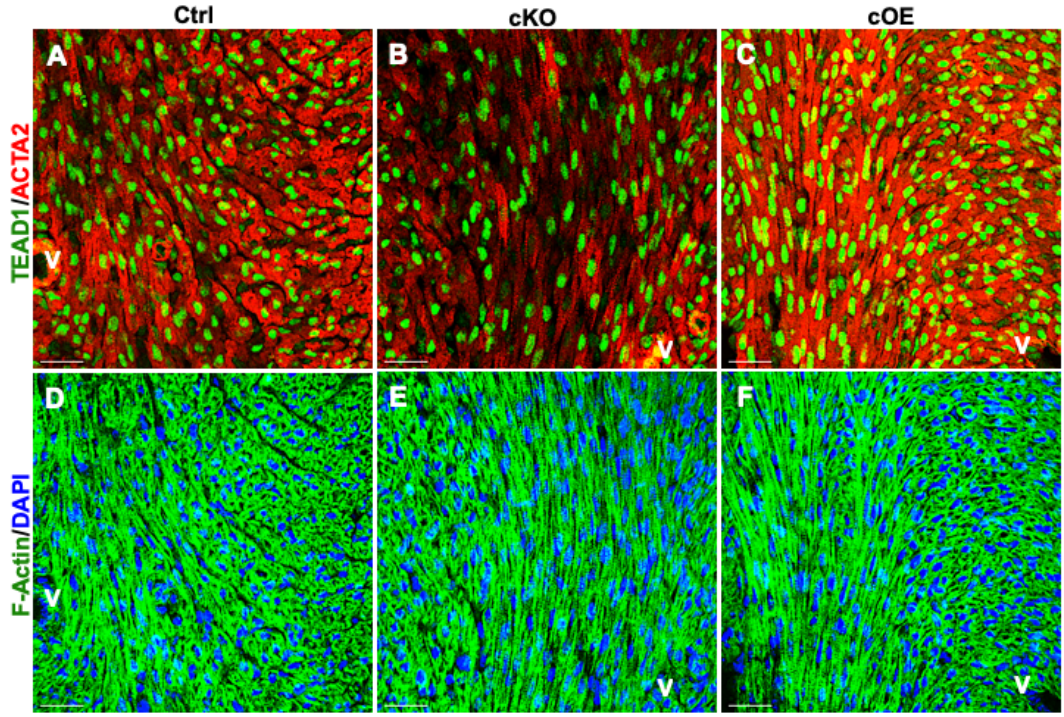

Figure 56. ***Decreased ACTA2 in cardiomyocytes of P3 pTead1-cKO hearts.*** *Representative fluorescent images of P3 heart sections. Cardiomyocytes of control (**A**) and eTead1-cOE hearts (**C**) are strongly positive for ACTA2. On the contrary, cardiomyocytes of pTead1-cKO hearts (**B**) display a reduced ACTA2 signal. Notice that F-Actin signal in cardiomyocytes and ACTA2 in vessels (V) is of comparable intensities in the studied groups (panels D, E, F). Green – TEAD1 / F-Actin, red – ACTA2, blue – DAPI; V - Vessels. Scale bar: 30 µm.*

The differences between groups in ACTA2 abundance and distribution patterns were even more pronounced in P12 and P24 hearts (Figures 57 and 58). As shown in Figure 58, ACTA2 and TEAD1 signals in P24 mutant cardiomyocytes were almost negligible, whereas all cardiomyocytes in control hearts remained TEAD1^{pos} and several of them showed a strong ACTA2 signal (Figure 58) implying that ACTA2 abundance declines in parallel with TEAD1. These finding were further strengthened by immunofluorescent analysis of control and *Tead1*-overexpressing hearts, which clearly showed that ACTA2 is more abundant in *Tead1*-overexpressing cardiomyocytes compared to control cardiomyocytes (Figure 59).

As expected, ACTA2 intensity was unaltered in SMCs of coronary vessels in all studied groups including control, cardiomyocyte-specific Tead1 gain- and loss-of function hearts irrespective from the examined postnatal stages (Figures 56 - 59).

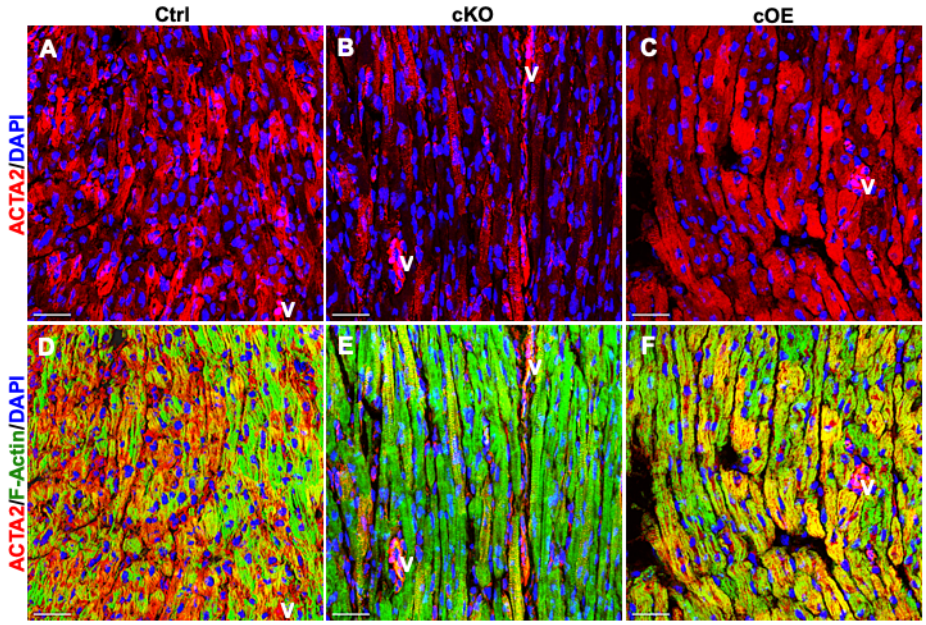

Figure 57. ***Reduced ACTA2 in cardiomyocytes of P12 pTead1-cKO hearts and increased ACTA2 in cardiomyocytes of eTead1-cOE hearts.*** *Cardiomyocytes in pTead1-cKO heart (panels **B**, **E**) are weakly positive for ACTA2. Cardiomyocytes in eTead1-cOE heart (panels **C**, **F**) are strongly positive for ACTA2 as compared to control cardiomyocytes (panels **A**, **D**). ACTA2 signal in vessels (V) is used as internal reference and its intensity is comparable in all groups. Red – ACTA2, green – F-Actin, blue – DAPI, V – Vessels. Scale bar: 30 µm.*

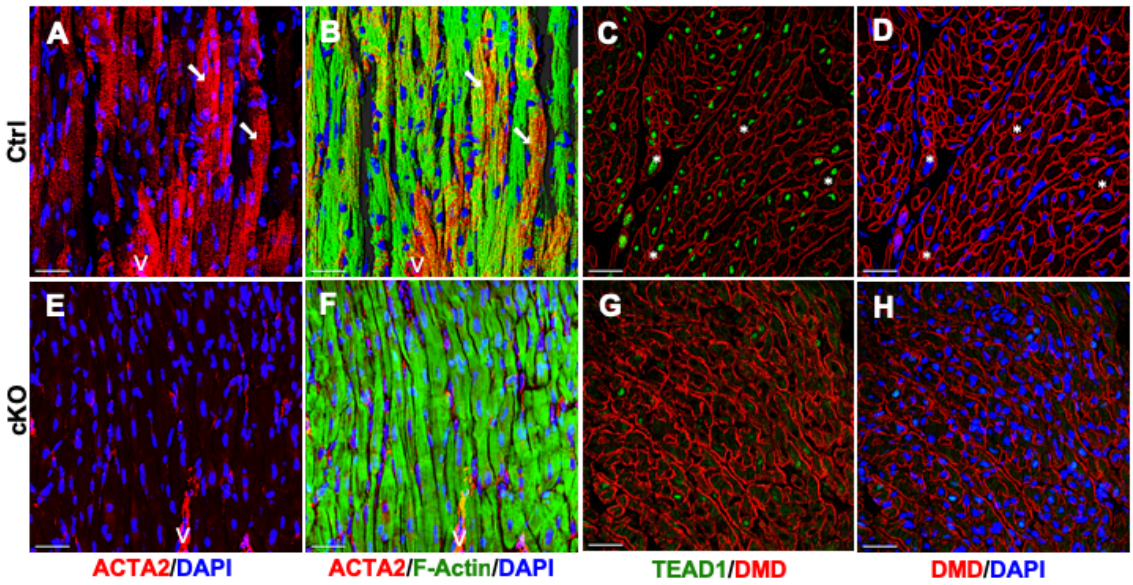

Figure 58. ***Reduced ACTA2 signal in P24 pTead1-cKO cardiomyocytes.*** *Representative fluorescent images of P24 control and pTead1-cKO hearts. (**A** – **D**) All cardiomyocyte of control hearts are TEAD1^{pos} (asterisk, panels C, D), whereas only a few cardiomyocytes are ACTA2^{pos} (arrows, panels A, B). (**E** – **H**) Cardiomyocytes in pTead1-cKO hearts are TEAD1^{neg} (panels G, H) and ACTA2^{neg} (panels E, F). The cardiomyocytes in control and in pTead1-cKO hearts are positive for F-Actin (panels B, F) and dystrophin (DMD, panels C, D, G, H). ACTA2 signal in vessels (V) is comparable in both groups (panels A, B, E, F). Red – ACTA2 / DMD, green – F-Actin / TEAD1, blue – DAPI; V – Vessels. Scale bar: 30 µm.*

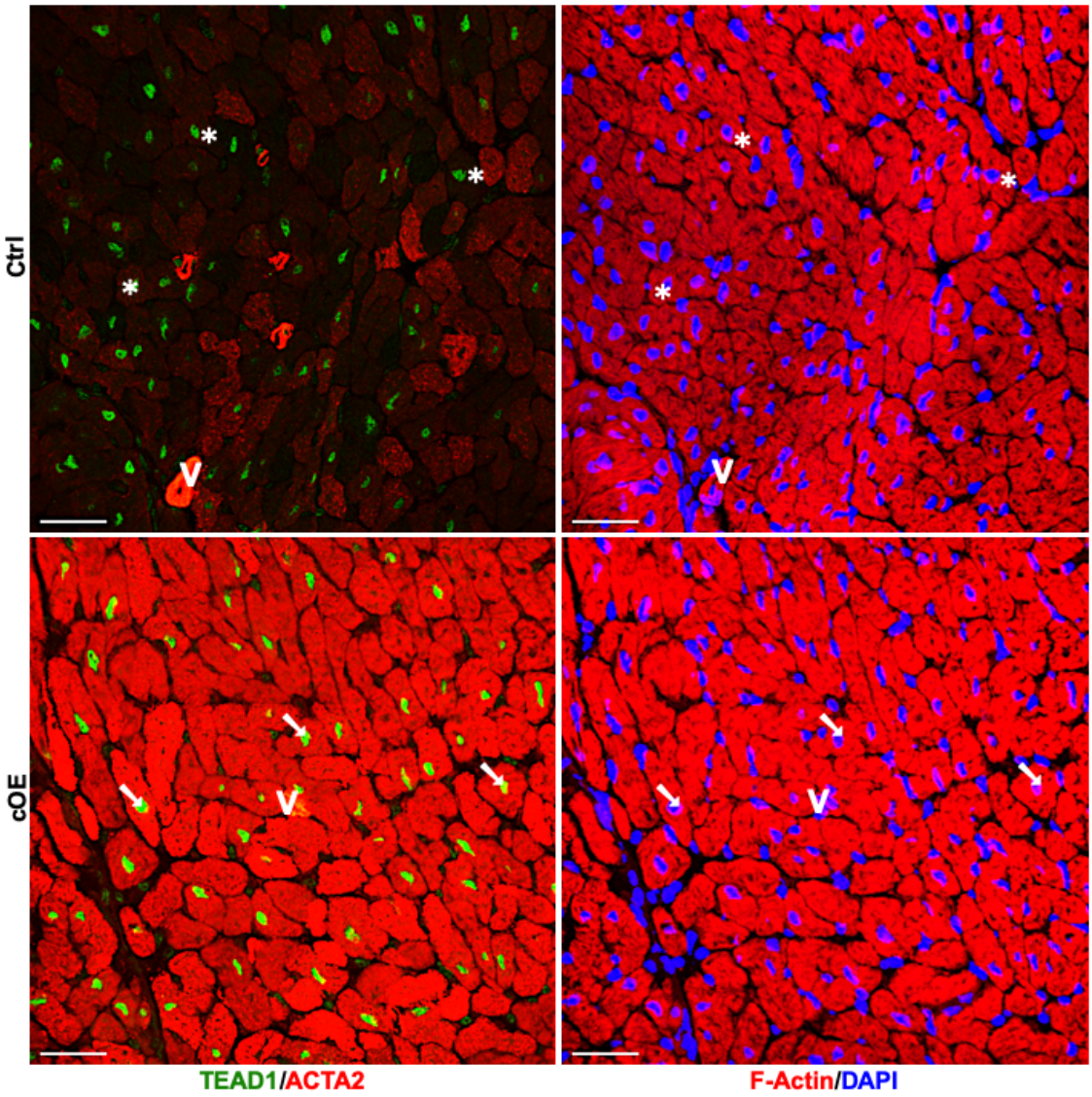

Figure 59. ***Tead1-overexpressing cardiomyocytes remain ACTA2 positive at P30.*** *Representative images of P30 heart sections co-stained for ACAT2, TEAD1 and F-Actin.* ***Upper panels****: In control hearts, all cardiomyocytes are F-Actin^{pos} and TEAD1^{pos} (asterisk), whereas only some cardiomyocytes are weakly positive for ACTA2.* ***Lower panels****: In contrast, in eTead1-cOE hearts the vast majority of cardiomyocytes are strongly positive for both TEAD1 and ACTA2 (arrows). ACTA2 signal intensity in vessels (V) and F-Actin signal in cardiomyocytes is equal in control and eTead1-cOE hearts. Green – TEAD1, red – ACTA2 / F-Actin, blue – DAPI. Scale bar – 30 µm.*

Several studies have linked ACTA2 re-expression and ultrastructural features of dedifferentiated cardiomyocytes [143, 144]. Therefore, transmission electron microscopy analysis of P16 hearts was performed and provided additional evidence for a higher abundance of terminally differentiated cardiomyocytes in pTead1-cKO mutants than in control hearts. A representative TEM image of undifferentiated cardiomyocytes frequently observed in control hearts is shown

in Figure 60. According with the previously described ultrastructural features [143, 144], undifferentiated cardiomyocytes are characterized by high content of mitochondria with varying size and shapes, glycogen deposits as well as low content of contractile structures. Differentiated cardiomyocytes observed in Tead1-cKO hearts are characterized by a high content of myofibrils, equally shaped mitochondria of mostly the same size and low glycogen deposits (Figure 60).

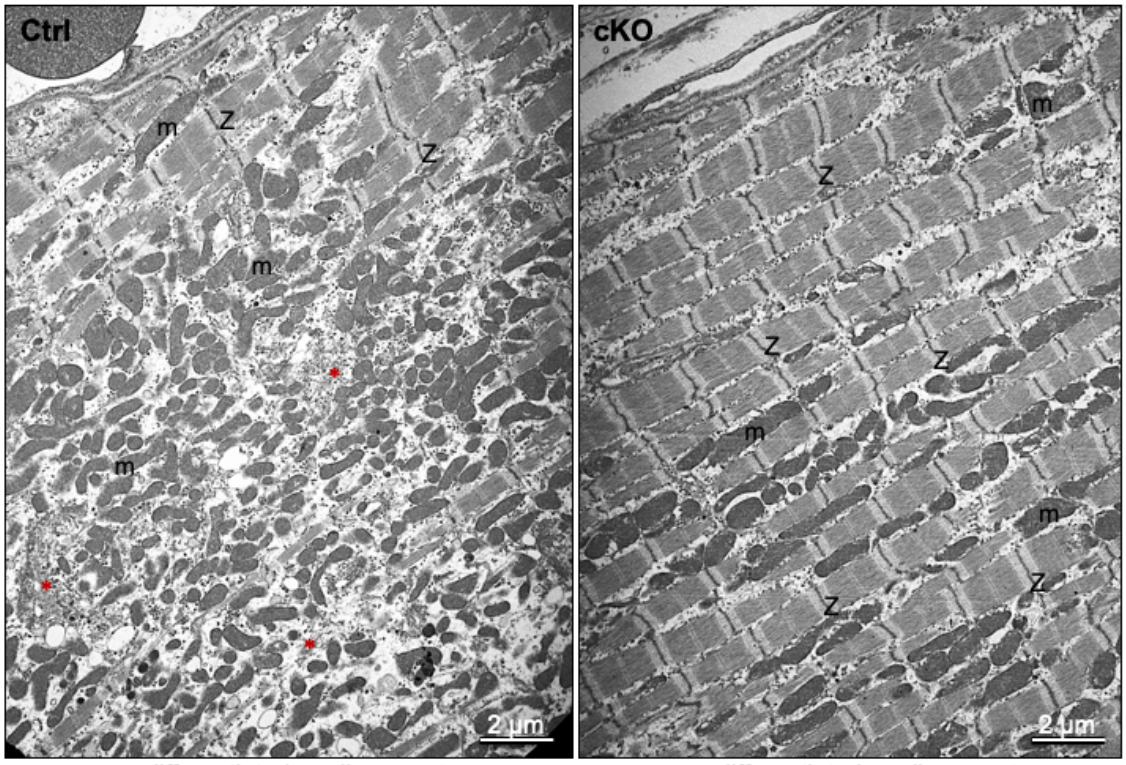

Figure 60. ***Typical ultrastructural features of differentiated versus undifferentiated cardiomyocytes in control and pTead1-cKO mutants (P16). Left panel:*** *Representative TEM image of undifferentiated cardiomyocytes (control) characterized by high glycogen depositions (red asterisk) and numerous mitochondria (m) with varying sizes and shapes as well as low content of contractile structures.* ***Right panel:*** *Fully differentiated (pTead1-cKO) cardiomyocytes characterized by densely packed myofibrils, equally shaped mitochondria (m) of mostly same size and low glycogen deposits. Z – Z-disks.*

3.9 Enhanced MYLK4 expression in cardiomyocytes bordering infarction

MYLK4 (Myosin Light Chain Kinase 4) has been previously reported to be strongly reduced in cardiomyopathies [145]. The present global transcriptomic analysis of early and late PCMs from pTead1-cKO hearts indicated that *Mylk4* is

one of the most downregulated genes upon *Tead1* deletion (Figure 47). In addition, elevated *Tead1* expression levels in late PCMs of TEAD1 GOF mice strongly increased *Mylk4* mRNA levels (Figure 47). For this reason, MYLK4 protein levels were analyzed in control cardiomyocytes and in the settings of acute (4 days) and chronic myocardial ischemia (21 days) after myocardial infarction (MI) in adult WT mice. Under normal conditions, MYLK4 is not detectable in cardiomyocytes, whereas vessels display a strong MYLK4 signal (data not shown). During the acute phase of MI, cardiomyocytes bordering infarction were MYLK4^{pos} (Figures 61A and 61B). In contrast, in the chronic phase, cardiomyocytes bordering post-infarction scars were almost MYLK4^{neg} (Figures 61E and 61F), indicating MYLK4 activation mainly in acute ischemic cardiomyocytes. It is worthy to note that cardiomyocytes in either acute or chronic MI displayed discernible TEAD1 signal confined to cardiomyocyte nuclei (Figures 61C, 61D, 61G and 61H).

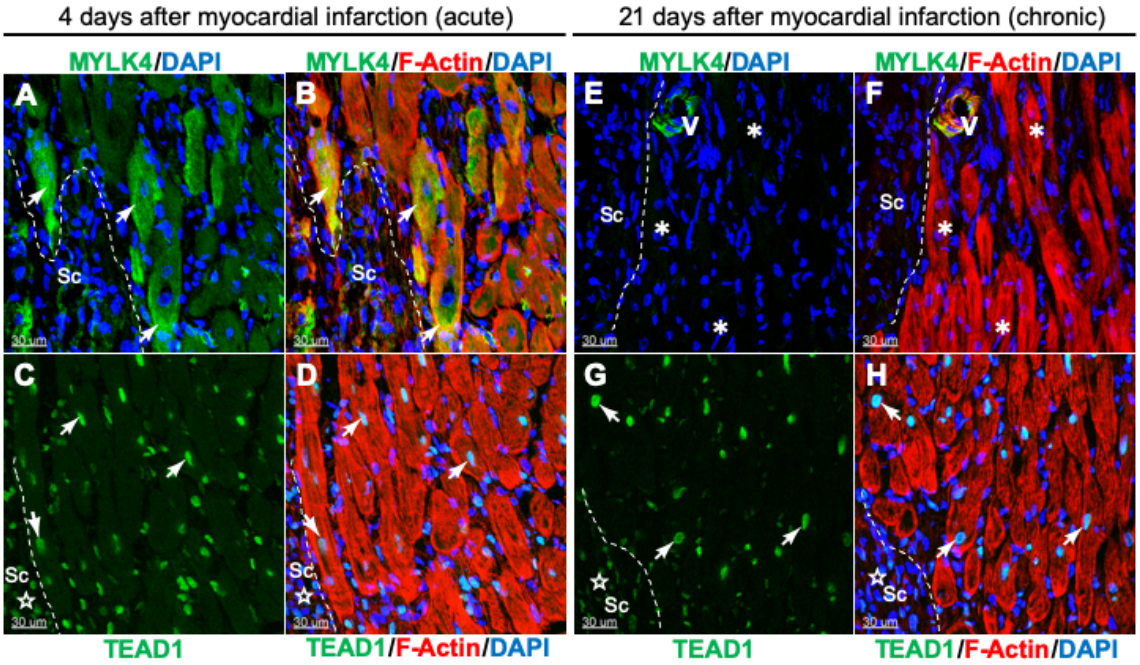

Figure 61. ***Transient myocardial MYLK4 expression in cardiomyocyte bordering infarction in acute (4 days) and chronic phases (21 days).*** *Panels* ***A - D****: Acute phase (4 d after MI). (****A*** *and* ***B****) show Mylk4^{pos} cardiomyocytes (arrows) bordering infarction. (****C*** *and* ***D****) Cardiomyocytes (arrows) and non-cardiomyocytes (star) are TEAD1^{pos}. Panels* ***E - H****: Chronic phase (21 d after MI). (****E*** *and* ***F****) Note that cardiomyocytes bordering infarction are MYLK4^{neg} (asterisk). (****G*** *and* ***H****) Cardiomyocytes (arrows) and non-cardiomyocytes (star) are TEAD1^{pos}. The scar area (Sc) is outlined with dashed white line. V labels MYLK4^{pos} vessels. Green – MYLK4 / TEAD1, red – F-Actin, blue – DAPI; V – Vessels, Sc – scar area.*

3.10 Induced Tead1 inactivation in isolated postnatal cardiomyocytes results in formation of inhomogeneous cell layer and retraction of filopodia

An obvious feature of cultured cardiomyocytes isolated from pTead1-cKO mutant hearts was an incomplete deletion of *Tead1*, which resulted in TEAD1-positive and -negative cardiomyocytes (Figures 41B and 56B). In order to achieve a complete *Tead1* inactivation in early PCMs (P3), a transgenic tamoxifen-inducible *MCM-Cre::Tead1*$^{fl/fl}$ strain, referred to as i(inducible)Tead1-cKO, was used. In this strain, the Cre-ER^{T2} fusion-protein is expressed under the control of *Myh6* promoter, which can be activated upon 4-Hydroxytamoxifen (4-HT) administration [111]. 4-HT treated control cardiomyocytes displayed characteristic spreading morphology and formed homogenous, synchronously beating cell monolayers (Figure 62, left panel). In contrast, iTead1-cKO cardiomyocytes retracted their filopodia and lost intercellular contacts resulting in heterogeneous, asynchronously beating cell layers (Figure 62, right panel).

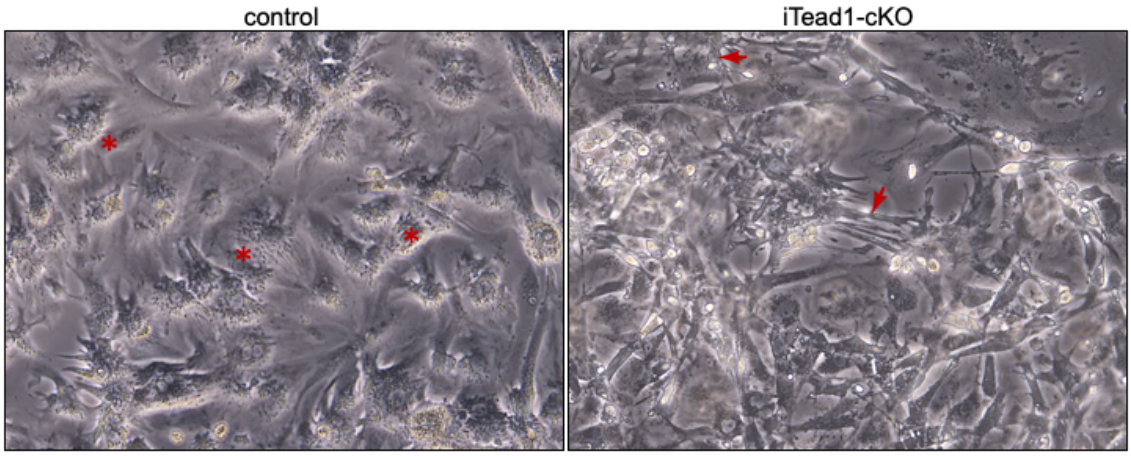

Figure 62. ***Isolated Tead1-deficient early PCMs undergo atrophy.*** *Representative bright field images of isolated postnatal cardiomyocytes from control and iTead1-cKO after 8 days of 4-HT treatment.* ***Left panel:*** *Treated control cardiomyocytes appear as homogeneous cell culture and display a distinctive spreading morphology (red asterisk).* ***Right panel:*** *In contrast, treated iTead1-cKO myocytes retract initially formed filopodia (red arrows), which results in a heterogeneous cell layer.*

To verify whether *Tead1* deletion in cultured early PMCs reflect the *in vivo* observed downregulation of *Acta2*, co-immunostaining for TEAD1 and ACTA2 was performed. Similar with our *in vivo* observations, *Tead1*-deficient PCMs in culture displayed a concomitant loss of ACTA2 signal, as visualized by

immunofluorescence (Figure 63). However, a complete deletion of *Tead1* was not achieved after 8 days of treatment as depicted by the presence of TEAD1^{pos} cardiomyocytes. Importantly, F-Actin staining of 4-HT treated control and iTead1-cKO cardiomyocytes showed regular sarcomeric cross-striations indicating that sarcomerogenesis in iTead1-cKO cardiomyocytes is not disturbed (Figure 63).

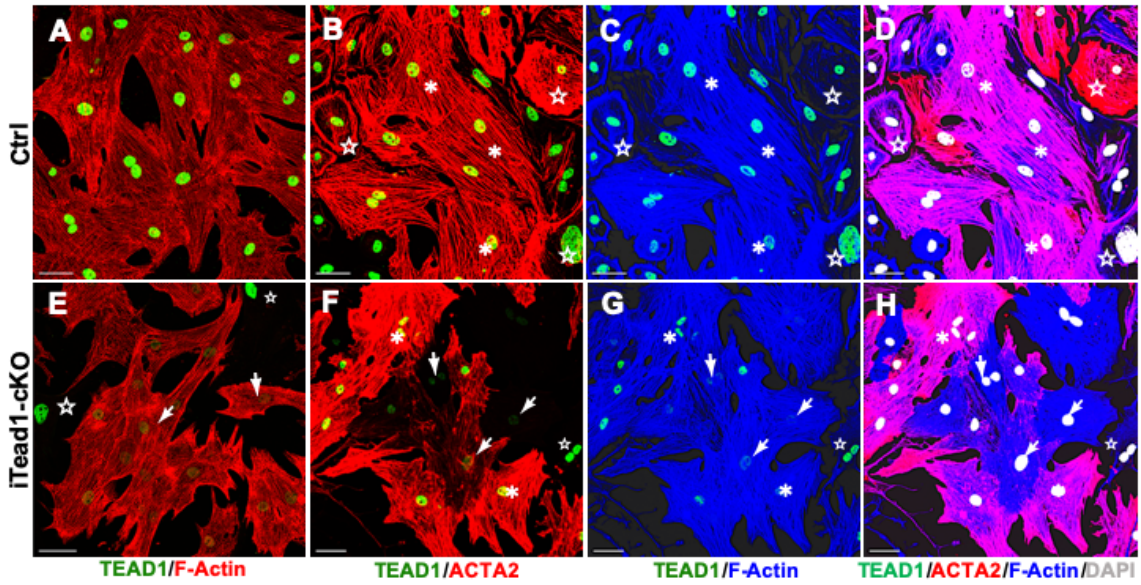

Figure 63. ***Tead1 deletion reduces ACTA2 in P3 PCMs.*** *(**A** and **E**) Representative fluorescent images of F-Actin cross-striation in isolated control (A) and iTead1-cKO (E) early PCMs. (Panels **F** - **H**) ACTA2 signal is diminished in Tead1-deficient myocytes (arrows) compared to TEAD1^{pos}/Acta2^{pos} myocytes (asterisks). (Panels **B** - **D**) Control cardiomyocytes are TEAD1^{pos} / ACTA2^{pos}. Non-cardiomyocytes are depicted with stars. Green – TEAD1, red – F-Actin / ACTA2, blue – F-Actin, white – DAPI. Scale bar: 30 µm.*

To achieve a higher *Tead1* deletion efficiency, an adenovirus expressing a codon of improved *Cre*-recombinase (Ad-Cre), based on knockout approach was used in cultured postnatal cradiomyocytes. In order to determine the optimal virus to cardiomyocytes ratio (multiplicity of infection, MOI), isolated early PCMs conditionally expressing fluorescent Cre reporter (*R26-CAGG-GFP*) were infected with serial dilutions of virus titter (MOI of 10 -100) and scored for infection efficiency and cell survival. Infected cardiomyocytes were analyzed in IncuCyte® live cell analysis system to monitor cell confluence and GFP expression. The MOI of 20 was selected for further experiment because of optimal higher recombination efficiency and low toxicity (Figure 64).

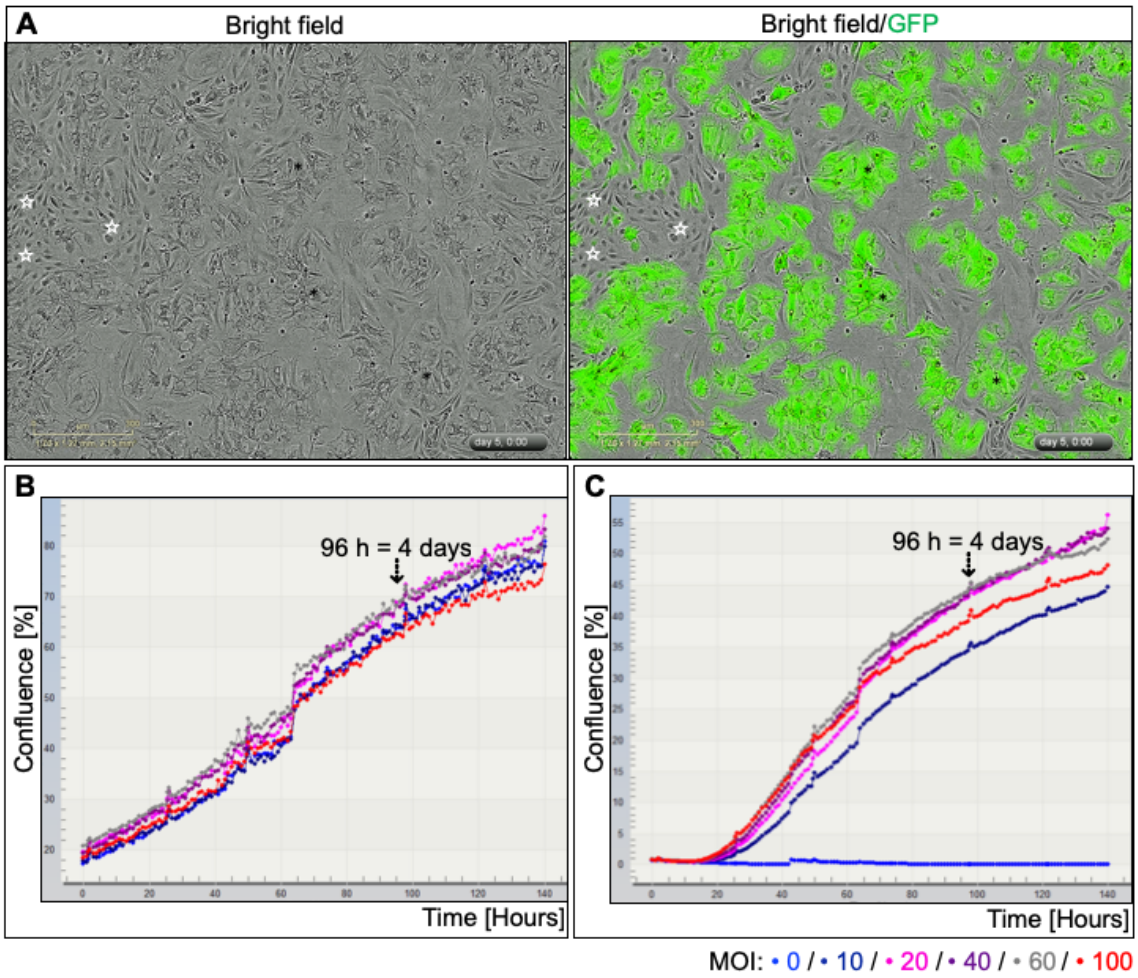

Figure 64. ***Dose and time-dependent efficiency of Ad-Cre mediated GFP expression in early PCMs.*** *(**A**) Representative bright field (left panel) and merged with GFP (right panel) images of infected GFP^{pos} cardiomyocytes (green, asterisk). Note that cells displaying non-cardiomyocyte morphologies (white stars, presumably fibroblasts) are GFP^{neg}. (**B**) Step-wise increase of Ad-Cre infected myocytes achieving 70% cell confluency at 96 h after transduction. (**C**) Step-wise increase in confluency of recombined GFP^{pos} cells in dependence on MOI of Ad-Cre. Note that non-infected myocytes (blue line) display no GFP signal. Blue – no virus, Dark blue – MOI of 10, Magenta – MOI of 20, Purple – MOI of 40, Grey – MOI of 60, Red – MOI of 100; h – hours.*

Next, isolated *Tead1*$^{fl/fl}$ early PCMs, carrying homozygous conditional *Tead1* allele, were infected with Ad-Cre (MOI of 20) for 6 h to induce *Tead1* deletion in culture. The infection resulted in efficient recombination after 4 days, which reduced *Tead1* mRNA level by approximately 90%, consistent with the undetectable TEAD1 protein in western blot analysis (Figures 65E and 65F). In addition, expression levels of *Acta2* and *Crhr2* were also 3-fold and 16-fold, respectively, reduced compared to control cardiomyocytes, which were infected with an empty adenovirus (Ad-empty) (Figure 65E). Time-laps microscopy revealed reduced proliferation of Ad-Cre infected cardiomyocytes 4 days after

infection (Figures 65A - 65D). The observed increases in cell proliferation 8 days after transduction occurred presumably due to non-cardiomyocytes proliferation, e.g. fibroblasts (Figure 65C).

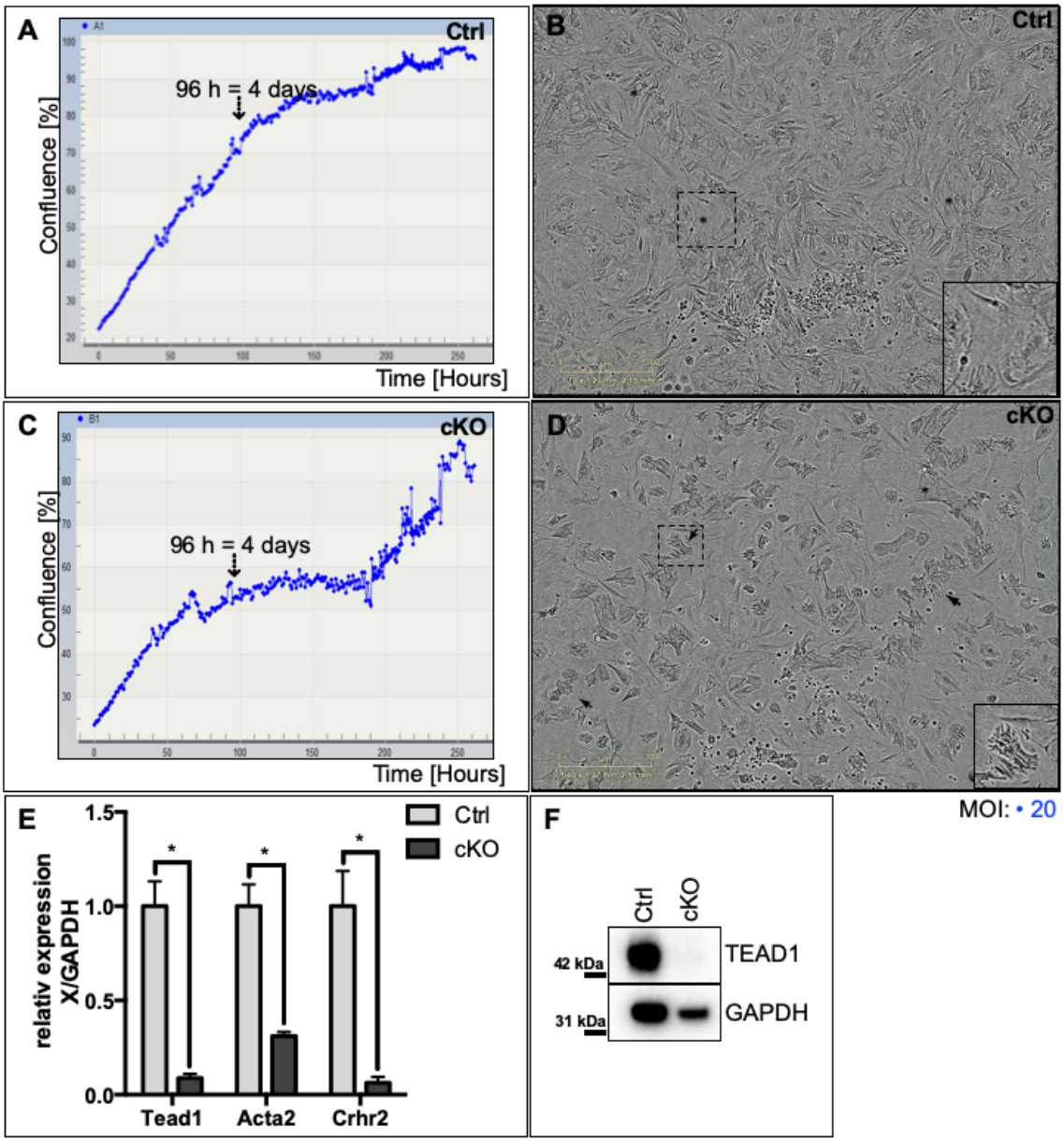

Figure 65. ***Ad-Cre mediated Tead1 deletion in isolated PCMs supresses cell growth.*** *(**A**) The curve represents the time course of confluency of control (Ctrl) infected (Ad-empty) cardiomyocytes. (**B**) Control cardiomyocytes forms a homogenous cell layer with spread cardiomyocytes (asterisk and boxed region). (**C**) The curve represents Tead1-deficient cardiomyocytes after Ad-Cre infection showing inhibition of cell proliferation and confluency 4 days after infection. (**D**) Tead1-deficient cardiomyocytes appear atrophied and retract the initially formed filopodia thereby loosing cell-to-cell contacts (arrows and boxed region) 4 days after transduction. (**E**) Significant expression reductions of Tead1 (by 90%), Acta2 (by 65%) and Crhr2 (by 94%) 4 days after Ad-Cre transduction. Values are normalized to Gapdh mRNA levels. Data are means ± SD, ∗ = $P < 0.05$, $n = 3$. (**F**) Western blot displays strong TEAD1 protein reductions 4 days after Ad-Cre infection. GAPDH serves as a loading control.*

Moreover, EdU-based proliferation assay revealed that *Tead1*-deficient cardiomyocytes displayed a 10-fold lower proliferation rate compared to control infected cultures (Figure 66). In addition, 4 days after Ad-Cre transduction all cardiomyocytes were TEAD1^{neg} and appeared atrophied (Figures 66B, 66D and 66F).

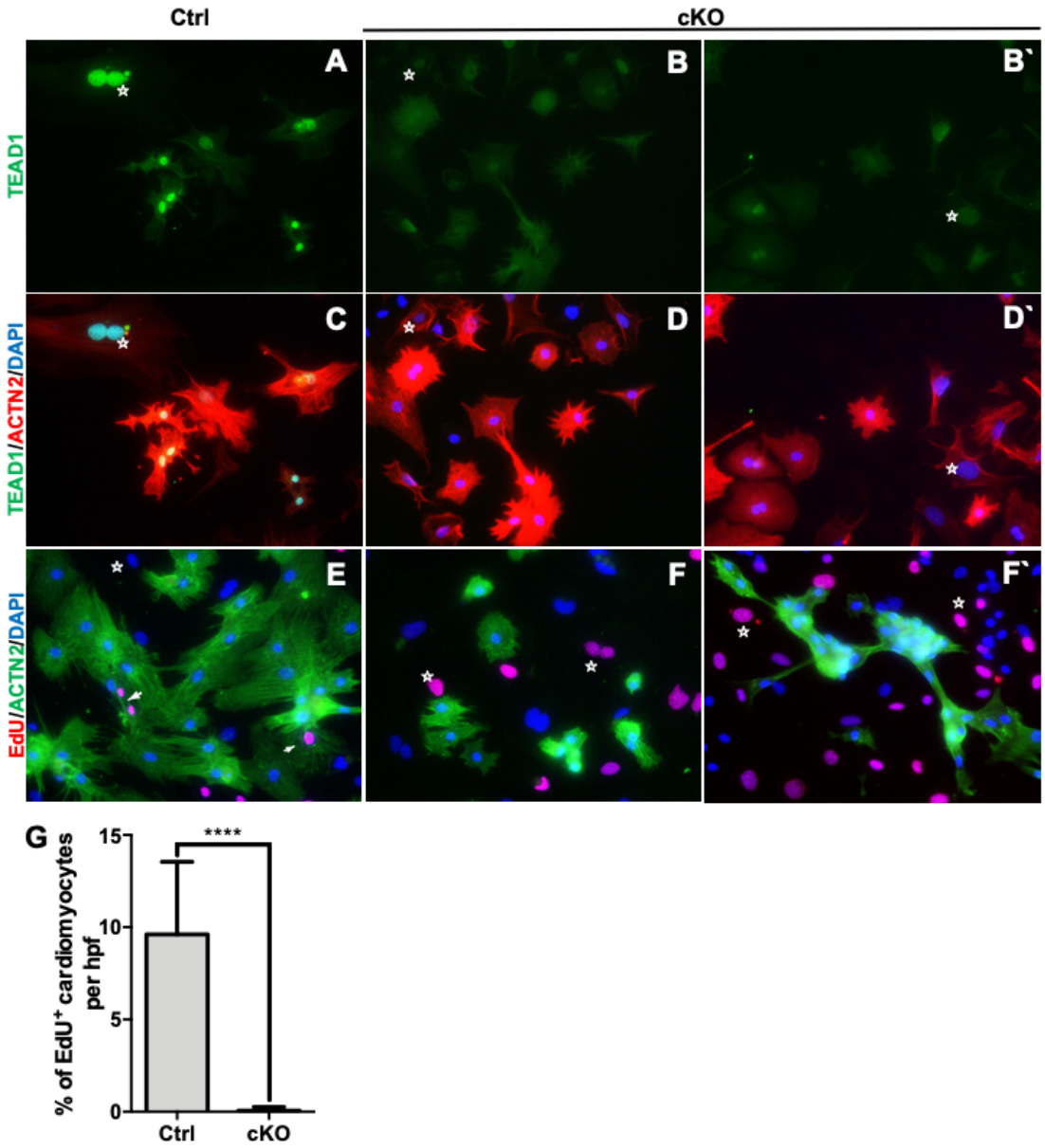

Figure 66. ***Adeno-Cre mediated Tead1 deletion in isolated early PCMs results in reduced proliferation 4 days after infection.*** *(**A**, **C**, **E**) Representative fluorescent images of control infected cultures showing EdU^{pos} PCMs (white arrows, E) with nuclear TEAD1 signal (panels A, C). (**B, D, F**) Ad-Cre infected PCMs are TEAD1^{neg} (panels B, D) and EdU^{neg} cells (F). Non-cardiomyocytes are indicated with white stars in all images. (**G**) Ad-Cre infected cultures of PCMs display a 90 % reduction of proliferating EdU^{pos} cardiomyocytes compared to control infected cultures. Green – TEAD1 / ACTN2, red – EdU / ACTN2, blue – DAPI; hpf – high-power field. Data are means ± SD; **** = P < 0.001.*

3.11 FGF2-TEAD1 pathways crosstalk in adult rat cardiomyocytes

It is well established, that the cytokine FGF2 (Fibroblast Growth Factor 2) functions as a potent regulator of multiple cellular functions, including cell proliferation, differentiation, survival and migration [146-150]. In particular, it has been shown that FGF2 in the myocardium acts as a cardioprotective cytokine during ischemia and afterload-induced hypertrophy (reviewed in [147]). Moreover, FGF2 stimulation of cultured adult cardiomyocytes switches the expression of contractile genes from “adult” to “fetal” program [151]**.** Due to the fact that Acta2 expression is strongly stimulated by FGF2 [151], and given that Acta2 expression depends highly on TEAD1 (Figures 47-51, 55-59 and 63), we analyzed TEAD1 protein level in adult rat cardiomyocytes (ARCs) upon FGF2 stimulation. Furthermore, it has been reported that stimulation of α_1-adrenergic pathway in ARCs induces TEAD1 binding to *Myh7* promoter thereby enhancing *Myh7* expression [105]. In order to figure out, if either FGF2 or α_1-adrenergic pathway induces *Tead1* expression in ARCs, we performed independent FGF2 and epinephrine stimulations combined with TEAD1 western blot analysis and time-lapse imaging. Interestingly, only FGF2 stimulation severely increased TEAD1 protein level, whereas TEAD1 protein was unaltered in epinephrine stimulated ARC, comparable to bovine serum albumin (BSA) stimulated controls (Figure 67A).

A hallmark of FGF2 stimulated ARCs dedifferentiation is the loss of typical road shape characteristics and cell size increases upon spreading [148, 152], which can quantitatively be measured using time-lapse imaging. In order to analyze if FGF2 signaling is mediated *via* TEAD1, we performed siRNA-mediated knockdown (KD) of *Tead1* (siTead1) and *FGFR1* (siFGFR-1) in FGF2 stimulated ARCs. The main reason for targeting FGFR1 (FGF Receptor 1) is the fact that this receptor is highly abundant in cardiomyocytes [146, 153, 154].

Since FGF2 acts as a pro-hypertrophic cytokine, FGF2 stimulated control treated with non-targeting control siRNA (siCtrl) ACRs strongly increased in cell size compared to BSA treated siCtrl myocytes (Figures 67D and 67E). Interestingly, siTead1 cardiomyocytes did not increase in cell size upon FGF2 stimulation. Comparable to siTead1 KD cardiomyocytes, FGF2 stimulation of siFGFR1 KD

ARCs inhibited myocyte hypertrophy as judged by the percent of cell confluence and cell size (Figures 67D and 67E). Moreover, siTead1 as well as siFGFR1 rat cardiomyocytes recapitulated the atrophic phenotype observed in another cell system of isolated *Tead1*-deficient mouse cardiomyocytes (Figures 41B, 42B, 62, 65C and 65D), suggesting that TEAD1 is regulated likely *via* FGF2 pathway.

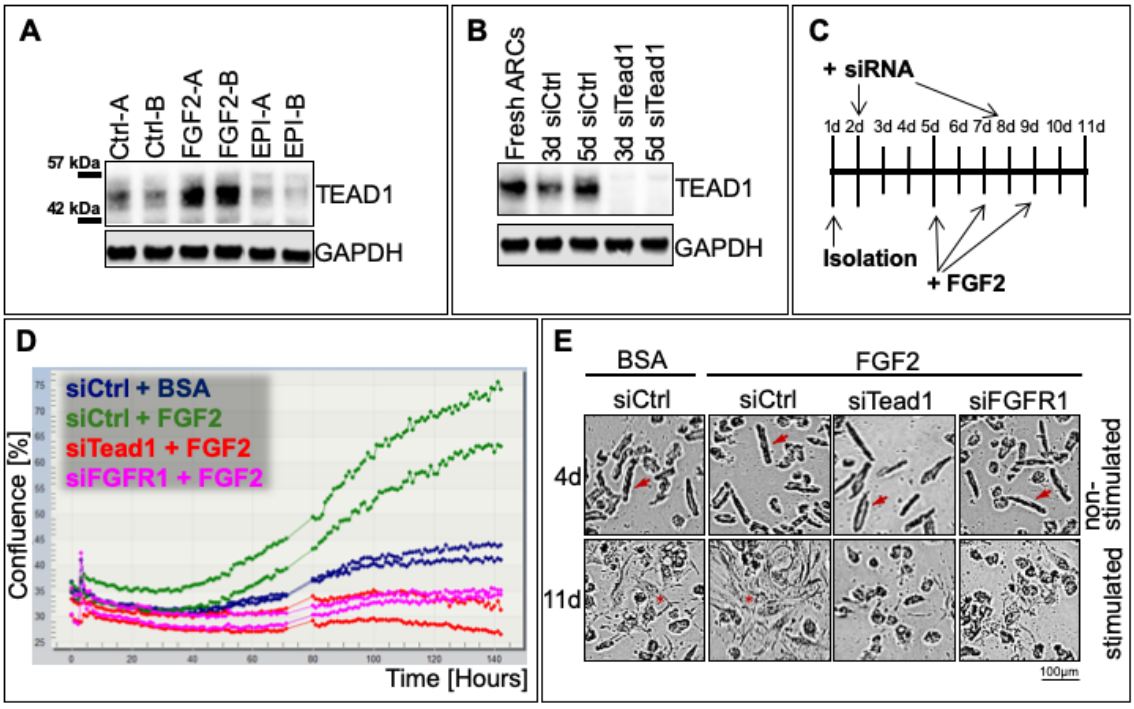

Figure 67. ***FGF2 enhances TEAD1 expression in cardiomyocytes.*** *(**A**) Increased TEAD1 protein level in FGF2 stimulated ARCs, whereas epinephrine (EPI) stimulation has no impact on TEAD1 protein level. (**B**) Efficient siRNA mediated Tead1 knockdown (KD) in ARCs. (**C**) Schematic outline of the performed siRNA mediated KD and FGF2 stimulation experiments. (**D**) Tead1 (red lines) as well as FGFR1 (magenta lines) KDs display an atrophic phenotype upon FGF2 stimulation, whereas siCtrl FGF2 stimulated cardiomyocytes (green lines) appear hypertrophied in comparison to non-stimulated ARCs (blue lines). (**E**) Images of siTead1, siFGFR1 and siCtrl treated road shaped ARCs (red arrows) before (4d, upper panels) and after FGF2 stimulation (11d, lower panels) in comparison to non-stimulated siCtrl ARCs. Note that siCtrl cardiomyocytes after FGF2 stimulation (11d) dedifferentiate as characterized by morphology changes e.g. spreading, increasing in the size (red asterisk). EPI – epinephrine, d – day(s)*

4 DISCUSSION

The adult mammalian heart is a dynamic organ, which can adapt to workload alteration by physiological and morphological changes. The contraction of all cardiomyocytes within the myocardium is highly coordinated and synchronized to guarantee an adequate cardiac output, which is constantly increasing from embryonic development to postnatal heart growth. While embryonic heart development is mainly promoted by cardiomyocyte proliferation, the postnatal heart growth is predominantly supported by cardiomyocyte hypertrophy and terminal differentiation that limits heart regeneration [20, 24, 25, 27].

Cardiogenesis is a precisely regulated process governed by signaling pathways and transcription factor networks, including GATA4, NKX2.5 (NK2 homeobox 5), ISL1 (Islet 1), TBX1 and 5 (transcription factor T-box 1 and 5) (reviewed in [155, 156]).

The present study indicates, that transcription enhancer factor 1 (TEAD1) is an important regulator of multiple genes responsible for cardiomyocyte proliferation, differentiation and growth, which are the hallmarks of cardiomyocyte plasticity. Moreover, during development as well as under pathological conditions, like hypertrophy, TEAD1 regulates the myocardial fetal gene program [12, 14-19, 73, 99, 105]. In addition, it has been suggested that TEAD TFs and their transcriptional co-activator YAP1 act downstream of the Hippo-signaling pathway, which controls multiple cellular processes including regeneration, proliferation, stem cell maintenance as well as organ size regulation [89, 90, 140, 157, 158]. In line with these observations, it has been shown that α-adrenergic stimulation of cardiomyocytes activates *via* TEAD1 the fetal gene *Myh7* re-expression thus facilitating hypertrophic cell growth [15, 64, 105].

It has been shown, that constitutive *Tead1* deletion in mouse is embryonic lethal at E11.5 due to heart malformations characterized by ventricular wall thinning and hypotrabeculation, whereas myofiber ultrastructure is not altered [12]. In order to identify whether cardiomyocytes are the primary cause of this phenotype we have conditionally inactivated *Tead1* in this cell type during early cardiac development and observed similar morphological heart malformations. In addition, we showed that the proliferation rate of embryonic cardiomyocytes was

significantly reduced, whereas the number apoptotic cells was highly increased. In contrast, embryonic cardiomyocytes overexpressing *Tead1* displayed enhanced proliferation accompanied by an unaltered apoptosis rate. However, the increased proliferation of embryonic cardiomyocytes in the latter strain had no impact on adult heart size and function, suggesting compensatory mechanisms. The present study demonstrated that cardiomyocyte-specific deletion of *Tead1* in postnatal stage resulted in heart failure because of dilated cardiomyopathy (DCM) characterized by reduced cardiomyocyte proliferation and increased apoptosis rates associated with severe interstitial fibrosis. Importantly, the lethal heart phenotype of these conditional *Tead1*-deficient mice was rescued by cardiomyocyte-specific *Tead1* overexpression.

Combined global expression profiling of *Tead1*-deficient cardiomyocytes and genome wide TEAD1 binding studies in cardiomyocytes, enabled us to identify cardiomyocyte-specific direct TEAD1 target genes encoding cytoskeletal and contractile proteins, linker proteins between cellular and extracellular matrix, smooth muscle proteins and proteins involved in cardiomyocyte metabolism. Furthermore, our experiment using isolated adult rat cardiomyocytes stimulated with FGF2 demonstrated that TEAD1 protein level was increased downstream of the FGF2-FGFR1-signaling pathway, which has been previously described to be involved in cardioprotection, cardiomyocyte development, proliferation, hypertrophy as well as angiogenesis in the heart ([151] and reviewed in [147]).

4.1 Embryonic cardiomyocyte-specific Tead1 deletion results in embryonic lethality

Since constitutive *Tead1* mutants displayed severe embryonic heart malformations and are embryonically lethal [12], an alternative conditional targeted strategy for specific *Tead1* deletion in early embryonic cardiomyocytes was used in the present study. In addition to the previously reported embryonic heart phenotype comprising ventricular wall thinning and hypotrabeculation, we detected reduced cardiomyocyte proliferation and increased apoptosis rates in our conditional *Tead1* mutant. Furthermore, on the ultrastructural level we observed loosely distributed cardiomyocytes with undeveloped intercalated discs and decreased number of sarcomeric structures resulting in shorter myofibers.

The present study demonstrating increased cardiomyocyte proliferation in *Tead1* knockout hearts is in good agreement with those obtained in embryonic hearts with conditional inactivation of *Yap1*, which is a well-established TEAD1 transcriptional co-activator [89]. In addition to reduced cardiomyocyte proliferation observed in *Yap1* mutants, our *Tead1* mutants displayed increased apoptosis rates, indicating a potential role of TEAD1 in cardiomyocyte death and survival.

4.2 Specific *Tead1* deletion in postnatal cardiomyocytes leads to severe heart failure

In order to overcome embryonic lethality of mice with early cardiomyocyte-specific *Tead1* deletion, we have conditionally inactivated *Tead1* in cardiomyocytes during postnatal stages. These mice died within 4 weeks after birth because of severe heart failure. *In vivo* analysis of *Tead1* mutant mice using magnetic resonance imaging technique demonstrated contractile dysfunctions characterized by reduced left ventricular ejection fraction and biventricular dilation. Histological analysis demonstrated ventricular wall thinning, cardiomyocyte atrophy and enlargement of the intercellular space. Ultrastructural analysis of *Tead1* mutant hearts revealed elongation and thinning of cardiomyocytes, an enlargement of the intercellular space as well as severe myocardial fibrosis. Morphometric analysis of isolated cardiomyocytes from *Tead1* mutant hearts confirmed the elongation and thinning. Additionally, *Tead1* mutant hearts displayed a decrease in cardiomyocyte proliferation and significant increases in cardiomyocyte apoptosis rate, which might also explain the occurrence of myocardial fibrosis in these mice. The above-mentioned functional disturbances and morphological alterations are compatible with the clinical diagnosis of dilated cardiomyopathy (DCM).

DCM is defined by a pathologically abnormal myocardium and an enlargement of the heart, which often affects all four chambers, especially in late disease stages. Most commonly, DCM is associated with reduced left ventricular (LV) contraction function, although in early stage of the disease the LV may be dilated, with only minimally reduced function (as reviewed in [159]). Recent studies have revealed an increasing number of gene mutations linked to DCM including structural,

sarcomere, costamere, Z band, nuclear membrane genes as well as genes regulating transcriptional networks downstream of signaling pathways *e.g.* AKT-, GPCR-, NFAT-, WNT- and Hippo-pathways (reviewed in [30, 160-163]). Regarding the latter pathway, it has been shown that cardiomyocyte-specific overexpression of *Mst1*, the core-component of the Hippo-signaling pathway in mouse, leads to severe DCM associated with increased cardiomyocytes apoptosis, ventricular wall thinning and depressed cardiac function [79]. On the other hand, postnatal cardiomyocyte-specific inactivation of *Yap1*, which is inhibited by Hippo-pathway activation and is one of known TEAD1 cofactors, resulted also in severe cardiomyopathy and heart failure [157, 158]. Given that TEAD1 acts downstream of Hippo-pathway, our data in pTead1-cKO mice showing a DCM phenotype concur well with above mentioned observations.

Cardiac interstitial and replacement fibrosis due to cardiomyocytes loss are a hallmark of DCM. As reviewed by Dobaczewski [164], elevated TGF-β expression levels in myocardium are associated with fibrosis and play an important role in cardiac remodeling in DCM and heart failure. In line with this, our gene set enrichment analysis of global expression changes in *Tead1*-deficient cardiomyocytes displayed enrichments of genes encoding the TGF-β signaling pathway such as *Thbs1* (Thrombospondin1), *Eng* (Endoglin), *Furin*, *Map3k7*, *Rab31* and *Tgfβ1* (Transforming-Growth Factor β1). Therefore, upregulation of the TGF-β pathway observed in our postnatal *Tead1* mutant hearts might have contributed to myocardial fibrosis in these mice.

Certainly, myocardial fibrosis, disturbed balance between cell proliferation and cell death, cardiomyocyte elongation as well as ventricular thinning might have played important roles in contractile cardiac dysfunction observed in *Tead1* mutants. However, the ultrastructural analysis revealed no obvious degenerative alterations in *Tead1*-deficient cardiomyocytes. Therefore, it is tempting to speculate that contractile dysfunction of *Tead1* mutant hearts in the absence of striking morphological alterations in cardiomyocyte sarcomeric structures may culminate in heart failure. In favor of this hypothesis speaks numerous studies showing that overt heart failure and contractile insufficiency may occur even in the absence of degenerative changes in individual cardiomyocytes [165].

In agreement with our data on postnatal cardiomyocyte-specific *Tead1* inactivation, a recent report showed that inducible cardiomyocyte-specific *Tead1* deletion in adult murine cardiomyocytes results in severe DCM [18]. Moreover, a recently published study of the same research group supports our observations and shows that loss of *Tead1* expression using *Myh6*-Cre in mouse cardiomyocytes resulted in postnatal lethality at P5-P9. Interestingly, this heart phenotype was characterized by reduced cardiomyocyte proliferation, severe fibrosis and heart failure due to DCM [108]. However, our study revealed additional effects of cardiomyocyte-specific *Tead1* inactivation including impaired cardiomyocyte differentiation and maturation characterized by disturbed myofibrillogenesis. Importantly, these phenotypic changes in our postnatal *Tead1* deletion model occurred at later postnatal stages (at 2-4 weeks). It is worthy to note that in comparison to our postnatal MCK-Cre mediated *Tead1* deletion, the earlier occurred heart phenotype in the Liu *et al*. study might result from utilizing an earlier *Myh6*-Cre delete allele.

4.3 *Tead1* overexpression stimulates embryonic cardiomyocyte proliferation resulting in hypertrabeculation

Myocardial trabeculation increases cardiac output and permits nutrition as well as oxygen uptake in the embryonic myocardium prior to coronary vascularization without increasing heart size, thereby playing an essential role in the fetal heart growth and function. It is well accepted that trabecular cardiomyocytes are at a more advanced differentiation stage and therefore proliferate 2-times less than cardiomyocytes in the compact layer (reviewed in [164]). Although the mechanisms, which regulate cell cycle exit of trabecular cardiomyocytes are only partially understood, several studies suggested that trabecular layer growth mainly results from migrating cardiomyocytes of the compacted myocardium (reviewed in [166, 167]). In this context, the present conditional overexpression of *Tead1* in embryonic cardiomyocyte resulted in enhanced proliferation, especially in the trabecular layer leading to transient ventricular hypertrabeculation during embryogenesis. However, this feature had no detrimental impact on subsequent postnatal heart growth.

The biological functionality and compatibility of TEAD1-Flag-HA (*Tead1*-Rescue strain) was assessed by compound *Tead1* allele comprising the conditional cardiomyocyte-specific knockout combined with the gain-of-function (GOF) transgene. As expected, there were no differences between control and *Tead1*-Rescue mice in life span. The present results obtained in mice with cardiomyocyte-specific overexpression of *Tead1* demonstrating increased proliferation rates of trabecular cardiomyocytes during embryogenesis are in good accordance with the published observations in mice harboring constitutive active YAP1 (*Yap1[S127A]*) [89, 158]. Taken together, these data indicate highly coordinated activities of TEAD1 and YAP1 in the proliferation of trabecular cardiomyocytes. This conclusion is furthermore supported by data showing that YAP1 regulation of cardiomyocyte proliferation requires direct interaction with TEAD, which was demonstrated by two independent approaches using either a dominant negative peptide specifically blocking YAP1-TEAD interaction or a YAP1 point mutation-defective TEAD interaction [89]. These observations suggest that high levels of TEAD1 combined with YAP1 might plausibly extend the window of postnatal cardiomyocyte proliferation.

Interestingly, overexpression of two different constitutive nuclear active YAP1 mutants (*Yap1[S112A]*, *Yap1[S127A]*) in embryonic cardiomyocytes resulted in increased cardiomyocyte proliferation and thickening of the myocardium [89, 158]. However, it is worth noting that both YAP1 forms differ in the heart phenotype severity. While *Myh6*-Cre driven *Yap1[S112A]* overexpression resulted in non-lethal heart hyperplasia, doxycycline-induced activation of *Yap1[S127A]* led to myocardial overgrowth, ventricular wall thickening and marked expansion of the trabecular myocardium resulting in embryonic lethality. Such differences in the phenotype severity of both *Yap1* overexpression approaches might either be explained by different activities of the YAP1 mutants or by divergent activation levels of the utilized overexpression systems (*e.g.* Cre-mediated *versus* doxycycline-inducible). *Tead1* overexpression in the present study probably reflects the milder phenotype of embryonic *Yap1[S112A]* overexpression. One should, however, consider that transcriptional activation of TEAD TFs strongly depends on the presence of cofactors, which provide either coactivator, *e.g.* YAP1, or corepressor, *e.g.* VGLL-4, functions modulating thereby transcriptional network of TEAD TFs targeted genes [82, 86]. This

assumption is in line with published observations showing that YAP1 protein is robustly present in postnatal as well as juvenile cardiomyocytes and declines with age [86, 89]. The endogenous downregulation of TEAD1 coactivators, *e.g.* YAP1, in adult cardiomyocytes might compensate the hyperplastic phenotype in *Tead1*-overexpressing mice examined in the present study.

In contrast to YAP1, the protein level of the TEAD TFs repressor, VGLL-4, increases from low level in the new-born heart to high level in the adult heart [86], which might counteract *Tead1* overexpression observed in our study. It has been shown, that VGLL-4 restrains proliferation of postnatal cardiomyocytes by inhibiting TEAD1-YAP1 interaction and targeting TEAD1 for degradation. Moreover, in early postnatal cardiomyocytes TEAD1 and VGLL-4 interaction is inhibited by acetylation of the VGLL-4 TDU-domain, whereas adult cardiomyocytes lack this acetylation. This finally results in a switch of interaction partners from high-proliferative YAP1 to low-proliferative VGLL-4 in mature cardiomyocytes. Of note, an acetylation-resistant *Vgll-4* (*Vgll4[R]*) cardiomyocyte-specific overexpression induced severe myocardial dysfunction, myocardial wall thinning, reduced cardiomyocyte proliferation and increased fibrosis, whereas overexpression of the wild type *Vgll-4* did not significantly affected heart growth or function [86]. In this regard, the hyperproliferative phenotype of *Tead1*-overexpressing embryonic and early postnatal cardiomyocytes as well as the unaltered phenotype in adult hearts observed in the present study might be explained by VGLL-4 dependent TEAD1 degradation in adult cardiomyocytes. In fact, this could be one of the explanations for compensatory mechanism underlying an unaltered morphology of adult *Tead1* GOF mutants, although these mice displayed cardiomyocyte hyperproliferation during development and maturation. One strategy to overcome TEAD1 dependence on coactivators as well as corepressors in cardiomyocytes might be the overexpression of a constitutive active TEAD1, a chimeric protein of TEA DNA-binding domain of TEAD TFs fused to a strong transactivation domain of VP16 herpes simplex virus protein, which was previously reported in mouse fibroblasts [137, 168, 169].

It is worth to mention, that the previously published postnatal MCK-promoter driven *Tead1* overexpression resulted in late onset (10 month) of cardiac dysfunctions, myocardial fibrosis as well as reactivation of the fetal gene program

e.g. Acta1 and *Myh7* [17]. Importantly, comparable to our 8 weeks old *Tead1*-overexpressing mice, this MCK-driven *Tead1* overexpression showed no phenotypical changes at earlier time points. Moreover, inducible cardiomyocyte-specific overexpression of *Yap1[S127A]* during postnatal stages showed increased cardiomyocyte proliferation capacity without any obvious heart alterations [89]. Interestingly, long-lasting induction of *Yap1[S127A]* overexpression resulted only in slightly decreased heart function and modest myocardial fibrosis, however cardiomyocyte size was not increased, indicating mild effects of chronic *Yap1[S127A]* overexpression [90]. These findings are comparable to present data obtained in *Tead1*-overexpressing hearts.

4.4 TEAD1 regulates multiple cardiomyocyte-specific genes involved in proliferation, differentiation and survival.

Several studies have demonstrated transcriptional gene regulation by the ubiquitously expressed transcription factor TEAD1 in combination with co-activators/-repressors *e. g.* YAP1, WWTR1, VGLLs in various cell types [84, 86, 97, 140, 170]. Moreover, increased specificity of TEAD TFs mediated gene expression is accomplished by interactions with numerous cell-type and -processes specific transcription factors including MAX, SRF, MEF2, IRF2BP2, FOXO, SMADs [14, 16, 96, 98, 100, 101]. In particular, TEAD1 muscle-specific gene regulation is predominantly provided by binding to a specific DNA sequence, called MCAT-element, which was initially identified in the promoter region of the malonyl-coA-acyl carrier protein transacylase gene [10, 70, 171]. Moreover, some studies revealed that TEAD1 exerts repressive functions on gene expression in the context of target genes, cell types and conditions [86, 102, 137]. For instance, binding of TEAD TFs to MCAT-elements represses *Acta2* transcription in cultured adult smooth muscle cells (SMCs), whereas in cultured myoblasts, fibroblasts and endothelial cells TEAD TFs binding mediates a transcriptional activation of *Acta2* [63]. Altogether, these observations indicate, that TEAD1 regulates gene expression either in combination with activating and repressing cofactors, respectively, or cooperatively with additional transcription factors to guarantee precise gene expression depending on cell-type and context.

A number of studies have examined the TEAD1 DNA binding sites in various cell types including skeletal muscle, cancer cell lines in an effort to specify chromatin occupancy and transcriptional activity of TEAD1 [15, 18, 48, 136, 170]. While these studies have provided important insights into the potential mechanistic role of TEAD1 in various cell-types, so far no study has systematically examined functional significance of genome-wide TEAD1-DNA binding on global transcription, specifically in isolated cardiomyocytes. It should be noted, that several TEAD1 gene specific binding studies in cardiomyocytes have addressed selected targets *e.g. Myh7* [15] , although no global TEAD1 chromatin binding profiles were performed so far.

In order to identify cardiomyocyte-specific TEAD1 target genes, we performed a global transcriptome analysis of *Tead1*-deficient and overexpressing postnatal cardiomyocytes, respectively, combined with genome-wide TEAD1-binding studies in wild-type (WT) postnatal cardiomyocytes. Cardiomyocyte-specific deletion and overexpression of *Tead1* in early postnatal cardiomyocytes resulted in expression changes of approximately 400 genes and 600 genes, respectively. The number of dysregulated genes upon *Tead1* deletion and overexpression in late postnatal cardiomyocytes was increased and comprised approximately 1000 and 700 genes, respectively, which might be explained either by an increased Cre-mediated recombination efficiency in later stages or secondary effects *e.g.* replacement fibrosis. Our gene set enrichment analysis of *Tead1*-deficient cardiomyocytes revealed decreased expression of gene clusters involved in cardiac muscle contraction, fatty acid metabolism and oxidative phosphorylation, which goes in line with previously reported inactivation of *Tead1* in adult cardiomyocytes [18]. Alterations of the latter pathway were also observed in mouse myoblast upon *Tead1/4* deletion [48, 117]. As expected, these gene clusters were transcriptionally upregulated upon *Tead1* overexpression indicating a direct function of TEAD1 in these transcriptional pathways.

In addition, the gene clusters responsible for cell-to-cell communication *(β-Catenin*), cell adhesion (*Fibronectin*, *Laminins*, *Collagen 4*) and focal adhesion (*Actinin 1* and *4*, *Integrin α 5*, *Collagen 4*) proteins were upregulated upon *Tead1* deletion in our postnatal mutants. Upregulation of these gene clusters in *Tead1* mutants might contribute to a premature cardiomyocyte differentiation resulting in disturbed hypertrophic growth and proliferation. On the other hand, increased

expression of cell-contact proteins might reflect an increased mechanical stress on remaining *Tead1*-deficient cardiomyocytes (as reviewed in [172, 173]). In contrast, *Tead1*-overexpressing cardiomyocytes displayed a downregulation of these gene clusters, which might indicate a prolonged maturation process supporting enhanced proliferation of *Tead1*-overexpressing cardiomyocytes. In addition, the extended proliferation potential of *Tead1*-overexpressing cardiomyocytes might have been supported by upregulation of genes involved in Insulin-, mTOR-, ERBB- and WNT-signaling pathways [174-178].

In order to specify genes, which might be directly regulated by TEAD1, genome-wide TEAD1 binding studies using chromatin immunoprecipitation sequencing (ChIP-seq) analysis in freshly isolated WT cardiomyocytes were performed and further compared with the transcriptome analysis of isolated *Tead1*-deficient cardiomyocytes. Due to technical limitations, *e.g.* inefficient *Tead1* deletion in early postnatal cardiomyocytes and insufficient isolation of late postnatal cardiomyocytes, for TEAD1 DNA-binding studies, the ChIP-seq analysis of early neonatal cardiomyocytes (P3) and transcriptome profiling of late postnatal cardiomyocytes (P15-P19) were merged. In total, 63 candidates were downregulated upon *Tead1* deletion and displayed TEAD1 binding to corresponding promoter regions. Surprisingly, only 36 out of the 63 candidates contained well-defined TEAD TFs binding-sites known as MCAT-elements. However, several studies have shown that TEAD TFs have the ability to bind related regulatory sequences including MCAT-like, SV40 GT-IIC, Sph I, Sph II regulatory element, which share sequence similarities to MCAT-motives [40, 46, 179, 180]. Since TEAD TFs binding-sites comprise short degenerated sequences of 6 nucleotides, multiple sequence combinations arise, which were restricted in our analysis to the most abundant MCAT variants. Integration of TEAD1 ChIP-seq data with that of chromatin modification showed 26 genes, which were associated with active H3K9Ac-marked (histone 3 acetylation on lysine 9) regulatory elements [139].

Based on our analysis data, we depicted genes, which are regulated by TEAD1 and have been reported to exert important functions in muscle cells. As has been shown previously, TEAD1 activates ***Myh7*** (Myosin Heavy Chain β-Subunit) expression in rat cardiomyocytes *via* binding to MCAT-elements, which is in line with our ChIP-seq and transcriptome analysis clearly indicating TEAD1 binding

to a MCAT-element containing *Myh7* promoter region [15, 17, 18]. Moreover, downregulation of *Myh7* upon *Tead1* deletion in postnatal cardiomyocytes underlines this result. Due to the fact that *Myh7* is barely expressed in fully differentiated cardiomyocytes under non-pathological conditions (reviewed in [104]), we did not observed *Myh7* downregulation in late postnatal *Tead1*-deficient cardiomyocytes, although *Myh7* was upregulated upon *Tead1* overexpression.

The present study also identified ***Acta2*** (Smooth Muscle Actin) as a potential TEAD1 downstream target gene in cardiomyocytes. *Acta2* has been previously shown in myofibroblasts and developing smooth muscle cells to be regulated by TEAD1 *via* MCAT elements [60, 63]. Moreover, mutations in MCAT-elements resulted in delayed *Acta2* expression in smooth muscle cells as well as loss of *Acta2* expression in cardiac and skeletal muscles during embryogenesis, indicating a complex regulation of *Acta2* expression determined by the cell type and developmental stage, respectively [60].

It is well established, that smooth muscle genes are implicated in cardiomyocyte differentiation and maturation [35, 141, 142]. In line with these observations, our transcriptomic and genome-wide TEAD1 binding profiling as well as immunohistochemical data strongly indicate that TEAD1 regulates expression of *Acta2* during cardiomyocyte differentiation and maturation. Specifically, *Acta2* in embryonic and postnatal cardiomyocytes was reduced in *Tead1*-deficient or increased in *Tead1*-overexpressing cardiomyocytes. Moreover, ultrastructural analysis of *Tead1*-deficient hearts revealed numerous prematurely differentiated cardiomyocytes characterized by compact contractile structures, uniform mitochondria and low glycogen content in comparison to age-matched control cardiomyocytes characterized by sparely arranged contractile filaments, glycogen depositions and polymorphic mitochondria as previously described [143, 144]. These findings indicate an important role of TEAD1 and its downstream targets including *Acta2* in the proper cardiomyocyte differentiation and maturation. This assumption is further supported by the observations of Xin *et al.* who showed that ACTA2 protein was up-regulated in adult cardiomyocytes overexpressing constitutive active *Yap[S112A]*, which is one of the TEAD1 cofactors [158].

The expression level of *Myocardin* (*Myocd)*, a well-known *Acta2* upstream transcriptional regulator [107], was unaltered in *Tead1*-deficient and overexpressing cardiomyocytes, indicating that TEAD1 acts as a MYOCD-independent activator of *Acta2* expression in this particular cell type. This observation is supported by *Myocd* promoter studies, which showed that TEAD1 binding site were dispensable for *Myocd* promoter activation in embryonic heart [16].

Among well-known TEAD1 downstream targets, we identified 24 novel cardiomyocyte-specific TEAD1 regulated genes, including ***Adprhl1*** (ADP-Ribosylhydrolase Like 1), ***Coro6*** (Coronin, Actin Binding Protein 6), ***Syde2*** (Synapse Defective Rho GTPase Homolog 2), ***Fbxl22*** (F-Box and Leucine Rich Repeat Protein 22), ***Popdc2*** (Popeye Domain Containing 2), ***Hsd17b7*** (Hydroxysteroid 17-Beta Dehydrogenase 7) and ***Trim55*** (Tripartite Motif Containing 55/Muscle-Specific RING Finger Protein 2, Murf-2). These genes are known to be responsible for heart development, cardiomyocyte contractility, cytoskeleton arrangement and maturation, which are essential features of proper biomechanical function ensuring an adequate adaptation of cardiac chambers to increased biomechanical forces [181-187].

Furthermore, we have identified potential TEAD1 targets, which are involved in regulation of cardiomyocyte energy homeostasis including ***Prkaa2*** **(**AMP-Activated, α-2 Catalytic Subunit), ***Ckmt2*** (Creatine Kinase, Mitochondrial 2, Sarcomeric), ***Nnt*** (Nicotinamide Nucleotide Transhydrogenase) and ***Scd4*** (Stearoyl-Coenzyme A Desaturase 4) [188-193]. Multiple studies have demonstrated, that the shift of anaerobic glycolysis to mitochondrial respiration during differentiation is required to cover energy demands of differentiated cells (reviewed in [194]). For example, protein kinase PRKAA2 activates multiple catabolic pathways, including fatty acid metabolism, to ensure high levels of ATP production [195]. It is likely that downregulation of genes involved in oxidative phosphorylation in *Tead1*-deficient cardiomyocytes might be one of the causes for increased apoptosis rate in mutant hearts. Surprisingly, the previously reported direct TEAD1 target genes *Serca2a* and *Ppp1R1A* in adult cardiomyocytes were unaltered in our postnatal *Tead1*-deficient cardiomyocytes, which might reflect the differences in TEAD1 mediated gene transcription in postnatal *vs.* adult cardiomyocytes [18].

In addition, we identified a set of TEAD1 target genes including ***FoxO3*** (Forkhead Box O3), ***Crhr2*** (Corticotropin-Releasing Hormone receptor 2), ***Irf2bp2*** (Interferon Regulator Factor 2 Binding Protein 2), ***Ogn*** (Osteoglycin / Mimecan), ***Klhl21*** (Kelch Like Family Member 21) ***Klhl38*** (Kelch Like Family Member 38), ***Mylk3*** (Myosin Light Chain Kinase Family Member 3), ***Abcc8*** (ATP-Binding cassette Subfamily C Member 8) and ***Crip2*** (Cysteine Rich Protein 2) [100, 196-206], which are involved in various biological processes. FOXO3 is a member of FOXO transcription factors family and regulates multiple target genes, which are involved in diverse cellular processes including the ubiquitin-proteasome system and autophagy in cardiomyocytes [207]. These results are in line with TEAD1 DNA binding assays and transcriptome profiling studies of myoblast indicating a direct regulation of *Foxo3* expression by TEAD1 [208]. However, in our analysis *Foxo3* downregulation was restricted to late postnatal cardiomyocytes, which might be explained either by the redundancy of other TEAD TFs or insufficient *Tead1* recombination in early postnatal cardiomyocytes. Moreover, FOXO3 was previously shown to interfere with the Hippo-pathway by activating *Mst1* expression and thereby negatively regulating YAP1 activity in cardiomyocytes [209, 210].

The present study also identified a set of genes, which were strongly downregulated upon *Tead1* deletion and upregulated upon *Tead1* overexpression, respectively, however the proximal promoter regions of these genes were not occupied by TEAD1. This gene set contains 2 candidates including ***Mylk4*** (Myosin Light Chain Kinase Family Member 4) and ***Sntb1*** (Syntrophin Beta 1) [145, 211]. One explanation for the undetectable TEAD1 regulatory occupancy in this gene set might be explained by our settings of bioinformatic analysis, which were restricted to TSS region plus 5000 bp up- and downstream. In this cases TEAD1 might bind to more distal located regulatory regions of these genes, which were not included in our analysis.

A peculiar gene of the TEAD1-occupied promoter region resembles ***Nmrk2*** (Nicotinamide Riboside Kinase 2 / MIBP Muscle Integrin-Binding Protein), which expression was downregulated upon *Tead1* deletion in early postnatal cardiomyocytes, thus indicating a direct TEAD1 regulation of *Nmrk2* at this stage [212]. However, in later cardiomyocyte stages, *Nmrk2* activation seems to

become TEAD1 indispensable, which is indicated by an increased *Nmrk2* expression upon TEAD1 deletion.

Surprisingly, the expression of two well-established YAP1-TEAD target genes ***Ctgf*** (Connective Tissue Growth Factor) and ***Amotl2*** (Angiomotin Like 2) was unaltered upon *Tead1* deletion and overexpression in postnatal cardiomyocytes, although both promoters were occupied by TEAD1 and transcriptionally active, represented by H3K9Ac marks [48, 140]. The unaltered expression of *Ctgf* and *Amotl2* in our study indicates a TEAD1-independent transcription in postnatal cardiomyocytes. However, during late postnatal stages *Ctgf* expression increased upon TEAD1 deletion, indicating a potential repressive function of TEAD1 during cardiomyocyte maturation. Similar observations were described for TEAD4 in C2C12 cells during differentiation, where it acts as a repressor of *Ctgf* [213].

Interestingly, our data demonstrated that TEAD1 binds in own transcriptionally active promoter represented by a H3K9Ac mark, suggesting that TEAD1 positively regulates its own expression. A similar autoregulatory transcriptional activation loop was previously reported for TEAD4 in myoblast differentiation [48]. Moreover, the present study showed that TEAD1 also binds to the *Tead4* promoter region, however the expression levels of *Tead4* as well as of *Tead2* and *Tead3* remained unchanged upon *Tead1* deletion.

In line with a recently reported observation in adult cardiomyocytes [18], we found that *Tead1* specific inactivation in postnatal cardiomyocytes resulted in a 4-fold upregulation of *Vgll-2* (VITO-1), a skeletal muscle specific TEAD1 coactivator, which promotes muscle differentiation by enhancing the expression of muscle-specific genes [84, 95]. However, we could not detect a TEAD1 binding in the *Vgll-2* promoter region, indicating a compensatory effect caused by TEAD1 inactivation.

In conclusion, our combined transcriptomic and genome-wide binding study of TEAD1 in cardiomyocytes resulted in more that 60 TEAD1 directly regulated genes, which correlates with the number of direct TEAD4 targets identified by the comparison of RNA-seq and ChIP-chip data in C2C12 cells [48]. In total, we observed 1675 TEAD1 binding sites, 606 of them were located in the promoter regions, which we defined as transcription start site (TSS) plus 5000 nucleotides up- and down-stream, respectively. This indicates that multiple TEAD1 binding

regulatory sites might be located in far distal promoter regions, reflecting the low number of candidates.

4.5 The role of TEAD1 in cardiomyocyte FGF2-signaling

Multiple studies have shown that FGF2-signaling in the myocardium is predominantly mediated by the abundant high-affinity tyrosine kinase receptor FGFR-1, and regulates cellular processes including proliferation, maturation, hypertrophic growth, dedifferentiation of cardiomyocytes and re-expression of fetal contractile gene program [146, 148-151, 153, 154], which resembles the phenotype of *Tead1* mutants. Our *ex-vivo* experiments in adult rat cardiomyocytes clearly showed the increased TEAD1 protein levels upon FGF2 stimulation. Moreover, siRNA mediated knock-down of *Tead1* as well as *Fgfr1* in adult rat cardiomyocytes resulted in attenuated hypertrophic growth in response to FGF2 stimulation, which is characterized by cardiomyocyte spreading and dedifferentiation. Numerous studies showed that dedifferentiated cardiomyocytes share common characteristics compared to early postnatal ones [152, 214], which supports atrophic phenotype of *Tead1*-deficient postnatal cardiomyocytes in the present study. Of note, *Tead2*, *Tead3* as well as *Tead4* siRNA mediated knockdowns did not affected cardiomyocyte morphology upon FGF2 stimulation suggesting that these TEAD TFs family members can not compensate TEAD1 function in FGF2-FGFR1 pathway. Taken together, our results indicate a potential novel FGF2 mediated TEAD1 regulatory pathway, however, the exact regulatory mechanism needs to be further investigated. The potential role of TEAD1 in FGF2-signaling and its biological effects is depicted in Figure 68. Similar findings were reported in mouse fibroblasts upon FGF1 or FGF2 stimulation, which resulted in an enhanced *Tead4* expression [57].

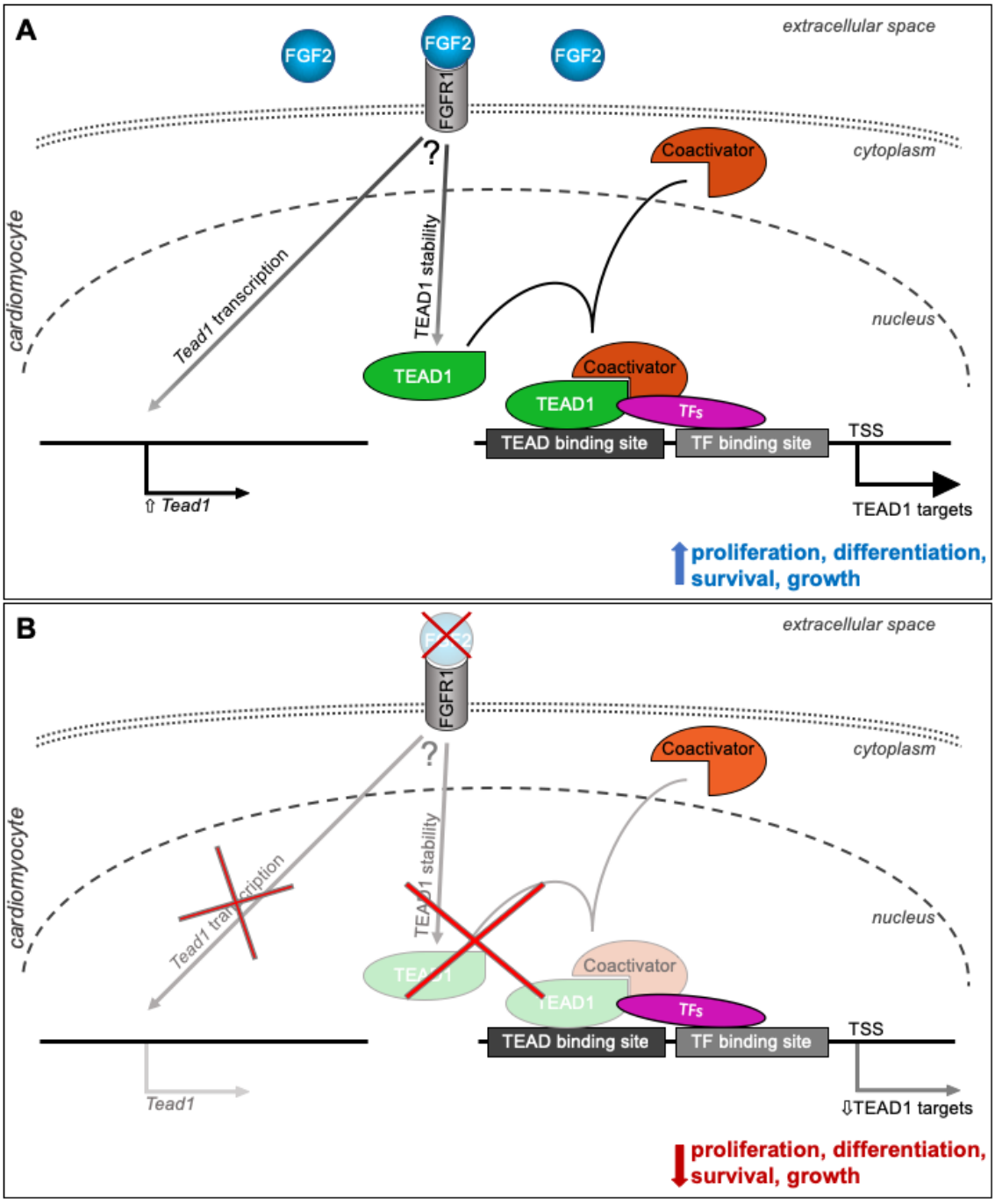

Figure 68. ***Schematic representation of the hypothetical TEAD1 function in cardiomyocyte FGF2-signaling.*** *(**A**) Active FGF2-FGFR1 pathway might act via Tead1 transcription activation or TEAD1 protein stability. TEAD1-Coactivator (e.g. YAP1) interaction in combination with additional TFs activates TEAD1 target genes expression and thereby stimulates cardiomyocyte proliferation, differentiation, survival and growth. (**B**) Inactive FGF2-FGFR1 pathway might cause reduced TEAD1 stability or expression level, resulting in decreased cardiomyocytes proliferation, growth, survival and impaired differentiation. TF(s) – transcription factor(s); TSS - Transcription Start Site*

In summary, the present study demonstrates that cardiomyocyte-specific *Tead1* loss in embryonic and postnatal hearts caused end-stage dilated cardiomyopathy. This pathological phenotype was characterized by reduced proliferation, increased apoptosis and atrophy of *Tead1*-deficient cardiomyocytes. In contrast, embryonic cardiomyocyte-specific *Tead1* overexpression led to hypertrabeculation characterized by increased number of proliferating cardiomyocytes without noticeable phenotypic changes in postnatal as well as adult hearts. Based on transcriptional profiling in combination with genome-wide mapping of TEAD1 binding, this study identified multiple novel TEAD1 target genes responsible for cardiomyocyte growth, differentiation, contraction, energy homeostasis, sarcomere and cytoskeleton organization of maturating cardiomyocytes. Moreover, the present work showed that in cardiomyocytes, TEAD1 potentially exerts its biological functions downstream of FGF2-FGFR1 pathway, which is well established in induction of cardiomyocyte proliferation, differentiation and growth. These findings clearly demonstrate that *Tead1* loss and subsequent dysregulation of TEAD1 downstream targets during cardiomyocyte development and maturation leads to decreased proliferation and premature differentiation resulting in limited cardiomyocyte plasticity (Figure 69). These processes are crucial prerequisite for proper embryonic and postnatal heart growth.

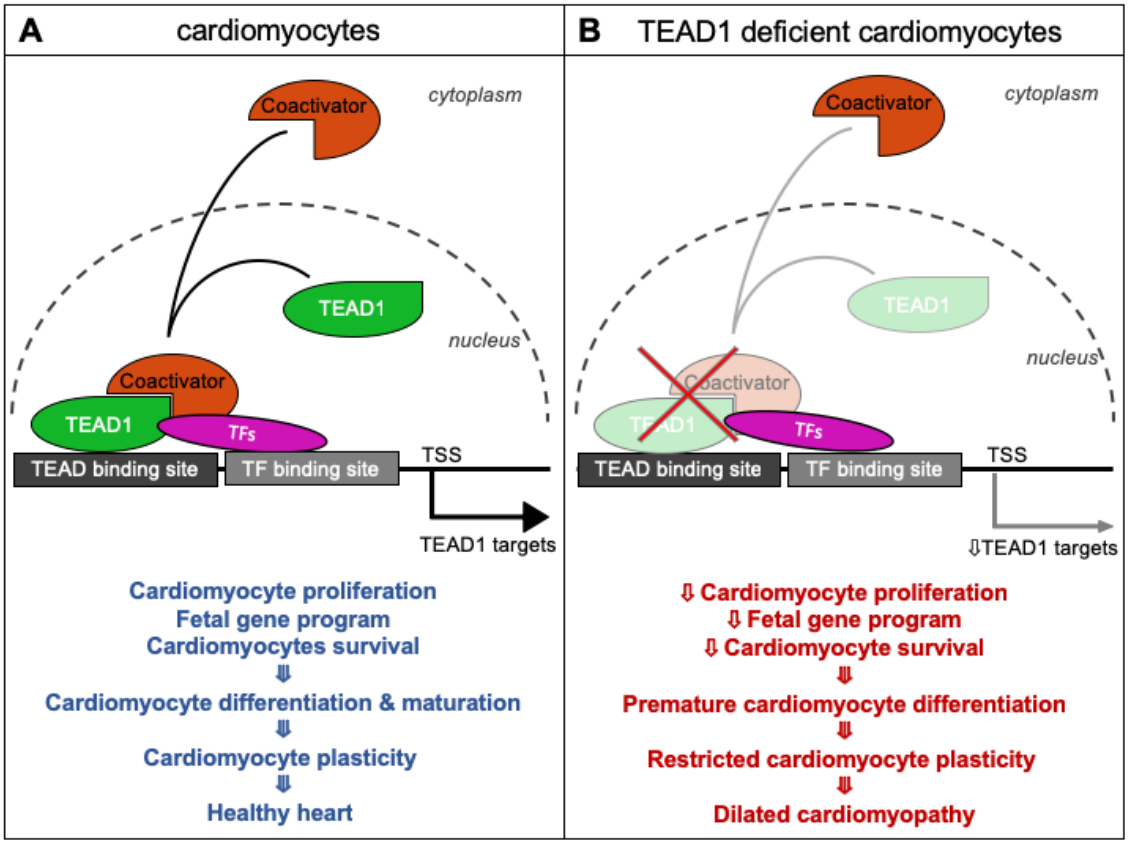

Figure 69. ***Schematic view on effects of TEAD1 regulated gene network in differentiating cardiomyocytes.*** *(**A**) TEAD1-Coactivator interaction in combination with additional TFs activates transcription of downstream target genes involved in variety of cellular processes, e.g. proliferation, survival, differentiation, in healthy heart. (**B**) Tead1 loss results in reduced expression of target genes thereby impairing numerous cellular processes e.g. proliferation, survival, differentiation, which causes premature cardiomyocyte differentiation leading to limited cardiomyocyte plasticity and onset of dilated cardiomyopathy. TF(s) – Transcription Factor(s), TSS - Transcription Start Site.*

4.6 Future directions

This study provides novel insights into TEAD1 regulated transcriptional network as well as functional consequences of *Tead1* inactivation during embryonic and postnatal cardiomyocyte differentiation and maturation. Importantly, this study demonstrated that TEAD1 acts as a regulator of cardiomyocyte proliferation and differentiation processes, which are essential for sustained cardiac function during heart maturation. Furthermore, the expression of TEAD1 regulated genes is not coordinated by a single transcription factor, rather, it is controlled by multiple mechanisms including cognate transcription factors as well as cofactors, their combinatorial interactions, posttranslational modifications and accessibility to DNA. The orchestrated protein interaction between TEAD1, cofactors and other transcription factors exerts a strong impact on the diversity of TEAD1 target genes expression in particular for embryonic, postnatal and adult cardiomyocytes. Towards a more comprehensive understanding of TEAD1 function in cardiomyocyte, detailed interactome studies comparing different conditions, *e.g.* stages and disease, are needed.

Multiple studies have addressed TEAD TFs function in various cell types, however functional insights in cardiomyocytes are limited to TEAD1 and TEAD4. In order to analyze the potential functional redundancy of TEAD TFs in cardiomyocytes, a combinatorial inactivation of TEAD TF family members is required. Since our cardiomyocyte-specific *Tead1* gain-of-function hearts were phenotypically unaltered, the expression of a constitutive active *Tead1* version would uncouple TEAD1 from the requirement of additional cofactors and uncover potential regenerative functions in mature myocardium.

The present study suggests that the FGF2-FGFR1 signaling pathway is one, but not the only, plausible upstream TEAD1 activator in cardiomyocytes, however, additional pathways should be analyzed, in order to determine positive or negative impact on TEAD1 biological function.

Finally, a more comprehensive understanding of TEAD1 role in cardiomyocytes will contribute to the understanding of cardiac diseases pathogenesis and development of novel therapeutic strategies.

IV. ABBREVIATIONS

4-HT	4-Hydroxytamoxifen
Abcc8	ATP-Binding Cassette Subfamily C Member 8
Acta1	Skeletal Muscle α-Actin
Acta2	Smooth Muscle α-aActin 2
Ad-Cre	Adenovirus expressing a codon of improved Cre-recombinase
Adprhl1	ADP-Ribosylhydrolase Like 1
Adra1c	α1c-Adrenergic Receptor
AFA	Adaptive Focused Acoustics
Ajuba	LIM Domain-Containing Protein Ajuba
Amotl2	Angiomotin Like 2
Amp	Ampicillin
APS	Ammoniumperoxodisulfat
ARCs	Adult Rat Cardiomyocytes
BSA	Bovine Serum Albumin
C	Capillary
CAMS	Cell Adhesion Molecules
CAT	Chloramphenicol acetyltransferase
cDNA	Complimentary DNA
ChIP-seq	Chromatin immunoprecipitation sequencing
Chrnb1	β-Acetylcholine Receptor
Ckmt2	Creatine Kinase, mitochondrial 2 (Sarcomeric)
CL	Compact Layer
COL1	Collagen 1
Coro6	Coronin, Actin Binding Protein 6
Crhr2	Corticotropin-Releasing Hormone receptor 2
Crip2	Cysteine Rich Protein 2
CTGF	Connective Tissue Growth Factor
Ctrl.	Control
DAPI	4′,6-diamidino-2-phenylindole
DAPI	4′,6-diamidino-2-phenylindole
DCM	Dilated Cardiomyopathy
dd.	Distilled Deionized
DMD	Dystrophin
DMEM	Dulbecco's Modified Eagle Medium

DNA	Deoxyribonucleic Acid
dNTP	DeoxyriboNucleotide TriPhosphate
E	day of embryonic development
e.g.	for example (Latin)
EB	Extraction Buffer
ECM	Extracellular Matrix
EdU	5-Ethynyl-2'-Deoxyuridine
EPI	Epinephrine
Epi	Epicardium
ES	Enrichment Score
et al.	and others (Latin)
etc.	and son on (Latin)
EtOH	Ethanol
ex vivo	out of living (Latin)
FAM	Fluorescein Amidite
FBS	Fetal Bovine Serum
Fbxl22	F-Box And Leucine Rich Repeat Protein 22
FC	Fold Change
FCS	Fetal Calf Serum
FGF	Fibroblast Growth Factor
FGFR1	FGF Receptor 1
for	forward
Foxo2	Forkhead Box A2
FoxO3	Forkhead Box O3
Gapdh	Glyceraldehyde-3-Phosphate Dehydrogenase
GFP	Green Fluorescent Protein
GOF	Gain-Of-Function
GSEA	Gene Set Enrichment Analysis
h	Hours
HE-stained	stained with Hematoxylin and Eosin
HEK	Human Embryonic Kidney
hpf	high-power field
HRP	Horseradish Peroxidase
Hsd17b7	Hydroxysteroid 17-Beta Dehydrogenase 7
i.p.	*intraperitoneal*
ICM(s)	Isolated Cardiomyocyte(s)
ID	Intercalated Disk

IGV	Integrative Genomic Viewer
In Situ	in place (Latin)
in vitro	in the glass (Latin)
in vivo	within the living (Latin)
IP	Immunoprecipitation
IRES	Internal Ribosomal Entry Site
IRF2BP2	Interferon Regulator Factor 2 Binding Protein 2
kb	kilobase
KD	Knockdown
KHB	Krebs-Henseleit Bicarbonate Buffer
Klhl21	Kelch Like Family Member 21
Klhl38	Kelch Like Family Member 38
KO	*knockout*
LA	Left Atrium
LATS	Large Tumour Suppressor Kinases
LB	Lysis Buffer
LOF	Loss-Of-Function
Luc	Luciferase
LV	Left Ventricle
LVEF	Left Ventricular Ejection Fraction
m	Mitochondria
MAX	MYC Associated Factor X
MCAT	Muscle Specific Cytidine-Adenosine-Thymidine-Sequence
MCK	Muscle Creatine Kinase
MCM	MerCreMer
MEF2	Myocyte Enhancer Factor 2
MI	Myocardial Infarction
min	minute(s)
MOI	Multiplicity Of Infection
MRI	Magnetic Resonance Imaging
mRNA	messenger RNA
MST	STE20-like protein kinase
MTOR	Mechanistic Target Of Rapamycin Kinase
Myh6	Myosin Heavy Chain 6, cardiac muscle α Isoform, α-MHC
Myh7	Myosin Heavy Chain 7, cardiac muscle β Isoform, β-MHC
Mylk3	Myosin Light Chain Kinase Family Member 3
Mylk4	Myosin Light Chain Kinase Family Member 4

Myocd	Myocardin
N(UC)	Nucleus
neg	negative
Nmrk2	Nicotinamide Riboside Kinase 2 / MIBP Muscle Integrin-Binding Protein
Nnt	Nicotinamide Nucleotide Transhydrogenase
Nppa	Natriuretic Peptide A
Nppb	Natriuretic Peptide B
OD	Optical Density
OE	Overexpression
Ogn	Osteoglycin / Mimecan
P	postnatal day
P/S	Penicillin / Streptomycin
PAA	Polyacrylamide
PBS	Phosphate Buffered Saline
PCM(s)	Postnatal Cardiomyocyte(s)
PCR	Polymerase Chain Reaction
PFA	Paraformaldehyde
PFU	Plague forming units
Popdc2	Popeye Domain Containing 2
pos	positive
Ppp1R1A	Protein Phosphatase 1 Regulatory Inhibitor Subunit 1A
Prkaa2	AMP-activated, a-2 catalytic subunit
qRT-PCR	Quantitative Real-Time Polymerase Chain Reaction
RA	Right Atrium
rev	reverse
RNA	Ribonucleic Acid
ROSA26	Reverse Oriented Splice Acceptor, Clone 26
rpm	rotation per minute
RT	Room Temperature
RV	Right Ventricle
Scd4	Stearoyl-Coenzyme A Desaturase 4
Serca2a	ATPase Sarcoplasmic/Endoplasmic Reticulum Ca2+ Transporting 2
siRNA	Small interfering RNA
SMCs	Smooth Muscle Cells
Sntb1	Syntrophin Beta 1
SRF	Serum Response Factor
SRY	Sex-Determining Region Y

Syde2	Synapse Defective Rho GTPase Homolog 2
TEAD (TEF)	Transcription Enhancer Factor
TEAD1	Transcription Enhancer Factor 1 (protein symbol in mouse)
Tead1	Transcription Enhancer Factor 1 (gene and mRNA symbol in mouse)
TEM	Transmission Electron Microscopy
TF(s)	Transcription Factor(s)
TG	Transgenic
TGFβ	Transforming Growth Factor β
TL	Trabecular Layer
Tnni3	Troponin I3, cardiac type
Tnnt2	Troponin T2, cardiac type
Tpm1	α-Tropomyosin
Trim55	Tripartite Motif Containing 55/Muscle-Specific RING Finger Protein 2, Murf-2
TUNEL	Terminal deoxynucleotidyl transferase dUTP nick end labeling
U	Unit
V	Vessel(s)
VEGF	Vascular Endothelial Growth Factor
Vg	Vestigial
VGLL-1	Vestigial Like Family Member 1
VGLL-2	Vestigial Like Family Member 2, VITO-1
VGLL-3	Vestigial Like Family Member 3
VGLL-4	Vestigial Like Family Member 4
VIC	fluorescent dye dev. by Applied Biosystems
vs.	against (Latin)
WT	Wild-Type
Wwtr1	WW Domain Containing Transcription Regulator 1 (TAZ)
XMLC	Xenopus laevis myosin light-chain 2
YAP1	Yes-Associated Protein 1
Z	Z-disk(s)
β-PKC	β-Protein Kinase C

V. REFERENCES

1. Mestroni, L., et al., *Familial dilated cardiomyopathy: evidence for genetic and phenotypic heterogeneity. Heart Muscle Disease Study Group.* J Am Coll Cardiol, 1999. **34**(1): p. 181-90.
2. Klaassen, S., et al., *Mutations in sarcomere protein genes in left ventricular noncompaction.* Circulation, 2008. **117**(22): p. 2893-901.
3. Olson, T.M., et al., *Actin mutations in dilated cardiomyopathy, a heritable form of heart failure.* Science, 1998. **280**(5364): p. 750-2.
4. Knoll, R., et al., *The cardiac mechanical stretch sensor machinery involves a Z disc complex that is defective in a subset of human dilated cardiomyopathy.* Cell, 2002. **111**(7): p. 943-55.
5. Vincentz, J.W., et al., *Hand factor ablation causes defective left ventricular chamber development and compromised adult cardiac function.* PLoS Genet, 2017. **13**(7): p. e1006922.
6. Kikuchi, K., et al., *Primary contribution to zebrafish heart regeneration by gata4(+) cardiomyocytes.* Nature, 2010. **464**(7288): p. 601-5.
7. Lien, C.L., et al., *Control of early cardiac-specific transcription of Nkx2-5 by a GATA-dependent enhancer.* Development, 1999. **126**(1): p. 75-84.
8. van Oort, R.J., et al., *MEF2 activates a genetic program promoting chamber dilation and contractile dysfunction in calcineurin-induced heart failure.* Circulation, 2006. **114**(4): p. 298-308.
9. He, A., et al., *Co-occupancy by multiple cardiac transcription factors identifies transcriptional enhancers active in heart.* Proc Natl Acad Sci U S A, 2011. **108**(14): p. 5632-7.
10. Mar, J.H. and C.P. Ordahl, *A conserved CATTCCT motif is required for skeletal muscle-specific activity of the cardiac troponin T gene promoter.* Proc Natl Acad Sci U S A, 1988. **85**(17): p. 6404-8.
11. Xiao, J.H., et al., *Cloning, expression, and transcriptional properties of the human enhancer factor TEF-1.* Cell, 1991. **65**(4): p. 551-68.
12. Chen, Z., G.A. Friedrich, and P. Soriano, *Transcriptional enhancer factor 1 disruption by a retroviral gene trap leads to heart defects and embryonic lethality in mice.* Genes Dev, 1994. **8**(19): p. 2293-301.
13. Gupta, M.P., M. Gupta, and R. Zak, *An E-box/M-CAT hybrid motif and cognate binding protein(s) regulate the basal muscle-specific and cAMP-inducible expression of the rat cardiac alpha-myosin heavy chain gene.* J Biol Chem, 1994. **269**(47): p. 29677-87.
14. Gupta, M.P., et al., *Transcription enhancer factor 1 interacts with a basic helix-loop-helix zipper protein, Max, for positive regulation of cardiac alpha-myosin heavy-chain gene expression.* Mol Cell Biol, 1997. **17**(7): p. 3924-36.
15. McLean, B.G., et al., *Basal and alpha1-adrenergic-induced activity of minimal rat betaMHC promoters in cardiac myocytes requires multiple TEF-1 but not NFAT binding sites.* J Mol Cell Cardiol, 2003. **35**(5): p. 461-71.
16. Creemers, E.E., et al., *Myocardin is a direct transcriptional target of Mef2, Tead and Foxo proteins during cardiovascular development.* Development, 2006. **133**(21): p. 4245-56.
17. Tsika, R.W., et al., *TEAD-1 overexpression in the mouse heart promotes an age-dependent heart dysfunction.* J Biol Chem, 2010. **285**(18): p. 13721-35.
18. Liu, R., et al., *Tead1 is required for maintaining adult cardiomyocyte function, and its loss results in lethal dilated cardiomyopathy.* JCI Insight, 2017. **2**(17).

19. Ikeda, S., et al., *Hippo Deficiency Leads to Cardiac Dysfunction Accompanied by Cardiomyocyte Dedifferentiation During Pressure Overload.* Circ Res, 2019. **124**(2): p. 292-305.
20. Hashimoto, H., et al., *Time-lapse imaging of cell cycle dynamics during development in living cardiomyocyte.* J Mol Cell Cardiol, 2014. **72**: p. 241-9.
21. Toyoda, M., et al., *jumonji downregulates cardiac cell proliferation by repressing cyclin D1 expression.* Dev Cell, 2003. **5**(1): p. 85-97.
22. Soufan, A.T., et al., *Regionalized sequence of myocardial cell growth and proliferation characterizes early chamber formation.* Circ Res, 2006. **99**(5): p. 545-52.
23. Yuan, X. and T. Braun, *Multimodal Regulation of Cardiac Myocyte Proliferation.* Circ Res, 2017. **121**(3): p. 293-309.
24. Soonpaa, M.H., et al., *Cardiomyocyte DNA synthesis and binucleation during murine development.* Am J Physiol, 1996. **271**(5 Pt 2): p. H2183-9.
25. Ikenishi, A., et al., *Cell cycle regulation in mouse heart during embryonic and postnatal stages.* Dev Growth Differ, 2012. **54**(8): p. 731-8.
26. Mahmoud, A.I., et al., *Meis1 regulates postnatal cardiomyocyte cell cycle arrest.* Nature, 2013. **497**(7448): p. 249-253.
27. Li, F., et al., *Rapid transition of cardiac myocytes from hyperplasia to hypertrophy during postnatal development.* J Mol Cell Cardiol, 1996. **28**(8): p. 1737-46.
28. Dickhuth, H.H., et al., *[Endurance training and cardial adaptation (athlete's heart)].* Herz, 2004. **29**(4): p. 373-80.
29. Dorn, G.W., 2nd and T. Force, *Protein kinase cascades in the regulation of cardiac hypertrophy.* J Clin Invest, 2005. **115**(3): p. 527-37.
30. Heineke, J. and J.D. Molkentin, *Regulation of cardiac hypertrophy by intracellular signalling pathways.* Nat Rev Mol Cell Biol, 2006. **7**(8): p. 589-600.
31. Leone, M., A. Magadum, and F.B. Engel, *Cardiomyocyte proliferation in cardiac development and regeneration: a guide to methodologies and interpretations.* Am J Physiol Heart Circ Physiol, 2015. **309**(8): p. H1237-50.
32. Laflamme, M.A. and C.E. Murry, *Heart regeneration.* Nature, 2011. **473**(7347): p. 326-35.
33. Reuter, S., et al., *Recombinant neuregulin 1 does not activate cardiomyocyte DNA synthesis in normal or infarcted adult mice.* PLoS One, 2014. **9**(12): p. e115871.
34. Eming, S.A., T.A. Wynn, and P. Martin, *Inflammation and metabolism in tissue repair and regeneration.* Science, 2017. **356**(6342): p. 1026-1030.
35. Black, F.M., et al., *The vascular smooth muscle alpha-actin gene is reactivated during cardiac hypertrophy provoked by load.* J Clin Invest, 1991. **88**(5): p. 1581-8.
36. Taegtmeyer, H., S. Sen, and D. Vela, *Return to the fetal gene program: a suggested metabolic link to gene expression in the heart.* Ann N Y Acad Sci, 2010. **1188**: p. 191-8.
37. Lowes, B.D., et al., *Changes in gene expression in the intact human heart. Downregulation of alpha-myosin heavy chain in hypertrophied, failing ventricular myocardium.* J Clin Invest, 1997. **100**(9): p. 2315-24.
38. Prabhu, S.D. and N.G. Frangogiannis, *The Biological Basis for Cardiac Repair After Myocardial Infarction: From Inflammation to Fibrosis.* Circ Res, 2016. **119**(1): p. 91-112.
39. Xin, M., E.N. Olson, and R. Bassel-Duby, *Mending broken hearts: cardiac development as a basis for adult heart regeneration and repair.* Nat Rev Mol Cell Biol, 2013. **14**(8): p. 529-41.
40. Davidson, I., et al., *The HeLa cell protein TEF-1 binds specifically and cooperatively to two SV40 enhancer motifs of unrelated sequence.* Cell, 1988. **54**(7): p. 931-42.

41. Andrianopoulos, A. and W.E. Timberlake, *The Aspergillus nidulans abaA gene encodes a transcriptional activator that acts as a genetic switch to control development.* Mol Cell Biol, 1994. **14**(4): p. 2503-15.
42. Heise, B., et al., *The TEA transcription factor Tec1 confers promoter-specific gene regulation by Ste12-dependent and -independent mechanisms.* Eukaryot Cell, 2010. **9**(4): p. 514-31.
43. van der Felden, J., et al., *The transcription factors Tec1 and Ste12 interact with coregulators Msa1 and Msa2 to activate adhesion and multicellular development.* Mol Cell Biol, 2014. **34**(12): p. 2283-93.
44. Halder, G., et al., *The Vestigial and Scalloped proteins act together to directly regulate wing-specific gene expression in Drosophila.* Genes Dev, 1998. **12**(24): p. 3900-9.
45. Ferguson, G.B. and J.A. Martinez-Agosto, *The TEAD family transcription factor Scalloped regulates blood progenitor maintenance and proliferation in Drosophila through PDGF/VEGFR receptor (Pvr) signaling.* Dev Biol, 2017. **425**(1): p. 21-32.
46. Jacquemin, P., et al., *A novel family of developmentally regulated mammalian transcription factors containing the TEA/ATTS DNA binding domain.* J Biol Chem, 1996. **271**(36): p. 21775-85.
47. Tsika, R.W., et al., *Overexpression of TEAD-1 in transgenic mouse striated muscles produces a slower skeletal muscle contractile phenotype.* J Biol Chem, 2008. **283**(52): p. 36154-67.
48. Joshi, S., et al., *TEAD transcription factors are required for normal primary myoblast differentiation in vitro and muscle regeneration in vivo.* PLoS Genet, 2017. **13**(2): p. e1006600.
49. Kaneko, K.J., et al., *Transcription factor TEAD2 is involved in neural tube closure.* Genesis, 2007. **45**(9): p. 577-87.
50. Sawada, A., et al., *Redundant roles of Tead1 and Tead2 in notochord development and the regulation of cell proliferation and survival.* Mol Cell Biol, 2008. **28**(10): p. 3177-89.
51. Yagi, R., et al., *Transcription factor TEAD4 specifies the trophectoderm lineage at the beginning of mammalian development.* Development, 2007. **134**(21): p. 3827-36.
52. Nishioka, N., et al., *Tead4 is required for specification of trophectoderm in pre-implantation mouse embryos.* Mech Dev, 2008. **125**(3-4): p. 270-83.
53. Chen, H.H., et al., *Transcription enhancer factor-1-related factor-transgenic mice develop cardiac conduction defects associated with altered connexin phosphorylation.* Circulation, 2004. **110**(19): p. 2980-7.
54. Yasunami, M., et al., *Molecular characterization of cDNA encoding a novel protein related to transcriptional enhancer factor-1 from neural precursor cells.* J Biol Chem, 1995. **270**(31): p. 18649-54.
55. Azakie, A., et al., *DTEF-1, a novel member of the transcription enhancer factor-1 (TEF-1) multigene family.* J Biol Chem, 1996. **271**(14): p. 8260-5.
56. Maeda, T., et al., *Mouse DTEF-1 (ETFR-1, TEF-5) is a transcriptional activator in alpha 1-adrenergic agonist-stimulated cardiac myocytes.* J Biol Chem, 2002. **277**(27): p. 24346-52.
57. Hsu, D.K., et al., *Identification of a murine TEF-1-related gene expressed after mitogenic stimulation of quiescent fibroblasts and during myogenic differentiation.* J Biol Chem, 1996. **271**(23): p. 13786-95.
58. Stewart, A.F., et al., *Cloning of human RTEF-1, a transcriptional enhancer factor-1-related gene preferentially expressed in skeletal muscle: evidence for an ancient multigene family.* Genomics, 1996. **37**(1): p. 68-76.
59. Stewart, A.F., et al., *Transcription factor RTEF-1 mediates alpha1-adrenergic reactivation of the fetal gene program in cardiac myocytes.* Circ Res, 1998. **83**(1): p. 43-9.

60. Gan, Q., et al., *Smooth muscle cells and myofibroblasts use distinct transcriptional mechanisms for smooth muscle alpha-actin expression.* Circ Res, 2007. **101**(9): p. 883-92.
61. Xu, M., et al., *The endothelium-dependent effect of RTEF-1 in pressure overload cardiac hypertrophy: role of VEGF-B.* Cardiovasc Res, 2011. **90**(2): p. 325-34.
62. Rindt, H., et al., *In vivo analysis of the murine beta-myosin heavy chain gene promoter.* J Biol Chem, 1993. **268**(7): p. 5332-8.
63. Swartz, E.A., A.D. Johnson, and G.K. Owens, *Two MCAT elements of the SM alpha-actin promoter function differentially in SM vs. non-SM cells.* Am J Physiol, 1998. **275**(2 Pt 1): p. C608-18.
64. Karns, L.R., K. Kariya, and P.C. Simpson, *M-CAT, CArG, and Sp1 elements are required for alpha 1-adrenergic induction of the skeletal alpha-actin promoter during cardiac myocyte hypertrophy. Transcriptional enhancer factor-1 and protein kinase C as conserved transducers of the fetal program in cardiac growth.* J Biol Chem, 1995. **270**(1): p. 410-7.
65. Ishiji, T., et al., *Transcriptional enhancer factor (TEF)-1 and its cell-specific co-activator activate human papillomavirus-16 E6 and E7 oncogene transcription in keratinocytes and cervical carcinoma cells.* EMBO J, 1992. **11**(6): p. 2271-81.
66. Jiang, S.W., K. Wu, and N.L. Eberhardt, *Human placental TEF-5 transactivates the human chorionic somatomammotropin gene enhancer.* Mol Endocrinol, 1999. **13**(6): p. 879-89.
67. Sawada, A., et al., *Tead proteins activate the Foxa2 enhancer in the node in cooperation with a second factor.* Development, 2005. **132**(21): p. 4719-29.
68. Mar, J.H. and C.P. Ordahl, *M-CAT binding factor, a novel trans-acting factor governing muscle-specific transcription.* Mol Cell Biol, 1990. **10**(8): p. 4271-83.
69. Simpson, P.C., et al., *Adrenergic hormones and control of cardiac myocyte growth.* Mol Cell Biochem, 1991. **104**(1-2): p. 35-43.
70. Yoshida, T., *MCAT elements and the TEF-1 family of transcription factors in muscle development and disease.* Arterioscler Thromb Vasc Biol, 2008. **28**(1): p. 8-17.
71. Berberich, C., et al., *Two adjacent E box elements and a M-CAT box are involved in the muscle-specific regulation of the rat acetylcholine receptor beta subunit gene.* Eur J Biochem, 1993. **216**(2): p. 395-404.
72. O'Connell, T.D., D.G. Rokosh, and P.C. Simpson, *Cloning and characterization of the mouse alpha1C/A-adrenergic receptor gene and analysis of an alpha1C promoter in cardiac myocytes: role of an MCAT element that binds transcriptional enhancer factor-1 (TEF-1).* Mol Pharmacol, 2001. **59**(5): p. 1225-34.
73. Pasquet, S., et al., *Transcription enhancer factor-1-dependent expression of the alpha-tropomyosin gene in the three muscle cell types.* J Biol Chem, 2006. **281**(45): p. 34406-20.
74. Johnson, R. and G. Halder, *The two faces of Hippo: targeting the Hippo pathway for regenerative medicine and cancer treatment.* Nat Rev Drug Discov, 2014. **13**(1): p. 63-79.
75. Tapon, N., et al., *salvador Promotes both cell cycle exit and apoptosis in Drosophila and is mutated in human cancer cell lines.* Cell, 2002. **110**(4): p. 467-78.
76. Hariharan, I.K. and D. Bilder, *Regulation of imaginal disc growth by tumor-suppressor genes in Drosophila.* Annu Rev Genet, 2006. **40**: p. 335-61.
77. Aragona, M., et al., *A mechanical checkpoint controls multicellular growth through YAP/TAZ regulation by actin-processing factors.* Cell, 2013. **154**(5): p. 1047-59.
78. Wackerhage, H., et al., *The Hippo signal transduction network in skeletal and cardiac muscle.* Sci Signal, 2014. **7**(337): p. re4.

79. Yamamoto, S., et al., *Activation of Mst1 causes dilated cardiomyopathy by stimulating apoptosis without compensatory ventricular myocyte hypertrophy.* J Clin Invest, 2003. **111**(10): p. 1463-74.
80. Odashima, M., et al., *Inhibition of endogenous Mst1 prevents apoptosis and cardiac dysfunction without affecting cardiac hypertrophy after myocardial infarction.* Circ Res, 2007. **100**(9): p. 1344-52.
81. Matsui, Y., et al., *Lats2 is a negative regulator of myocyte size in the heart.* Circ Res, 2008. **103**(11): p. 1309-18.
82. Yagi, R., et al., *A WW domain-containing yes-associated protein (YAP) is a novel transcriptional co-activator.* EMBO J, 1999. **18**(9): p. 2551-62.
83. Kanai, F., et al., *TAZ: a novel transcriptional co-activator regulated by interactions with 14-3-3 and PDZ domain proteins.* EMBO J, 2000. **19**(24): p. 6778-91.
84. Gunther, S., et al., *VITO-1 is an essential cofactor of TEF1-dependent muscle-specific gene regulation.* Nucleic Acids Res, 2004. **32**(2): p. 791-802.
85. Pobbati, A.V., et al., *Structural and functional similarity between the Vgll1-TEAD and the YAP-TEAD complexes.* Structure, 2012. **20**(7): p. 1135-40.
86. Lin, Z., et al., *Acetylation of VGLL4 Regulates Hippo-YAP Signaling and Postnatal Cardiac Growth.* Dev Cell, 2016. **39**(4): p. 466-479.
87. Vassilev, A., et al., *TEAD/TEF transcription factors utilize the activation domain of YAP65, a Src/Yes-associated protein localized in the cytoplasm.* Genes Dev, 2001. **15**(10): p. 1229-41.
88. Pobbati, A.V. and W. Hong, *Emerging roles of TEAD transcription factors and its coactivators in cancers.* Cancer Biol Ther, 2013. **14**(5): p. 390-8.
89. von Gise, A., et al., *YAP1, the nuclear target of Hippo signaling, stimulates heart growth through cardiomyocyte proliferation but not hypertrophy.* Proc Natl Acad Sci U S A, 2012. **109**(7): p. 2394-9.
90. Lin, Z., et al., *Cardiac-specific YAP activation improves cardiac function and survival in an experimental murine MI model.* Circ Res, 2014. **115**(3): p. 354-63.
91. Lin, Z. and W.T. Pu, *Releasing YAP from an alpha-catenin trap increases cardiomyocyte proliferation.* Circ Res, 2015. **116**(1): p. 9-11.
92. Mahoney, W.M., Jr., et al., *The transcriptional co-activator TAZ interacts differentially with transcriptional enhancer factor-1 (TEF-1) family members.* Biochem J, 2005. **388**(Pt 1): p. 217-25.
93. Hau, J.C., et al., *The TEAD4-YAP/TAZ protein-protein interaction: expected similarities and unexpected differences.* Chembiochem, 2013. **14**(10): p. 1218-25.
94. Sun, C., et al., *Common and Distinctive Functions of the Hippo Effectors Taz and Yap in Skeletal Muscle Stem Cell Function.* Stem Cells, 2017.
95. Mielcarek, M., et al., *VITO-1, a novel vestigial related protein is predominantly expressed in the skeletal muscle lineage.* Mech Dev, 2002. **119 Suppl 1**: p. S269-74.
96. Maeda, T., D.L. Chapman, and A.F. Stewart, *Mammalian vestigial-like 2, a cofactor of TEF-1 and MEF2 transcription factors that promotes skeletal muscle differentiation.* J Biol Chem, 2002. **277**(50): p. 48889-98.
97. Chen, H.H., S.J. Mullett, and A.F. Stewart, *Vgl-4, a novel member of the vestigial-like family of transcription cofactors, regulates alpha1-adrenergic activation of gene expression in cardiac myocytes.* J Biol Chem, 2004. **279**(29): p. 30800-6.
98. Gupta, M., et al., *Physical interaction between the MADS box of serum response factor and the TEA/ATTS DNA-binding domain of transcription enhancer factor-1.* J Biol Chem, 2001. **276**(13): p. 10413-22.
99. Maeda, T., M.P. Gupta, and A.F. Stewart, *TEF-1 and MEF2 transcription factors interact to regulate muscle-specific promoters.* Biochem Biophys Res Commun, 2002. **294**(4): p. 791-7.
100. Teng, A.C., et al., *IRF2BP2 is a skeletal and cardiac muscle-enriched ischemia-inducible activator of VEGFA expression.* FASEB J, 2010. **24**(12): p. 4825-34.

101. Fujii, M., et al., *Convergent signaling in the regulation of connective tissue growth factor in malignant mesothelioma: TGFbeta signaling and defects in the Hippo signaling cascade.* Cell Cycle, 2012. **11**(18): p. 3373-9.
102. Liu, F., et al., *The transcription factor TEAD1 represses smooth muscle-specific gene expression by abolishing myocardin function.* J Biol Chem, 2014. **289**(6): p. 3308-16.
103. Swynghedauw, B., *Molecular mechanisms of myocardial remodeling.* Physiol Rev, 1999. **79**(1): p. 215-62.
104. Baldwin, K.M. and F. Haddad, *Effects of different activity and inactivity paradigms on myosin heavy chain gene expression in striated muscle.* J Appl Physiol (1985), 2001. **90**(1): p. 345-57.
105. Kariya, K., L.R. Karns, and P.C. Simpson, *An enhancer core element mediates stimulation of the rat beta-myosin heavy chain promoter by an alpha 1-adrenergic agonist and activated beta-protein kinase C in hypertrophy of cardiac myocytes.* J Biol Chem, 1994. **269**(5): p. 3775-82.
106. Simpson, P.C., et al., *Transcription of early developmental isogenes in cardiac myocyte hypertrophy.* J Mol Cell Cardiol, 1989. **21 Suppl 5**: p. 79-89.
107. Wang, Z., et al., *Myocardin is a master regulator of smooth muscle gene expression.* Proc Natl Acad Sci U S A, 2003. **100**(12): p. 7129-34.
108. Liu, R., et al., *Tead1 is required for perinatal cardiomyocyte proliferation.* PLoS One, 2019. **14**(2): p. e0212017.
109. Breckenridge, R., et al., *Pan-myocardial expression of Cre recombinase throughout mouse development.* Genesis, 2007. **45**(3): p. 135-44.
110. Bruning, J.C., et al., *A muscle-specific insulin receptor knockout exhibits features of the metabolic syndrome of NIDDM without altering glucose tolerance.* Mol Cell, 1998. **2**(5): p. 559-69.
111. Sohal, D.S., et al., *Temporally regulated and tissue-specific gene manipulations in the adult and embryonic heart using a tamoxifen-inducible Cre protein.* Circ Res, 2001. **89**(1): p. 20-5.
112. Srinivas, S., et al., *Cre reporter strains produced by targeted insertion of EYFP and ECFP into the ROSA26 locus.* BMC Dev Biol, 2001. **1**: p. 4.
113. O'Connell, T.D., M.C. Rodrigo, and P.C. Simpson, *Isolation and culture of adult mouse cardiac myocytes.* Methods Mol Biol, 2007. **357**: p. 271-96.
114. Besser, J., et al., *MiRNA-1/133a clusters regulate adrenergic control of cardiac repolarization.* PLoS One, 2014. **9**(11): p. e113449.
115. Lorchner, H., et al., *Myocardial healing requires Reg3beta-dependent accumulation of macrophages in the ischemic heart.* Nat Med, 2015. **21**(4): p. 353-62.
116. Boettger, T., et al., *Acquisition of the contractile phenotype by murine arterial smooth muscle cells depends on the Mir143/145 gene cluster.* J Clin Invest, 2009. **119**(9): p. 2634-47.
117. Subramanian, A., et al., *GSEA-P: a desktop application for Gene Set Enrichment Analysis.* Bioinformatics, 2007. **23**(23): p. 3251-3.
118. Davis, M.P., et al., *Kraken: a set of tools for quality control and analysis of high-throughput sequence data.* Methods, 2013. **63**(1): p. 41-9.
119. Dobin, A., et al., *STAR: ultrafast universal RNA-seq aligner.* Bioinformatics, 2013. **29**(1): p. 15-21.
120. Harmanci, A., J. Rozowsky, and M. Gerstein, *MUSIC: identification of enriched regions in ChIP-Seq experiments using a mappability-corrected multiscale signal processing framework.* Genome Biol, 2014. **15**(10): p. 474.
121. Robinson, J.T., et al., *Integrative genomics viewer.* Nat Biotechnol, 2011. **29**(1): p. 24-6.
122. Ramirez, F., et al., *deepTools: a flexible platform for exploring deep-sequencing data.* Nucleic Acids Res, 2014. **42**(Web Server issue): p. W187-91.

123. Zerbino, D.R., et al., *WiggleTools: parallel processing of large collections of genome-wide datasets for visualization and statistical analysis.* Bioinformatics, 2014. **30**(7): p. 1008-9.
124. Anders, S. and W. Huber, *Differential expression analysis for sequence count data.* Genome Biol, 2010. **11**(10): p. R106.
125. Quinlan, A.R. and I.M. Hall, *BEDTools: a flexible suite of utilities for comparing genomic features.* Bioinformatics, 2010. **26**(6): p. 841-2.
126. Salic, A. and T.J. Mitchison, *A chemical method for fast and sensitive detection of DNA synthesis in vivo.* Proc Natl Acad Sci U S A, 2008. **105**(7): p. 2415-20.
127. Roduit, R. and D.F. Schorderet, *MAP kinase pathways in UV-induced apoptosis of retinal pigment epithelium ARPE19 cells.* Apoptosis, 2008. **13**(3): p. 343-53.
128. Mollova, M., et al., *Cardiomyocyte proliferation contributes to heart growth in young humans.* Proc Natl Acad Sci U S A, 2013. **110**(4): p. 1446-51.
129. Trask, R.V. and J.J. Billadello, *Tissue-specific distribution and developmental regulation of M and B creatine kinase mRNAs.* Biochim Biophys Acta, 1990. **1049**(2): p. 182-8.
130. Soriano, P., *Generalized lacZ expression with the ROSA26 Cre reporter strain.* Nat Genet, 1999. **21**(1): p. 70-1.
131. Gill, C., R. Mestril, and A. Samali, *Losing heart: the role of apoptosis in heart disease--a novel therapeutic target?* FASEB J, 2002. **16**(2): p. 135-46.
132. Hesse, M., A. Welz, and B.K. Fleischmann, *Heart regeneration and the cardiomyocyte cell cycle.* Pflugers Arch, 2018. **470**(2): p. 241-248.
133. Zambrowicz, B.P., et al., *Disruption of overlapping transcripts in the ROSA beta geo 26 gene trap strain leads to widespread expression of beta-galactosidase in mouse embryos and hematopoietic cells.* Proc Natl Acad Sci U S A, 1997. **94**(8): p. 3789-94.
134. Osman, I., et al., *TEAD1 (TEA Domain Transcription Factor 1) Promotes Smooth Muscle Cell Proliferation Through Upregulating SLC1A5 (Solute Carrier Family 1 Member 5)-Mediated Glutamine Uptake.* Circ Res, 2019. **124**(9): p. 1309-1322.
135. Mori, S., et al., *Human Papillomavirus 16 E6 Upregulates APOBEC3B via the TEAD Transcription Factor.* J Virol, 2017. **91**(6).
136. Zanconato, F., et al., *Genome-wide association between YAP/TAZ/TEAD and AP-1 at enhancers drives oncogenic growth.* Nat Cell Biol, 2015. **17**(9): p. 1218-27.
137. Landin Malt, A., et al., *Alteration of TEAD1 expression levels confers apoptotic resistance through the transcriptional up-regulation of Livin.* PLoS One, 2012. **7**(9): p. e45498.
138. Ventura-Clapier, R., A. Garnier, and V. Veksler, *Energy metabolism in heart failure.* J Physiol, 2004. **555**(Pt 1): p. 1-13.
139. Karmodiya, K., et al., *H3K9 and H3K14 acetylation co-occur at many gene regulatory elements, while H3K14ac marks a subset of inactive inducible promoters in mouse embryonic stem cells.* BMC Genomics, 2012. **13**: p. 424.
140. Zhao, B., et al., *TEAD mediates YAP-dependent gene induction and growth control.* Genes Dev, 2008. **22**(14): p. 1962-71.
141. Clement, S., et al., *Expression and function of alpha-smooth muscle actin during embryonic-stem-cell-derived cardiomyocyte differentiation.* J Cell Sci, 2007. **120**(Pt 2): p. 229-38.
142. Bildyug, N., E. Bozhokina, and S. Khaitlina, *Contribution of alpha-smooth muscle actin and extracellular matrix to the in vitro reorganization of cardiomyocyte contractile system.* Cell Biol Int, 2016. **40**(4): p. 472-7.
143. Borgers, M., *Hibernating myocardium: Programmed cell survival or programmed cell death?* Exp Clin Cardiol, 2002. **7**(2-3): p. 69-72.
144. Driesen, R.B., et al., *Re-expression of alpha skeletal actin as a marker for dedifferentiation in cardiac pathologies.* J Cell Mol Med, 2009. **13**(5): p. 896-908.

145. Herrer, I., et al., *RNA-sequencing analysis reveals new alterations in cardiomyocyte cytoskeletal genes in patients with heart failure.* Lab Invest, 2014. **94**(6): p. 645-53.
146. Mima, T., et al., *Fibroblast growth factor receptor is required for in vivo cardiac myocyte proliferation at early embryonic stages of heart development.* Proc Natl Acad Sci U S A, 1995. **92**(2): p. 467-71.
147. Detillieux, K.A., et al., *Biological activities of fibroblast growth factor-2 in the adult myocardium.* Cardiovasc Res, 2003. **57**(1): p. 8-19.
148. deAlmeida, A. and D. Sedmera, *Fibroblast Growth Factor-2 regulates proliferation of cardiac myocytes in normal and hypoplastic left ventricles in the developing chick.* Cardiol Young, 2009. **19**(2): p. 159-69.
149. Sheikh, F., et al., *Overexpression of FGF-2 increases cardiac myocyte viability after injury in isolated mouse hearts.* Am J Physiol Heart Circ Physiol, 2001. **280**(3): p. H1039-50.
150. Jiang, Z.S., et al., *Acute protection of ischemic heart by FGF-2: involvement of FGF-2 receptors and protein kinase C.* Am J Physiol Heart Circ Physiol, 2002. **282**(3): p. H1071-80.
151. Parker, T.G., S.E. Packer, and M.D. Schneider, *Peptide growth factors can provoke "fetal" contractile protein gene expression in rat cardiac myocytes.* J Clin Invest, 1990. **85**(2): p. 507-14.
152. Harder, B.A., et al., *Differential protein localization in sarcomeric and nonsarcomeric contractile structures of cultured cardiomyocytes.* J Struct Biol, 1998. **122**(1-2): p. 162-75.
153. Sugi, Y., et al., *Developmental expression of fibroblast growth factor receptor-1 (cek-1; flg) during heart development.* Dev Dyn, 1995. **202**(2): p. 115-25.
154. Hughes, S.E., *Differential expression of the fibroblast growth factor receptor (FGFR) multigene family in normal human adult tissues.* J Histochem Cytochem, 1997. **45**(7): p. 1005-19.
155. Bruneau, B.G., *Signaling and transcriptional networks in heart development and regeneration.* Cold Spring Harb Perspect Biol, 2013. **5**(3): p. a008292.
156. Akazawa, H. and I. Komuro, *Roles of cardiac transcription factors in cardiac hypertrophy.* Circ Res, 2003. **92**(10): p. 1079-88.
157. Del Re, D.P., et al., *Yes-associated protein isoform 1 (Yap1) promotes cardiomyocyte survival and growth to protect against myocardial ischemic injury.* J Biol Chem, 2013. **288**(6): p. 3977-88.
158. Xin, M., et al., *Hippo pathway effector Yap promotes cardiac regeneration.* Proc Natl Acad Sci U S A, 2013. **110**(34): p. 13839-44.
159. Jefferies, J.L. and J.A. Towbin, *Dilated cardiomyopathy.* Lancet, 2010. **375**(9716): p. 752-62.
160. Olson, E.N. and M.D. Schneider, *Sizing up the heart: development redux in disease.* Genes Dev, 2003. **17**(16): p. 1937-56.
161. Chang, A.N. and J.D. Potter, *Sarcomeric protein mutations in dilated cardiomyopathy.* Heart Fail Rev, 2005. **10**(3): p. 225-35.
162. McNally, E.M., J.R. Golbus, and M.J. Puckelwartz, *Genetic mutations and mechanisms in dilated cardiomyopathy.* J Clin Invest, 2013. **123**(1): p. 19-26.
163. Hou, N., et al., *Activation of Yap1/Taz signaling in ischemic heart disease and dilated cardiomyopathy.* Exp Mol Pathol, 2017. **103**(3): p. 267-275.
164. Dobaczewski, M., W. Chen, and N.G. Frangogiannis, *Transforming growth factor (TGF)-beta signaling in cardiac remodeling.* J Mol Cell Cardiol, 2011. **51**(4): p. 600-6.
165. Chandrashekhar, Y., et al., *Cardiomyocytes from hearts with left ventricular dysfunction after ischemia-reperfusion do not manifest contractile abnormalities.* J Am Coll Cardiol, 1999. **34**(2): p. 594-602.
166. Pasumarthi, K.B. and L.J. Field, *Cardiomyocyte cell cycle regulation.* Circ Res, 2002. **90**(10): p. 1044-54.

167. Samsa, L.A., B. Yang, and J. Liu, *Embryonic cardiac chamber maturation: Trabeculation, conduction, and cardiomyocyte proliferation.* Am J Med Genet C Semin Med Genet, 2013. **163C**(3): p. 157-68.
168. Kessler, D.S., *Siamois is required for formation of Spemann's organizer.* Proc Natl Acad Sci U S A, 1997. **94**(24): p. 13017-22.
169. Ota, M. and H. Sasaki, *Mammalian Tead proteins regulate cell proliferation and contact inhibition as transcriptional mediators of Hippo signaling.* Development, 2008. **135**(24): p. 4059-69.
170. Zhang, H., et al., *TEAD transcription factors mediate the function of TAZ in cell growth and epithelial-mesenchymal transition.* J Biol Chem, 2009. **284**(20): p. 13355-62.
171. Cooper, T.A. and C.P. Ordahl, *A single cardiac troponin T gene generates embryonic and adult isoforms via developmentally regulated alternate splicing.* J Biol Chem, 1985. **260**(20): p. 11140-8.
172. Samarel, A.M., *Costameres, focal adhesions, and cardiomyocyte mechanotransduction.* Am J Physiol Heart Circ Physiol, 2005. **289**(6): p. H2291-301.
173. Tallawi, M., et al., *Effect of substrate mechanics on cardiomyocyte maturation and growth.* Tissue Eng Part B Rev, 2015. **21**(1): p. 157-65.
174. Bersell, K., et al., *Neuregulin1/ErbB4 signaling induces cardiomyocyte proliferation and repair of heart injury.* Cell, 2009. **138**(2): p. 257-70.
175. Heallen, T., et al., *Hippo pathway inhibits Wnt signaling to restrain cardiomyocyte proliferation and heart size.* Science, 2011. **332**(6028): p. 458-61.
176. Xin, M., et al., *Regulation of insulin-like growth factor signaling by Yap governs cardiomyocyte proliferation and embryonic heart size.* Sci Signal, 2011. **4**(196): p. ra70.
177. Laplante, M. and D.M. Sabatini, *mTOR signaling in growth control and disease.* Cell, 2012. **149**(2): p. 274-93.
178. D'Uva, G., et al., *ERBB2 triggers mammalian heart regeneration by promoting cardiomyocyte dedifferentiation and proliferation.* Nat Cell Biol, 2015. **17**(5): p. 627-38.
179. Berger, L.C., et al., *Interaction between T antigen and TEA domain of the factor TEF-1 derepresses simian virus 40 late promoter in vitro: identification of T-antigen domains important for transcription control.* J Virol, 1996. **70**(2): p. 1203-12.
180. Watanabe, T., et al., *Regulation of troponin T gene expression in chicken fast skeletal muscle: involvement of an M-CAT-like element distinct from the standard M-CAT.* J Biochem, 1997. **121**(2): p. 212-8.
181. Smith, S.J., et al., *The cardiac-restricted protein ADP-ribosylhydrolase-like 1 is essential for heart chamber outgrowth and acts on muscle actin filament assembly.* Dev Biol, 2016. **416**(2): p. 373-88.
182. Spaich, S., et al., *F-box and leucine-rich repeat protein 22 is a cardiac-enriched F-box protein that regulates sarcomeric protein turnover and is essential for maintenance of contractile function in vivo.* Circ Res, 2012. **111**(12): p. 1504-16.
183. Kirchmaier, B.C., et al., *The Popeye domain containing 2 (popdc2) gene in zebrafish is required for heart and skeletal muscle development.* Dev Biol, 2012. **363**(2): p. 438-50.
184. Soni, S., et al., *A Proteomics Approach to Identify New Putative Cardiac Intercalated Disk Proteins.* PLoS One, 2016. **11**(5): p. e0152231.
185. Lo, H.F., et al., *Association of dysfunctional synapse defective 1 (SYDE1) with restricted fetal growth - SYDE1 regulates placental cell migration and invasion.* J Pathol, 2017. **241**(3): p. 324-336.
186. McElhinny, A.S., et al., *Muscle-specific RING finger-2 (MURF-2) is important for microtubule, intermediate filament and sarcomeric M-line maintenance in striated muscle development.* J Cell Sci, 2004. **117**(Pt 15): p. 3175-88.

187. Jokela, H., et al., *Hydroxysteroid (17beta) dehydrogenase 7 activity is essential for fetal de novo cholesterol synthesis and for neuroectodermal survival and cardiovascular differentiation in early mouse embryos.* Endocrinology, 2010. **151**(4): p. 1884-92.
188. Fassett, J.T., et al., *AMPK attenuates microtubule proliferation in cardiac hypertrophy.* Am J Physiol Heart Circ Physiol, 2013. **304**(5): p. H749-58.
189. Anderson, C.M., et al., *Cooperative activation of cardiac transcription through myocardin bridging of paired MEF2 sites.* Development, 2017. **144**(7): p. 1235-1241.
190. Huang, T.T., et al., *Genetic modifiers of the phenotype of mice deficient in mitochondrial superoxide dismutase.* Hum Mol Genet, 2006. **15**(7): p. 1187-94.
191. Bainbridge, M.N., et al., *Loss of Function Mutations in NNT Are Associated With Left Ventricular Noncompaction.* Circ Cardiovasc Genet, 2015. **8**(4): p. 544-52.
192. Eimre, M., et al., *Distinct organization of energy metabolism in HL-1 cardiac cell line and cardiomyocytes.* Biochim Biophys Acta, 2008. **1777**(6): p. 514-24.
193. Dobrzyn, P., T. Bednarski, and A. Dobrzyn, *Metabolic reprogramming of the heart through stearoyl-CoA desaturase.* Prog Lipid Res, 2015. **57**: p. 1-12.
194. Gaspar, J.A., et al., *Unique metabolic features of stem cells, cardiomyocytes, and their progenitors.* Circ Res, 2014. **114**(8): p. 1346-60.
195. Gwinn, D.M., et al., *AMPK phosphorylation of raptor mediates a metabolic checkpoint.* Mol Cell, 2008. **30**(2): p. 214-26.
196. Van Aelst, L.N., et al., *Osteoglycin prevents cardiac dilatation and dysfunction after myocardial infarction through infarct collagen strengthening.* Circ Res, 2015. **116**(3): p. 425-36.
197. Chang, D.F., et al., *LIM-only protein, CRP2, switched on smooth muscle gene activity in adult cardiac myocytes.* Proc Natl Acad Sci U S A, 2007. **104**(1): p. 157-62.
198. Jain, M.K., et al., *Embryonic expression suggests an important role for CRP2/SmLIM in the developing cardiovascular system.* Circ Res, 1998. **83**(10): p. 980-5.
199. Maerki, S., et al., *The Cul3-KLHL21 E3 ubiquitin ligase targets aurora B to midzone microtubules in anaphase and is required for cytokinesis.* J Cell Biol, 2009. **187**(6): p. 791-800.
200. Courtheoux, T., et al., *Cortical dynamics during cell motility are regulated by CRL3(KLHL21) E3 ubiquitin ligase.* Nat Commun, 2016. **7**: p. 12810.
201. Tsuda, T., et al., *Corticotropin releasing hormone receptor 2 exacerbates chronic cardiac dysfunction.* J Exp Med, 2017. **214**(7): p. 1877-1888.
202. Cong, B., et al., *Estrogens protect myocardium against ischemia/reperfusion insult by up-regulation of CRH receptor type 2 in female rats.* Int J Cardiol, 2013. **168**(5): p. 4755-60.
203. Ni, Y.G., et al., *Foxo transcription factors blunt cardiac hypertrophy by inhibiting calcineurin signaling.* Circulation, 2006. **114**(11): p. 1159-68.
204. Schips, T.G., et al., *FoxO3 induces reversible cardiac atrophy and autophagy in a transgenic mouse model.* Cardiovasc Res, 2011. **91**(4): p. 587-97.
205. Seguchi, O., et al., *A cardiac myosin light chain kinase regulates sarcomere assembly in the vertebrate heart.* J Clin Invest, 2007. **117**(10): p. 2812-24.
206. Emdin, C.A., et al., *Genetic Variation at the Sulfonylurea Receptor, Type 2 Diabetes, and Coronary Heart Disease.* Diabetes, 2017. **66**(8): p. 2310-2315.
207. Chi, Y., et al., *Forkhead box O (FOXO) 3 modulates hypoxia-induced autophagy through AMPK signalling pathway in cardiomyocytes.* Biosci Rep, 2016. **36**(3).
208. Qiu, H., et al., *TEAD1-dependent expression of the FoxO3a gene in mouse skeletal muscle.* BMC Mol Biol, 2011. **12**: p. 1.
209. Evans-Anderson, H.J., C.M. Alfieri, and K.E. Yutzey, *Regulation of cardiomyocyte proliferation and myocardial growth during development by FOXO transcription factors.* Circ Res, 2008. **102**(6): p. 686-94.

210. Wang, P., et al., *The alteration of Hippo/YAP signaling in the development of hypertrophic cardiomyopathy.* Basic Res Cardiol, 2014. **109**(5): p. 435.
211. Yoshizawa, K., et al., *Analyses of beta-1 syntrophin, syndecan 2 and gem GTPase as candidates for chicken muscular dystrophy.* Exp Anim, 2003. **52**(5): p. 391-6.
212. Li, J., R. Mayne, and C. Wu, *A novel muscle-specific beta 1 integrin binding protein (MIBP) that modulates myogenic differentiation.* J Cell Biol, 1999. **147**(7): p. 1391-8.
213. Benhaddou, A., et al., *Transcription factor TEAD4 regulates expression of myogenin and the unfolded protein response genes during C2C12 cell differentiation.* Cell Death Differ, 2012. **19**(2): p. 220-31.
214. Poindexter, B.J., et al., *Calcium signaling mechanisms in dedifferentiated cardiac myocytes: comparison with neonatal and adult cardiomyocytes.* Cell Calcium, 2001. **30**(6): p. 373-82.

VI. LIST OF FIGURES

VII. LIST OF TABLES